

Clemson University

TigerPrints

All Dissertations

Dissertations

12-2021

Development of Tissue Engineered Scaffolds for Cardiovascular Repair and Replacement in Pediatric Patients

Dipasha Sinha

Clemson University, dipashs@clemson.edu

Follow this and additional works at: https://tigerprints.clemson.edu/all_dissertations

Recommended Citation

Sinha, Dipasha, "Development of Tissue Engineered Scaffolds for Cardiovascular Repair and Replacement in Pediatric Patients" (2021). *All Dissertations*. 2940.

https://tigerprints.clemson.edu/all_dissertations/2940

This Dissertation is brought to you for free and open access by the Dissertations at TigerPrints. It has been accepted for inclusion in All Dissertations by an authorized administrator of TigerPrints. For more information, please contact kokeefe@clemson.edu.

Clemson University

TigerPrints

All Dissertations

Dissertations

12-2021

Development of Tissue Engineered Scaffolds for Cardiovascular Repair and Replacement in Pediatric Patients

Dipasha Sinha

Follow this and additional works at: https://tigerprints.clemson.edu/all_dissertations

DEVELOPMENT OF TISSUE ENGINEERED SCAFFOLDS FOR
CARDIOVASCULAR REPAIR AND REPLACEMENT
IN PEDIATRIC PATIENTS

A Dissertation
Presented to
the Graduate School of
Clemson University

In Partial Fulfillment
of the Requirements for the Degree
Doctor of Philosophy
Bioengineering

by
Dipasha Sinha
December 2021

Accepted by:
Dr. Narendra Vyavahare, Committee Chair
Dr. Agneta Simionescu
Dr. Jiro Nagatomi
Dr. Ying Mei

ABSTRACT

Congenital Heart Diseases (CHD) are abnormalities present in the heart and great vessels at birth. It is one of the most frequently diagnosed congenital disorders, affecting approximately 40,000 live birth each year in the United States. The incidence of new CHD patients and the relative distribution of defects have not changed over time and remain a birth rate function. Out of the new patients found to have CHD each year, an estimated 2,500 patients have a defect that requires a substitute, non-native valve, or conduit artery to replace structures that are congenitally absent or hypoplastic. Materials in current use for conduit and valve replacement involve varying degrees of stiffness and flexibility, durability, calcification, susceptibility to infection, thrombosis, and a lack of growth potential for the replacement.

Biomaterials developed using tissue engineering principles could overcome the limitations encountered with current strategies. This research aims to develop potentially superior valves and conduits using acellular xenograft tissues that are physically cross-linked to protect the Extracellular Matrix (ECM) from rapid degradation. The hypothesis is that such a replacement graft would allow cellular ingrowth of host cells and potentially enable regenerative growth and remodeling of the graft. A decellularization protocol was developed, and the most effective crosslinker protecting the extracellular matrix structure was identified. The decellularized scaffolds crosslinked with Penta galloyl glucose (PGG) were analyzed *in-vitro* for stability and mechanical properties, in subcutaneous rat and in

valve replacement in sheep-models to determine the biocompatibility and functionality of the developed scaffolds.

Tissue-engineered scaffolds prepared from decellularized PGG treated tissues were found to have mechanical properties comparable to that of native tissues, while being more resistant to enzymatic degradation. Subcutaneous implantation of scaffolds demonstrated their biocompatibility and superior resistance to calcification compared to currently available glutaraldehyde fixed tissues. The tissue-engineered conduits and valves implanted in large animal models also demonstrated adequate implant functionality, cellular infiltration, implant remodeling, and growth of the implants. PGG treated decellularized xenografts could be an effective replacement option for pediatric patients, reducing the need for reoperations required with current devices.

DEDICATION

To my parents Pradip Sinha and Sabita Sinha, for supporting me through all the decisions I have made in my life and having immense faith in me. I would not be the person I am without them.

ACKNOWLEDGMENTS

I would like to express my sincere gratitude to all the people who have helped me throughout this journey. First and foremost, my advisor Dr. Narendra Vyavahare, for providing me with the opportunity to perform this research and for his direction and perspective whenever I needed it. His mentorship, innovation, and critical thinking have amazed me and are a great source of aspiration for my journey forward.

Secondly, all my committee members, Dr. Agneta Simionescu, Dr. Jiro Nagatomi, and Dr. Ying Mei, for providing me with valuable guidance and insights into my research. They have generously offered their help whenever I needed it and helped bring their perspective into this research.

A significant work involved in this research comes from animal studies. My sincere gratitude to Dr. John Parrish, Travis Pruitt, Cynthia Nigro, Melody Willey, and everyone at Godley Snell Research Center who have helped me with all my animal studies. I would also like to thank our collaborator Dr. John E. Mayer and his group at Harvard Medical School, who have performed the sheep studies for us. Moreover, I would like to acknowledge all the rats who gave their lives for the studies in this research. I hope their sacrifice contributes to significant advancements in science.

My gratitude to everyone at the Advanced Material Science Laboratory (AMRL) facility in Clemson for helping with the electron microscopy imaging in this research. Especially George Wetzal for providing his help and advice on the imaging studies to complete this research.

I would like to thank Dr. Guzeliya Korneva, and Dr. Agnes Nagy Mehesz for being the best mentors and teaching me all the subtleties of research and scientific thinking. I am also grateful to Dr. LaBerge and the Department of Bioengineering for giving me the opportunity as a graduate student. I extend my gratitude to all the administrative staff in the department who have made things easy for me.

All my present and past lab members, namely, Dr. Vaideesh Parsaram, Dr. Saketh Karamched, Dr. Xioayang Wang, Dr. Nandakumar Natarajan, Dr. Christian Macks, Dr. Saphala Dhital, Dr. Shivani Arora, Tyler Gibson, Hannah Gore, Fatema Tuj Zohora, and Greg Halsey. All of you have immensely helped me in my lab experiments, as well as provided me motivation to pursue a career in research.

I would like to say a huge thank you to all my friends in the United States who have made the grad school journey a lot easier and more fun. Also, my friends from IIT Kharagpur who have cheered me on from all over the world.

Finally, I would also like to acknowledge the financial support provided by the National Institutes of Health and the Hunter endowment to Dr. Vyavahare.

TABLE OF CONTENTS

	Page
TITLE PAGE.....	i
ABSTRACT	ii
DEDICATION.....	iv
ACKNOWLEDGMENTS	v
LIST OF TABLES.....	x
LIST OF FIGURES	xi
LIST OF ABBREVIATIONS	xiv
CHAPTER	
I. INTRODUCTION.....	1
II. LITERATURE REVIEW.....	6
2.1 The Cardiovascular System.....	6
2.2 Congenital Heart Diseases (CHD).....	16
2.3 Treatment for CHD.....	24
2.4 Tissue Engineering Strategies	28
2.5 Conduit Replacement Strategies	34
2.6 Valve Replacement Strategies.....	40
2.7 Decellularization Strategies.....	45
2.8 Sterilization and crosslinking of decellularized scaffolds	50
2.9 Diabetes and wound healing.....	57
III. PROJECT RATIONALE AND SPECIFIC AIMS.....	64
IV. SPECIFIC AIM 1: ASSESSMENT OF THE EFFICIENCY OF POLYPHENOLS IN STABILIZING ELASTIN AND COLLAGEN IN SCAFFOLDS	70
4.1 Introduction	70
4.2 Materials and method	71

Table of Contents (Continued)	Page
4.3 Results	80
4.4 Discussions	91
4.5 Conclusions	94
V. SPECIFIC AIM 2: DEVELOPMENT OF TISSUE ENGINEERED BOVINE JUGULAR VEIN CONDUITS FOR PEDIATRIC PATIENTS	96
5.1 Introduction	96
5.2 Materials and method	98
5.3 Results	106
5.4 Discussions	124
5.5 Conclusions	127
VI. SPECIFIC AIM 3: DEVELOPMENT OF TISSUE ENGINEERED VALVE LEAFLET PATCH FOR PULMONARY VALVE REPAIR IN PEDIATRIC PATIENTS	129
6.1 Introduction	129
6.2 Materials and method	131
6.3 Results	141
6.4 Discussions	164
6.5 Conclusions	167
VII. SPECIFIC AIM 4: EVALUATION OF PGG TREATED BOVINE PERICARDIUM SCAFFOLDS AS INTRA-MUSCULAR IMPLANTS IN DIABETIC CONDITIONS.....	169
7.1 Introduction	169
7.2 Materials and method	170
7.3 Results	179
7.4 Discussions	202
7.5 Conclusions	204
VIII. CONCLUSIONS AND FUTURE RECOMMENDATION.....	205
8.1 Conclusions	205
8.2 Recommendations for future studies	207
APPENDIX	214

Table of Contents (Continued)	Page
REFERENCES	216

LIST OF TABLES

Table		Page
1	Currently available conduit replacement strategies.....	39
2	Properties of Quercetin, Hesperidin, D-Salicin and All-trans retinoic acid	57
3	Polyphenol concentrations used for treatment of decellularized tissues	76
4	PGG concentrations used for BJV treatment.....	98
5	PGG quantification in PBS wash solutions	107
6	Jansen scoring of subcutaneous BJV implants	119
7	Jansen scoring of subcutaneous PAV implants	160
8	Statistics of cells stained positive from flow cytometry.....	163
9	IHC semi-quantification for CD68 staining	193
10	IHC semi-quantification for CD80 staining	194
11	IHC semi-quantification for CD163 staining	195
12	IHC semi-quantification for CD3 staining	196
13	IHC semi-quantification for TNF-alpha staining	197
14	IHC semi-quantification for i-NOS staining	198
15	IHC semi-quantification for MMP-9 staining	199
16	IHC semi-quantification for vimentin staining.....	200
17	IHC semi-quantification for smooth muscle actin staining.....	201

LIST OF FIGURES

Figure		Page
1	Schematic representation of the systemic and pulmonary circulatory system	6
2	Anatomy of the heart and heart valves	7
3	Structure of blood vessels.....	9
4	Histology of heart valves.....	10
5	Overview of collagen fibril formation process.....	12
6	Elastogenesis: Synthesis of elastin fibers	13
7	Crosslinking of elastin and mechanism of elastic stretch and recoil	14
8	Schematic representation of stress-strain relationship in heart valves during motion	15
9	Total CHD birth prevalence over time	17
10	Septal defects in CHD	19
11	Valve defects in CHD.....	20
12	Total anomalous partial venous connection	21
13	Tetralogy of Fallot.....	22
14	Dextro-transposition of the great arteries	22
15	Patent ductus arteriosus and truncus arteriosus	23
16	Gore cardioform atrial septal defect occluder deployment using Mullin's sheath.....	25
17	Fontan, Rastelli, Ross-Konno procedure.....	26
18	Corrective surgery for tetralogy of fallot.....	27

List of Figures (Continued)

Figure		Page
19	Load bearing properties vs time for tissue engineered scaffolds.....	30
20	CT follow-up showing calcification in glutaraldehyde conduit	39
21	Mechanical heart valves	41
22	Autologous pericardial tissue reconstructions using Ozaki procedure.....	43
23	Histology of glutaraldehyde fixed tissues in elastase degradation	51
24	Structure of Penta galloyl glucose (PGG)	54
25	Stages of normal process of wound healing	59
26	Effects of diabetes on wound healing.....	59
27	Decellularization process and polyphenol treatment of native tissues	72
28	DNA quantification of bovine jugular vein.....	81
29	DNA quantification of bovine pericardium, porcine fascia, and bovine inferior vena cava	82
30	Hematoxylin and eosin staining of native and decellularized tissues	83
31	Resistance to elastase treatment for polyphenol treated decellularized tissues	85
32	Resistance to collagenase treatment for polyphenol treated decellularized tissues	86
33	Insoluble elastin deposition within cell cultures treated with polyphenols.....	88

List of Figures (Continued)

Figure		Page
34	Immunocytochemical analysis of HAoSMC cultures using Elastin and Fibrillin I	90
35	Semi-quantitative analysis of elastin and fibrillin ICC	91
36	Washing protocol for PGG treated BJV	99
37	Schematic representation of subcutaneous implantation of BJV leaflets and walls in rats	103
38	Schematic representation of PGG treated BJV conduit replacement in sheep	106
39	PGG quantification in methanol extracts from BJV	107
40	VVG staining of BJV treated with different concentrations of PGG.....	107
41	Gross view of PGG treated decellularized bovine jugular vein conduit	109
42	Elastase treatment of BJV conduits treated with different concentrations of PGG.....	110
43	Collagenase treatment of BJV conduits treated with different concentrations of PGG.....	111
44	Native and PGG treated decellularized BJV histology	112
45	PGG concentration in BJV stored for up-to 24 months.....	113
46	Elastase challenge with stored BJV	114
47	Maximum stress and strain in BJV tissues from uniaxial testing.....	116
48	Alizarin red staining of subcutaneous BJV explants	117

List of Figures (Continued)

Figure	Page
49 ICP analysis of elemental calcium and phosphorous in subcutaneous BJV implants.....	118
50 H&E staining of glut and PGG BJV subcutaneous implants	119
51 H&E staining of BJV subcutaneous explants.....	120
52 IHC staining of subcutaneously implanted BJV.....	122
53 Sheep implants of PGG treated BJV conduits.....	123
54 PGG treated leaflet patch repair unit	131
55 Biaxial testing set-ups for porcine aortic valve leaflets.....	134
56 Suture retention strength measurement	136
57 Schematic representation of subcutaneous study of PAV in rats	137
58 DNA quantification for porcine aortic valves	142
59 DNA quantification of porcine pulmonary valves	142
60 Gross view of native, decellularized, and PGG treated Valve leaflets	143
61 Porcine aortic valve histology	144
62 Porcine pulmonary valve histology	146
63 Elastase and collagenase treatment of native, decellularized, and PGG treated PAV	147
64 Elastase and collagenase treatment of native, decellularized, and PGG treated PPV.....	148
65 Stress-strain biaxial curves for porcine aortic valves	149

List of Figures (Continued)

Figure	Page
66 Average maximum peaks at 60% strain for biaxial testing in porcine aortic valves.....	150
67 Peak tangent moduli for biaxial testing in porcine aortic valves.....	150
68 Average thickness of native, decellularized, and PGG treated porcine pulmonary valves.....	151
69 Stress-strain biaxial curves for porcine pulmonary valves.....	152
70 Average maximum peaks at 60% strain and peak tangent modulus for biaxial testing in porcine pulmonary valves.....	153
71 Suture pull-through testing for porcine aortic valves.....	154
72 Suture pull-through testing for porcine pulmonary valves.....	155
73 Gross view of PGG subcutaneous implants.....	156
74 Micro-CT imaging of porcine aortic valve explants.....	157
75 Alizarin red staining of porcine aortic valve subcutaneous explants.....	158
76 Calcium and phosphorous quantification in explanted aortic valves.....	159
77 Hematoxylin and Eosin staining of aortic valve subcutaneous explants.....	160
78 IHC staining of subcutaneously explanted aortic valves.....	162
79 Representative dot-plots of flow cytometry of subcutaneously implanted aortic valves.....	162
80 PGG treated decellularized porcine aortic valves explanted from sheep.....	163
81 Experimental designs for the study of antimicrobial properties of PGG treated decellularized scaffolds.....	174

List of Figures (Continued)

Figure	Page
82 Intra-muscular abdominal wound healing surgery	177
83 Pico-green dsDNA quantification in bovine pericardium	179
84 Hematoxylin and Eosin staining of bovine pericardium	180
85 Decellularized and PGG treated decellularized bovine pericardium scaffolds in <i>S aureus</i> cultures (Day 1).....	181
86 Growth of bacteria in <i>S aureus</i> cultures with addition of scaffolds incubated from Day 1	182
87 SEM imaging of decellularized and PGG treated decellularized bovine pericardium without bacterial incubation	183
88 SEM images of decellularized bovine pericardium with bacterial cultures.....	183
89 SEM images of PGG treated bovine pericardium with bacterial cultures.....	184
90 Bacterial growths in cultures after addition of elastase and collagenase enzyme digestion extracts	185
91 Weight and blood glucose levels of HFD/STZ induced diabetic rats.....	186
92 Gross view of decellularized and PGG treated bovine pericardium as intra-muscular implants in healthy rats.....	187
93 Gross view of decellularized and PGG treated bovine pericardium as intra-muscular implants in diabetic rats.....	188
94 Histology of decellularized and PGG treated decellularized pericardium intra-muscular implants in healthy rats for 2 weeks	190

List of Figures (Continued)

Figure	Page
95 Histology of decellularized and PGG treated decellularized pericardium intra-muscular implants in healthy rats for 4 weeks	190
96 Histology of decellularized and PGG treated decellularized pericardium intra-muscular implants in diabetic rats for 4 weeks	191
97 Histology of decellularized and PGG treated decellularized pericardium intra-muscular implants in healthy rats for 6 weeks	191
98 Histology of decellularized and PGG treated decellularized pericardium intra-muscular implants in diabetic rats for 6 weeks	192
99 Representative IHC images for CD68 staining in intra-muscular implants.....	193
100 Representative IHC images for CD80 staining in intra-muscular implants.....	194
101 Representative IHC images for CD163 staining in intra-muscular implants.....	195
102 Representative IHC images for CD3 staining in intra-muscular implants.....	196
103 Representative IHC images for TNF-alpha staining in intra-muscular implants	197
104 Representative IHC images for CD68 staining in intra-muscular implants.....	198
105 Representative IHC images for i-NOS staining in intra-muscular implants.....	199
106 Representative IHC images for vimentin staining in intra-muscular implants	200

List of Figures (Continued)

Figure		Page
107	Representative IHC images for Alpha-SMA staining in intra-muscular implants	201
108	PGG quantification in enzyme treatment extracts	214

LIST OF ABBREVIATIONS

CHD:	Congenital Heart Diseases
PTFE:	Polytetrafluoroethylene ethylene
PGG:	Penta galloyl Glucose
AV Valve:	Atrioventricular Valve
SL Valves:	Semilunar Valve
GAGs:	Glycose amino Glycans
SMC:	Smooth Muscle Cells
PGs:	Proteoglycans
SMCs:	Smooth Muscle Cells
ECM:	Extra Cellular Matrix
ER:	Endoplasmic Reticulum
EDS:	Ethers Danlos Syndrome
EBPs:	Elastin Binding Proteins
US:	United States
ASD:	Atrial Septal Defect
VSD:	Ventricular Septal Defect
AVSD:	Atrioventricular Septal Defect
d-TGA:	Dextro-transposition of the great arteries
TAPVC:	Total (or partial) Anomalous Pulmonary Venous Connection
PDA:	Patent ductus arteriosus

List of abbreviations (continued)

PLA:	Poly(lactic) acid
PGA:	Poly(glycolic) acid
PLGA:	poly (lactic-co-glycolic) acid
PU:	polyurethanes
PGS:	Polyglycerol sebacate
FDA:	Food and Drug Administration
PCL:	poly(ϵ -caprolactone)
PHAs:	Polyhydroxyalkanoates
P4HB:	poly-4-hydroxybutyrate
UPy:	supramolecular 2-ureido-4[1H]-pyrimidone
RVOT:	Right Ventricular Outflow Tract
MSC:	Mesenchymal Stem Cells
HEC:	Human Endothelial Cells
AOA TM :	Alpha-Oleic Acid
ATRA:	All-trans Retinoic Acid
TA:	Tannic Acid
PBS:	Phosphate Buffered Saline
SDS:	Sodium Dodecyl Sulfate
DOC:	Deoxy Cholate
EDTA:	Ethylenediaminetetraacetic acid

List of abbreviations (continued)

TRIS:	Tris (hydroxyethyl) aminomethane
DNA:	Deoxyribonucleic Acid
PAA:	Peracetic Acid
EDC:	1-Ethyl-3-(3-dimethyl aminopropyl)-carbodiimide
NDGA:	nordihydrogualeic acid
TEVG:	Tissue Engineered Vascular Grafts
EPCs:	Endothelial progenitor cells
PKC:	Protein Kinase C
AGEs:	Advanced Glycosylation End products
IL:	Interleukin
TNF:	Tumor Necrosis Factor
MMPs:	Matrix Metalloproteinase
TIMP:	Tissue Inhibitors of MMPs
VEGF:	Vascular Endothelial Growth Factors
bFGF:	basic Fibroblast Growth Factors
SDF 1-alpha:	Stromal Cell derived Factor-1 alpha
NOD:	Non Obese Diabetic
OHS:	Obese hypersensitive
BB:	Bio Breeding rat
KDP:	Komeda-diabetes prone

List of abbreviations (continued)

LETL:	Long Evans Tokushima Lean
LEW-iddm:	Lewis- Insulin Dependent Diabetes Mellitus
HFD:	High Fat Diet
STZ:	Streptozotocin
Glut:	Glutaraldehyde
PPV:	Porcine Pulmonary Valve
PAV:	Porcine Aortic Valve
TA:	Tannic Acid
DNase:	Deoxyribonuclease
dsDNA:	double stranded Deoxyribonucleic acid
RNA:	Ribonucleic acid
RNAse:	Ribonuclease
Pen/ Strep:	Penicillin/ Streptomycin
DI:	De Ionized
HEPES:	(4-(2-hydroxyethyl)-1-piperazineethanesulfonic acid)
CaCl ₂ :	Calcium Chloride
NaN ₃ :	Sodium Azide
CO ₂ :	Carbon dioxide
RPM:	Revolutions per minute
NBF:	Neutral Buffered Formalin

List of abbreviations (continued)

HAoSMC:	Human Aortic Smooth Muscle Cells
DMSO:	Dimethyl Sulfoxide
BCA:	Bicinchoninic Assay
IgG:	Immunoglobulin G
DAPI:	4', 6 – diamidino - 2- phenylindole
TEM:	Transmission Electron Microscopy
ANOVA:	Analysis of Variance
HSD:	Honest Significant Difference
BJV:	Bovine Jugular Vein
BVC:	Bovine Vena Cava
H&E:	Hematoxylin and Eosin
LOX:	Lysyl oxidase
ICC:	Immuno Cyto-chemistry
VVG:	Verhoeff's-Van Geisen
ICP:	Inductively Coupled Plasma
HCl:	Hydrochloric Acid
IHC:	Immunohistochemistry
H ₂ O ₂ :	Hydrogen Peroxide
DAB:	Diaminobenzene
HSP:	Heat Shock Protein

List of abbreviations (continued)

SMA:	Smooth Muscle Actin
SIS:	Sub-intestinal Submucosa
F-C:	Folin-Ciocalteu's
CCD:	Charged Coupled Device
SD:	Sprague Dawley
CT:	Computed Tomography
NaOH:	Sodium Hydroxide
NPPPV:	Native Porcine Pulmonary Valves
DPPPV:	Decellularized Porcine Pulmonary Valves
PPPPV:	PGG treated decellularized porcine pulmonary valves
LB:	Lysogeny Broth
CFU:	Colony Forming Units
SEM:	Scanning Electron Microscopy
MIC:	Minimum Inhibitory Concentration
iNOS:	inductive nitric oxide synthase

CHAPTER ONE

INTRODUCTION

Congenital Heart Diseases (CHD) are one of the most prevalent defects present at birth, affecting approximately 0.8% to 1.2% of live births worldwide (1). Risk factors for incidence of CHD are largely unknown, but some factors like chromosomal aneuploidies, genetic defects, and conditions of diabetic mellitus, phenyl-ketonuria, rubella, alcohol use, maternal obesity, exposure to thalidomide, retinoic acid, and organic solvents attribute to ~15% of known CHD cases. The incidence and distribution of CHD worldwide has remained stable from 1990 – 2017, indicating little improvement in its prevention over the years (2).

Defects in the heart and blood vessels present at birth range from minor defects to critical conditions lead to impaired blood flow within the body. The typical human cardiovascular system is a closed system consisting of systemic and pulmonary circulations, with unidirectional flow of blood maintained by the heart valves and blood vessels. (3). Deformities in CHD, occurring as septal defects, stenotic or regurgitant aortic or pulmonary valves, valve atresia, dextro-transposition of the great arteries, or a Tetralogy of Fallot, disrupts this normal flow of blood within the body (4). These deformed structures need to be treated to restore normal blood flow.

Treatment strategies for CHD deformities utilize catheterization techniques or open-heart surgeries. Cardiac catheterization is a minimally invasive technique that can be used to repair minor deformities within the heart. Critical conditions, however, require

surgical interventions. Surgical strategies like the Ross-Konno procedure, Rastelli procedure, and Fontan procedure require the use of non-native conduit arteries, valves, and patches to repair and replace deformed structures (5). The gold standard for these replacements is homograft from donors; however, the insufficient number of heart donors in combination with donor-recipient heterogeneity and the wide range of deformities present in CHD makes the treatment more challenging. This leads to high mortality rates among infants and financial burden on the healthcare system (6).

Early intervention is required in congenital defects for normal physical and cognitive development of the patients (7). However, most of the currently available artificial replacements cannot keep up with the rapid changes in the size and structure of the heart from neonatal stages to childhood and adulthood. Synthetic conduit replacements made from polytetrafluoroethylene (PTFE) or Dacron tubes display various degrees of stiffness, kinking, stenosis, and calcification. Bioprosthetic conduits, commonly developed from glutaraldehyde treated bovine jugular veins, display severe calcification and stenosis upon implantation (8, 9). Mechanical valve replacements require the use of blood coagulants throughout the patient's life, whereas bioprosthetic heart valves generally display high levels of degradation upon implantation (10). Moreover, none of the currently available conduit or valve replacement strategies allow for growth with the patients, leading to failure of implants usually after 10-12 years of implantation (11).

To reduce multiple surgical interventions, and overcome the limitations of currently available biomaterials, tissue engineering techniques for preparation of these scaffolds seem to be the most promising. Tissue engineered scaffolds are 'patient specific' and can

adapt to the alterations in the recipient's body. The desired replacement conduit or valve should be biodegradable, biocompatible, flexible, durable, with an absence of immunogenicity, thrombosis, and calcification (12). The scaffolds should be composed of materials with specific morphological, functional, and mechanical properties to support cell attachment and proliferation at the implantation site. Additionally, they should allow neovascularization, allowing for oxygenation for the implanted tissue. The tissue engineered scaffolds should also resist rapid degradation upon implantation to prevent implant failure.

Decellularization of native tissues have been shown to reduce the incidence of calcification by removing the principal sites of calcification (13). To prevent rapid degradation of the decellularized scaffolds, the extracellular matrix components within the scaffolds need to be stabilized (14). Penta galloyl glucose (PGG), a derivative of tannic acid, has been shown to effectively stabilize elastin and collagen within extracellular matrices owing to its hydrophobic core and various hydroxy groups (15). PGG has also been shown to be non-toxic to human smooth muscle cells, as well as possess various therapeutic properties like anti-inflammatory, anti-oxidative, and anti-microbial, which might be beneficial in its use in cardiovascular applications (16-18).

In this research, we initially established the efficiency of the decellularization procedure in different tissues and determined the best stabilizing agent capable of protecting elastin and collagen from rapid degradation. Subsequently, decellularized and PGG treated conduits and valves were developed from native tissues and characterized in vitro. The PGG treated scaffolds were found to be biocompatible and resist calcification in

subcutaneous rat models. Sheep pulmonary conduit replacement with PGG treated valved conduits showed the regeneration and growth potential of the scaffolds. PGG treated porcine aortic and pulmonary valves were however found to be unsuitable in the pulmonary position.

Additionally, the PGG treated decellularized bovine pericardium scaffolds were evaluated as intra-muscular implants in diabetic conditions. Diabetes is a chronic condition resulting in delayed wound healing due to elevated pro-inflammatory phase and reduction in anti-inflammatory cells and cytokines. PGG as a therapeutic agent possesses anti-oxidant properties as well as anti-bacterial properties. The effects of these therapeutic properties of PGG treatment of scaffolds in diabetic conditions were analyzed. Overall, the goal of this research was to develop tissue-engineered scaffolds from decellularized, PGG treated scaffolds and determine the biocompatibility, growth, and regeneration potential of these developed scaffolds.

The dissertation is arranged into the following chapters:

- Chapter II presents a comprehensive overview of the Cardiovascular system, anatomy of the heart and great vessels, extracellular matrix in the cardiovascular system, congenital heart diseases, current treatment strategies for congenital defects, tissue engineering strategies, animal models for assessment of biocompatibility and functionality of tissue engineered scaffolds, diabetic wound healing, scaffolds used in diabetic

wound healing conditions, and animal models for the development of Type II diabetes.

- Chapter III presents the specific aims of this research and the approaches employed to achieve those aims.
- Chapter IV assesses the consistency of the decellularization procedure for different tissue types, and the effectiveness of different polyphenols and retinoic acid at crosslinking the extracellular matrix components within the decellularized scaffolds.
- Chapter V presents the development and characterization of conduit replacements from decellularized and PGG treated bovine jugular vein valved conduits, as well as biocompatibility and functionality assessment of these conduits in animal models.
- Chapter VI describes the development and characterization of valve replacements from decellularized PGG treated porcine aortic valves and porcine pulmonary valves and the assessment of these valves as pulmonary valve repair units in sheep.
- Chapter VII evaluates PGG treated decellularized bovine pericardium scaffolds as intra-muscular implants in healthy and diabetic rats.
- Chapter VIII presents the conclusions of this research and discusses future recommendations for the discussed research.

CHAPTER TWO
LITERATURE REVIEW

2.1 The Cardiovascular System

The cardiovascular system, also known as the circulatory system, is one of the most important organ systems, facilitating blood circulation and mass transportation (19). It is a closed tubular system within which a muscular heart propels blood into the blood vessels. There are primarily two circuits of blood vessels, the pulmonary and systemic circulations, composed of arterial, capillary, and venous components (Figure 1) (20).

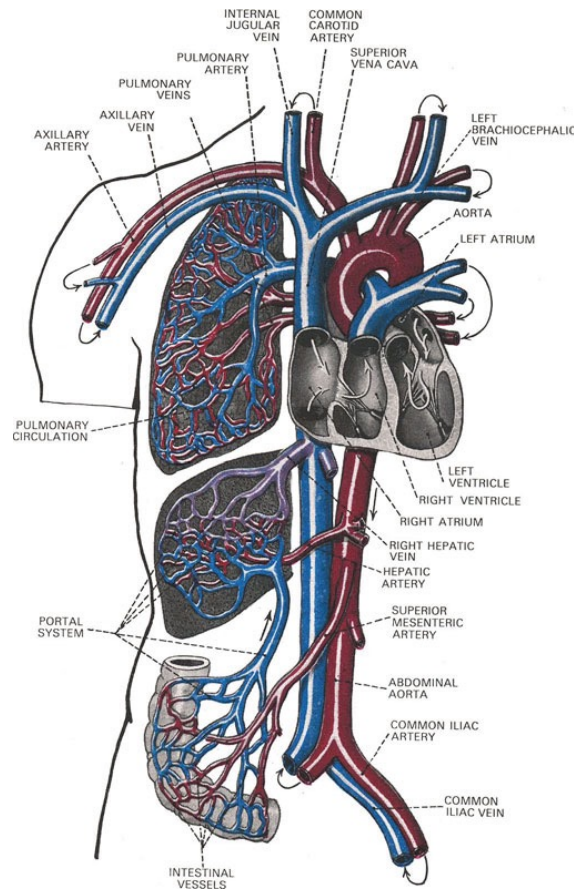


Figure 1: Schematic representation of the systemic and pulmonary circulatory system

The cardiovascular system performs the major function of transport of nutrients, gases, and waste products within the body. It plays a vital role in maintaining homeostasis by continuously regulating the blood flowing throughout the system, transporting nutrients, electrolytes, gases, and other essential cytokines to the different body tissues and organs (3). Protection against foreign microbes and toxins is carried out by white blood cells, antibodies, and complement proteins circulating through the blood. Clotting factors present within the blood prevent blood loss after injuries (21).

Anatomy of the heart and great vessels

The heart is a muscular organ, somewhat conical in shape, and enclosed within an outer fibrous pericardium, and a thinner delicate layer of serous pericardium. The layers of the serous pericardium form a pericardial cavity, enclosing some fluids that facilitate the movement of the heart within the pericardial cavity (20). The muscles of the heart are composed of three layers of outer epicardium, middle myocardium, and inner endocardium (22).

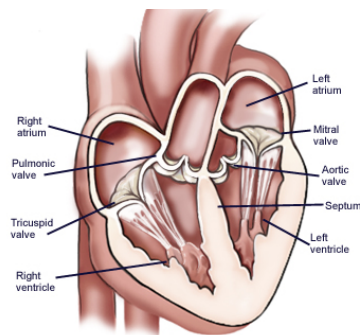


Figure 2: Anatomy of the heart and heart valves

The heart is composed of four chambers, left and right atria, and left and right ventricles. Blood from the right ventricles pass through the pulmonary artery, into the lungs, and back into the left atria through the pulmonary veins, completing the pulmonary cycle. From the left atria, blood flows into the left ventricle, from where it is pumped into the rest of the body (except the lungs) through the aorta (Figure 2). The aorta branches out into numerous smaller arteries, arterioles, and finally thin-walled capillaries, which are permeable to vital cellular nutrients and waste products that are received and redistributed. Blood within the capillaries is collected in veins through venules and returned to the right atria via the superior and inferior vena cava.

All blood vessels (arteries and veins) are composed of three primary layers: the intima, media, and adventitia (Figure 3). The innermost intima layer, lined with endothelial cells, are in direct contact with blood. The internal elastic lamina forms a barrier between the intima and medial layers in arteries. The media layer is composed of elastic fibers arranged in circular sheets and consists of numerous layers of smooth muscle cells which control the diameter of the vessel by contracting and relaxing to neural or chemical signals. The outer most layer of adventitia is composed mostly of fibrous tissue whose collagen fibers impart tensile strength and prevent excessive vasodilation (23). The cells within the arteries and veins require nourishment and produce waste. However, owing to the fast flow of blood through the great vessels, as well as the thickness of the vessels, diffusion of nutrients and waste is not possible through the walls. Larger arteries and veins, therefore, contain smaller vessels within their walls called *vasa vasorum*, to provide them with this critical exchange. In addition, since large veins are often under low pressure, they are

equipped with valves to maintain the unidirectional flow of blood. The walls of the veins immediately proximal to the valves, often show a slight bulge, called the *venous sinus* (24).

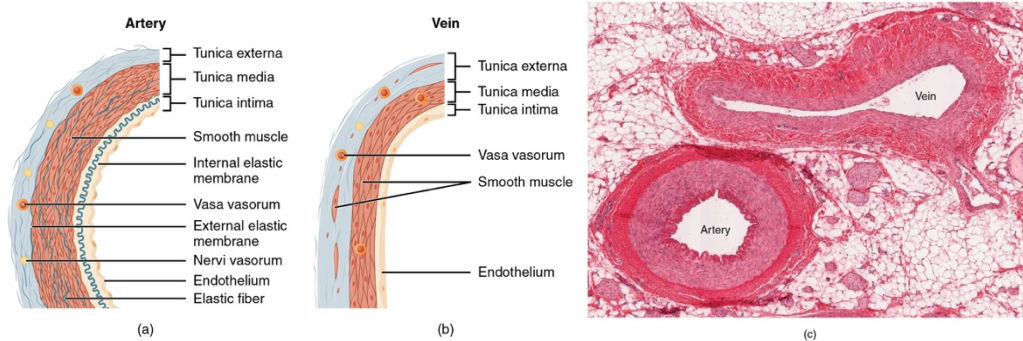


Figure 3: Structure of blood vessels (a) arteries and (b) veins have the same general features, but arteries have thicker walls to resist higher pressure of blood flow. (c) a micrograph showing relative difference in thickness between arterial and venous structures (25)

Blood within the heart flows through valvular openings, which permit the flow of blood only from the atria to ventricle, but not in the reverse direction. In the adult heart, the atrial and ventricular cavities are completely separated from each other via the impervious inter-atrial and inter-ventricular septum respectively. In fetal heart however, blood can flow within the atria through the *foramen ovale*, and for a short time between the ventricles through the interventricular foramen (26).

The human heart consists of four valves. The tricuspid and the mitral atrioventricular valves (AV) separate the atria and ventricles, while the pulmonary and the aortic semilunar valves (SL) separate the ventricles from the great arteries (27). All the valves are tricuspid (3 cusps or leaflets), except the mitral valve, which has only two cusps.

AV valves have a specialized support structure, while SL valves have a unique self-contained support structure within the arterial roots (28, 29). The SL valves are composed of different sized cusps and do not have symmetrical geometries.

Additionally, they are tethered to the inner walls of the ventricles by *chordae tendinea*, which prevents valve collapse during systole. AV valves, on the other hand, have similar-sized leaflets, attached to the basal wall at the basal attachment, and the free leaflets coapting to direct blood flow. Neighboring leaflets of the AV valves meet at the highest point to form a commissure. The aortic valve also has coronary artery ostioles behind two of the leaflets, leading to the nomenclature of non-coronary, left and right coronary leaflets (30).

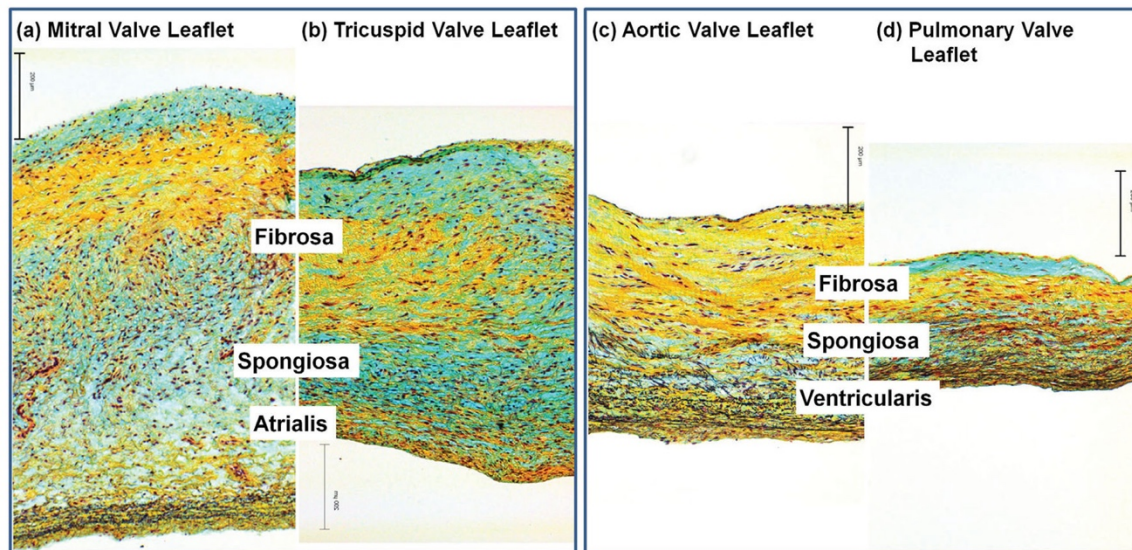


Figure 4: Histology of (a) Mitral valve, (b) Tricuspid valve, (c) Aortic valve, and (d) Pulmonary valve. SL valves have fibrosa, spongiosa, and atrialis layers, while AV valves have fibrosa, spongiosa, and ventricularis layers (31)

SL heart valves have a tri-layer tissue structure composed of fibrosa, spongiosa, and ventricularis layers (Figure 4). The fibrosa is composed primarily of Type I collagen fibers and is the main load bearing layer. The ventricularis layer, composed of dense network of elastin and collagen fibers assist in reducing radial strains during maximum forward flow. The middle spongiosa layer is composed of Glycose aminoglycans (GAGs) and Proteoglycans (PGs) that act as a lubricant for the other two layers as they shear and deform. Fibrosa and ventricularis layers consist primarily of endothelial cells, while the spongiosa is composed of interstitial cells like smooth muscle cells (SMC), fibroblasts and myofibroblasts (25).

Extracellular matrix in the cardiovascular system

As mentioned in previous sections, the extracellular matrix in the great vessels and heart valves are composed primarily of elastin, collagen, and glycosaminoglycans. This ECM composition is tissue-specific and varies with conditions and stages of development, homeostasis, and disease (32).

In media and adventitia layers of blood vessels, collagen type-I and type-III are the most predominant. Type-V collagens have been found to be concentrated in the media and basement membranes (33). In addition to type I, III, and V fibrillar collagen, type-VI collagen associated with fibrillin-1 in blood vessels and serve to connect elastic lamellae to the basement membrane of SMCs or SMCs to other ECM structures (34). Similarly, in valves, collagen types I, III, and V are the most predominant, imparting stiffness and integrity to the valve leaflets (35).

Collagen formation in the body starts with procollagen chains synthesized in the endoplasmic reticulum (ER) (Figure 5). The pro-collagen chains are brought together by interactions between the C-pro-peptides, and they fold to form rod-like triple-helical domain flanked by globular N- and C-pro-peptides. Post-translational modifications occur in pro-collagen within the ER. Procollagen molecules are then transported across Golgi stacks, the N- and C-propeptides are removed, and it results in collagen molecules assembled into fibrils. Triple helical collagen molecules are covalently crosslinked into fibrils (36).

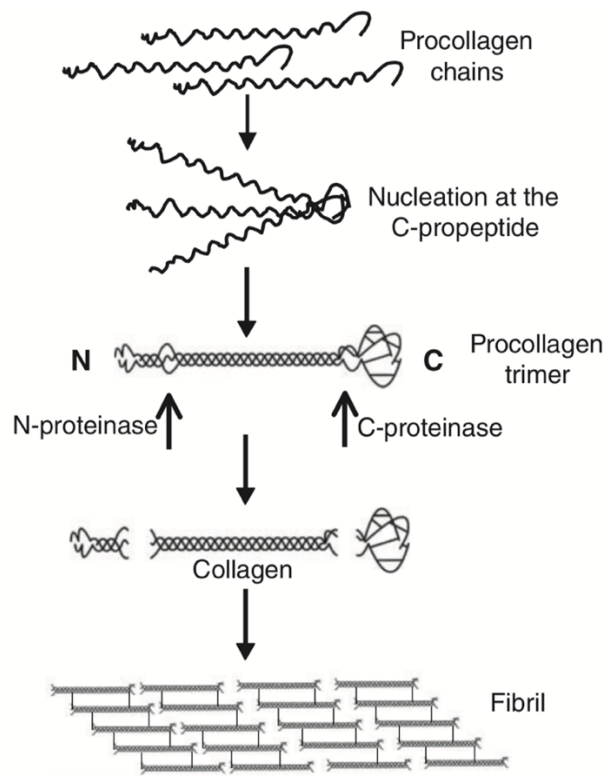


Figure 5: Overview of collagen fibril formation process from procollagen in fibroblasts (36)

In addition to being the primary source of tensile strength within the tissues, collagen also interacts with vascular cells and plays an essential role in pathobiology and cell biology (33, 37). Mutations, deficiencies, or different compositions in the collagen within vasculatures lead to diseased conditions like *Osteogenesis imperfecta* (Collagen-I mutation), Ethers Danlos Syndrome (EDS) (Collagen III procollagen mutation), Bethlem myopathy and Ulrich’s disease (mutation of collagen-VI) (38-41).

The other major ECM component found in heart valves and blood vessels is elastin. Elastin is the main structural component of elastic fibers and is a largely unstructured protein compared to collagen. This unstructured nature accounts for the ability of elastin to stretch and recoil. Elastin is composed of two primary components: a core comprising 90% of the fiber, and a scaffold of microfibrils, composed of fibrillin-1 and -2 (42). The

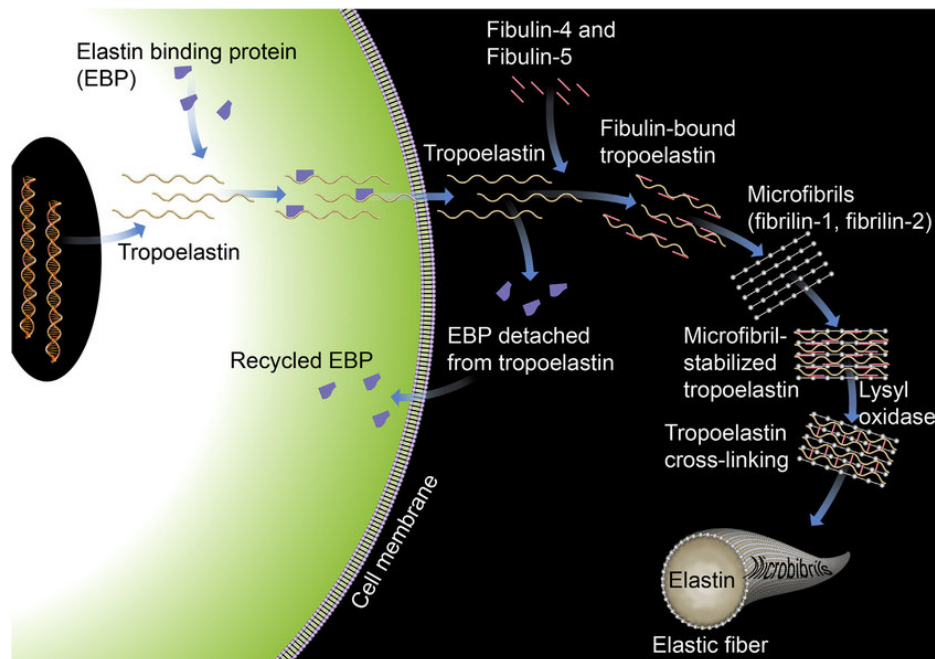


Figure 6: Elastogenesis: Synthesis of elastic fibers from tropoelastin

primary structure of elastin, tropoelastin, is expressed within elastogenic cells (including SMCs, endothelial cells, fibroblasts, and chondroblasts), after which it is trafficked to the

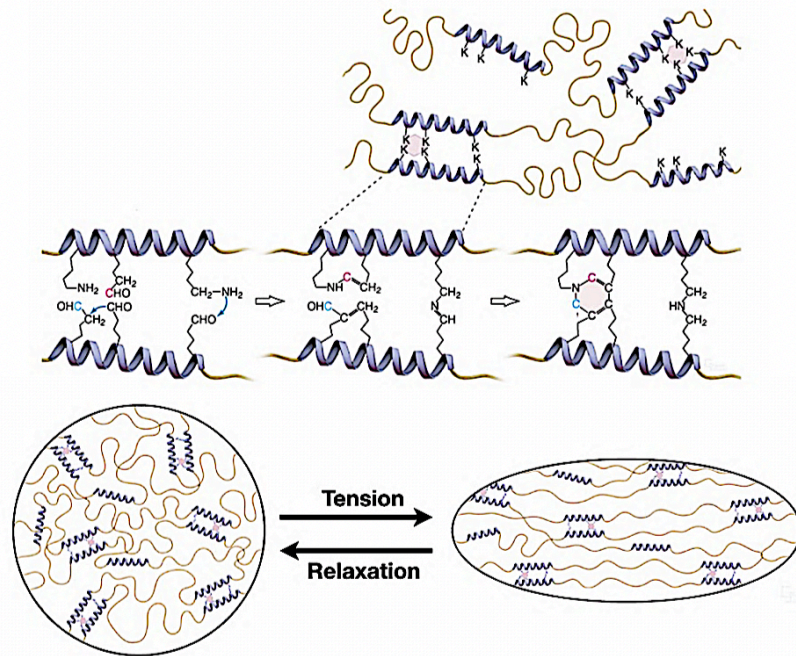


Figure 7: Crosslinking of elastin and mechanism of elastic stretch and recoil (52)

extracellular regions for cross-linking and assembly. This transport is mediated by elastin binding proteins (EBPs), which prevent intracellular aggregation and proteolysis of the tropoelastin (Figure 6). Tropoelastin molecules cluster by forming self-aggregated spherules, and they are crosslinked by lysyl oxidase into the networks of elastic fibers by depositing the spherules onto microfibrils and forming intramolecular and intermolecular crosslinks (42-45).

Most of the elastin synthesis in humans occurs at a young age. With the increase in age, elastin expression is reduced, resulting in decreased elastin production and difficulties

in elastin repair (46). Elastin is the major component in arterial walls, comprising ~50% of the dry weight (43). It is found throughout the medial layer of blood vessels, present as fenestrated elastic laminae. The microfibrils embedded within the amorphous core of elastin allow its elastic recoil (Figure 7). Elastic laminae in the blood vessels render tissue integrity as well as elastic recoil (33). Within valves, elastin is present in the ventricularis, aligned mostly in the radial direction, limiting radial stress during leaflet openings (47-50).

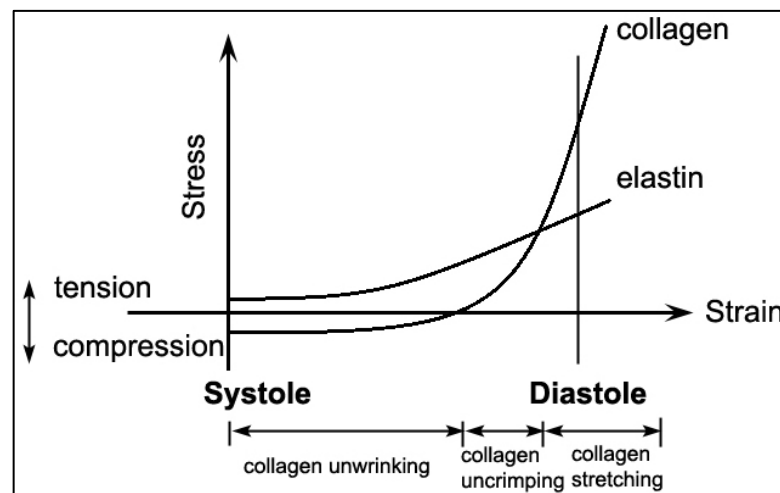


Figure 8: Schematic representation of stress-strain relationship in heart valves during motion (51)

The structure and arrangement of collagen along with elastin determine the mechanical properties of blood vessels and valves. Within valves, as demonstrated Figure 8, biomechanical cooperation exists between the collagen and elastin layers. During valve opening, elastin is extended at minimal load, while collagen uncrimps and corrugates. Near full closure, this load-bearing capability is shifted from elastin to collagen; while the stress

rises steadily, coaptation is maintained. Finally, during systole, the contracted configuration of the cusps is restored by elastin (51).

In addition to resistance to tensile forces, cardiovascular extracellular matrix also possesses resistance to compressive forces. This is rendered by Glycosaminoglycans (GAGs) and proteoglycans (PGs) within the ECM. GAGs, which are long chains of repeating disaccharides, retain large amounts of water to resist compression. GAGs are further classified into proteoglycans and hyaluronidases, depending on the arrangement of the GAG molecules (52). The presence of GAGs within cardiovascular ECM ensures smooth movement of the various structures.

2.2 Congenital Heart Diseases (CHD)

Congenital heart diseases (CHD) are deformities present in the heart and blood vessels at birth. These deformities might change the normal flow of blood through the heart (53). CHDs are the most common forms of birth defects and can range from mild deformities (like a hole in the heart) to severe defects (such as missing or poorly formed parts of the heart) (54).

Approximately 0.8% - 1.2% of live births worldwide are affected by congenital heart defects (1, 55, 56). In the United States (US), CHD affects approximately 40,000 newborns each year. The total number of patients living with CHD is now estimated to be approaching 2 million patients (57). Statistical studies have determined that from 1990 to 2017, the incidence of CHD has remained constant in both males and females, indicating there has been little or no improvement in its prevention over the years (Figure 9) (1, 58).

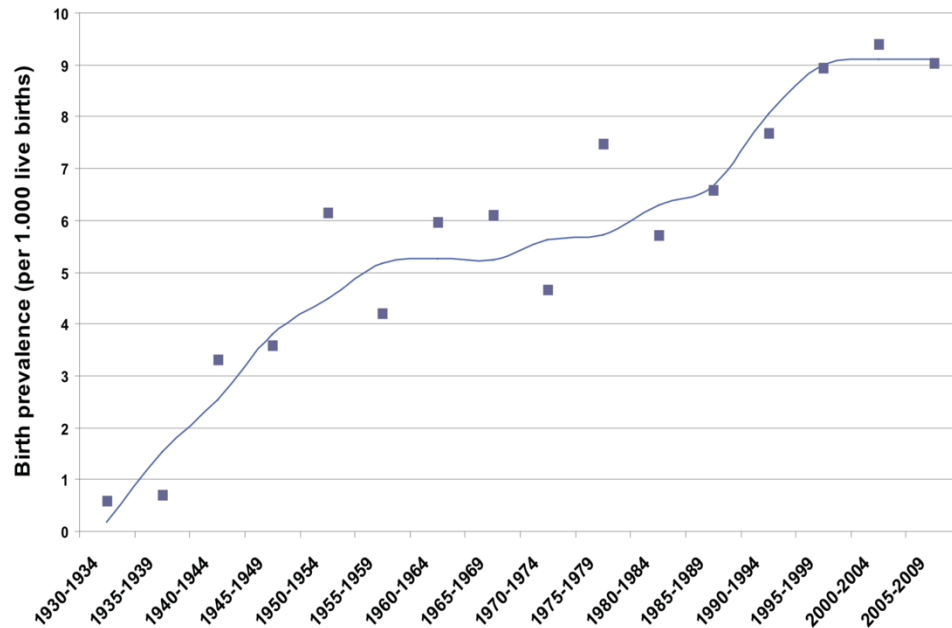


Figure 9: Total CHD Birth prevalence over time (55)

Only ~15% of the cases of CHD can be attributed to a known cause (59). Chromosomal aneuploidies like Down’s syndrome, Turner syndrome, DiGeorge syndrome, trisomy 13, and trisomy 18 might lead to deformations in the heart structures. Conditions with defects in single genes like Alagille syndrome, Holt–Orem syndrome, and Noonan syndrome contribute to 3% - 5% of CHD cases. Known environmental risk factors leading to defects include maternal diabetes mellitus, phenylketonuria, obesity, alcohol use, febrile illnesses, rubella infection, use of thalidomide and retinoic acid, as well as exposure to organic solvents (60, 61).

More than 80% deaths in CHD patients happen before five years of age, thereby emphasizing the importance of early screening and correction of the deformities (1).

Types of CHD

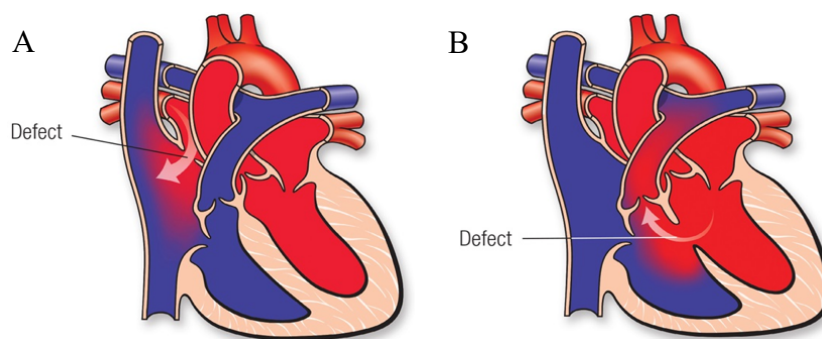
Congenital defects in the heart occur in various forms that might be present individually or in combination. Some of the more common CHD conditions are as follows (2, 62-68):

Septal Defects:

Atrial Septal Defect (ASD): A defect in the septum between the left and right atria, leading to leaking of oxygenated blood into the right atria.

Ventricular Septal Defect (VSD): A defect in the septum between the ventricles leading to leakage of oxygenated blood into the right ventricle, which might in turn cause higher pressure in the lungs or less oxygenated blood circulation throughout the body.

Atrioventricular Septal Defect (AVSD): A large defect in the heart affecting blood flow in all the four chambers (left and right atria and left and right ventricles). In a complete AVSD conditions, both the mitral valve and the tricuspid valves are malformed, whereas in a partial defect, only one of the valves might be deformed.



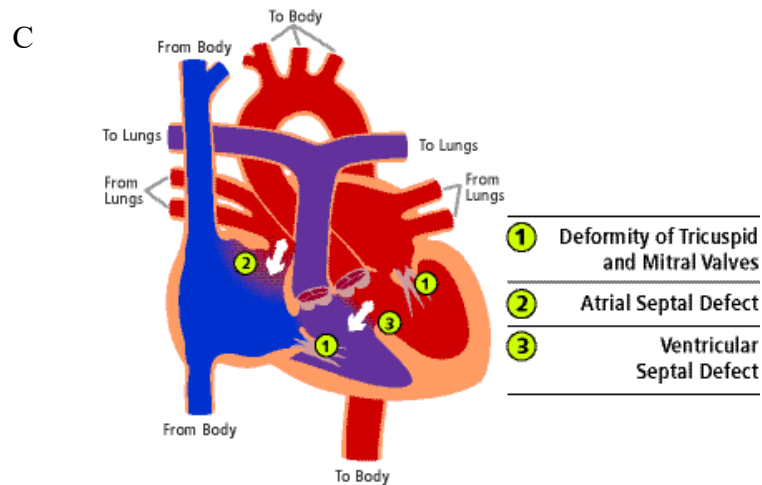


Figure 10: Septal defects in CHD: (A) Atrial Septal Defect (ASD), (B) Ventricular Septal Defect (VSD); (C) Atrioventricular Septal Defect (AVSD)

Valve Defects:

Atresia: Valve atresia refers to a valve that is malformed or not formed at all, resulting in no opening for the flow of blood. In CHD, usually, atresia occurs in the pulmonary or tricuspid position.

Ebstein's anomaly: Defect in the tricuspid valve that prevents its proper closing. This leads to leakage of blood in the opposite direction, and it usually exists with ASD conditions.

Valve stenosis: Stenosis of the aortic or pulmonary valve where the respective valves are narrower than usual, leading to pressure build-up in the heart, and over time, hypertrophy in the heart muscles.

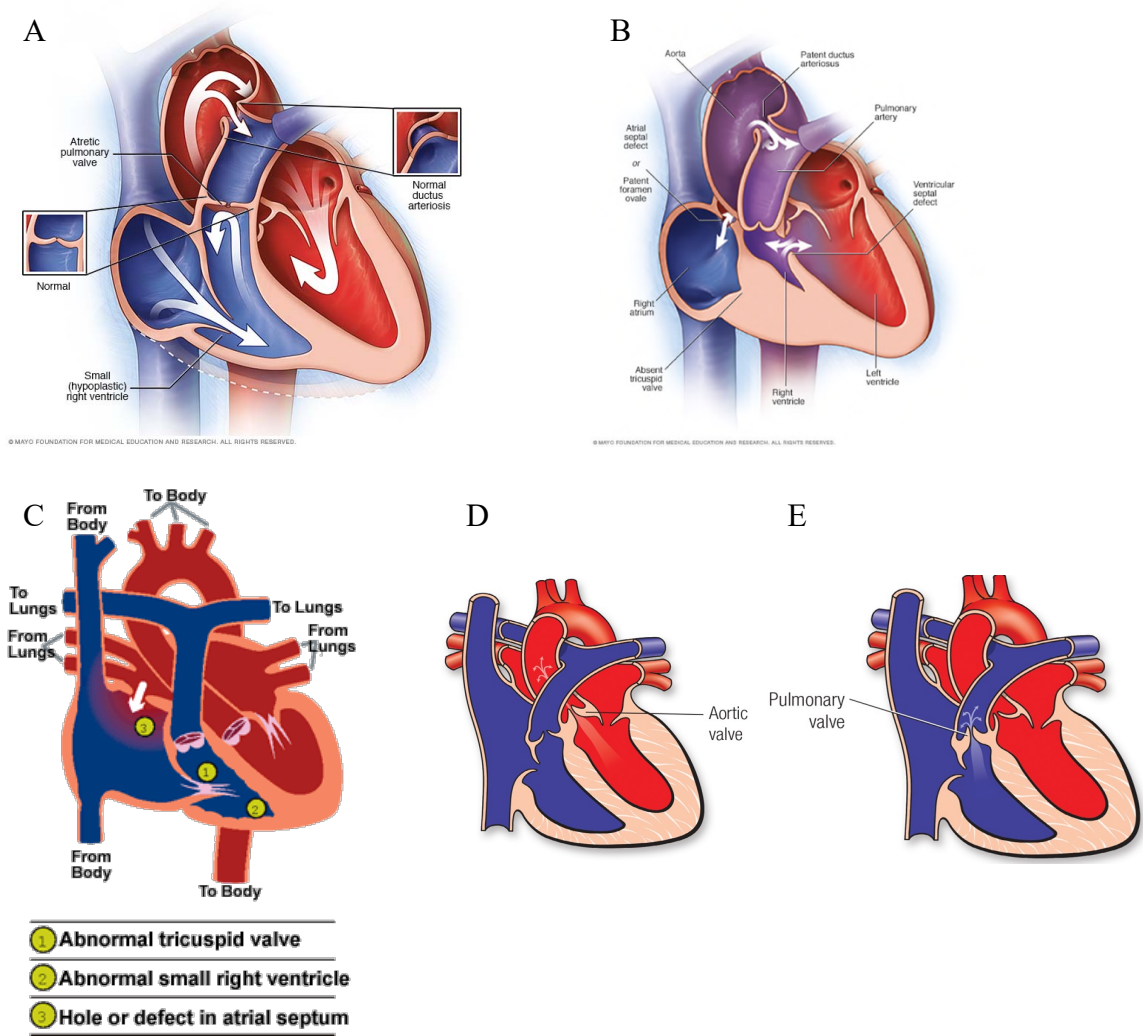


Figure 11: Valve defects in CHD: (A) Pulmonary Valve Atresia; (B) Tricuspid Valve Atresia; (C) Ebstein's Anomaly (D) Aortic Valve Stenosis; (E) Pulmonary Valve Stenosis (62)

Combined Defects:

Total (or partial) Anomalous Pulmonary Venous Connection (TAPVC): This condition refers to abnormalities in the connection of the pulmonary veins to the heart. In TAPVC, the pulmonary veins are connected to the right atria instead of the left, leading to

oxygenated blood delivery to the right side of the heart (Figure 12). Usually, the condition coexists with ASD to enable blood leakage to the left atria and its circulation throughout the body.

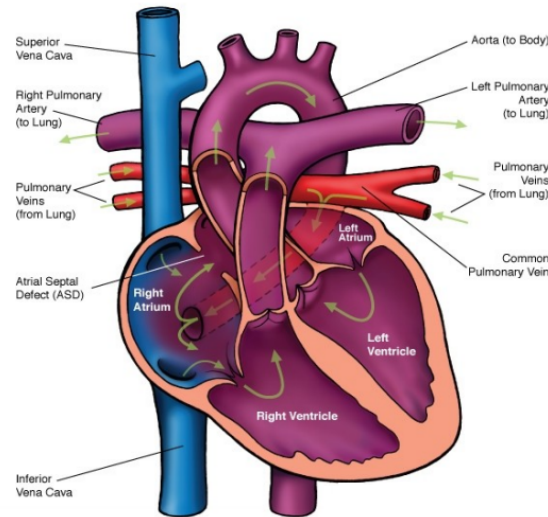


Figure 12: Total Anomalous Partial Venous Connection (TAPVC) representing pulmonary valve attachment to the right atria along with ASD

Tetralogy of Fallot: Tetralogy of Fallot is a combination of four different heart defects present at birth. The defects include a defect in the ventricular septum (VSD), stenotic pulmonary valve with narrowed pulmonary artery, a malformed aortic valve that is present right above the ventricular defect, along with right ventricular hypertrophy (Figure 13). The combination of these conditions creates a critical defect that might lead to reduced circulation of oxygen throughout the body resulting in bluish skin, heart arrhythmias, higher risk of endocarditis, along with delayed growth and development.

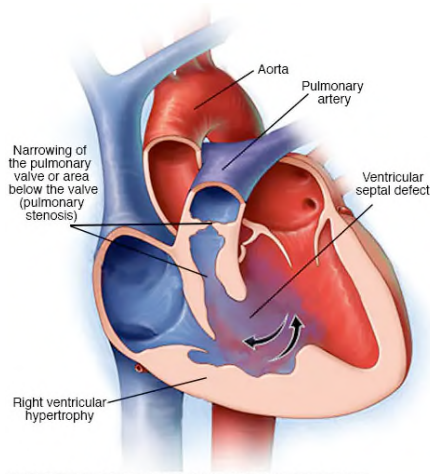


Figure 13: Tetralogy of Fallot condition demonstrating pulmonary stenosis, ventricular hypertrophy and VSD (62)

Dextro-transposition of the great arteries (d-TGA): The main arteries from the heart, the pulmonary artery and the aorta are swapped in their connection to the heart in this condition (Figure 14). This results in low oxygenated blood being circulated through the body via the right atria and the aorta attached to the right ventricle.

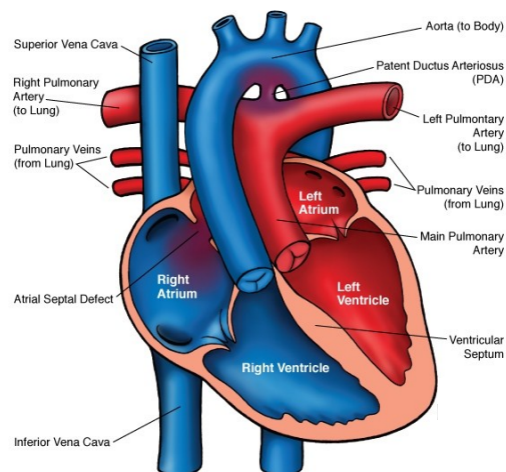


Figure 14: Dextro-transposition of the great arteries with swapping of the connections of the main arteries

Patent ductus arteriosus (PDA): This condition refers to a hole in the aorta. In fetal condition, the blood is oxygenated through the umbilical cord even after skipping the pulmonary circulation (Figure 15.A). However, after birth, the hole within the aorta should close to enable oxygenated blood flow throughout the body.

Truncus arteriosus: The condition refers to the presence of a single large artery instead of two to carry blood throughout the body. Instead of separate pulmonary and aortic valves, only a single truncus valve is present which might be narrowed and leaky, allowing back-flow of blood through the valve (Figure 15.B). This leads to accumulation of more blood in the lungs and less oxygenated blood through the body. The deprivation of oxygenated blood in the body might lead to higher pressure on the heart muscles leading to hypertrophy.

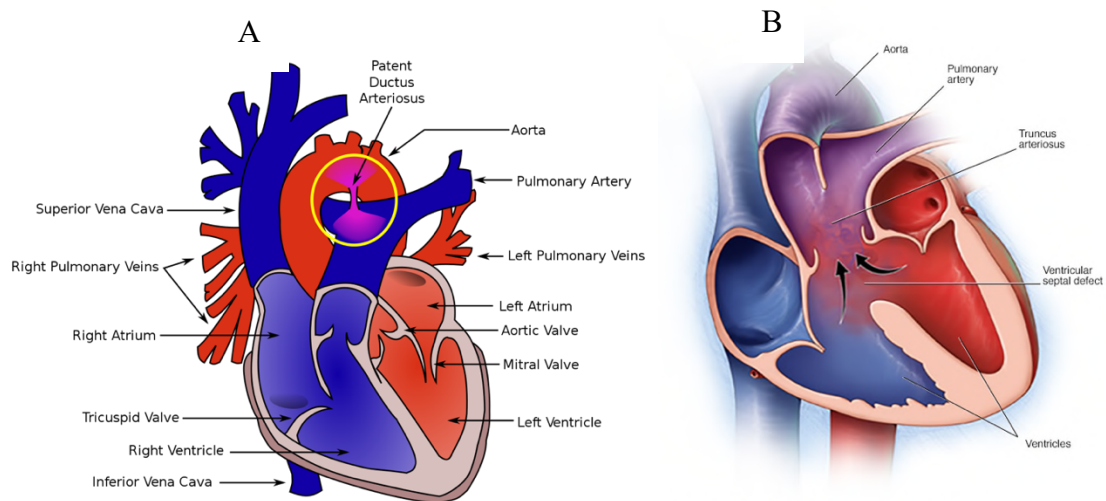


Figure 15: (A) Patent ductus arteriosus representing defect in aorta; (B) truncus arteriosus with merged blood vessels (62)

2.3 Treatment for CHD

Minor defects in the heart, like holes within the septum or small holes in the aortas usually close without any interference. Critical congenital defects, however, require surgical intervention or catheterization to repair the defects.

Cardiac Catheterization

Cardiac catheterization is a procedure in which a small, flexible, hollow tube (a catheter) is inserted through a patient's arm, neck, or groin into the blood vessels and guided into the aorta and the heart with the help of X-ray images (63). Once the catheter is in place, it can be used for the repair of minor defects. Usually, a catheterization procedure is used for the treatment of atrial septal defects and patent ductus arteriosus. It can also be used for reopening stenotic valves or narrowed arteries (62, 69). The earliest use of catheterization for the treatment of congenital defects dates to 1976, when the first catheter device was developed for the repair of atrial septal defects (70). Subsequently, there has been significant development in catheterization repair of heart defects (Figure 16).

Catheterization is a minimally invasive technology; however, in most cases of congenital heart diseases, the deformities might be too complex to repair via catheterization. In such cases, open-heart surgeries are required to repair or replace deformed structures. Out of the new patients diagnosed with CHD each year, an estimated 2,500 patients require the use of non-native conduits and valves to repair structures congenitally absent or hypoplastic.

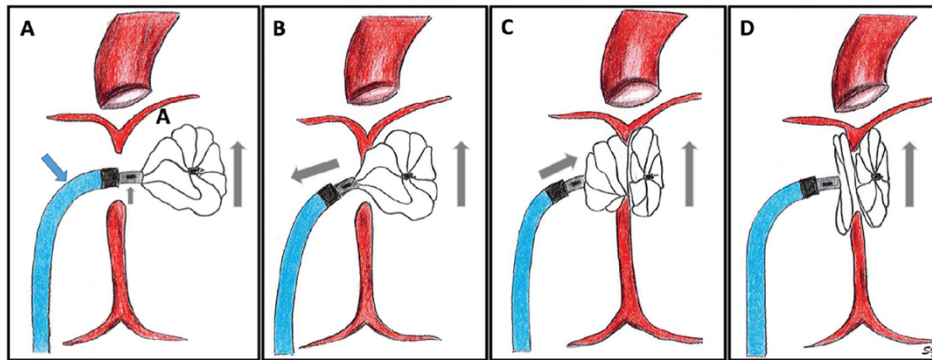


Figure 16: Gore cardioform atrial septal defect occluder deployment using Mullin's sheath (A) Left atrial disc deployment (B) As delivery system is withdrawn, the sheath maintains disc orientation (C) Right atrial disc deployment (D) on either side of septum (71)

Surgical Interventions

Septal defects including ASD, VSD, AVSD, and TAPVC are repaired using pericardium or synthetic patches to prevent leakage of blood through the atria or ventricle walls. Repair patches are also used for conditions of the interrupted aortic arch and double inlet left ventricle. Valve defects like absent pulmonary valve, aortic or pulmonary stenotic valves are usually replaced using homograft, mechanical or bioprosthetic valves. Pulmonary and tricuspid atresia conditions are repaired using valved conduits (72).

CHD conditions of pulmonary atresia with the intact ventricular wall, tricuspid atresia, double inlet ventricle, and hypoplastic left heart syndrome are corrected using the Fontan surgery (Figure 17.A). The procedure aims at directing the systemic flow of venous blood through the lungs without passing through any ventricles (73). Recent modifications in the Fontan operation connect each vena cava to the pulmonary artery using valved conduits, thereby completely bypassing the right atria and ventricle (74, 75).

Rastelli procedure is the standard surgical treatment for correction of ventricular septal defect, dextro-transposition of the arteries, and pulmonary stenosis (Figure 17.B) (76). An intracardiac tunnel is used to connect the left ventricle to the aorta, and the right ventricle is connected to the pulmonary artery using an extracardiac valved conduit (77, 78).

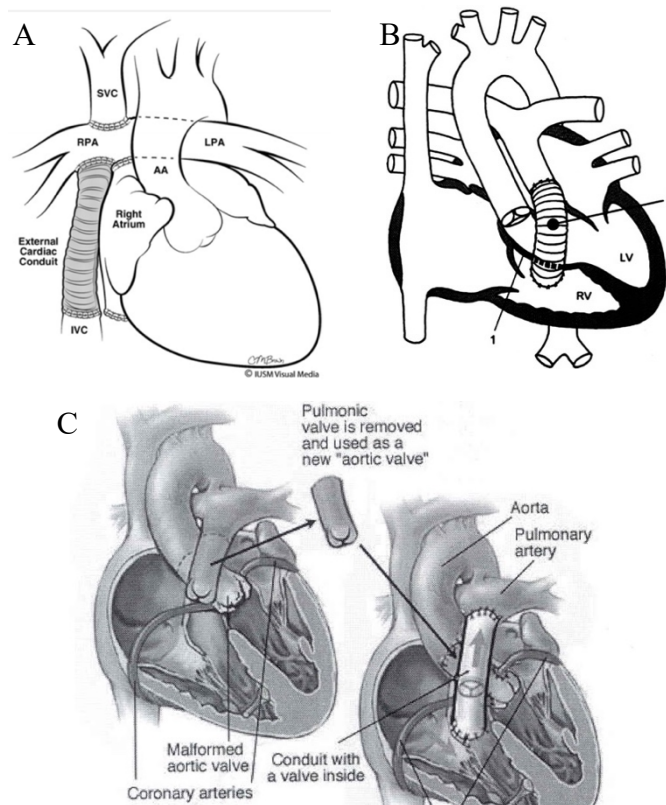
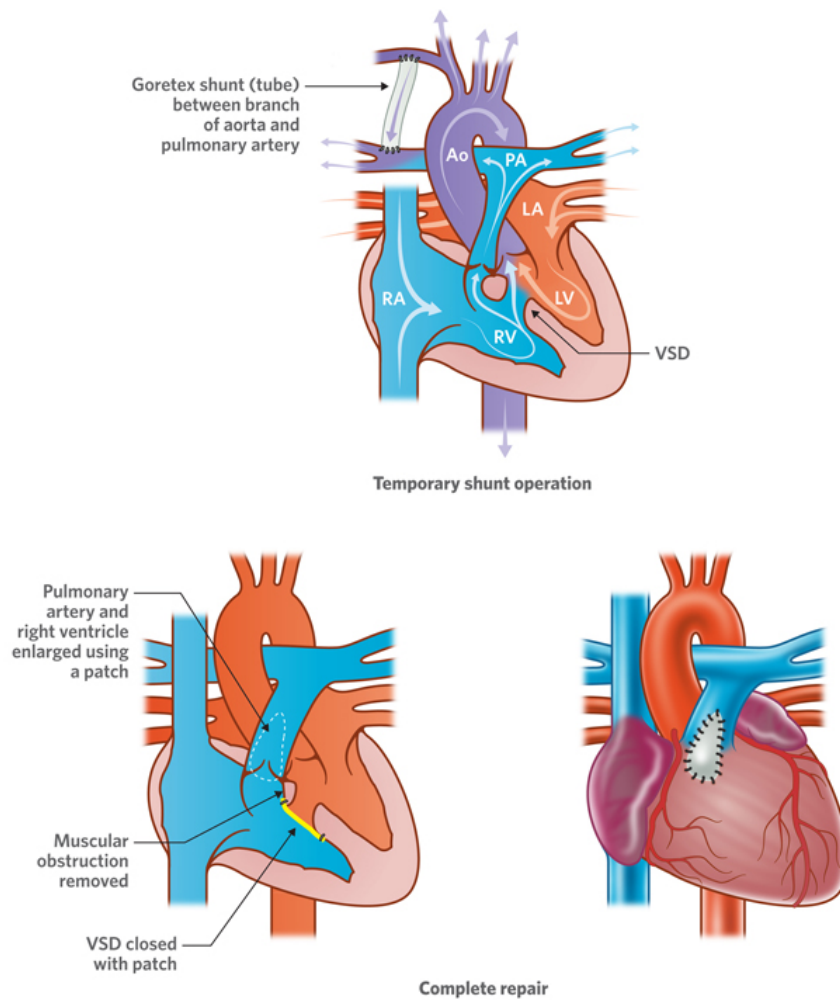


Figure 17: (A) Fontan procedure using an extracardiac conduit to bypass the ventricles (B) Rastelli procedure for correction of d-TGA using 1-an intracardiac tunnel, 2-an extracardiac conduit (C) Ross-Konno procedure for replacement of aortic valve with pulmonary valve, and repair of the pulmonary valve using a valved conduit

Damaged or malformed aortic valves are usually replaced using the Ross procedure. In this procedure, the patient's damaged aortic valve is replaced using their own

pulmonary valve. A donor conduit or valve is then implanted in the place of the pulmonary valve (79, 80). As a modified Ross-Konno procedure, the left ventricular outflow tract is also enlarged to enhance blood flow (Figure 17.C) (81).

Complex Tetralogy of Fallot condition is surgically corrected using an intracardiac repair. The VSD defect is closed using a patch, and the narrowed pulmonary valve is repaired or replaced to increase blood flow to the lungs (Figure 18) (82).



© The Royal Children's Hospital, Melbourne, Australia

Figure 18: Corrective surgery for Tetralogy of Fallot (83)

2.4 Tissue engineering Strategies

Tissue engineering is an interdisciplinary field that applies the principles of life sciences and engineering towards developing biological substitutes that help restore, maintain, or improve tissue functions or whole organs (84, 85). As described by Langer and Vacanti in 1993, tissue engineering principles utilize the body's natural growth and regeneration processes for the repair and replacement of damaged or non-functional tissues with healthy, native tissues. Tissue engineering approaches include utilization of biodegradable polymeric scaffolds, decellularized extracellular matrix, as well as stem cells, and cells harvested from patients.

As discussed previously, repair and replacement of cardiovascular deformities for patients with congenital heart disorders, as well as with acquired cardiovascular defects, requires the use of substitute tissues or grafts. To fabricate tissue replacements, three main approaches are employed for cardiovascular tissue engineering: (1) Direct transplantation of cells; (2) Decellularized or Acellular scaffolds; and (3) Tissue substitutes with cells seeded on scaffolds (9).

For direct transplantation of cells, isolated cells are injected directly into the body, and the differentiation and proliferation of these injected cells help restore the function of the damaged tissue. Several studies have shown the ability of injected cardiomyocytes as well as autologous skeletal myofibroblasts in restoring myocardial contractility and function (86-88). However, with autologous cell injection, several problems exist with cell survival, integration, and differentiation.

The second approach for tissue engineering involves the use of decellularized or acellular scaffolds. Decellularized scaffolds have widely been used in developing valve and conduit replacements for cardiovascular diseases. The advantage of utilizing decellularized scaffolds is the absence of cellular isolation and expansion *in vitro*. This reduces the chances of contamination that might occur from *in-vitro* cell culture. The approach relies on the infiltration of cells from the patient after implantation (89, 90). Although studies with decellularized scaffold implantations have shown cellular repopulation, the complete repopulation of decellularized scaffolds with cells is a challenge (90, 91). Moreover, decellularized scaffolds by themselves, do not have significant resistance to enzymatic degradation, and therefore need to be crosslinked (92). The effect of the crosslinking reagent also needs to be considered for *in vivo* implantation of these scaffolds (93).

The third approach in tissue engineering is the use of tissue constructs with live cells. Autologous cells are isolated from the patient and expanded *in-vitro*. The cells are then seeded on the prepared scaffold allowing cellular growth, differentiation, and formation of a new extracellular matrix. Suitable biochemical and mechanical cues are provided within a bioreactor. The constructs are then implanted back into the patient to improve the functioning of the diseased tissue or organ. The use of cell-seeded tissue constructs has three requirements: cells, scaffolds, and bioreactor. Cells seeded onto scaffolds should be non-immunogenic, therefore autologous cells (94). For cardiovascular tissue, usually smooth muscle cells, myofibroblasts, and endothelial cells from arteries and veins are used (95, 96). When cardiomyocytes have limited growth capability, embryonic

and adult stem cells capable of differentiating into multiple cardiovascular cell types are used (97, 98). Biomaterials or scaffolds are obtained from natural or synthetic sources. Scaffold materials have been discussed in later chapters. Lastly, bioreactors used for tissue engineering applications are aimed at replicating environmental factors seen in human biological systems and to provide mechanical and biochemical stimulation for cell growth and ECM remodeling. (99, 100) Rotating-wall vessel bioreactors, perfusion bioreactors, and pulsatile flow bioreactors have generally been used for cardiovascular applications (101-103). While progress in bioreactor technology is still being made, problems of bioreactor control, sterility, and tailoring device-specific variability still need to be addressed (103).

Biomaterials for Tissue Engineering Scaffolds

Tissue engineering techniques require the use of porous scaffolds serving as a three-dimensional structure for cellular attachment and subsequent remodeling and tissue generation. An ideal tissue-engineered scaffold should be able to resist enzymatic degradation and provide mechanical support to withstand mechanical stresses at

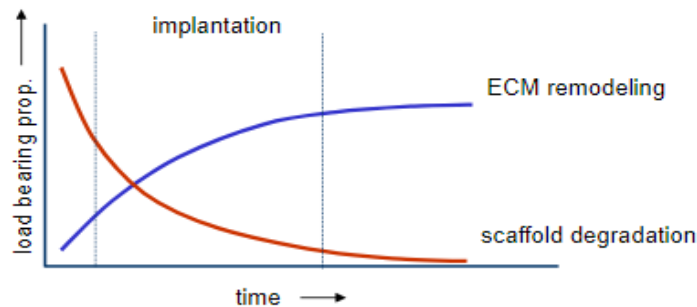


Figure 19: Load bearing properties vs time for tissue engineered scaffolds

implantation. Over time, to restore normal functioning of the tissues, scaffolds should degrade and allow cellular infiltration and remodeling of the implants (Figure 19). Several biomaterials, including synthetic and natural materials, have been utilized for the development of scaffolds for tissue engineering.

Synthetic Scaffolds:

Synthetic scaffolds used for tissue engineering applications can be biodegradable or non-biodegradable. Non-degradable materials like polytetrafluorethylene (PTFE) and Dacron have extensively been used as vascular graft replacements. Owing to the non-biodegradability of these materials, there might be physical barriers to the long term adaptation of these grafts. Additionally, despite their excellent mechanical strength, non-biodegradable scaffolds have been associated with graft kinking, scarring, inflammatory response, and increased risk of infection (104).

Biodegradable synthetic materials like poly(lactic) acid (PLA), poly(glycolic) acid (PGA), and poly (lactic-co-glycolic) acid (PLGA) are approved by the Food and Drug Administration (FDA) for human use (105). The degradation rate of these polymers can be controlled by adjusting the molecular weight, crystallinity, and the ratio of the combining units for these copolymers (106). PLA and PGA polymers have been investigated as biomaterials for heart valves, vascular grafts, and cardiac patches (107-109). Additionally, poly(ϵ -caprolactone) (PCL), polyurethanes (PU), and Polyglycerol sebacate (PGS) have also been used as bioresorbable scaffolds for tissue engineering (108, 110-118). Polyhydroxyalkanoates (PHAs) and poly-4-hydroxybutyrate (P4HB) fabricated scaffolds

tested as heart valve materials have not shown favorable results after 17 weeks of the implant (119). Recently, polycaprolactone-based UPy (supramolecular 2-ureido-4[1H]-pyrimidone) composed scaffolds, have shown promising results as conduit and valve replacement materials (120).

Synthetic scaffolds for tissue engineering might have the advantage of providing adequate mechanical properties, as well as the ability to modulate the polymer properties like degradation time, microstructure, and mechanical properties. However, they might not be an ideal attachment site for cells due to their surface characteristics. Moreover, toxicity and inflammatory responses from the degradation products of biodegradable polymers continue to be of concern (121).

Natural Scaffolds:

An alternative to synthetic scaffolds is the use of naturally derived materials. Chitosan, collagen, alginates, gelatin, Matrigel, and decellularized extracellular matrices have been extensively used for cardiovascular tissue engineering applications.

The first complete tissue-engineered blood vessel conduit, composed of collagen gel, was developed by Weinberg in 1986 (122). Although the scaffold promoted cellular attachment, it had mechanical limitations even after being reinforced with Dacron. Cyclical mechanical conditioning of collagen gel scaffolds resulting in cell-mediated ECM reorganization has significantly improved the strength of collagen scaffolds in later years (123, 124).

Similarly, gelatin scaffolds demonstrate poor mechanical resistance and are often used in combination with synthetic polymers (125-128). Alginates have evolved as attractive hydrogel matrices for cardiovascular tissue engineering. When used in combination with chitosan and alginates generate polyelectrolyte complexes with highly porous structures demonstrating reduced fibrosis, increased vascularization, and integration with host tissue (129-131). However, concerns remain over the long-term stability of alginate hydrogels and their ability to induce homeostasis. Chitosan has similar structures to GAGs in the extracellular matrix and also exhibits antimicrobial properties. However, there might be uncontrolled dissolution with chitosan scaffolds (125, 126, 132).

Decellularization of organs and tissues is another attractive approach to developing scaffolds for cardiovascular tissue engineering. The extracellular matrix is obtained from native tissues (allogenic or xenogeneic sources) by decellularization procedures involving minimal loss and disruption of the matrix and maximum removal of native cells. Due to the removal of native cells, the remaining ECM matrix is resistant to inflammatory responses. Additionally, it has been observed that the spatial orientation of the extracellular fibers affects the ability of cells to self-organize into tissue mimics (121). Since derived from natural functioning tissues, decellularized scaffolds provide the structural and biochemical cues required for cellular organization and proliferation. For cardiovascular approaches, porcine sub intestinal mucosa (SIS), bovine jugular veins, porcine aortic and pulmonary valves, as well as bovine pericardium decellularized scaffolds have been extensively used. However, the decellularization process needs to be standardized and

quality assessment investigated for effective use of decellularized scaffolds for tissue engineering applications (121).

2.5 Conduit Replacement Strategies

As discussed in the surgical treatments of CHD, valved conduits are required for the repair and replacement of deformed structures. The replacement conduits can be obtained from homograft tissues, synthetic or bioprosthetic sources. Homograft pulmonary conduits remain the preferred replacement of pulmonary arteries and veins; however, they might not always be readily available. Currently available synthetic and bioprosthetic conduit replacements come with their own limitations. Table 1 below lists some of the currently available conduit replacement strategies with the outcomes of their clinical trials.

Type	Material	Year Intro- duced	Clinical Trials	Outcomes
Synthetic or Composite	Handmade ePTFE conduits with bulging sinuses and fan- shaped ePTFE valve	2001	Pediatric	Implantation in 1776 patients for RVOT reconstruction; 0.5% conduit related unknown death, 15.9% reintervention, 10.7% required explantation caused by relative stenosis, 0.5% infection (133)
	Woven/knit Dacron tubes	1957	Pediatric	Kinking,, rigid, cannot revive lost biomechanical function

Gelatin/Collagen impregnated Dacron grafts	2002	Pediatric	High incidence of stenosis, fibrotic neointima (8)
Hancock conduit: Dacron conduit with porcine aortic valve	1975	Pediatric, Adults	Implantation in adults showed favorable results, however, not recommended in children because of high profile valve; shows calcification and stenosis after long-term implantation; persistent post-operative inflammation might be an indication of graft failure in later stages (134-137)
Xeltis pulmonary valved conduit: Conduit wall composed of polycaprolactone-based UPy (supramolecular 2-ureido-4[1H]-pyrimidone), valve leaflets made of polycarbonate based	2020	Pediatric	No calcification or stenosis observed after implantation in patients, significant pulmonary regurgitation in a substantial number of patients (138) Modified design of the conduit resulted in reduced onset of early regurgitation (120)

UPy; produced by
electrospinning

Bioprosthesis	Labcor Conduit: stentless porcine tricomposite valve assembled in bovine pericardium tube, crimped to achieve tubular configuration, glutaraldehyde treated (139)	1996	Pediatric	Implantation of Labcor conduits in patients resulted in high incidence of post-operative fever. (140) Furthermore, early, and late mortality rate was 5%, peripheral conduit narrowing due to inflammatory infiltration and pseudo-intimal reaction (141-143)
	Glutaraldehyde treated porcine aortic valves and main pulmonary artery sutured together, coupled with 0.1% partially degraded heparin (144)	1997	Animal studies	5-month implant in sheep did not show any pathological changes, thrombosis, reduced calcification
	Contegra: Bovine jugular vein conduits fixed with glutaraldehyde	2001	Animal studies, Pediatric, Adults	Sheep implants of contegra conduits have showed spots of calcification in jugular vein walls. (145) Implantation of

			conduits in patients have shown development of circumferential stenotic membrane requiring reintervention, as well as a high incidence of development of endocarditis (146-148)
Shelhigh No-react: Glutaraldehyde treated porcine conduit detoxified using heparin process (149)	2001	Pediatric	Implanted conduits resist calcification; however, foreign-body-type reactions result in pseudo-intimal peel formation and early conduit stenosis (150)
Bovine pericardial conduit containing di- epoxy treated porcine aortic root (151)	2001	Pediatric	Calcification after implantation in patients (83.7% and 58.8% after 4 and 6 years of implant), explant obstruction (152)
Di-epoxy treated bovine pericardial valved conduit	2001	Pediatric	Explant obstruction, calcification after implantation (152)
Matrix P plus: decellularized porcine pulmonary valve surrounded by	2007	Pediatric	38% reoperation due to obstructed grafts, stenosis formation observed due to inflammatory infiltration and

three glutaraldehyde fixed equine pericardial patches			severe fibrogenic pseudo intimal reaction (153)
Decellularized and photo-oxidatively crosslinked bovine jugular vein (154)	2008	Animal studies	Implants in dogs showed host cell repopulation of leaflets, little calcification, some endothelialization after 6 months (155)
Decellularized extracellular matrix made from porcine small intestinal submucosa (SIS) (CorMatrix®)	2016	Animal studies	Pulmonary conduit replacement in sheep resulted in 50% morbidity along with leaflet thickening, pulmonary stenosis, and valve regurgitation (156)
Glutaraldehyde treated bovine pericardial valved conduit		Pediatric	Calcification observed after 6 years of implant, conduit thrombosis, endocarditis (152)
Wharton's Jelly (gelatinous inner portion of umbilical cord) mesenchymal stem cell (MSC)	2021	Animal studies	Cellularized conduit implanted in 2 Landrace pigs; 6-month follow up showed patent conduits with no rupture, stenosis, deformation,

seeded decellularized	thrombosis, calcification; re-
porcine SIS	endothelialization observed
	(157)

Table 1: Currently available conduit replacement strategies

Synthetic replacements for valved conduits are often faced with the limitation of rigidity of the tubes, which makes them an unsuitable option for neonates (137). Bioprosthetic conduits, on the other hand, have been found to have the advantage of easy handling (158). However, most bioprosthetic conduits are crosslinked with Glutaraldehyde to protect extracellular matrix degradation. Implantation of Glutaraldehyde treated bioprosthetic conduits have resulted in stenosis, calcification, and ultimately conduit failure (Figure 20).

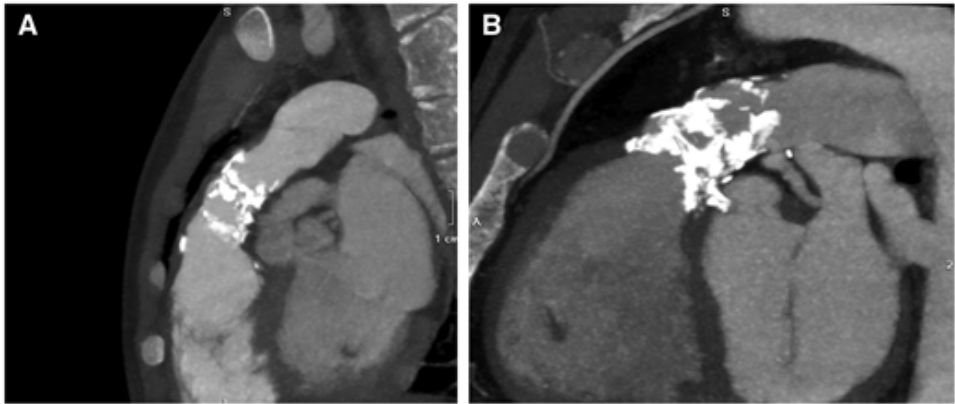


Figure 20: CT at follow-up showing calcification in (A) 16 mm bovine jugular vein treated with glutaraldehyde treated eight years after truncus arteriosus repair; (B) 19 mm bovine pericardial valved conduit treated with glutaraldehyde treated six years after Ross-Konno procedure (159)

A few synthetic and bioprosthetic conduits, like Xeltis (electrospun synthetic conduit) and Wharton's jelly MSC seeded decellularized scaffolds, have shown significant improvements over traditionally available replacements; however, the long-term functioning and patency of these conduits are yet to be assessed (120, 157).

2.6 Valve Replacement Strategies

Valve replacements are required for the treatment of critical congenital conditions like pulmonary stenosis or narrowing of the right ventricle. Valve repair or replacement might also be necessary for conditions of pulmonary atresia or Tetralogy of Fallot conditions (160). Commercially available valve replacements are either mechanical valves, synthetic valves, or bioprosthetic valves.

Mechanical heart valves

Mechanical heart valves have been in use since the 1950s (161). They are primarily composed of silicone rubber, stellite alloys, Teflon, titanium, or pyrolytic carbon (162-176); materials that are highly durable and do not degrade. Figure 21 shows some of the commercially available mechanical heart valve devices.

Mechanical valves, however, have several drawbacks. Risk of valve thrombosis and subsequent systemic embolism in patients with mechanical valve prosthesis requires life-long treatment with anti-coagulant therapies (177, 178). Obstruction in mechanical valves is also relatively frequent and is associated with thrombus and pannus formation

(179, 180). Mechanical erosion due to cavitation has also been observed in several mechanical valves (181).

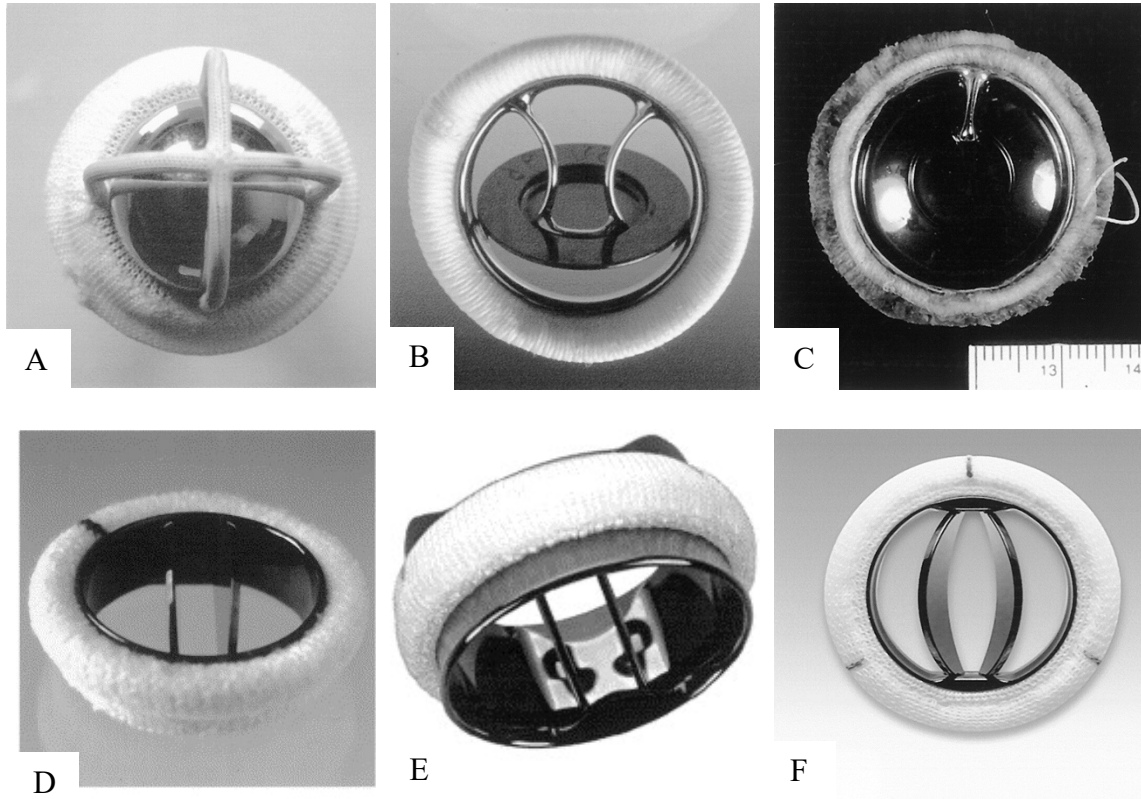


Figure 21: Mechanical heart valves; (A) Starr-Edwards prosthesis, (B) AorTech Ultracor mechanical valve, (C) Bjork-Shiley monostrut valve (D) Edwards bileaflet valve (E) On-X aortic valve (F) Edwards Mira valve (161)

Donor Valves

Donor heart valves or homografts are a more favorable replacement option compared to mechanical valves. Unlike mechanical heart valves, donor heart valves have a lower risk of infection, blood clots, do not require the administration of blood thinners, and demonstrate improved blood flow (182, 183).

With homograft valves, there, however, arises the concern of storage of the valves and the immunogenicity from donor valves. The cellular components in homograft valves have been observed to rapidly decrease along with loss of normal tissue architecture during the first year of implantation (184). Additionally, they suffer from limited durability, resulting in reoperations in young patients (183). Moreover, homograft valve replacement units might not always be easily available or be available in pediatric sizes.

Bioprosthetic heart valves (BHV)

Bioprosthetic or tissue valves are obtained from animal or human tissue sources. Like donor valves, bioprosthetic valves do not require life-long anti-coagulation therapy; however, they are also prone to degradation requiring reoperations and valve replacement (185, 186).

Tissue-engineered valves developed from autologous tissue are often decellularized to remove any donor cell immunogenicity. Efforts have been made to recellularize acellular allograft matrices with primary human endothelial cells (HEC) (187). Allograft valve tissues, however, face the same problem of availability as with homograft vessels.

Another allograft valve reconstruction method was pioneered by Dr. Ozaki. In this model, tissues are harvested from the patient's pericardium, cut into the appropriate sizes, treated with glutaraldehyde at room temperature for a few minutes, and sutured in place of the defective valve (Figure 22) (188). This procedure has shown optimum short-term results in young patients; however, long-term results remain to be seen (189-191).

Additionally, since the tissues are glutaraldehyde fixed, surgical annular enlargement is required at a later time for pediatric patients as the patient grows (192).

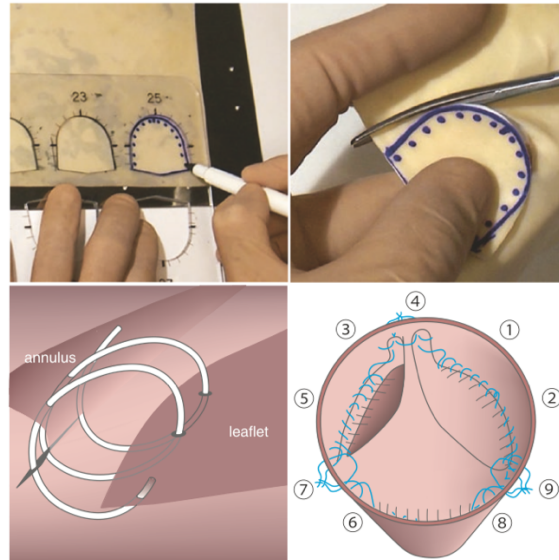


Figure 22: Autologous pericardial tissue valve reconstruction using Ozaki procedure (193)

Xenograft bioprosthetic valves are derived primarily from bovine pericardium or porcine aortic valves. Pericardium valves are developed by mimicking the native heart valve as much as possible by designing crosslinked animal-derived tissue into a tri-leaflet structure around a polymeric or metallic stent (194). The advantages of pericardium are its ease of handling and the ease of pericardium sheets to be cut into desired sizes. However, pericardium tissue lacks the intrinsic tri-layer structure found in heart valves. Moreover, glutaraldehyde is the most commonly used approved crosslinker, and glutaraldehyde treated tissues prevent cellular infiltration and growth, and remodeling of the valves (195).

Porcine aortic valves much closely resemble the native tri-layer structure of valves. Porcine valves, however, have a muscle shelf supporting the right coronary cusp, and they also possess less fibrous continuity between the mitral and aortic valves. The presence of

a shelf within the valve might lead to additional risk of calcification and reduced valve motion (10, 196-198). To overcome these challenges, optimal leaflets are individually selected and matched for the appropriate size (194).

Bioprosthetic heart valves can also be stented or non-stented. Stented valves have a stent made out of artificial materials, either metallic or plastic, which are covered with a fabric sewing ring to provide a frame for the valves. Early stented valves demonstrated high failure rates due to tearing at the commissures. Modern approaches to stented valves utilize flexible polymers, increasing the ease of valve implantation procedures. Stented valves are also widely used for percutaneous intracatheter delivery strategies (199-205). Stentless valves, on the other hand, do not have any struts to support the valve leaflets. The absence of struts allows for a greater effective orifice area (206). The increased size also allows for a better approximation of the patient's normal valve. Although stentless valves rely greatly on surgeons' expertise, they have been shown to demonstrate better hemodynamics, lesser obstruction to blood flow, reduced risk of endocarditis, and increased durability compared to stented valves (207-213).

Several bioprosthetic valves are commercially produced for pulmonary and aortic valve replacements. One of the first valves to be used in clinical applications was the SynerGraft valve made of decellularized porcine aortic valve (214, 215). It resulted in rapid degradation and structural failure after implantation in patients, along with extensive calcification and inflammatory responses (216). Subsequently, improvements have been made in the crosslinking of heart valves, and presently, the most commonly used valves are produced by Medtronic, Edwards Lifesciences, and St Jude Medical (217). Medtronic

valves are fabricated from a line of porcine aortic valve leaflets crosslinked with glutaraldehyde and treated with anti-calcification agent AOATM (alpha-oleic acid) as well as proprietary physiological fixation (218). St. Jude Medical Inc and Edwards Lifesciences utilize bovine pericardium tissues wrapped in proprietary material around proprietary stents and crosslinked with glutaraldehyde or formaldehyde to mimic native aortic valves (194, 219, 220). However, as discussed in previous sections, these fixed valves are not composed of 'living tissue' and do not have the capacity to grow with the patients, therefore making them unsuitable for pediatric valve replacements.

2.7 Decellularization strategies

Various approaches have been employed to decellularize native tissues producing decellularized scaffolds composed of extracellular matrix components without any native cells. Although there is no universal consensus for adequate decellularization, the following three criteria generally apply to decellularization of tissues: (1) < 50 ng DNA/mg dry weight of decellularized tissue; (2) DNA fragments < 200 base pairs in length; (3) No visible nuclear material from Hematoxylin and Eosin (H&E) or DAPI staining (221-224). Decellularization methods can be broadly classified as physical, enzymatic, and chemical, as well as a combination of two or more of these.

Physical Decellularization

Physical approaches for decellularization involve the mechanical separation of a cellular layer from the underlying extracellular matrix (223). Physical characteristics like

temperature, force, and pressure are modulated to facilitate the removal of cells from the matrix (225).

Freeze-thaw cycles, sonication, pressure gradients, and pressurization techniques aim at disrupting the cell membrane and causing cell lysis (226-233). Scraping of cells is also occasionally used to mechanically remove cells from the ECM (234). All these approaches, however, have a very high potential of disrupting the ECM structure within the native tissue. Electroporation has been used to decellularize tissues by the formation of micropores in cell membranes leading to cell lysis. However, It is more a suitable technique for small size tissues (235, 236). Moreover, solvents used for electroporation might be toxic. Perfusion, capable of removing cells as well as debris from the ECM is an effective technique with less damage; however, it requires the presence of vasculature within the tissue (233, 237, 238). Tissues without innate vasculature can be decellularized physically by immersion and agitation into decellularization solution. It provides a more homogenous exposure to detergents than static decellularization without significantly altering the ECM structure. However, compared to perfusion, there might be more damage to tissue because of the limited diffusion of chemicals by agitation (239-241).

Although physical methods of decellularization are an essential step to the removal of cells and debris, they need to be optimized to produce minimal damage to the native ECM of the tissues.

Enzymatic Decellularization

Enzymes specifically target cellular components or ECM structures without disrupting the whole tissue. Nuclease, trypsin, lipase, dispase, and phospholipase are commonly used enzymes for the effective removal of cells and unwanted ECM constituents.

DNase and RNase are routinely used in decellularization procedures to remove any remaining nuclear material. The treatment is usually done after detergent treatment to allow infiltration of the enzyme within the tissue. Although nucleases selectively remove nuclear components, treatment for a very long period might negatively affect tissue matrix components and mechanical stability (242). Additionally, proper washing of decellularized tissues after nuclease treatment is required since incomplete washing and remaining nuclease within the scaffold might invoke immunogenic response as well as inhibit the recellularization of scaffolds (243).

Another commonly used enzyme in decellularization procedures is trypsin. Trypsin functions by cleaving peptide bonds on the carboxyl-side of lysine and arginine, leading to the release of cells from the extracellular matrix (92). Typically, cardiovascular tissues are treated with 0.1% trypsin for 24-96 hours after nuclease treatments. Decellularization protocols using trypsin have observed gross maintenance of the ECM components, as well as limited toxicity from the enzyme (244). Some studies have, however, also found that trypsin does not effectively remove all resident cells from native tissues (245). Remains of native cells might cause immunogenic response as well as calcification after implantation. Therefore, longer incubation times might be required. However, longer incubations might

also lead to the destruction of elastin and collagen within the tissue matrix. The time and concentration of trypsin treatment, therefore, needs to be optimized for the decellularization protocol.

Chemical Decellularization

Detergents, acids, bases, hypertonic, and hypotonic solutions are utilized as chemical reagents for decellularization.

Ionic detergents like SDS and SDC solubilize cytoplasmic membranes of cells and nucleus as well as disassociate DNA from proteins. (246-248) Triton X-100/200, a non-ionic detergent, is frequently used in decellularization procedures. Triton also solubilizes cell membranes and dissociates DNA from proteins without disrupting the interaction between proteins (249). Zwitterionic detergents like CHAPS, SB-10, and SB-16 also function similarly by solubilizing cell membranes and disrupting DNA-protein, lipid-protein, and lipid-lipid interactions (250-252). All detergent treatments might alter ECM structures and reduce the GAG and fibronectin/ laminin content within ECM. However, a mild combination of the detergents within the decellularization solution has been shown to maintain the ECM structures within decellularized valves (253).

Acids and bases help catalyze the degradation of biomolecules, cellular and nuclear components. Peracetic acid (PAA), hydrochloric acid, ammonium hydroxide, sodium hydroxide, and sodium sulfide have been utilized in decellularization procedures (254, 255). Similar to detergents, acids and bases can also lead to ECM alteration and removal of components of ECM, and therefore need to be used in mild concentrations. Peracetic

acid at 0.1% concentration has been shown to have minimal effects on ECM structure (256).

Hypotonic and hypertonic solutions disrupt cell membranes due to differences in osmotic pressures and cause cell lysis. Protein removal has been observed to be more effective in hypertonic solutions, while hypotonic solutions effectively remove DNA (257). Additionally, these solutions are removed by washing and therefore cause very little toxicity. They also maintain ECM structures relatively well compared to other chemical treatments. Hypotonic/ hypertonic treatments might however not be very effective by themselves and are routinely used in combination with other detergents or enzymes (255).

Other Decellularization Approaches

In addition to the more conventional methods of decellularization as mentioned above as well as a combination of these procedures, some groups have also developed novel decellularization procedures. Casali *et al.* has developed a supercritical CO₂-based decellularization procedure in the porcine aorta that maintains the scaffold hydration and mechanical properties while effectively removing most cellular components (258). Vacuum-assisted decellularization, achieved by using negative pressure to accelerate the decellularization procedure has been developed by Wang *et al* (259, 260). This approach, while being highly effective in combination with physical, chemical, and enzymatic treatments, might lead to ECM damage due to prolonged exposure to vacuum. Apoptosis inducing agents like camptothecin, and rotenone has been pioneered for decellularization

of nerve and lung tissues (261, 262). However, further research needs to be conducted to apply these novel decellularization methods extensively.

2.8 Sterilization and crosslinking of decellularized scaffolds

Sterilization

Scaffolds, after decellularization need to be sterilized to remove micro-organisms from the matrix. However, the sterilization technique should not alter the physical characteristics of the scaffold or induce toxicity (92).

One of the most commonly used sterilization techniques is irradiation by gamma rays (263). The process effectively removes micro-organisms but might alter the physical, chemical, and biocompatibility properties of the ECM (264). Ethylene oxide (EO) sterilization is another method that alkylates nuclear acids, rendering the macromolecules inactive (265). EO treatment might lead to the accumulation of toxic residues within the scaffold (266). Antibiotic treatment of the decellularized scaffold is capable of inhibiting bacterial growth but does not effectively hinder the growth of virus and spores (267, 268).

Additionally, treatment with Peracetic acid is another method for sterilization of decellularized scaffolds. The decomposition products from peracetic acid treatment are non-toxic, but it might alter the physical characteristics of the scaffold (269, 270). This necessitates combining two or more sterilization techniques in mild concentrations to develop a balance between effective removal of micro-organisms and maintenance of the physical and chemical properties of the scaffold.

Crosslinking or stabilization of scaffolds

Decellularized scaffolds are susceptible to enzymatic degradation (14). To prevent their rapid degradation on implantation, extracellular components within the scaffolds need to be either chemically crosslinked or stabilized. Crosslinking also helps in improving or maintaining the mechanical strength of the scaffolds. Crosslinking strategies of decellularized scaffolds can be broadly divided into physical, chemical, and natural crosslinking.

Glutaraldehyde is the most commonly used crosslinker for scaffolds used in tissue-engineering applications. Glutaraldehyde significantly improves the mechanical strength of scaffolds; however, it has been shown to crosslink only the collagen within the ECM. Elastic fibers still degrade rapidly after glutaraldehyde crosslinking (Figure 23) (15).

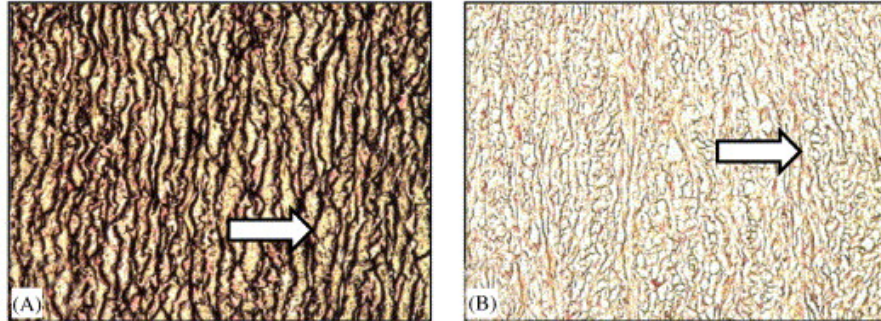


Figure 23: Histology of glutaraldehyde fixed aortic samples (A) before and (B) after elastase treatment showing loss of elastin. (Adapted from (15))

Additionally, Glutaraldehyde crosslinking has been associated with toxicity and calcification after scaffold implantation, leading to the final failure of the implant. (271) Glutaraldehyde crosslinked bioprosthetic heart valves have been severely associated with calcification. Devitalization and cellular alterations within heart valves result in the

formation of debris within the cells, which act as nucleation sites for calcification. In normal cells, low levels of intracellular calcium are maintained. However, after cell death, high concentrations of calcium can infiltrate cells, react with remaining phosphorous within tissues, and can ultimately lead to calcification. Anti-calcification strategies have been developed to detoxify the adverse effects of glutaraldehyde, as well as improve cellular adhesion and proliferation on these scaffolds. Pre-treatment with citric acid and amino acid solutions has been shown to improve cell attachment to glutaraldehyde treated tissues by removing free aldehyde groups (272, 273). Ethanol and its solutions have also been used to remove phospholipids and cholesterol molecules from scaffolds, which play a vital role in the induction of calcification (274, 275).

Another crosslinking agent commonly used is 1-Ethyl-3-(3-dimethyl aminopropyl)-carbodiimide or EDC. EDC crosslinking has been shown to protect collagen from enzymatic degradation; however, it has not been able to inhibit calcification within scaffolds, rendering them ineffective for cardiovascular uses (276, 277). Biological heart valves and vascular grafts have also been crosslinked with epoxy compounds, which interact with amino, carboxyl, and hydroxyl functional groups. This crosslinking approach creates linear crosslinking, and collagen is not effectively protected from enzymatic degradation. Moreover, epoxy crosslinking compounds have also been shown to exhibit toxicity causing immune responses similar to calcification in Glutaraldehyde fixed tissues (278).

Apart from chemical compounds, some natural substances like genipin, nordihydrogualeic acid (NDGA), tannic acid and procyanidins have been used as

crosslinking agents for tissue-engineered cardiovascular scaffolds. Natural crosslinkers are considered superior to chemical crosslinking owing to their non-cytotoxic and anti-calcification properties. Genipin crosslinked ECM scaffolds have been shown to exhibit a lower inflammatory response compared to glutaraldehyde, and there is no loss of the crosslinker during the preservation process (279-281). NDGA, a polyphenolic compound, crosslinks collagen with ECM rendering increased tensile strength to scaffolds. However, they are cytotoxic above 100 μ M concentrations (282).

Polyphenols like tannic acid and its derivatives, as well as procyanidins, a flavonoid have shown the ability to crosslink elastin along with collagen within extracellular matrices, thereby imparting superior resistance to cardiovascular scaffolds compared to traditional techniques (16, 283). These scaffolds have also been shown to resist calcification as well as increased biocompatibility in *in vitro* and *in vivo* experiments (284, 285). Therefore, natural crosslinking agents might be an excellent alternative to traditionally used chemical crosslinking and help alleviate some of the adverse effects of these crosslinking approaches.

Penta galloyl glucose (PGG) is a derivative of Tannic Acid that has previously shown to reduce biodegradation and calcification in Tissue Engineered Vascular Grafts (TEVG) (286). The structure of PGG is composed of a hydrophobic core with numerous external phenolic groups (Figure 24). On account of the structure of PGG, it is capable of binding to hydrophobic regions, as well as forming several hydrogen bonds. PGG shows a particularly high affinity for proline, which is present in abundance within collagen and elastin within the extracellular matrix (287, 288).

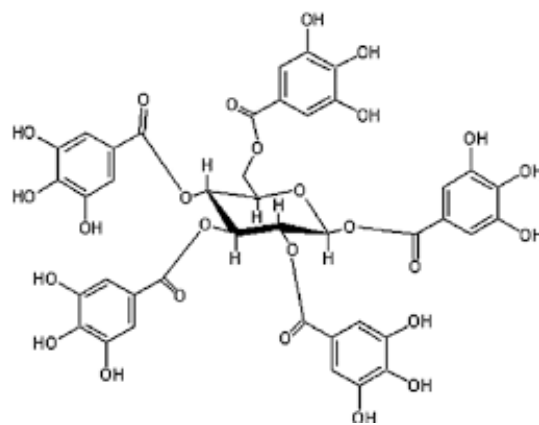
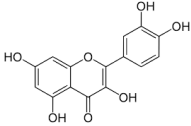
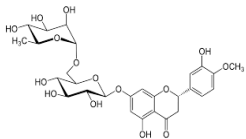


Figure 24: Structure of Penta-galloyl Glucose (PGG), a derivative of Tannic Acid

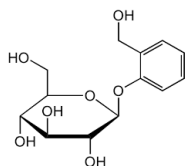
Similar to tannic acid, PGG possesses the ability to establish strong cohesive bonds between the structural proteins and protect them from enzymatic degradation (289). Moreover, it has been found to exhibit lower toxicity than Tannic acid at the local and systemic levels (16). , The addition of PGG to aneurysmal cell cultures, has been shown to improve the elastogenesis process within the cells. Local and systemic delivery of PGG has also been shown to reverse abdominal aortic aneurysms in rodents (290, 291). Additionally, PGG is a potent anti-oxidant, and has been shown to possess anti-cancer, anti-microbial, and anti-inflammatory activities (292). All of these functionalities make PGG an ideal crosslinker for cardiovascular tissue engineering applications.

In addition to PGG, polyphenols Quercetin, Hesperidin, D-Salicin, and All-trans Retinoic Acid have been shown to interact and modulate extracellular matrix components in cell cultures (Table 2). Some of these properties of polyphenols are similar to those of PGG, and therefore these other polyphenols might have the potential to interact and stabilize ECM components in scaffolds.

Compound	Advantages	Reference
<p data-bbox="337 352 464 384">Quercetin</p> 	<p data-bbox="578 352 951 604">Prevents in-vitro enzymatic degradation in porcine heart valves at concentrations of 1, 2.5, 5 and 10 mg ml</p> <p data-bbox="578 699 881 804">Interacts with bovine γ-globulin</p> <p data-bbox="578 898 976 1077">Stimulates collagen and elastin expression in human dermal fibroblasts</p> <p data-bbox="578 1171 954 1276">Decreases activity of MMP-2 in renovascular hypertension</p>	<p data-bbox="1036 426 1369 531">Wanyin J <i>et al.</i>, Acta Biomaterialia, 2010 (293)</p> <p data-bbox="1036 667 1369 846">Jianbo X <i>et al.</i>, Molecular Nutrition Food research, January 2011 (294)</p> <p data-bbox="1036 972 1369 1014">Edwin D, Cosmetics, 2021</p> <p data-bbox="1036 1140 1369 1318">Sherliane CP <i>et al.</i>, Atherosclerosis, 2018 (295)</p>
<p data-bbox="329 1381 469 1413">Hesperidin</p> 	<p data-bbox="578 1413 881 1518">Interacts with bovine γ-globulin</p> <p data-bbox="578 1654 902 1759">Antioxidant and collagen crosslinking</p>	<p data-bbox="1036 1381 1369 1560">Jianbo X <i>et al.</i>, Molecular Nutrition Food research, January 2011 (294)</p> <p data-bbox="1036 1623 1369 1793">Franziska B <i>et al.</i>, Materials, December 2020 (296)</p>

Promotes Osteogenesis and modulated collagen matrix organization and mineralization Patricia AM et al., Int Journal of Molecular Science, 2021 (297)

D-Salicin



Interacts with bovine γ -globulin Jianbo X *et al.*, Molecular Nutrition Food research, 2011 (294)

Influences rheological and film forming properties of collagen Katarzyna A et al., Molecules, 2021 (298)

Inhibits AGE-induced degradation of type ii collagen Feng G et al., Artificial cells, Nanomedicine, and Biotechnology, 2019 (299)

Protects retinal endothelial cells from IL-1 β -induced endothelial inflammatory response Yu S. et al., Artificial cells, Nanomedicine, and Biotechnology, 2019 (300)

Induces dermal elastin synthesis and elastin fiber formation Rosetti D *et al.*, International Journal of Cosmetic Science, 2010 (301)

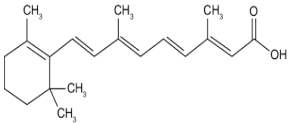
<p>All-trans Retinoic Acid</p> 	<p>Remodels extracellular matrix and suppresses laminin enhanced contractility of human retinal pigment epithelial cells</p> <p>Regulates TGF-β1-induced extracellular matrix production in nasal polyp-derived fibroblasts</p> <p>Regulates proliferation, migration, differentiation, and extracellular matrix turnover of human arterial smooth muscle cells</p>	<p>Yo-Chen C et al., Exp Eye Res, 2008 (302)</p> <p>Su-Jong K et al., Int forum allergy rhinol, 2020 (303)</p> <p>Dorothea IA et al., Cardiovascular Research, 2001 (304)</p>
--	---	---

Table 2: Properties of Quercetin, Hesperidin, D-Salicin and All-trans Retinoic Acid

2.9 Diabetes and wound healing

Diabetes is a chronic condition that develops due to insufficient production of insulin by the pancreas or the ineffectiveness of the body to utilize the insulin produced (305). Insulin is a hormone that regulates the metabolism of carbohydrates, fats, and proteins within the body by promoting glucose absorption from blood into fat, liver, and

skeletal muscle cells (306). Elevated levels of glucose, or hyperglycemia, is an effect of uncontrolled diabetes, resulting in damage to the body's systems, especially the vascular and nervous systems (305). Diabetes, in a combination of higher-than-optimal blood glucose conditions within the cardiovascular disease, chronic kidney conditions, and tuberculosis, leads to approximately 2.2 million deaths worldwide (307).

Diabetes incidence can be broadly classified into two groups. Type I diabetes, or childhood-onset diabetes, results from insufficient production of insulin in the pancreas. There is very little information on the cause and prevention of type I diabetes. Type II diabetes, on the other hand, also known as adult-onset diabetes, is a result of the ineffective use of insulin by the body (308). Type II is the most prevalent form of diabetes, accounting for almost 90-95% of all diabetes cases in the United States (309). Type II diabetes develops due to several factors, including overweight and obesity, physical inactivity, insulin resistance, and genetic predisposition (310). In the context of congenital heart disorders discussed previously in this chapter, it is also important to observe, pregnancies with type I and type II diabetes are at a higher potential risk of development of CHD conditions in the babies (311).

Among many complications induced by elevated blood sugar levels, the altered metabolism in diabetic conditions leads to impaired wound healing (312). The normal wound healing process progresses through stages of inflammation, proliferation, and remodeling (313, 314). The stages of normal wound healing along with the predominant cell types and the cellular events in each stage have been demonstrated in Figure 25 below (315)

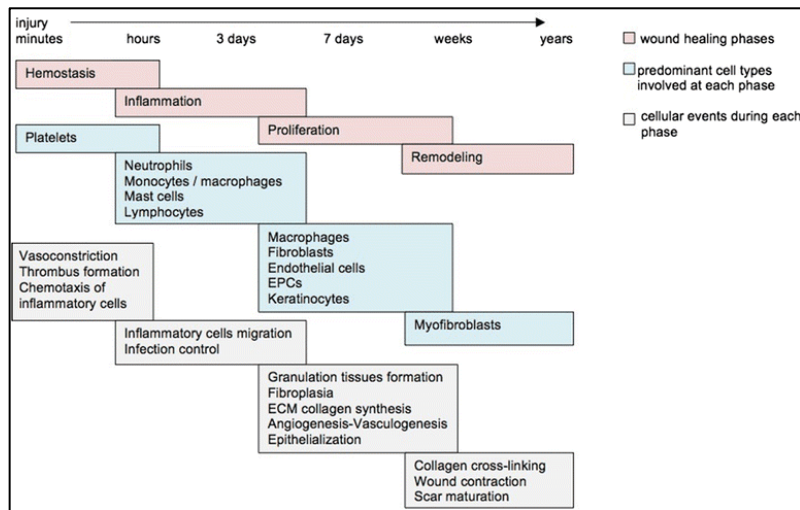


Figure 25: Stages of normal wound healing; EPCs: Endothelial progenitor cells, (315)

Impaired wound healing in diabetic conditions is manifold. Hyperglycemia leads to increased protein kinase C (PKC) activity, contributing to vascular complications (316). It also leads to non-enzymatic glycation of collagen and the formation of advanced glycosylation end products (AGEs), leading to dysfunctional endothelial cells and extracellular matrix along with reduced solubility of the extracellular matrix (Figure 26) (317-320).

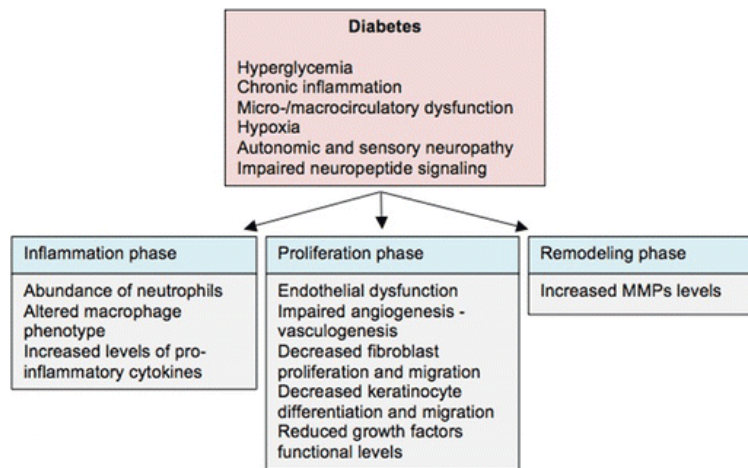


Figure 26: Effect of diabetes on wound healing; MMPs: Matrix metalloproteinases (315)

Chronic inflammation is caused by an increase in M1 macrophages compared to M2 macrophages (321). Additionally, an increase in pro-inflammatory cytokines like interleukin-1 (IL-1), interleukin-2 (IL-2), and tumor necrosis factor-alpha (TNF-alpha) leads to a prolonged inflammatory phase (322). Fibroblasts in diabetic wounds also display decreased proliferation, decreased migration, and increased apoptosis (323). Decreased keratinocyte differentiation and migration also leads to slower wound repair (324). Additionally, there is an increase in the levels of MMPs (matrix metalloproteinase) and a decrease in TIMPs (Tissue inhibitors of MMPs) (325-328).

Furthermore, the phagocytic and bactericidal activities of polymorphonuclear leukocytes in diabetic patients have been found to be impaired compared to patients with normal blood glucose levels (329, 330). These changes in metabolism and cellular dysfunction along with granulocyte impairment leads to slower wound healing in diabetic patients along with an increased risk of infection.

Scaffolds for diabetic conditions

As discussed previously, diabetic conditions lead to impaired wound healing due to imbalance of protease, the presence of reactive oxygen species, degraded essential growth factors, and impaired angiogenesis. Biomaterial scaffolds providing matrices for cellular attachment and proliferation are widely used in such conditions to facilitate wound healing and tissue regeneration. Several tissue-derived, hydrogel-based, and controlled release biomaterials have been used for wound repair in diabetic conditions.

Tissue-based scaffolds mimic the extracellular matrix of natural tissues and provide suitable microenvironments for cells. Allografts from cadavers, placental tissue, and porcine sub-intestinal mucosa have been used as tissue sources for wound healing scaffolds (331-334). Living skin substitutes seeded with allogenic fibroblasts or keratinocytes have been used for chronic skin wound healing (335, 336). Such substitutes are composed of natural (collagen) or synthetic (polyglactin scaffolds) components (337). Acellular scaffolds have been composed of porcine sub intestinal mucosa, decellularized human dermis, crosslinked bovine collagen, composites of collagen and cellulose as well as calcium alginate fibers (337-339). Additionally, biopolymeric scaffolds derived from N-acetyl glucosamine, hyaluronic acid, and crosslinked dextran and PEG acrylates have been reported to interact with fibroblast and endothelial cell infiltration stimulating chronic wound healing (340-342). Hydrogels can be engineered to mimic extracellular matrices of soft tissue, thereby providing a defined ECM for cellular infiltration, proliferation, and vascularization (343). L-Glutamine loaded Chitosan hydrogels have been shown to enhance collagen deposition and angiogenesis in diabetic wounds (344).

In addition to tissue supports, inductive signals like Vascular Endothelial Growth Factors (VEGF) and basic fibroblast growth factors (bFGF) have been shown to promote angiogenesis in wounds. Since these molecules degrade very rapidly in diabetic wound conditions, controlled release mechanisms have been fabricated to provide efficient concentrations of these molecules at the affected area (345). SDF 1-Alpha activated collagen scaffolds have been shown to restore pro-angiogenic wound healing in human diabetic adipose-derived stem cells (346). Nanoparticles, vectors (DNA, plasmid, virus),

as well as preloaded encapsulation within hydrogels have been used for controlled delivery of molecules at the wound site (347-349).

Animal models for Type II Diabetes

Type II diabetes is characterized by insulin resistance and increased apoptosis as well as decreased replication of the beta cells (350, 351). Animal models to study type II diabetes are therefore aimed towards the development of these physiological conditions to effectively analyze the effects of the condition. Due to species-specific differences, there are no perfect animal models for diabetes; however, several approaches have been investigated.

The development of type II diabetes in animal models has two main approaches: obesity-induced diabetes and beta-cell inadequacy induced diabetes. Since most cases of onset of type II diabetes in humans are associated with obesity, related animal models are widely used in diabetes research (352).

Obesity-induced type II diabetes can again be divided into two main categories: genetically obese animals and high fat-induced obesity. Depending on the genetic mutation or stress induction, different animal models mimic different physiological features of diabetes in humans. Animal models of type II diabetes have been developed in rats, mice, hamsters, pigs, and some invertebrates to study the pathophysiology and treatment of diabetes.

Mice and rat models of diabetes are the most common because of the ease of handling of these animals. Genetically developed diabetic rodent models include the

AKITA mice, GK Rats, Obese hypersensitive rats (OHS), Zucker diabetic fatty rats, and diabetic mice with mutations in either the leptin gene (ob/ob) or in the leptin receptor (db/db). Spontaneous auto-immune rodent models include NOD-mouse, diabetes-prone BB rats, KDP rat, LETL rat, and LEW-iddm rat. Most of these auto-immune disorder models more closely represent Type 1 diabetes (353, 354).

Chemically induced diabetic models in rats depend on the induction of diabetes using Alloxan or Streptozotocin. Alloxan is an analog of glucose that is cytotoxic and inhibits glucose-induced insulin emission as well as induces the formation of reactive oxygen species. About 20 -200 mg/kg doses of alloxan are used intravenously in rats for induction of diabetes. Streptozotocin (STZ) is also a toxic analog of glucose that targets pancreatic β -cells. In diabetic models, STZ can be administered in high doses or in multiple low doses. In high doses, it destroys pancreatic β -cells, while low doses induce inflammatory and immune responses similar to autoimmune diabetes (354, 355). Single doses of STZ produce characteristics similar to Type 1 diabetes, whereas low doses more closely resemble type 2 diabetes.

For wound healing applications, diabetic models of rats are extensively used. The High Fat Diet-STZ model for induction of type II diabetes in SD rats serve as an excellent model for wound healing applications. High-fat diet (HFD) in rats induces insulin resistance, whereas STZ injections lead to dysfunction in β -cells. This model, therefore, mimics the type 2 diabetes development in humans and can be ideal for studying effects (356, 357)

CHAPTER THREE

PROJECT RATIONALE AND SPECIFIC AIMS

As discussed previously, patients with congenital heart diseases have congenital or hypoplastic structures within their heart and great vessels. While many of these defects are small and can repair without any intervention, critical defects require surgical interventions to repair or replace the defect and restore normal blood flow. Valve, conduit, and patch replacements are required for absent pulmonary valves, aortic stenosis, double outlet right ventricle, extracardiac conduit, and pulmonary valve replacement in Tetralogy of Fallot conditions of congenital defects (358). Homograft replacements are the most desired but might not always be easily available. Synthetic or bio-prosthetic replacement options, on the other hand, have the advantage of being easily produced on a large scale. For conduit replacement, the more commonly used materials are Dacron, Gore-Tex, or Glutaraldehyde (Glut) fixed heterograft jugular veins (359) (360). Unfortunately, with most of the available materials, the conduits become stenotic over time, requiring their replacement. This results in multiple interventions ranging from catheterization with stents to replacement operations.

Current valve replacement strategies involve the use of mechanical or bioprosthetic valves. Mechanical valves are prone to thrombus formation and require the administration of life-long anticoagulants. Available bioprosthetic valves, on the other hand, eventually wear out. Valve repair is preferred over valve replacement, whenever possible, because of the lower incidence of infection, thrombosis, and reoperations with repair. One repair

procedure pioneered by Dr. Ozaki utilizes autologous pericardium tissue from the patient; pericardium is harvested from the patient, crosslinked with glutaraldehyde for a few minutes, cut into suitable size, and the patient's valve is repaired using sutures. (361) This procedure has shown acceptable short-term results in young patients with small aortic annuli. However, surgical annular enlargement might be required as the patients grow. (362) Moreover, the glutaraldehyde crosslinked pericardium tissue lacks the tri-layer structure of native valve leaflets and is incapable of growth or repair.

An ideal replacement graft for pediatric replacement should withstand the mechanical forces at the time of implantation as well as display capacity for remodeling to be efficient in the long term. Several approaches have been utilized in the past few decades to develop implants with growth potential, but with few successes. This research aims to develop superior valves, patches, and conduits by utilizing decellularized xenologous tissue that is treated to stabilize the elastin and collagen within the extracellular matrix. The decellularized PGG treated tissues would resist calcification due to the removal of the principal sites of calcification with the decellularization procedure. (363) Crosslinking with PGG would also protect the elastin and collagen within the decellularized tissues from rapid degradation. (364) PGG treated Engineered Tissue Vascular Grafts have been shown to exhibit good mechanical and biological properties *in vivo* by subdermal implantation in rats and were found to be non-thrombogenic in acute implantation studies in rabbits. (365) PGG treated valve leaflets with the attached portion of the wall would additionally maintain the native structure and functionality of the valve leaflets. The attached wall would also allow ease of surgical implantation by ensuring sutures pass through the wall and not the

valve leaflet, thereby minimizing manipulation of the functional leaflet structure. Moreover, the acellular grafts would be able to allow cellular infiltration and remodeling of the grafts with the potential to grow with young patients.

Additionally, the research aims to develop tissue biomaterials capable of resisting calcification and structural degradation from enzymatic digestion by treating decellularized tissue scaffolds with PGG. The approach would provide durable, off-the-shelf biomaterial that is robust, biocompatible, with significant implant life, compared to decellularized scaffolds and would allow cellular ingrowth of host cells, thereby potentially enabling regenerative growth and remodeling after implantation. The biocompatibility of the biomaterials was tested in subcutaneous implants as well as intra-muscular implants.

Furthermore, the functionality and efficiency of the PGG treated valved conduits and leaflet patches were evaluated in a large animal model circulatory environment. Along with implant functionality, this will determine the hemocompatibility of the biomaterial, as well as cellular infiltration, remodeling, and growth potential of the scaffold after implantation.

Aim 1: Assessment of the efficiency of polyphenols in stabilizing Elastin and Collagen in scaffolds

Approach: Decellularized scaffolds will be prepared from fresh tissues and will be treated with polyphenols Penta-Galloyl Glucose (PGG), All-Trans Retinoic Acid (ATRA), Hesperidin, D-Salicin, and Quercetin to determine the ability of the polyphenols to

crosslink the scaffolds. The efficiency of the polyphenol treatments to cross-link the elastin and collagen will be determined by subjecting the scaffolds to degradation by Elastase and Collagenase enzymes. Primary cultures of Human Aortic Smooth Muscle Cells (HAoSMCs) will be treated with polyphenols to determine effect of polyphenol treatment on the production of soluble tropoelastin by the cells as well as the deposition of healthy cross-linked elastin will be analyzed after 14-day cell-culture.

Aim 2: Development of tissue engineered bovine jugular vein conduits for pediatric patients

Approach: Tissue-engineered Bovine Jugular vein (BJV) conduits will be prepared from decellularized tissues crosslinked with PGG. The concentration of PGG for optimal crosslinking will be determined by the resistance of the scaffolds to resist degradation by elastase and collagenase enzymes. The potential of the prepared jugular vein conduit tissues to maintain their properties after long-term storage will be analyzed. The biocompatibility and functionality of the PGG treated jugular vein conduits will also be determined by implantation in sheep as pulmonary conduit replacement units.

Aim 3: Development of tissue-engineered valve leaflet patch for pulmonary valve repair in pediatric patients

Approach: Pulmonary valve repair units will be developed from porcine aortic valves (PAV) and porcine pulmonary valves (PPV) by decellularization and PGG treatment of the decellularized scaffolds. The tissue-engineered valves, with attached wall portions,

will be analyzed histologically for the decellularization efficiency, as well as their ability to resist degradation by elastase and collagenase enzymes. The mechanical properties of the native tissues and the decellularized and PGG treated scaffolds will be determined using biaxial mechanical testing. Suture retention strength of the PGG treated aortic walls will also be compared to that of Glutaraldehyde treated aortic wall tissues.

PGG treated porcine aortic valve and wall tissues will be implanted subcutaneously in rats for up to 90-days to determine their biocompatibility, as well as analyze their ability to resist calcification compared to Glutaraldehyde treated tissues. After subcutaneous implantation, the explants will be analyzed histologically, as well as using flow-cytometry to determine cellular infiltration within the subcutaneous implants.

PGG treated porcine aortic valves and porcine pulmonary valves with attached walls will also be implanted in sheep as pulmonary valve repair units to determine the functionality of the tissue-engineered scaffolds. The animals will be monitored for valve functionality during the implantation period. Explants will be analyzed by their gross histology as well as histologically to determine the infiltration of cells within the implanted scaffolds.

Aim 4: Evaluation of PGG treated Bovine Pericardium scaffolds as intramuscular implants in diabetic conditions

Approach: Bovine pericardium patches will be prepared by decellularization and PGG treatment of the native tissues. The tissue-engineered pericardium patches will be

analyzed for their ability to resist bacterial attachment in *Staphylococcus aureus* cultures. Patches will then be implanted in diabetic and non-diabetic rats as full-thickness abdominal wound healing patches for up to 6 weeks. The efficiency of the patches as intra-muscular implants in diabetic conditions will be compared to that under non-diabetic conditions using gross view analysis and histological analysis of the explants.

CHAPTER FOUR

SPECIFIC AIM 1: ASSESSMENT OF THE EFFICIENCY OF POLYPHENOLS IN STABILIZING ELASTIN AND COLLAGEN IN SCAFFOLDS

4.1 Introduction

Tissue-engineered scaffolds derived from xenogeneic sources need to be decellularized to remove the native cellular and nuclear components capable of inducing immunogenic response upon implantation (366, 367). The decellularization of native extracellular scaffolds also removes the principal sites for calcification, providing superior grafts compared to glutaraldehyde-fixed native tissues (368). The efficiency of the decellularization process itself might be dependent on the structure and arrangement of ECM components within the tissue (369, 370). To establish the consistency of the decellularization procedure, different tissues were decellularized using the developed decellularization protocol, and its effectiveness in removing native nuclear components was analyzed.

Additionally, despite their resistance to calcification and immunogenic responses, decellularized scaffolds are susceptible to enzymatic degradation by enzymes (371, 372). To protect decellularized scaffolds from rapid degradation by elastase and collagenase enzymes after implantation, the elastin and collagen within the ECM need to be crosslinked. PGG, the core structure of polyphenol Tannic Acid (TA), has been shown to stabilize elastin within the extracellular matrix of tissues while being less toxic than TA (373). Owing to its hydrophobic core and numerous external hydroxy groups, PGG is

capable of binding specifically to hydrophobic regions of elastin and collagen in addition to establishing numerous hydrogen bonds (374-376).

PGG has also been shown to promote elastogenesis within healthy and aneurysmal rat smooth muscle cell cultures(377). Elastogenesis is an elastic fiber assembly process that is highly upregulated during the late fetal and neonatal stages (378). Mature cells show poor recruitment, crosslinking, and elastin precursor organization into fibers (379). The presence of pro-elastogenesis compounds within the implanted scaffolds might therefore potentially enable elastin formation and remodeling within the scaffolds.

Polyphenols Quercetin, Hesperidin, and D-Salicin, have been shown to interact with γ -globulins (380). All-trans Retinoic Acid (ATRA) has been shown to influence ECM synthesis and ECM degradation in Human Arterial Smooth Muscle cell cultures (381). In this study, the ability of these polyphenols to interact and stabilize ECM components in decellularized scaffolds was studied. To this effect, the polyphenols were analyzed for their ability to crosslink collagen and elastin within ECM of decellularized scaffolds and prevent their rapid degradation. The ability of the polyphenols to deposit elastin and fibrillin within the extracellular matrix of smooth muscle cells was also determined.

4.2 Materials and methods

Decellularization of Native Tissues:

Fresh bovine pericardium, bovine jugular veins, bovine inferior vena cava, porcine fascia, and porcine aortic valve tissues were obtained from Animal Technologies, Inc. The tissues were inspected *ante mortem* and were found to be free from contagious diseases.

Blood was removed from the native tissues by washing with PBS, and any muscle within the tissue was trimmed.

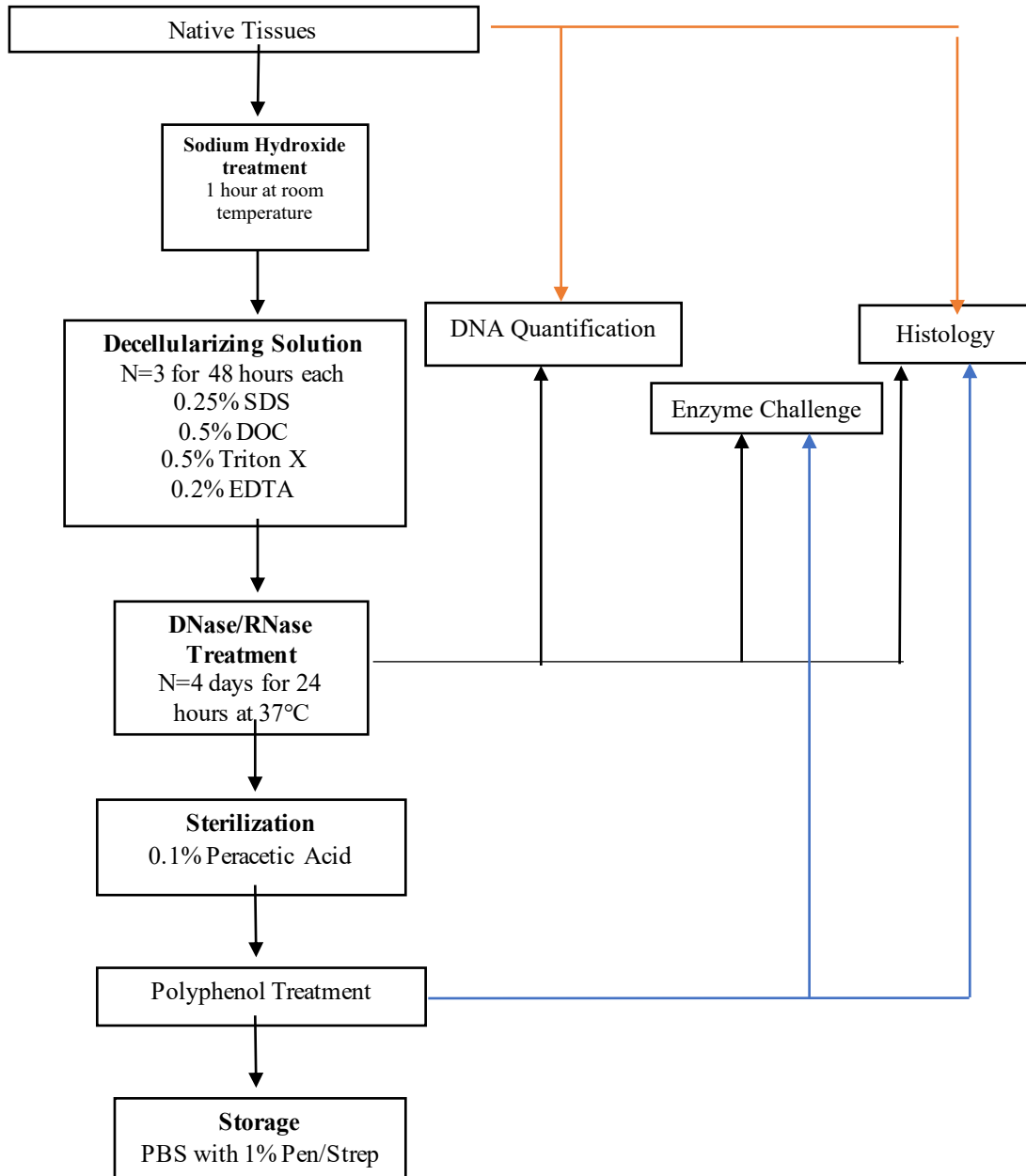


Figure 27: Decellularization process and Polyphenol Treatment of native tissues

Native tissues were incubated with 0.05 M sodium hydroxide (NaOH) for one hour at room temperature, following which, they were treated with a decellularizing solution composed of 0.25% sodium dodecyl sulfate (SDS) (Fisher BP349-100), 0.5% sodium Deoxycholate (DOC) (Carolina Biological 858740), 0.5% Triton X 100 (Alfa Aesar A16046), and 0.2% Ethylene Diamine Tetra-Acetic acid (EDTA) (Sigma Aldrich E6511) in 50 mM TRIS (tris (hydroxymethyl) amino-methane) (Bio-Rad 1610716) buffer (pH 7.4 \pm 0.05) for three days. Decellularization solution was replaced with fresh solution every day.

Tissues after treatment with decellularization solution were rinsed thoroughly and treated with 70% ethanol by shaking at room temperature and then incubated with DNase/RNase solutions. DNase (Worthington, 3840 /mg dry weight) and RNase (Fisher, 97.1 Kunitz/mg) was used at a concentration of 360 U/mL (for both DNase and RNase) to remove native nucleic acid components from the tissue. The DNase/ RNase treatment was done for four days at 37°C, and the solution was replaced with fresh DNase/RNase every 24 hours. The decellularized scaffolds were sterilized by shaking with sterile 0.1% Peracetic acid (pH 7.4 \pm 0.05) at room temperature for 24 hours. After sterilization, scaffolds were stored in sterile PBS with 1% penicillin/ streptomycin antibiotics. The decellularization procedure has been schematically represented in Figure 27.

DNA Quantification:

Native and decellularized tissues were lyophilized by freezing tissues at -80°C, and then placing them in a Freeze Dryer (Labconco, Kansas City, MO) for at least 24 hours.

All tissues were washed thoroughly in Deionized (DI) water before freezing to remove any salt contributing to false dry weight readings. DNA was extracted from lyophilized native and decellularized tissues using Qiagen Dneasy Blood and Tissue Kit (Cat. No. 69504). Briefly, 5-10 mg of the native and decellularized lyophilized tissues were cut into small pieces and placed in Buffer ATL and Proteinase K at 56°C until all of the tissue was digested. Ethanol was added to the digested samples to precipitate the nucleic acids, and the DNA was isolated in a microcentrifuge spin-column by washing with appropriate buffers and eluting bound DNA with equal volumes of buffer AE. The concentration of DNA obtained from each sample was quantified with ultrasensitive fluorescent nucleic acid stain Quant-It Pico green dsDNA Reagent kit. The fluorescence value for each sample was measured at 502/523 nm and compared to a set of standards of known concentrations of DNA to obtain the DNA concentration in the particular sample. Wherever required, the samples were diluted at the appropriate levels for the fluorescence reading to be within the range of the standards used. The DNA concentration for each sample was multiplied by the volume of buffer AE used for elution, and the total amount of DNA obtained was normalized to the dry weight of the tissue initially digested to determine the nanograms (ng) of DNA/ mg of the tissue sample.

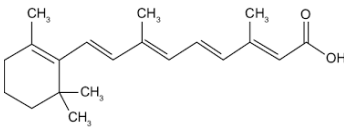
Histological Analysis:

Tissue samples were fixed in formalin for 48 hours, dehydrated by a series of changes through ethanol concentrations, and embedded in paraffin. Paraffin blocks of tissues were sectioned at 5 µm thickness, mounted on glass slides, and heated for 30

minutes on a slide warmer to adhere the tissue sections to the slides. Slides were baked overnight at 56°C in an oven. Subsequently, the slides were deparaffinized and stained with hematoxylin and eosin to determine cellular components within the tissue matrix.

Polyphenol treatment of decellularized scaffolds:

Decellularized tissues were treated with polyphenols PGG, All-trans retinoic acid, Hesperidin, D-Salicin, and Quercetin for 20 ± 2 hours by shaking at room temperature, protected from light. For the PGG treatment, 0.15% PGG (SA Ajinimoto Omnicem N.V., Belgium) was dissolved in 20% isopropanol in HEPES (4-(2-hydroxyethyl)-1-piperazineethanesulfonic acid) solution (pH 5.5). For treatment with All-Trans retinoic acid, 0.07% ATRA (Sigma Aldrich, US) was dissolved in 20% isopropanol in HEPES at pH 9. 0.28% Hesperidin (Sigma Aldrich, US) was dissolved in 10% DMSO in HEPES at pH 11.4. 0.2% D-Salicin (Sigma Aldrich, US) was dissolved in HEPES buffer at pH 7.4. Finally, for the Quercetin treatment, 0.16% Quercetin (Sigma Aldrich, US) was dissolved in 20% isopropanol in HEPES (pH 9.5). After the polyphenol treatments, the tissues were washed and stored in sterile PBS at 4°C. The polyphenol concentrations and buffers used have been summarized in Table 3.

Polyphenol	Structure	Maximum Dissolved	Buffer (pH)	Final Concentration
All-trans Retinoic Acid (ATRA)		3.5 mg/ml in Isopropanol	HEPES (9.0)	0.07%

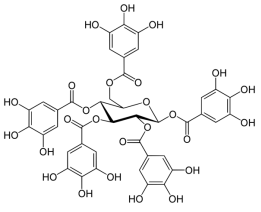
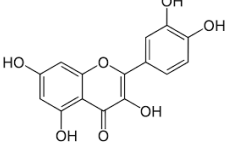
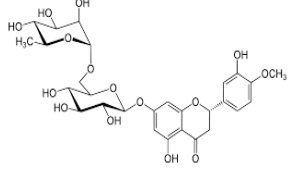
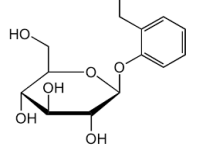
Penta-Galloyl Glucose (PGG)		11.6 mg/ml in Isopropanol	HEPES (5.5)	0.15%
Quercetin		8 mg/ml in Isopropanol	HEPES (9.5)	0.16%
Hesperidin		28 mg/ml in DMSO	HEPES (11.4)	0.28%
D-Salicin		43 mg/ml in Water	HEPES (7.4)	0.2%

Table 3: Polyphenol Concentrations used for Treatment of Decellularized Tissues

Enzyme (Elastase and Collagenase) Challenge:

Native, Decellularized, and Polyphenol treated decellularized tissues were rinsed thoroughly in water and lyophilized to obtain the dry weight of the tissues. The scaffolds were then subjected to treatment by elastase and collagenase to determine the ability of the polyphenol-treated scaffolds to resist rapid degradation by elastase and collagenase enzymes. 10-15 mg sections of lyophilized tissue were obtained for each sample. For the elastase challenge, the sections were placed in 1.2 mL of 5 U/mL Elastase enzyme with 1 mM Calcium Chloride (CaCl_2) and 0.02% Sodium Azide (NaN_3) in 100 mM TRIS buffer ($\text{pH } 7.8 \pm 0.05$) for 24 hours. For the collagenase treatment, 1.2 mL of 75 U/mL type VII Collagenase was used with 10 mM CaCl_2 and 0.02% NaN_3 in 50 mM TRIS buffer ($\text{pH } 8 \pm$

0.05) for 48 hours. The samples were placed in a warm room (37°C) with shaking at 650 RPM (revolutions per minute). The digested samples were rinsed in water and lyophilized at the end of the 24-hour or 48-hour time points. The dry weights of the digested samples were recorded and used to analyze the percent weight loss (% weight loss) after the collagenase/ elastase enzyme challenge. Digested tissue samples were also fixed in 10% NBF, tissue processed, embedded in paraffin, and sectioned using a microtome to determine the Extracellular Matrix structure after enzyme digestion.

Cell culture and Polyphenol treatment of cells:

Primary Human Aortic Smooth Muscle Cells (HAoSMCs) isolated from the human aorta were obtained from a commercial supplier (PromoCell, Heidelberg, Germany). Cells were cultured in T-75 flasks in low serum (5% v/v) smooth muscle cell growth media (PromoCell, Heidelberg, Germany). Growth media was prepared by adding the Supplement Mix consisting of Fetal Calf Serum, Epidermal Growth Factor (recombinant human), Basic Fibroblast Growth Factor (recombinant human), and Insulin (recombinant human) to the basal medium to final supplement concentrations of 0.05 mL/mL, 0.5 ng/mL, 2 ng/mL, and 5 µg/mL respectively. Cells were maintained in a humidified incubator at 37°C and 5% CO₂ and culture media were changed every three days.

Primary HAoSMCs were treated with polyphenol PGG, Quercetin, Hesperidin, D-Salicin and ATRA (10 µg/ml) for 14 days. Stock solutions of the polyphenols (5 mg/ml) in DMSO were filter sterilized through 0.2 µm filters before addition. Control groups were used with the addition of only DMSO. The cell culture media was changed every 3 days.

After 14-days of culture, soluble proteins and cell layers were collected and analyzed. Passage numbers 3-7 were used for all cell culture studies.

Protein quantification:

After 14-days of cell culture with polyphenols, the cell layers were washed with sterile DPBS and protein was extracted using Solulyze-M mammalian extraction buffer (Genlantis, San Diego, CA). Prior to extraction, one tablet of protease inhibitor cocktail (Sigma, St. Louis, MO), was added to 10 ml of the buffer to prevent protein degradation. After ~15 minutes of buffer incubation at room temperature, cell layers were scraped from the cell culture plate, collected, homogenized, and centrifuged at 12,000 x g for 15 minutes. Cell pelettes were washed, frozen and lyophilized, while the supernatant was used to determine the total soluble protein with Pierce BCA protein assay (Thermo Scientific, Rockford, IL).

Fastin Assay for Elastin quantification:

Insoluble elastin deposition within cell layers treated with polyphenols was quantified using Fastin assay (Accurate Scientific and Chemical Corporation, Westbury, NY). Lyophilized cell pelettes were digested using 0.5M Oxalic acid by boiling for 1 hour at 100°C in a water bath. Digested samples were quantified for the presence of α -elastin using fastin assay. The amount of elastin obtained from each sample was normalized to the total soluble protein content of each sample.

Immunocytochemistry (ICC) for Elastin and Fibrillin I:

HAoSMCs were treated with polyphenols for 14-days in culture as described before. At the end of 14-days, polyphenol treated SMC cultures were washed with sterile PBS and fixed at room temperature with 4% NBF for 15-20 minutes. Fixed cultures were blocked using 5% bovine serum albumin. The primary antibody, mouse anti-rat elastin or Fibrillin I antibody, was applied overnight at 4°C at a dilution of 1:100. Secondary fluorescent tagged antibody was used at 1:200 dilution for 1 hour at room temperature. Cell monolayers were stained with DAPI for 10 minutes and washed with PBS. Subsequently, the wells were filled with PBS, and samples were examined with a fluorescent microscope. All the samples were imaged under similar exposure for impartial analyses.

Semi-quantitative image analysis was done using FIJI ImageJ software. The elastin/ fibrillin I single-channel images were converted to 8-bit images, threshold adjusted to remove any background, and the Mean Grey area was obtained for each image. The cell count was obtained by threshold adjustment, watershed, and particle analysis from the DAPI channel images. Mean Grey area values were normalized to the cell counts obtained from each image to obtain the semi-quantitative elastin/ fibrillin I estimation (382, 383).

Statistical Analysis:

All *in-vitro* experiments, including cell cultures, were done in triplicates or more. The data was reported as the Mean \pm Standard Deviation. Data from different groups were analyzed by one-way analysis of variance (ANOVA) using Tukey's HSD. All statistical

analysis was done using JMP[®] Pro 15.2.0. Significance was reported at three different significance levels: *** $p \leq 0.01$, ** $p \leq 0.05$, * $p \leq 0.1$. Statistical significance has been reported in each result.

4.3 Results

Decellularization of Native Tissues:

The Decellularization process involved multiple 24-hour periods of treatment with DNase and RNase enzymes. The optimum number of the DNase/RNase treatment cycles was determined by measuring the DNA content in Bovine Jugular Vein tissues after every DNase/RNase treatment.

DNA quantification of BJV conduits after every DNase/RNase treatment cycle revealed a minimum of 4 treatment cycles necessary for optimum removal of DNA from the native tissues (Figure 28). Native BJV tissues had a DNA concentration of 980.89 ± 151.65 ng/mg dry weight of tissue. This concentration decreased to 257.9 ± 36.52 ng/mg after one DNase/RNase treatment: 126.62 ± 34.56 ng/mg after two DNase/RNase treatments, 64.4 ± 39.32 ng/mg after three treatments, and to 26.13 ± 9.91 ng/mg after four treatment cycles.

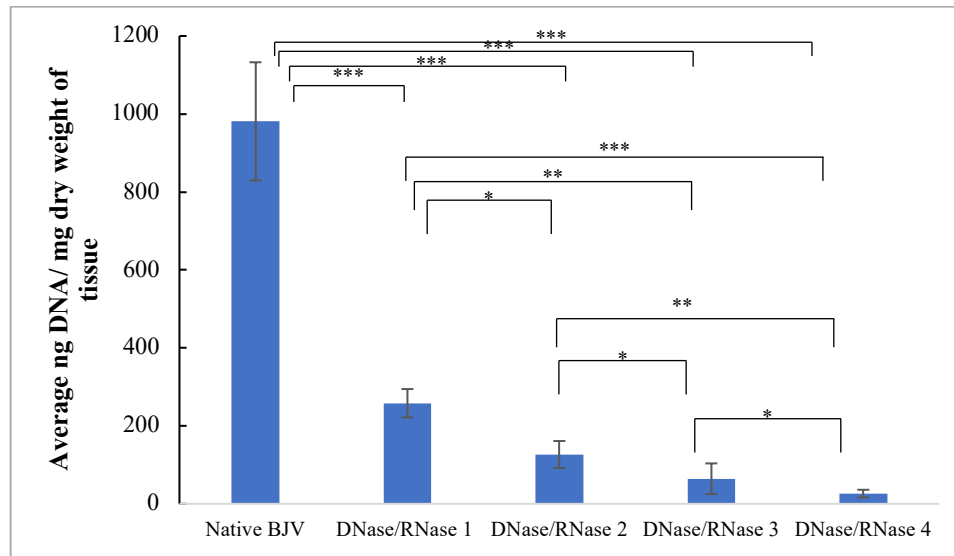


Figure 28: DNA quantification of Bovine Jugular Vein conduits to optimize the number of DNase/RNase treatment cycles. An acceptable level of DNA was obtained after 4 treatments

The optimum level of DNA achieved after four treatments was < 50 ng DNA/mg dry weight of the tissue. A significant decrease in the DNA content was observed after each DNase/RNase treatment cycle. The same treatment process applied to Native bovine pericardium, porcine fascia, bovine inferior vena cava, porcine aortic valves, and porcine pulmonary valves achieved successful decellularization of the native tissues with < 50 ng of DNA/ mg dry weight of tissue (384).

Native bovine pericardium tissues had average DNA concentrations of 2862.05 ± 2117.38 ng/mg, which decreased to 270.02 ± 28.93 ng/mg, demonstrating a 90.5% decrease. For porcine fascia, the DNA concentration of 2573.11 ± 842.3 ng/mg in native tissues decreased 99.2% to 19.79 ± 8.29 ng/mg. Bovine vena cava showed a reduction from 769.02 ± 140.84 ng/mg to 9.32 ± 0.17 ng/mg, demonstrating a 98.78% reduction. The

difference in the DNA content between the native and decellularized tissues was significantly different for all the tissue types (Figure 29).

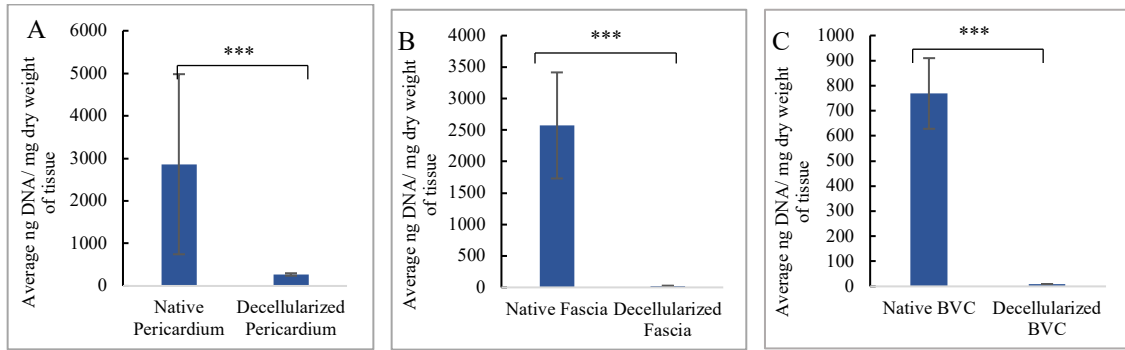
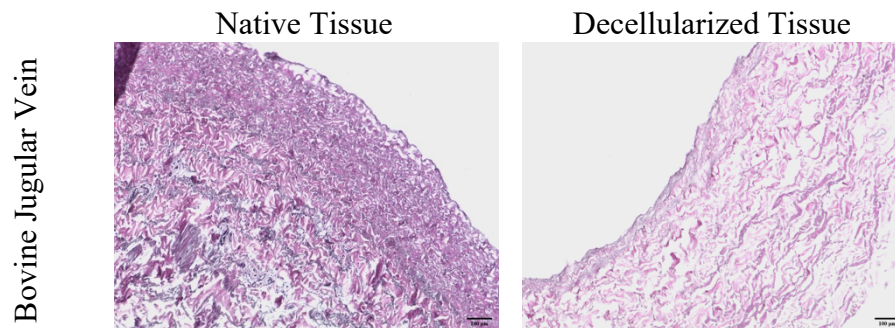


Figure 29: DNA Quantification in A. Bovine Pericardium; B. Porcine Fascia; C. Bovine Inferior Vena Cava (***, **, *: Represents different levels of significance, $N \geq 3$)

Histological analysis of the native and decellularized tissues revealed the removal of all visible cellular components from the native tissue after decellularization (Figure 30). Hematoxylin and Eosin staining of the native and decellularized scaffolds did not reveal any difference in the extracellular matrix before and after the decellularization process.



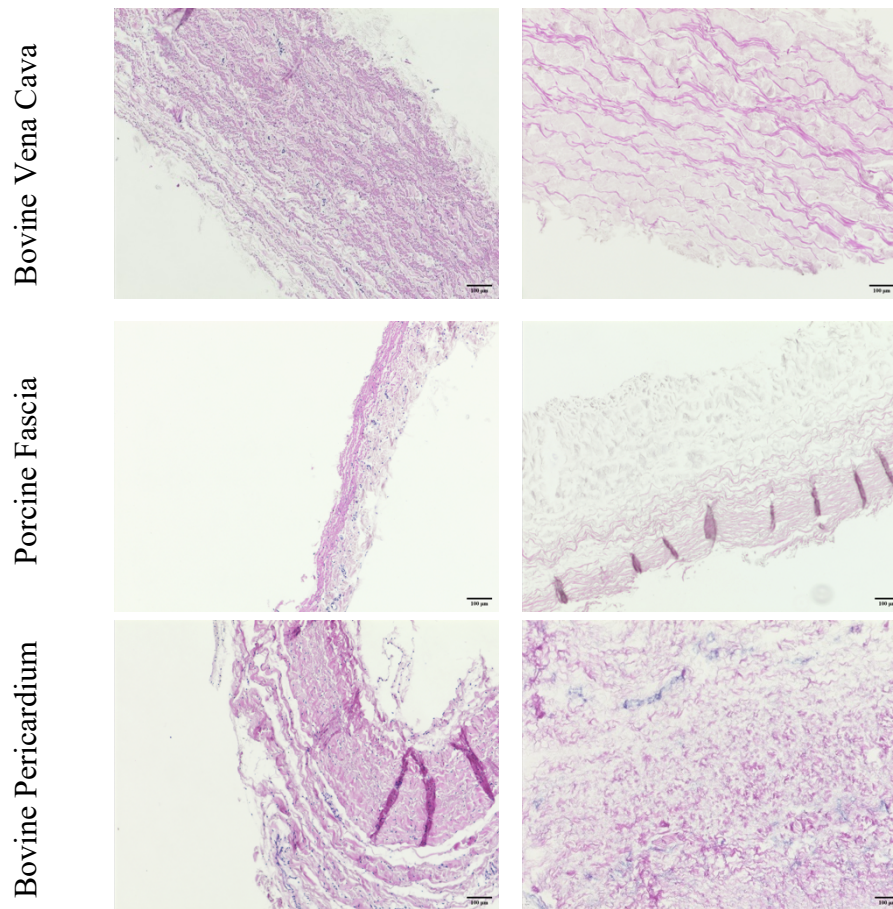


Figure 30: Hematoxylin and Eosin Staining of Native and Decellularized tissues showing absence of cells in decellularized tissues

Enzyme Resistance of Polyphenol Treated Scaffolds:

Polyphenol treated decellularized scaffolds prepared from bovine pericardium, porcine fascia, bovine jugular vein, and bovine inferior vena cava were compared to the respective decellularized tissues to determine the ability of the polyphenol treatment to provide resistance to the tissues against degradation by elastase and collagenase enzymes.

For the elastase treatment, there was no significant difference between any of the polyphenol treated groups and the decellularized pericardium and fascia tissues (Figure

31). For Bovine pericardium tissues, the % weight loss for decellularized, ATRA treatment, Hesperidin treatment, PGG treatment, Quercetin, and D-Salicin treatments were $16.92 \pm 0.54\%$, $14.56 \pm 3.84\%$, $4.35 \pm 1.36\%$, $10.2 \pm 2.78\%$, $9.67 \pm 2.25\%$, and $2.96 \pm 2.54\%$ respectively. In fascia tissues, the corresponding weight loss values were $11.36 \pm 2.63\%$, $4.58 \pm 2.52\%$, $8.72 \pm 4.74\%$, $8.5 \pm 4.04\%$, $6.02 \pm 5.62\%$ respectively.

BJV demonstrated significant decrease in the PGG and D-Salicin treated scaffolds compared to the native tissue (Figure 31). The average % weight loss for the decellularized BJV was $45.34 \pm 1.58\%$, while the PGG and D-Salicin treatments decreased this loss to $20.92 \pm 4.93\%$ and $19.51 \pm 2.5\%$ respectively. No significant difference was seen for the ATRA, Hesperidin, and Quercetin treatments, where the average losses were $33.52 \pm 2.77\%$, $64.6 \pm 9.89\%$, and $44.7 \pm 13.14\%$. Bovine inferior vena cava tissues, on the other hand, did not have any significant decrease in dry weight loss for any of the polyphenol treatments compared to the Decellularized tissues. % Weight loss of the decellularized vena cava tissues after elastase treatment was $20.72 \pm 5.13\%$ of the dry weight. After ATRA, Hesperidin, PGG, Quercetin, and D-Salicin treatments, the weight loss values were $23.5 \pm 3.47\%$, $27.21 \pm 0.77\%$, $21.02 \pm 4.73\%$, $24.76 \pm 14.71\%$, and $34.7 \pm 7.27\%$ respectively.

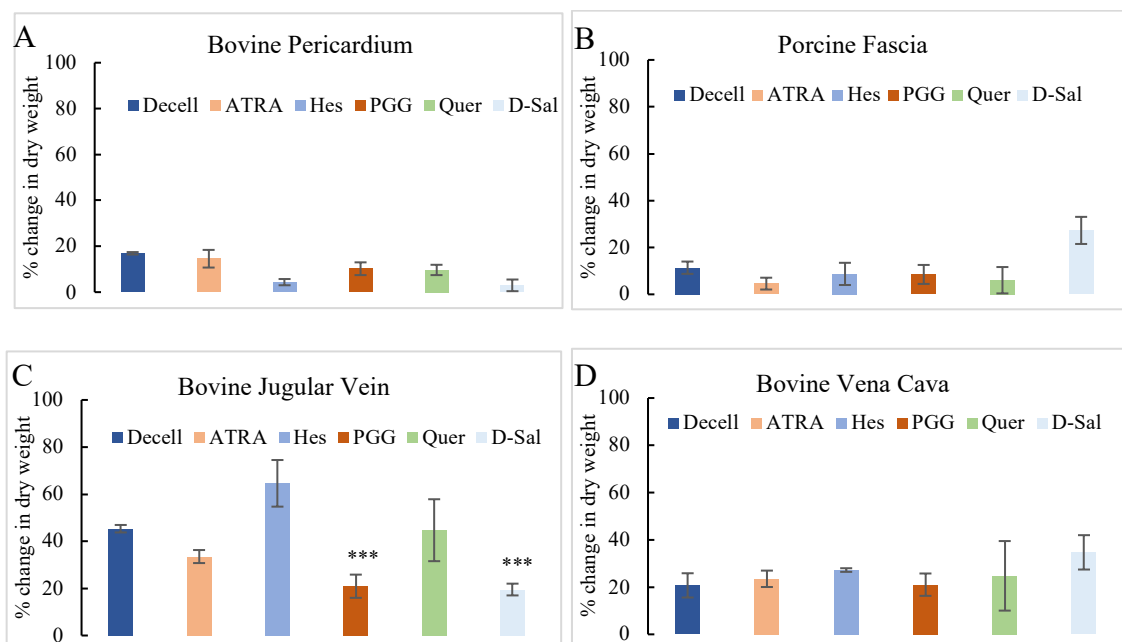


Figure 31: Resistance to Elastase treatment for polyphenol treated decellularized tissues; A: Bovine Pericardium; B: Porcine Fascia; C: Bovine Jugular Vein; D: Bovine Inferior Vena Cava; N=6; (***) statistically significant difference compared to decellularized group $p < 0.01$)

Collagenase treatment of the decellularized and polyphenol treated tissues showed a significantly high decrease in weight loss for some of the polyphenol treated groups (Figure 32). For the pericardium scaffolds, PGG treatment decreased the % loss in dry weight from 100% in decellularized tissues to $5.9 \pm 5.56\%$. The other treatments in pericardium resulted in $99.49 \pm 0.72\%$ loss for ATRA treatment, $99.1 \pm 0.66\%$ loss for Hesperidin, 100% loss for quercetin, and $99.9\% \pm 0.13\%$ loss for D-Salicin, none of which were significantly different from the decellularized group. A similar observation was made for the fascia scaffolds, where the PGG treatment decreased the weight loss from $97.88 \pm$

1.42% in the decellularized tissues to $3.78 \pm 1.97\%$ weight loss. In addition to PGG, ATRA, and Quercetin treatments also significantly reduced the weight loss from decellularized group to $36.51 \pm 16.83\%$ and $62.24 \pm 31.98\%$, respectively. The change in dry weight was, however, significantly less in the PGG treated tissues compared to both the ATRA and Quercetin treated groups. Hesperidin treatment resulted in weight loss of $89.54 \pm 14.11\%$, and D-Salicin in $61.75 \pm 8.22\%$, none of which was significantly different from the control group. For the jugular vein, the PGG treated group demonstrated a dry weight loss of $6.36 \pm 4.77\%$, which was significantly less than $68.62 \pm 17.51\%$ loss in the decellularized

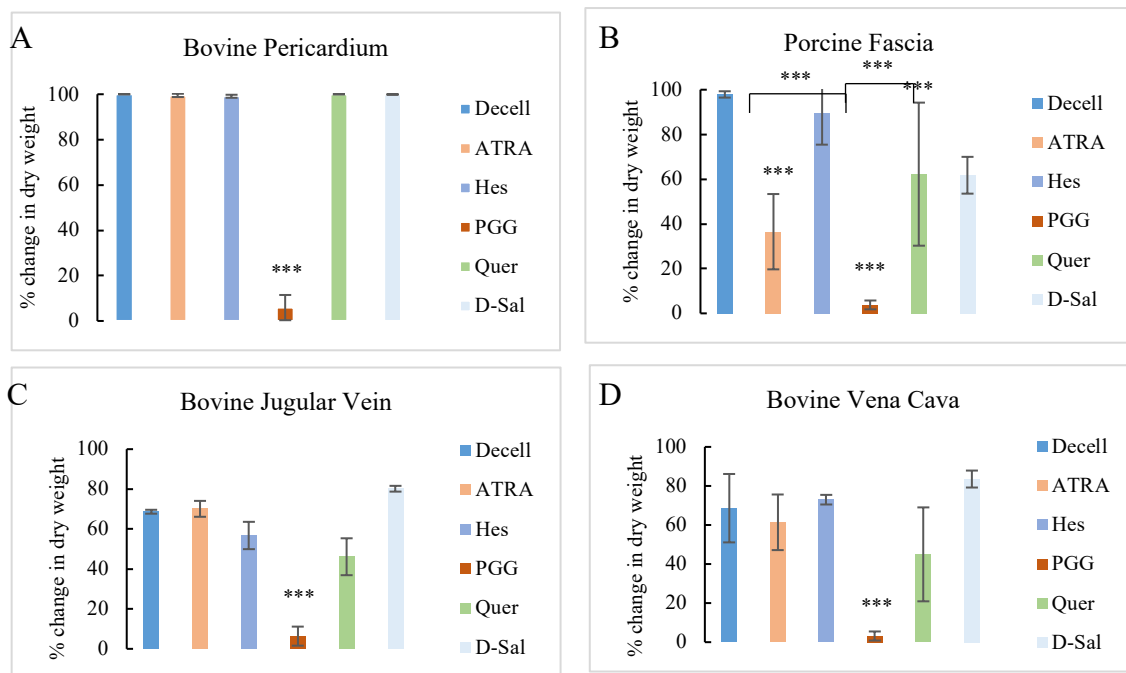


Figure 32 : Resistance to Collagenase treatment for polyphenol treated decellularized tissues; A: Bovine Pericardium; B: Porcine Fascia; C: Bovine Jugular Vein; D: Bovine Inferior Vena Cava; N=6; (* statistically significant difference compared to decellularized group $p < 0.01$)

tissues. None of the other polyphenol-treated jugular veins showed any significant decrease in weight loss. The average % weight losses for the other treatments were $70.11 \pm 3.98\%$ for ATRA, $56.76 \pm 6.84\pm$ for Hesperidin, $46.1 \pm 9.24\%$ for Quercetin, and $80.12 \pm 1.45\%$ for the D-Salicin treatment. Similarly, for the inferior vena cava tissues, PGG treatment significantly reduced the % decrease in dry weight after collagenase treatment from $68.62 \pm 17.51\%$ to $3.16 \pm 2.32\%$. The other groups had weight losses of $61.39 \pm 14.24\%$, $72.97 \pm 2.46\%$, $44.97 \pm 24.05\%$, and $83.54 \pm 4.34\%$ for ATRA, Hesperidin, Quercetin, and D-Salicin treatments, respectively.

Fastin Analysis for Polyphenol Treated HAoSMC cultures:

The addition of 10 $\mu\text{g/ml}$ of PGG, ATRA, Quercetin, Hesperidin, and D-Salicin demonstrated an increase in the average μg insoluble elastin/ μg soluble proteins within the HAoSMC cultures after 14 days (Figure 33). The average μg elastin/ μg soluble proteins for the control DMSO group was 0.34 ± 0.03 ; for the PGG, ATRA, Quercetin, Hesperidin, and D-Salicin treatments, the respective concentrations were 1.43 ± 0.64 , 1.29 ± 0.95 , 1.94 ± 0.77 , 0.69 ± 0.19 , and 0.83 ± 0.47 μg elastin/ μg soluble proteins. Normalized to the DMSO control group, there was a significant increase in the insoluble elastin production for PGG, Quercetin, and Hesperidin treatments. The elastin concentration within the quercetin group was significantly higher than that of the hesperidin treatment. No

significant difference was, however, observed between quercetin and PGG treatment groups.

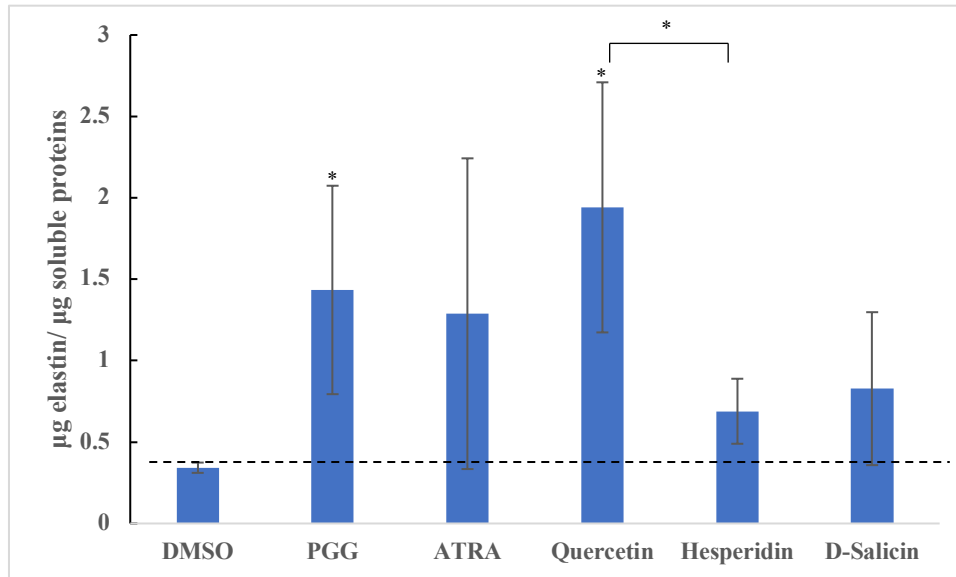
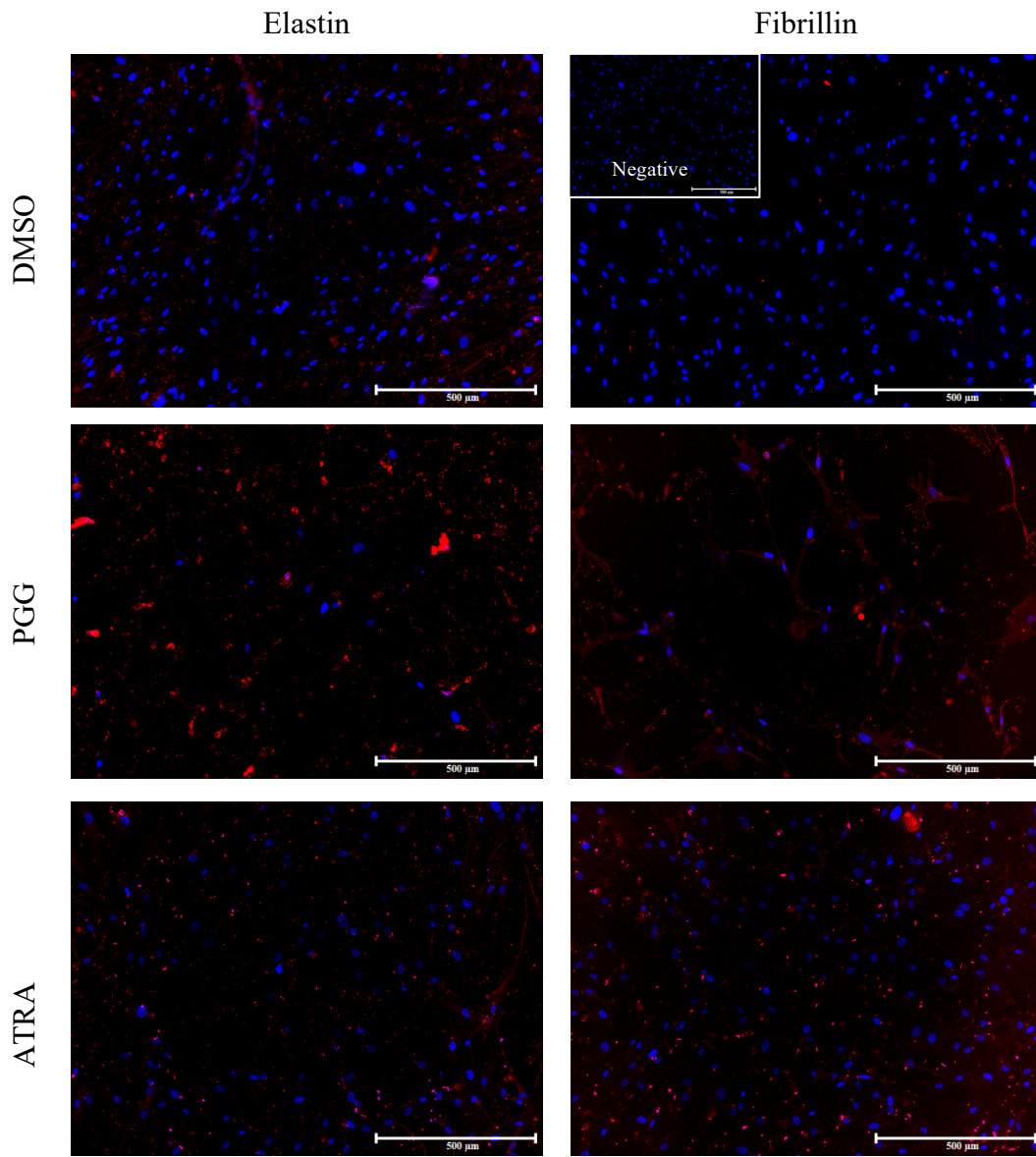


Figure 33: Insoluble elastin deposition within cell cultures treated with polyphenols; (μg Elastin/ μg soluble proteins); N=4

Immunocytochemistry (ICC) analysis for Elastin and Fastin Deposition in cell cultures:

ICC staining of elastin and fibrillin within the polyphenol treated HAoSMC cell cultures demonstrated the presence of the proteins after 14-days of culture. 10 $\mu\text{g}/\text{ml}$ of PGG, Quercetin, hesperidin, ATRA, and D-Salicin treatments demonstrated an increase in elastin deposition after 14-days of culture compared to DMSO control groups (Figure 34). A significant increase in fibrillin deposition was also observed within the PGG, Quercetin, ATRA, and Hesperidin treatment groups. The D-Salicin treatment did not show significantly higher fibrillin production after 14-days of culture.



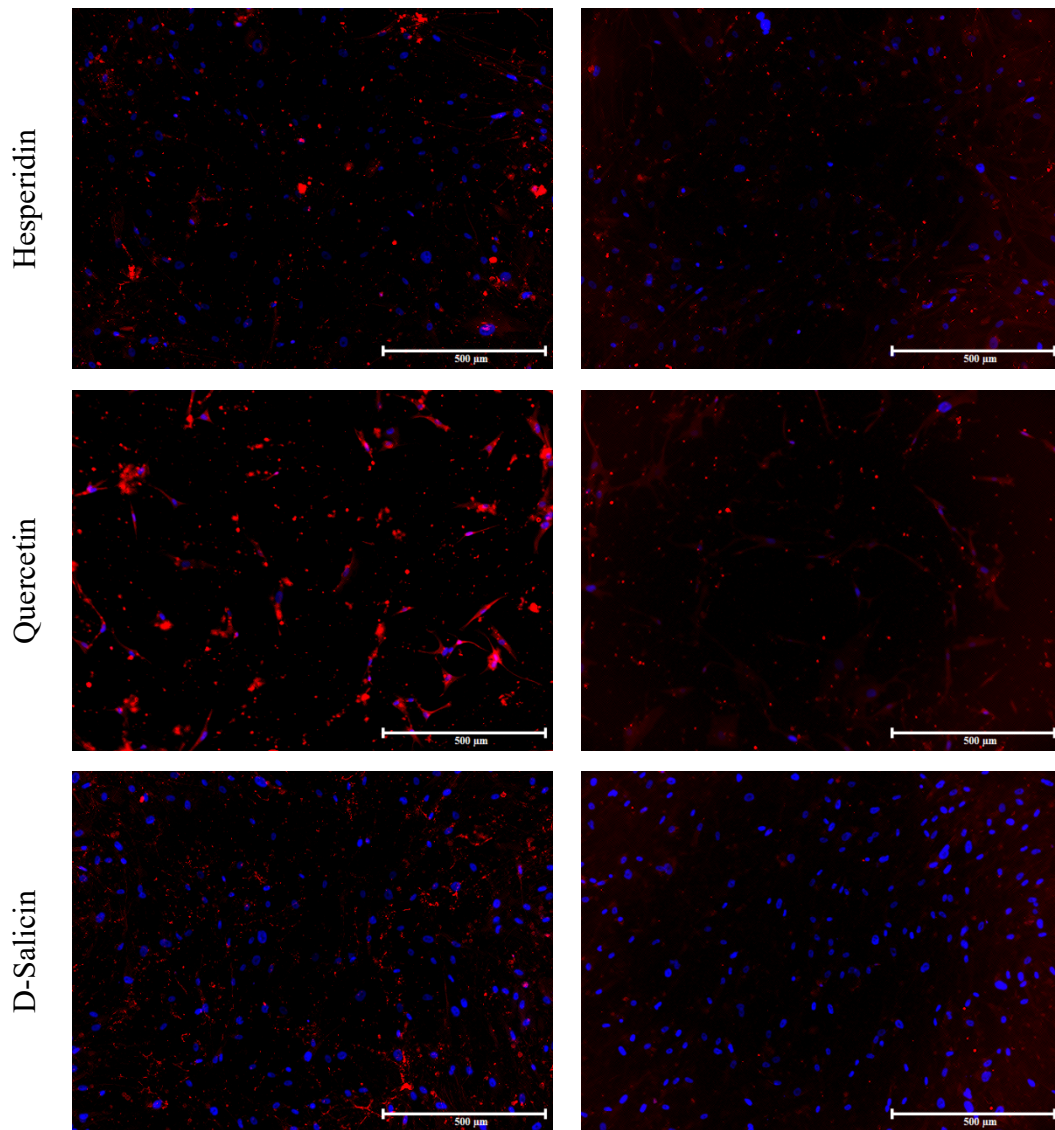


Figure 34: Immunocytochemical analysis of HAoSMC cultures using Elastin and Fibrillin antibodies

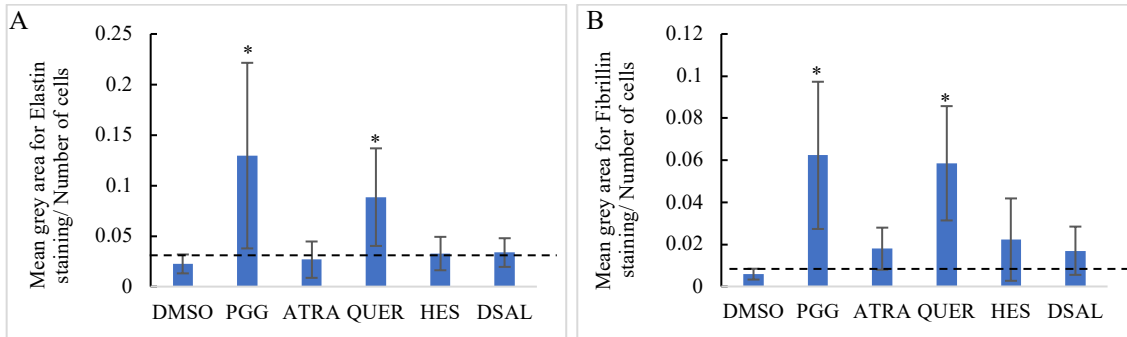


Figure 35: Semi-Quantitative analysis of (A) elastin and (B) fibrillin I ICC staining in polyphenol treated HAoSMC cultures; N=4

Semi-quantitative analysis of the elastin and fibrillin 1 staining showed significant increase in elastin and fibrillin proteins in both PGG and quercetin treated groups normalized to DMSO control groups (Figure 35). The other treatment groups did not show any significant increase.

4.5 Discussions

Tissue-derived scaffolds from xenogeneic sources used for development of biomaterials *in-vitro* are easily available, possess the inherent structure of native ECM, appropriate mechanical properties for physiological functioning of the biomaterials, and signals for cell binding, growth, and differentiation. The xeno-antigenicity of the scaffolds however needs to be addressed prior to implantation (385). Decellularization of xenogeneic materials is a commonly used procedure to remove native cellular and nuclear components from scaffolds. Decellularization protocol should effectively remove all xenogeneic materials from the scaffolds but preserve the native structure of the extracellular matrix within the scaffolds (386).

In this study, a detergent-based decellularization protocol was used for the removal of native cells. Tissues were briefly treated with NaOH before treatment with detergents. NaOH – PBS treatment of tissues has been shown to denature ds-DNA to a single strand as well as inactivate transmissible spongiform encephalitis (387). Optimization of the decellularization procedure using SDS, DOC, EDTA, TRIS, and DNase/ RNase solutions to remove cellular components from native tissues revealed four DNase/RNase treatment cycles necessary for the final concentration of dsDNA to be < 50 ng/ mg tissue dry weight. The same procedure applied to pericardium, fascia, and vena cava tissues also showed optimum removal of DNA. Although these tissues have the same basic component of ECM, collagen, and elastin, the relative arrangement of structure is different within the tissues, which might demand different decellularization approaches (388). The structure and arrangement of the ECM components were unaltered after the decellularization procedure, implying the process does not affect the ECM structure. This approach for decellularization of fresh tissues might be a better approach compared to lyophilization or freezing since tissue structure is altered by those approaches (366).

Polyphenol and ATRA treatment of decellularized tissues demonstrated that PGG was the most effective in protecting the elastin and collagen within the scaffolds from enzyme degradation. Some differences within tissues were observed for the same polyphenol treatments, however. For elastase treatment, there was a significant reduction in weight loss compared to the control decellularized group only in the BJV tissues. Almost 50% of the dry weight of BJV tissues is composed of elastin (389). However, in the pericardium, fascia, and vena cava, < 20% of the dry weight of tissues is composed of

elastin (390, 391). This might have been a contributing factor in the absence of significant weight loss for the polyphenol-treated scaffolds. It should, however, be noted, PGG has been reported to prevent elastin degradation better than glutaraldehyde treatment. Collagenase treatment, on the other hand, showed high weight losses since most of the tissue matrix is composed of collagen. PGG reduced collagen loss from all of the tissues consistently after treatment with the collagenase enzyme. For the fascia tissue, in addition to collagen, ATRA, and quercetin also demonstrated some protection against collagenase enzyme. A higher concentration or a different buffer treatment for these polyphenols might have been more effective in providing optimum collagen crosslinking.

Treatment of HAoSMC cultures with 10 µg/ml of polyphenols demonstrated an increase in the deposition of insoluble elastin significantly higher than the control DMSO group for PGG and quercetin treatments. The concentration of 10 µg/ml was obtained from previous studies reporting PGG treatment at these concentrations demonstrated higher deposition of insoluble elastin within rat aortic smooth muscle cell cultures, dermal fibroblasts as well as in lung fibroblast cells (392-394). Studies have reported the interaction of hesperidin with collagen structure, specifically binding to proteolytic cleavage sites, preventing its degradation by enzymes (395-398). ATRA has been reported to increase elastin deposition in HAoSMC cultures when grown in ATRA-doped polycaprolactone electrospun scaffolds (399). In addition, 0.1% ATRA has been shown to increase fibrillin I deposition in the photoaged dermis (400). However, the direct addition of ATRA in the used quantities did not produce any significant difference in insoluble elastin production.

PGG and quercetin treatments also increased the fibrillin I protein expression within the cell cultures compared to DMSO treatment. Fibrillin I, as mentioned in previous chapters, is a Calcium-binding protein that assembles to form microfibrils in elastic and non-elastic extracellular matrix structures (401). The increase in fibrillin deposition would corroborate with the increase in the production of elastin by the polyphenol treatments. It should also be noted that in addition to PGG, quercetin has been reportedly used for crosslinking of porcine dermal tissues. (402)

One limitation of the study is that the effect of polyphenols on elastogenesis was studied in two-dimensional cell cultures. Moreover, the effect of the polyphenols on essential elastogenic structures like fibulin 4,5, fibrillin-II, LOX proteins and MMPs were not studied. A better representation of the overall effect of the polyphenol treatments might also be obtained by looking at the effect of the polyphenols on deposition and remodeling of scaffolds in vivo or in a bioreactor.

4.6 Conclusion

In this aim, the efficiency developed decellularization protocol was compared in tissues with different ECM structures, proving the protocol was successful in decellularizing all kinds of tissues. The decellularization protocol did not alter the ECM structure within these tissues. Additionally, polyphenols PGG, Quercetin, Hesperidin, D-Salicin, and All-Trans Retinoic Acid were compared to their ability to crosslink elastin and collagen within the decellularized extracellular matrices. PGG was the most effective in protecting the treated scaffolds from rapid degradation by elastase and collagenase

enzymes. HAoSMC cultures treated with the polyphenols and ATRA for 14 days in culture demonstrated increased deposition of insoluble elastin as well as fibrillin I after treatment with PGG and quercetin for 14-days.

CHAPTER FIVE

SPECIFIC AIM 2: DEVELOPMENT OF TISSUE ENGINEERED BOVINE JUGULAR VEIN CONDUITS FOR PEDIATRIC PATIENTS

5.1 Introduction

Pulmonary conduit replacements are required in pediatric patients for the correction of critical congenital conditions like pulmonary stenosis, tetralogy of fallot, pulmonary atresia, truncus arteriosus, and transposition of the great arteries along with ventricular septal defects (403-405). Currently available replacement strategies for conduits involve the use of homograft or synthetically developed conduits. Homografts are not always easily available, whereas synthetically developed scaffolds lack the potential to grow along with the patients (406, 407).

Bioprosthetic conduits developed from glutaraldehyde fixed native tissues have been widely used for pulmonary conduit replacement, but these scaffolds fail rapidly after implantation due to calcification and stenosis in the implants leading to implant retrieval (408, 409). A major risk factor identified in pediatric conduit replacement is the young age of the patients leading to the narrow size of the conduits required (410). Studies have also shown that implantation of a larger size conduit does not have any specific advantage over narrower conduits (411). Moreover, while the currently available strategies might be a suitable option in older patients, in pediatric patients, owing to the growth and development of the patients throughout their lives, with currently available strategies, there arises a need for reinterventions and multiple surgeries throughout the patient's life (412).

There is, therefore, a need to develop replacement conduits that can grow along with pediatric patients. In addition to providing optimal mechanical strength on implantation, the implanted scaffold should be able to degrade over time, allowing cellular infiltration, thereby displaying a potential to grow and remodel along with the patient (413). To develop such conduit replacement scaffolds, decellularized bovine jugular vein conduits can be crosslinked with Penta galloyl glucose (PGG). Decellularization removes the principal sites of calcification within the scaffolds, and crosslinking with PGG (414, 415), as determined in *Chapter Four*, has been shown to protect the elastase and collagenase within the extracellular matrix of the scaffolds from rapid degradation by elastase and collagenase enzymes.

Moreover, compared to stented valves within Dacron or Bovine pericardium conduits, the continuity between the valve and the conduits in bovine jugular vein conduits is advantageous. BJV conduits have been found to be suitable under low pressure conditions; additionally, the distal and proximal ends of BJV allow for easy manipulation of the valved conduit during surgery (416). To be able to use as off-the-shelf conduits, the treated scaffolds should also be able to retain properties after storage for extended periods of time. In this aim, the PGG concentration required for optimal scaffold crosslinking has been optimized along with the *in vitro* characterization of the scaffolds, biocompatibility in subcutaneous implantations, and their functionality in a circulatory environment (417).

5.2 Materials and methods

Optimization of PGG treatment of Decellularized Bovine Jugular Vein

Decellularized Bovine Jugular Vein (BJV) conduits were treated with different concentrations of PGG to determine the concentration at which tissue crosslinking is maximized. The PGG concentrations used have been listed in Table 4. A stock solution of PGG was prepared at a concentration of 167 mg/ml in Isopropanol. The concentrated PGG solution was diluted to the desired concentrations using Isopropanol. PGG in Isopropanol solutions were added to HEPES buffer (pH 5.5) at a ratio of 10 mL PGG solution to 40 mL HEPES. The treatment procedure was used as described for the polyphenol treatment in *Chapter Four*. Briefly, sterilized decellularized tissues were treated in the prepared PGG solutions for 20 ± 2 hours by shaking at room temperature, protected from light.

PGG %	HEPES (ml)	Stock (ml)	Isopropanol (ml)	Concentration of PGG in Isopropanol (mg/ml)
0.05%	40	0.15	9.85	2.5
0.15%	40	0.45	9.55	7.5
0.25%	40	0.75	9.25	12.5
0.55%	40	1.6	8.4	27.5
0.85%	40	2.5	7.5	42.5
1%	40	3	7	50
2%	40	6	4	100
3.33%	40	10	0	167

Table 4: PGG concentrations used for Bovine Jugular Vein treatment optimization

After PGG treatment, the BJV scaffolds were washed with PBS to remove any excess PGG. The washing protocol was used as described in Figure 36. Measured volumes of PBS were used for washing at each step, and the PBS spent from washing was quantified for their PGG concentration to determine how much un-used PGG was washed out in every step. The washing was done to obtain a low final concentration of PGG in the PBS solution.

Subsequently, PGG treated tissues were washed in DI water and lyophilized. Lyophilized tissues were treated with 80% methanol, and PGG within the tissues was quantified as described below. Enzyme challenge with Elastase and Collagenase was also done to determine the resistance of the different PGG concentrations to enzymatic digestion.

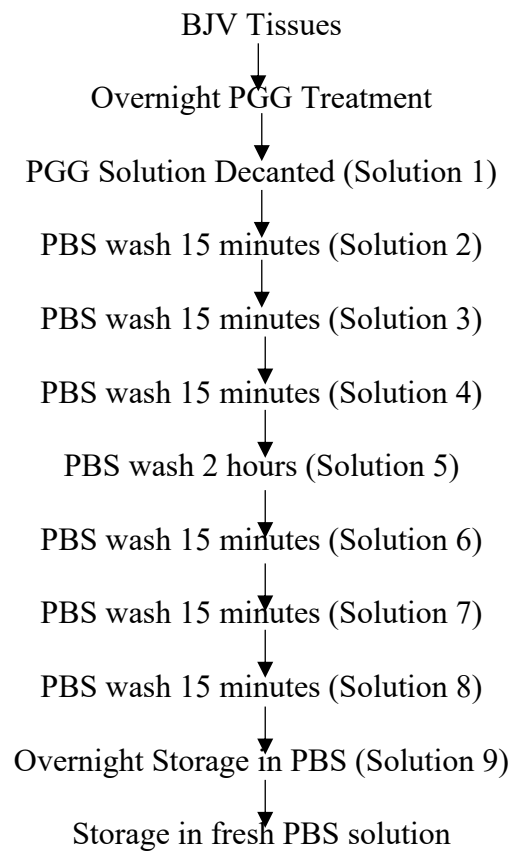


Figure 36: Washing Protocol for PGG treated Bovine Jugular Vein Conduits. PBS wash solutions were quantified for their PGG concentrations to ensure most of the un-used PGG was removed

Storage analysis for PGG treated Bovine Jugular Vein conduits:

Decellularized BJV scaffolds treated with 0.15% PGG were stored for up to 24 months in sterile PBS with 1% Pen/Strep antibiotics. After the storage points, tissues were washed with DI water and lyophilized. The lyophilized samples were analyzed for the stability of the PGG crosslinking after extended storage periods. For the PGG concentration analysis, PGG was extracted and quantified using F-C reagent, as mentioned below. Lyophilized samples were also treated with Elastase and Collagenase enzymes separately, and the PGG treated tissues' resistance to enzyme degradation was determined.

PGG extraction and quantification:

PGG was extracted using Methanol and quantified using F-C Reagent (418, 419) . Tissue samples were rinsed in water and lyophilized. 10-15 mg of lyophilized tissue was obtained for each sample, minced into 1 mm segments, and incubated in 80% methanol at room temperature for 15 minutes. The methanol extracts from each sample were quantified for their PGG concentrations using Folin-Ciocalteu's (F-C) reagent (Sigma-Aldrich, Germany). Briefly, 800 μ l of F-C reagent, diluted 1:10, was added to 200 μ l of each sample, vortexed, and incubated at 37°C for 5 minutes. Next, 600 μ l of sodium bicarbonate was added to the solutions, vortexed, and incubated at 37°C for 30 minutes. Finally, 250 μ l of the final solution was pipetted into 96-well plates, and the Absorption was read at 760 nm. The PGG concentration for each sample was determined by comparing to a calibration curve prepared with known concentrations of PGG. The total amount of PGG obtained for each sample was normalized to the initial weight of the tissue used for methanol extraction.

Enzyme (Elastase and Collagenase) Challenge:

The resistance of the scaffolds to resist enzymatic degradation was determined as a method described previously in Chapter IV (420). Briefly, lyophilized Native, Decellularized and PGG treated decellularized tissues were subjected to treatment by elastase and collagenase enzymes in 1 mM Calcium Chloride (CaCl_2) and 0.02% Sodium Azide (NaN_3) in 100 mM TRIS buffer ($\text{pH } 7.8 \pm 0.05$) for 24 hours and 48 hours respectively at 37°C . The percentage (%) dry weight loss of the scaffolds after enzyme treatment was used as an indication of the resistance of the scaffold to enzyme degradation.

Histological Analysis:

Formalin fixed samples were tissue processed, embedded in paraffin, sectioned at $5 \mu\text{m}$ thickness, mounted on glass slides and heated for 30 minutes to adhere the tissue sections to the slides. Slides were baked overnight at 56°C in an oven. Subsequently, the slides were deparaffinized and stained with hematoxylin and eosin to determine cellular components within the tissue matrix. Tissue sections were also stained with Masson's Trichrome, Verhoeff's-Van Geisen (VVG), and Alcian Blue to visualize the ECM structure of the native, decellularized, and PGG treated scaffolds.

Uniaxial mechanical testing of Bovine Jugular Vein:

Native, decellularized, and PGG treated Bovine jugular vein scaffolds were cut into 2 cm x 1 cm rectangular sections in both the circumferential and longitudinal directions. Uniaxial testing was performed on each section using Instron uniaxial tester (Instron,

Norwood, MA, USA). Samples were pre-loaded to 0.05 N and then stretched at a uniform rate of 1 N/s until tissue failure. The thickness of each sample was assessed before the uniaxial testing procedure. The stress-strain biomechanical characteristics of the scaffolds were analyzed. Tensile stress was calculated by dividing the load sustained by the specimen by the cross-sectional area. The tensile strain was determined by dividing the change in sample length by the original length of the sample. The modulus of elasticity (Young's modulus) was calculated by taking the slope of the stress-strain curve (421).

$$\text{Tensile Stress (MPa)} = \frac{\text{Load sustained in sample}}{\text{Cross sectional area}}$$

$$\text{Tensile Strain} = \frac{\text{Change in sample length}}{\text{Original sample length}}$$

$$\text{Modulus of elasticity (MPa)} = \frac{\text{Tensile Stress}}{\text{Tensile Strain}}$$

Subcutaneous Implantation in rats

PGG treated decellularized and glutaraldehyde fixed native bovine jugular vein leaflets and walls were implanted subcutaneously in 3-4-week-old Sprague Dawley (SD) rats to determine the biocompatibility of the scaffolds. For the surgical procedure, rats were anesthetized with inhalation of isoflurane. Each animal's eyes were instilled with artificial tears to prevent corneal ulcers. Using aseptic technique, one small, 1 cm incision was made on the rat's back. Blunt scissors were inserted into each incision and subcutaneous pockets

were created dorso-laterally by blunt dissection. Pre-prepared implants (PGG treated decellularized/ glutaraldehyde treated native leaflets or walls) were placed into each pouch to study the effects of *in-vivo* calcification. One glut leaflet/wall and one PGG leaflet/wall were implanted in each rat. The wound was closed with surgical staples, and the animals were allowed to recover and housed in animal quarters. At the designated time interval, rats were euthanized, and implants were retrieved. A gross view of the explants was observed for any capsule formation and implant degradation. The implant periods used were 30 days and 90 days. Twenty animals received PGG/ Glut BJV walls, and 20 animals received BJV leaflet implants. The surgical procedure has been schematically represented in Figure 37.

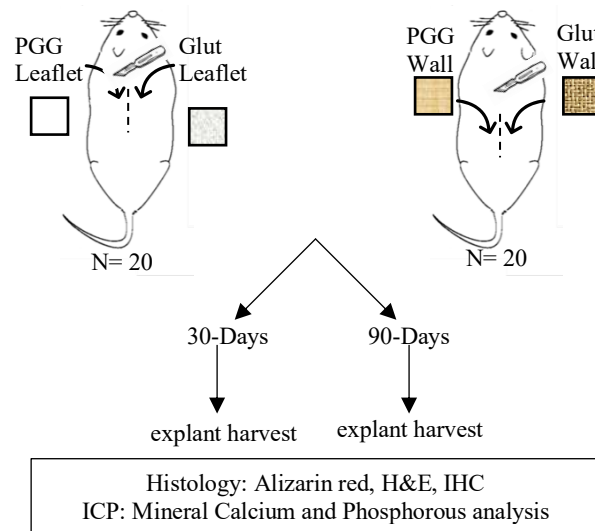


Figure 37: Schematic representation of subcutaneous implantation of BJV walls and leaflets in rats

ICP Calcium and Phosphorous mineral analysis:

Capsules (if any) were removed from the explants harvested subcutaneously from rats. Samples were frozen at -80°C, and lyophilized. Measured dry weights were hydrolyzed in 2 mL 6 N HCl overnights at 37°C. Acid hydrolyzed samples were dried under nitrogen gas at 96°C, and the residues were resuspended in DI water. Resuspended samples were filtered to remove any solid particles. The elemental calcium and phosphorous within the samples were analyzed with ICP Spectrometer (SPECTRO Analytical Instruments, Kiev, Germany) (422). Resuspended samples were diluted, wherever required, and the Ca/P content was normalized to the dry weights.

Immunohistochemical (IHC) analysis:

Histological tissue sections were deparaffinized, followed by antigen retrieval using a citrate heat-conducting method. Sections were permeabilized with 0.1% triton, and non-specific binding was blocked using the Background buster (Innovex Biosciences NB306). Peroxidase blocking was performed with 3% Hydrogen peroxide (H₂O₂) in the case of DAB (diaminobenzidine) detection system, followed by endogenous biotin blocking (Avidin/ Biotin blocking kit, Vector SP 2001). Sections were incubated with primary antibodies overnight at a dilution of 1:100 (or according to manufacturer recommendation) in 1% BSA (Bovine Serum Albumin) and 0.01% azide in PBS at 4°C. After overnight incubation and washing, sections were incubated with secondary antibodies labeled with DAB or fluorescent tag for 1 hr at room temperature, followed by appropriate nuclear staining, mounting, and imaging (Keyence BZ-X810). Inflammatory

responses in the explants were evaluated using immunohistochemistry for CD 3-T cells, CD 11c dendritic cells, and macrophage marker CD 68. Sectioned were also stained for Vimentin and α -Smooth Muscle Actin (α SMA) to determine infiltration of fibroblasts and myofibroblasts (423, 424). Collagen remodeling and new collagen formation were determined using Heat Shock Protein 47 (HSP-47) staining (425).

Implantation of PGG treated Bovine Jugular Vein conduits as pulmonary conduit replacement unit in sheep²

Three PGG-treated BJV tricuspid conduits were implanted in one sheep for one month and two sheep for three months. A cardiopulmonary bypass procedure was performed to resect the native pulmonary valve leaflets and main pulmonary artery. PGG treated decellularized bovine jugular vein valved conduit was used to replace the resected native tissues. Sheep were monitored for cardiopulmonary function throughout the implant period. At the end of one-month or two-months, animals were heparinized to prevent post-mortem thrombosis and then euthanized with pentobarbital sodium (80-100 mg/kg, IV). The gross view of explants was analyzed, and subsequently explants were analyzed histologically and using IHC to determine cellular infiltration. The conduits were also measured pre- and post-implant to determine any change in size of the conduits.

² Sheep Implant surgeries performed by Dr. John E. Mayer at Boston Children's Hospital

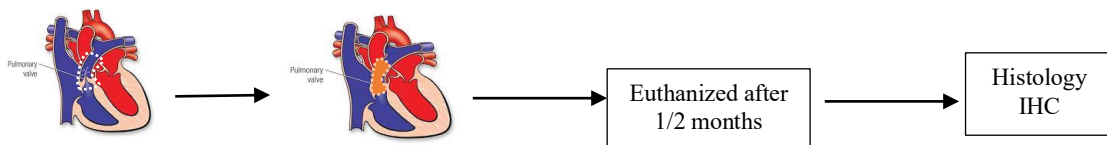


Figure 38: Schematic representation of PGG treated BJV conduit replacement in sheep

Statistical Analysis:

All *in-vitro* experiments were done in triplicates or more. The data was reported as the Mean \pm Standard Deviation. Data from different groups were analyzed by one-way analysis of variance (ANOVA) followed by Tukey’s HSD. All statistical analysis was done using JMP® Pro 15.2.0. Significance was reported at three different significance levels: *** $p \leq 0.01$, ** $p \leq 0.05$, * $p \leq 0.1$. Statistical significance has been reported in each result.

5.3 Results

Optimization of PGG concentration:

PGG quantification of the PBS solutions used for washing showed decrease in the un-used PGG with every wash until wash 9, indicated in Table 5. The final BJV conduits stored in fresh PBS with Pen/Strep antibiotics had $<25 \mu\text{g PGG/ ml}$ of PBS buffer which should not interfere with the PGG quantification done for the treated tissues subsequently.

PGG	Wash 1	Wash 2	Wash 3	Wash 4	Wash 5	Wash 6	Wash 7	Wash 8	Wash 9
0.05%	1152.80	113.98	9.96	5.14	4.62	2.41	1.76	6.19	1.11
0.15%	1791.07	59.27	17.26	12.83	17.52	4.88	6.19	6.58	1.37
0.25%	2989.46	90.53	23.77	17.52	20.65	10.22	7.10	6.06	2.54

0.55%	8759.98	8.47	44.09	34.32	35.23	18.43	14.26	11.66	4.36
0.85%	7783.03	120.49	31.72	27.68	54.25	28.20	20.38	7.23	6.32
1%	10231.92	282.01	152.08	49.43	71.58	35.89	23.25	19.08	11.66
2%	19245.91	278.10	83.69	41.75	69.10	36.28	30.41	21.43	14.78
3.33%	32493.36	632.41	85.25	37.97	90.99	67.93	41.36	36.02	24.68

Table 5: PGG Quantification in PBS wash solutions: μg PGG/ ml of PBS buffer (All values rounded up to 2 decimal places)

Quantification of PGG within the lyophilized BJV treated with 0.05% - 3.33% PGG demonstrated PGG concentrations ranging from 20-60 μg of PGG/ mg dry weight of tissue (Figure 39). This value was significantly higher than the control decellularized and native tissues. No significant difference was found in the PGG concentration for treatments 0.05% PGG – 0.55% PGG. BJV treated with 0.55% PGG had the highest concentration of extracted PGG with an average of $46.2 \pm 18.9 \mu\text{g}$ PGG/ mg tissue. This value was significantly higher than groups treated with 0.85% PGG, 1.0% PGG, and 2.0% PGG, where the average values were $25.7 \pm 3.4 \mu\text{g/ mg}$, $21 \pm 12.7 \mu\text{g/ mg}$, and $24.2 \pm 2.9 \mu\text{g/ mg}$ tissue weight respectively (Figure 39).

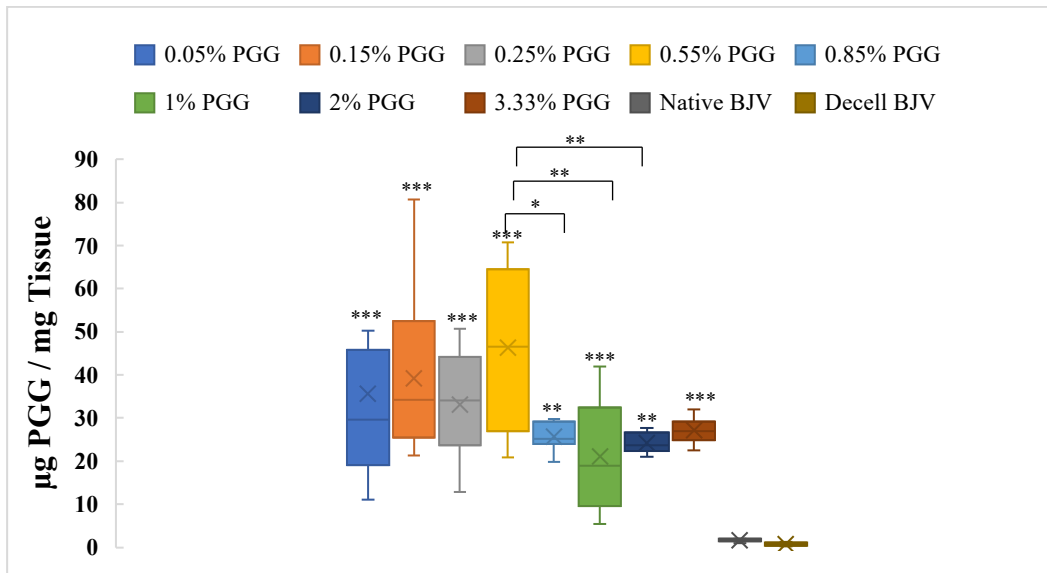


Figure 39: PGG quantification in Methanol extracts from BJV tissues treated with different concentrations of PGG (***, **, *: Indicates different levels of significance between groups and native/decellularized tissues, and among groups) N=5

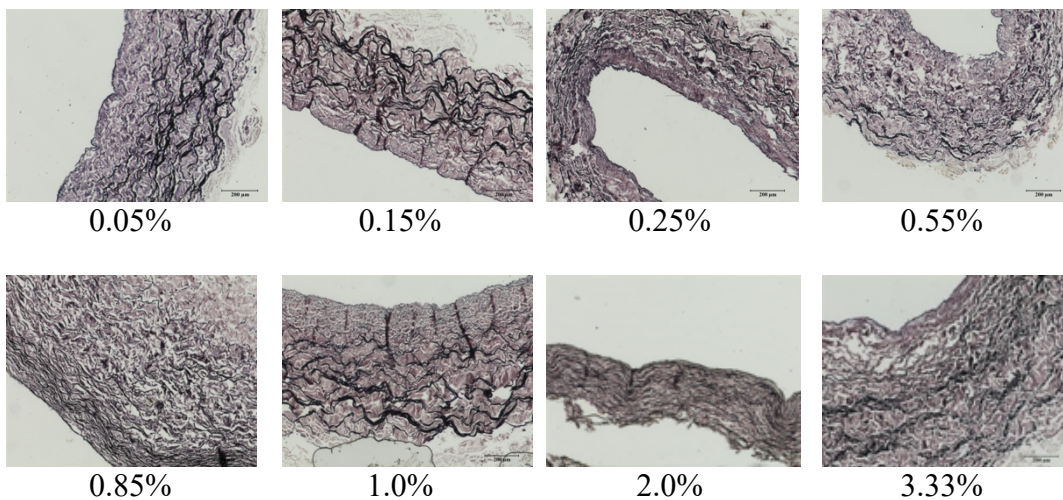


Figure 40: VVG staining of BJV treated with different concentrations of PGG showing preservation of elastin within scaffold matrix

Histological analysis of decellularized BJV treated with PGG concentrations ranging from 0.05% - 3.33% demonstrated the maintenance of the elastin structure within the extracellular matrix of the scaffolds (Figure 40). The gross view of the scaffolds have been demonstrated in Figure 41.

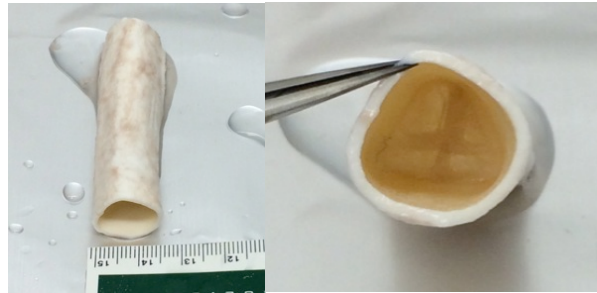


Figure 41: Gross view of PGG treated decellularized Bovine Jugular Vein Conduit

Elastase enzyme digestion of BJV scaffolds treated with 0.15% - 3.33% PGG demonstrated a significant decrease in % loss of dry weight compared to the native and decellularized tissues. The % weight loss of native and decellularized control groups ranged from 25% - 45% decrease in dry weight of tissues. 0.05% PGG treated BJV had an average of $25.7 \pm 3.3\%$ decrease in weight loss, which was not significantly different from the control groups (Figure 42). This value was also significantly higher than those for the other concentrations of PGG. BJV treated with 0.15% - 3.33% PGG demonstrated average weight losses ranging from 9% - 20%. No significant difference was observed among any of the PGG treatments within this range.

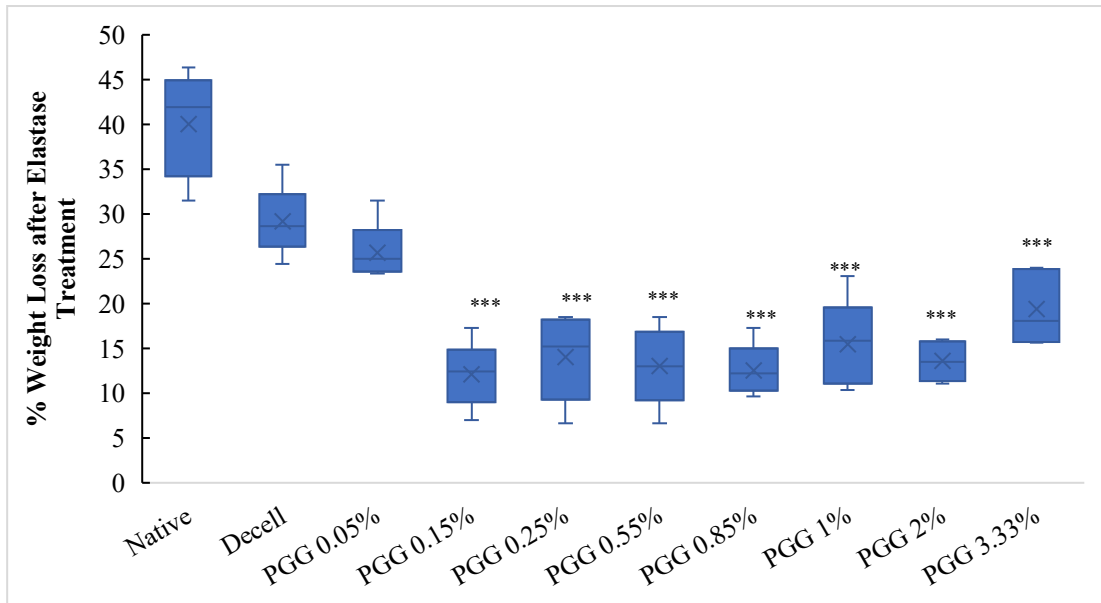


Figure 42: Elastase treatment of BJV conduits treated with different concentrations of PGG. (***: Indicates significance levels of difference in % weight loss) Significant decrease in % weight loss compared to Native, Decellularized, and 0.05% PGG treated group; N=5

Collagenase challenge on the PGG treated BJV also demonstrated a significant decrease in % weight loss for the treated groups compared to native and decellularized tissues. In this case, the 0.05% PGG treated BJV also had significantly lower weight losses than the control groups. The weight loss for the decellularized and native tissues ranged from 72% - 96%. The value for the 0.05% PGG was $41.4 \pm 28.3\%$. Weight losses for PGG treatments 0.15% - 3.33% ranged from 0.1% - 15%. These values were significantly lower than the control groups as well as the 0.05% PGG treated BJV. No significant difference

was observed within the range of 0.15% - 3.33% PGG treatments for collagenase treatment (Figure 43).

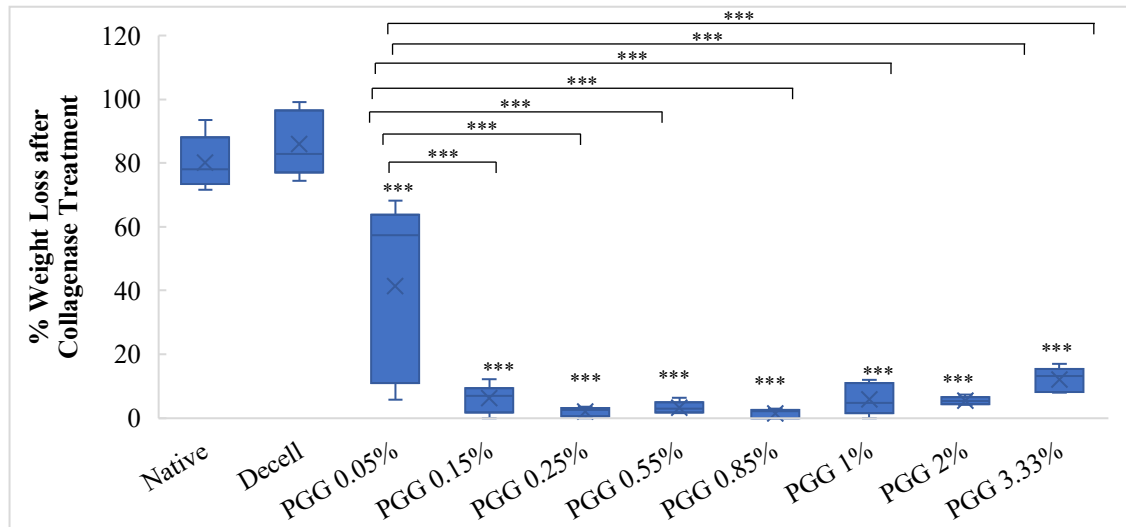


Figure 43: Collagenase treatment of BJV conduits treated with different concentrations of PGG. (***) Indicates significance levels of difference in % weight loss) Significant decrease in % weight loss compared to Native, Decellularized, and 0.05% PGG treated group' N=5

Histologically, 0.15% PGG treated decellularized BJV scaffolds demonstrated presence of elastin, collagen, and GAGs within the scaffold extracellular matrix (Figure 44). The arrangement and structure of ECM components was similar to those observed in native BJV tissues.

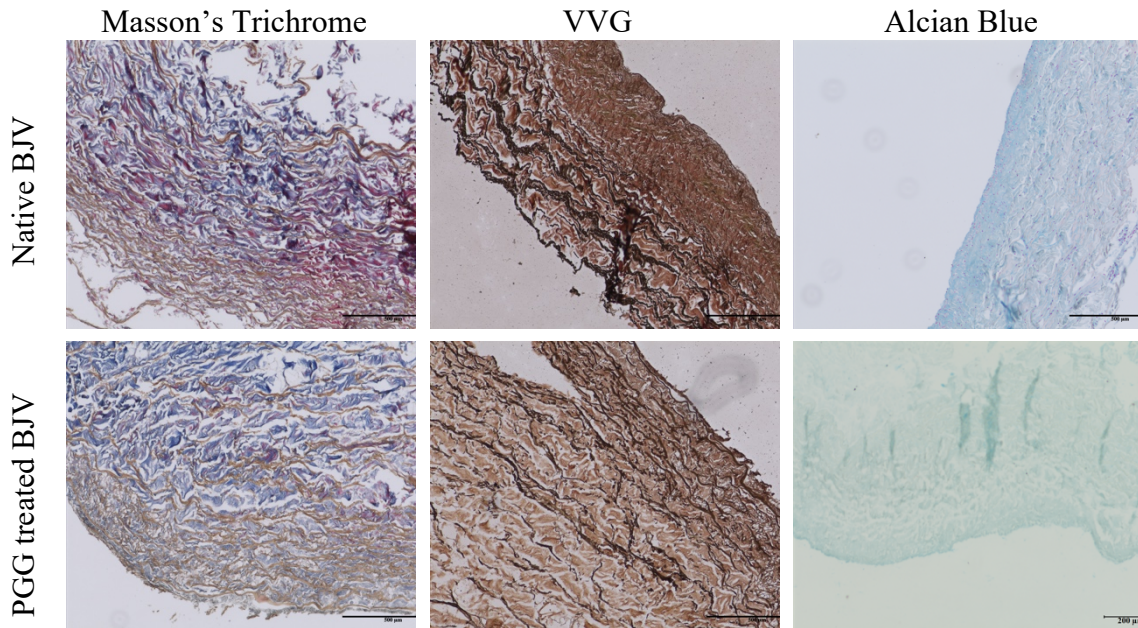


Figure 44: Native and PGG treated decellularized Bovine Jugular Vein Histology

Storage potential of PGG treated Bovine Jugular Vein:

Methanol extraction and quantification of PGG from BJV tissues treated with 0.15% PGG and stored for up to 24-months demonstrated PGG content ranging from 25 μg PGG/ mg – 55 μg PGG/ mg dry weight of tissue. Decellularized BJV demonstrated PGG concentrations of 0.08 ± 0.15 $\mu\text{g}/\text{mg}$. 0.15% PGG treated BJV had PGG concentrations of 29.3 ± 10 $\mu\text{g}/\text{mg}$, 28.8 ± 9.7 $\mu\text{g}/\text{mg}$, 41.2 ± 15.9 $\mu\text{g}/\text{mg}$, 55.5 ± 25.8 $\mu\text{g}/\text{mg}$, and 34.5 ± 16.1 $\mu\text{g}/\text{mg}$ for storage periods of 0 months, 6 months, 9 months, 13 months, 16 months, and 24 months respectively. The PGG concentrations obtained for the treatment groups were significantly higher compared to the control decellularized tissues. However, no significant difference was observed among PGG treated BJV tissues stored

in PBS for 3 months, 9 months, 13 months, 16 months, 24 months, and freshly prepared PGG treated BJV (Figure 45).

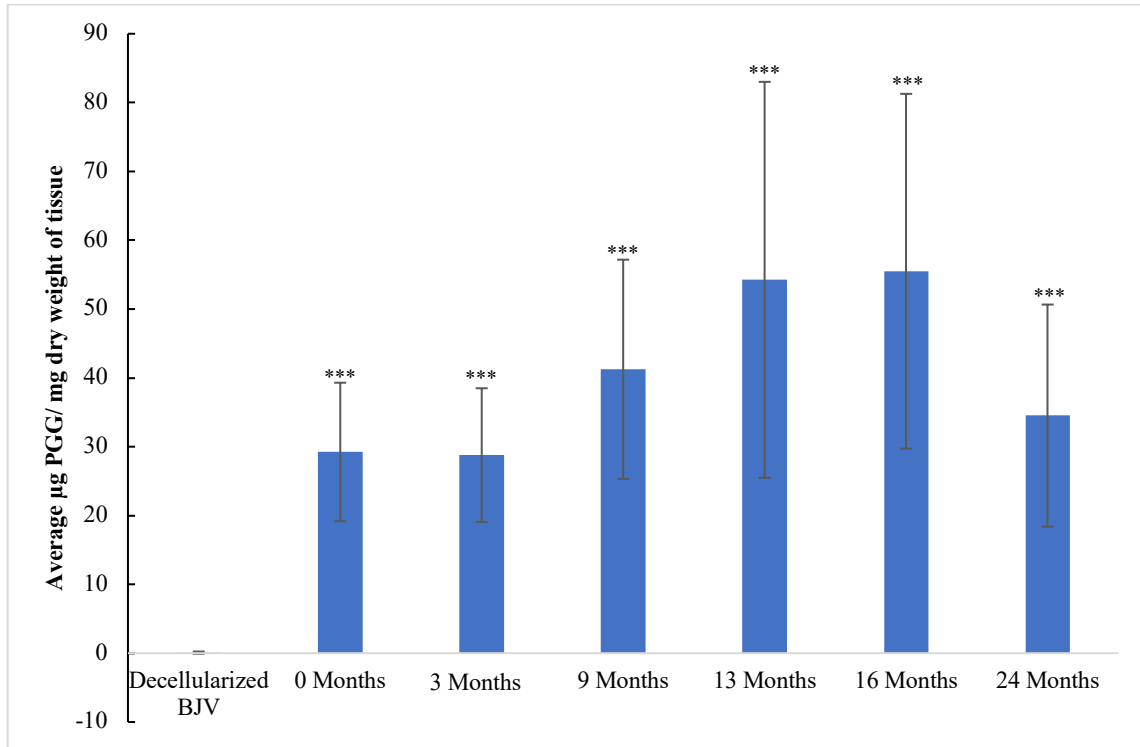


Figure 45: µg PGG/ mg dry weight of tissue for Bovine Jugular Vein Conduits stored for up-to 24-months; (***) Statistically significant difference in PGG concentration compared to decellularized tissues. No significant difference among groups.); N=8

Elastase treatment of the PGG treated BJV tissues demonstrated a significant decrease in weight loss after elastase treatment compared to the decellularized BJV. The weight loss for the Decellularized tissues was $27.6 \pm 6.3\%$, while for the PGG treated tissues, the weight loss values were $15.8 \pm 3.2\%$, $16.1 \pm 4.3\%$, $12.8 \pm 2\%$, $17.5 \pm 1.2\%$, 15

$\pm 3.2\%$, and $17.4 \pm 1.5\%$ for freshly prepared BJV, BJV stored for 3 months, 9 months, 13 months, 16 months, and 24 months respectively (Figure 46). There was no significant difference between the % dry weight losses among the freshly prepared PGG treated BJV, and those stored for up to 24 months in sterile PBS with Pen/Strep at 4°C.

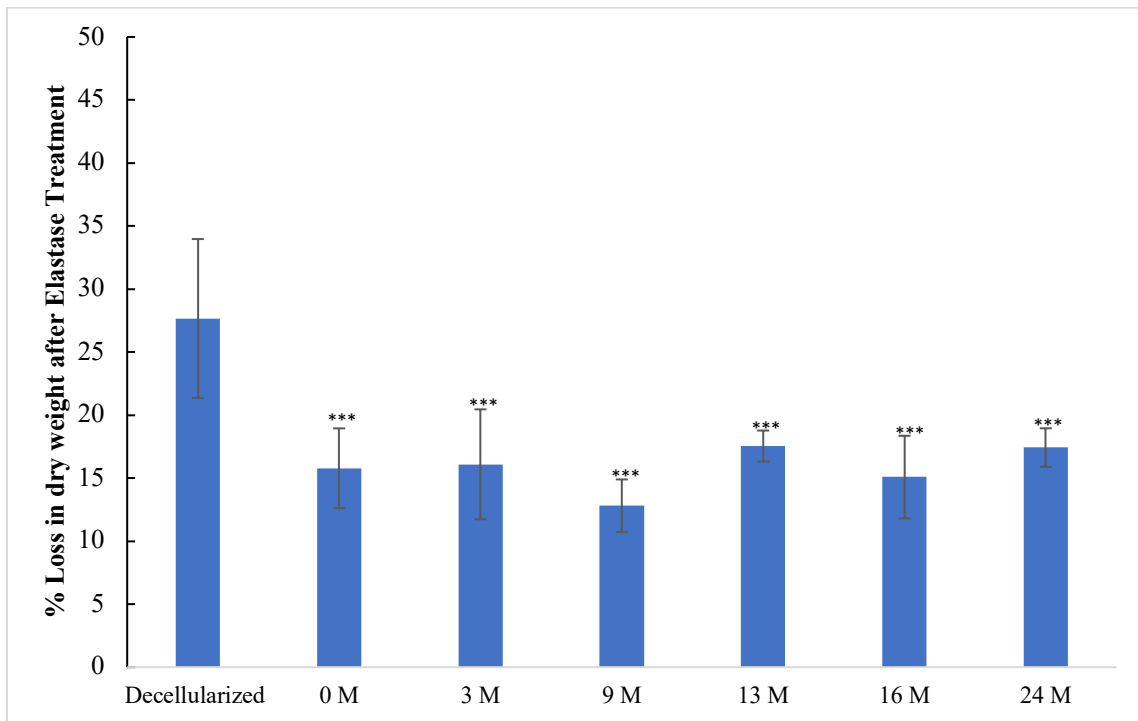


Figure 46: Elastase Challenge with 0.15% PGG treated Bovine Jugular Vein tissues stored for up-to 24-months (***) Statistically significant difference compared to decellularized BJV); N=8

Uniaxial Testing of BJV scaffolds:

The maximum stress required for tissue failure was comparable in native, decellularized, and PGG treated BJV scaffolds. In native BJV, the maximum stress was

$37.6 \pm 21.2 \times 10^5$ Pa in the circumferential direction and $21.6 \pm 19.4 \times 10^5$ Pa in the longitudinal direction. In decellularized scaffolds, these stresses increased to $41.5 \pm 8.9 \times 10^5$ Pa and $27 \pm 16.3 \times 10^5$ Pa in the circumferential and longitudinal directions, respectively. PGG treated scaffolds had maximum stresses of $47.4 \pm 14.1 \times 10^5$ Pa and $30.4 \pm 4 \times 10^5$ Pa in the circumferential and longitudinal directions, respectively (Figure 47.A). There was no significant difference, however, in the maximum stresses between the two directions or among the different groups (native, decellularized, and PGG treated).

The maximum strain at failure was 18.4 ± 9.2 and 27 ± 2.9 for the native BJV in the circumferential and radial directions. In decellularized scaffolds, the respective strains were 24.5 ± 1.4 and 31.6 ± 7.5 , and in PGG treated decellularized scaffolds, the circumferential and longitudinal strains for failure were 20.3 ± 5.7 and 28.3 ± 2 . There was no significant difference in the maximum strain at failure between the circumferential or longitudinal directions or between different treatments (Figure 47.B).

The peak tangent modulus, calculated from the maximum slope of the stress-strain curve for each sample was consistently higher in the circumferential direction compared to the longitudinal direction for native, decellularized, and PGG treated decellularized BJV. The peak tangent modulus was 4.7 ± 1.45 MPa in the circumferential direction and 2.37 ± 2.39 MPa in the longitudinal direction for native BJV. In decellularized BJV, the peak moduli were 3.19 ± 2.27 MPa in the circumferential direction and 1.78 ± 0.66 MPa in the longitudinal direction. PGG treated decellularized BJV had peak tangent modulus values of 4.66 ± 1.59 MPa and 1.36 ± 0.44 MPa in the circumferential and longitudinal directions

respectively. No significant difference was observed within the peak modulus in either directions or between the native, decellularized, and PGG treated groups. (Figure 47.C)

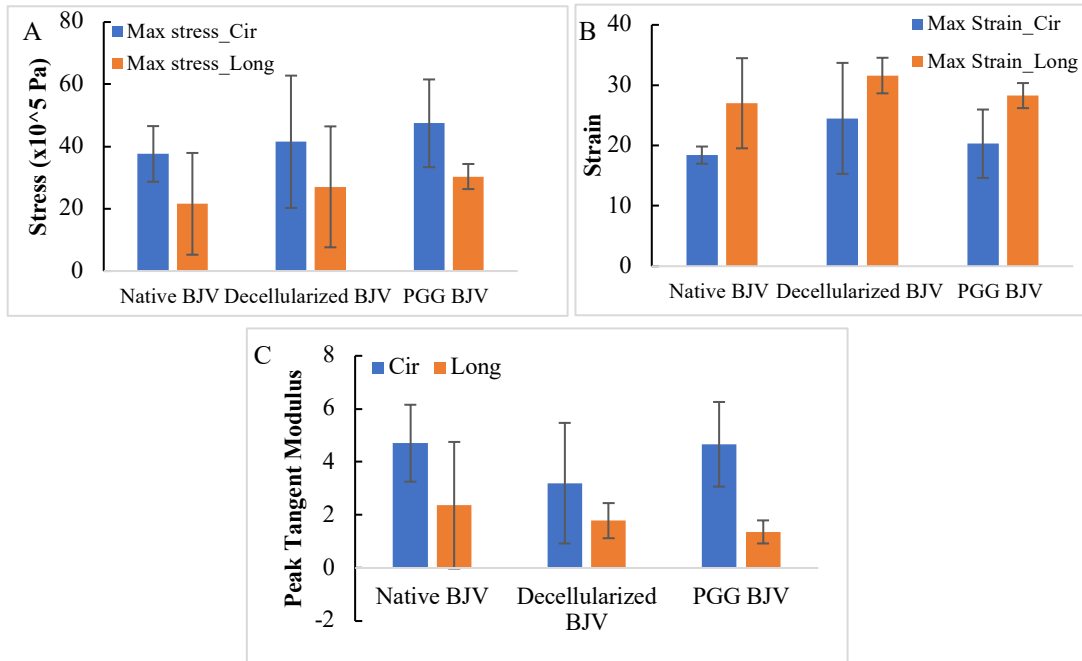


Figure 47: Maximum (A) stress, (B) strain and (C) Peak Tangent Modulus in native, decellularized, and PGG treated decellularized BJV scaffolds for failure in uniaxial testing; No significant difference observed among the groups; N=5

Subcutaneous Implantation in rats:

PGG treated BJV wall and leaflet subcutaneous implants in sheep demonstrated degradation of the implanted scaffolds after 30-days, and 90-days of implant. There was very less capsule formation around the PGG treated scaffolds. Glutaraldehyde treated tissues, on the other hand, developed thick capsules around the implanted tissues, with minimal degradation.

Alizarin red staining of the PGG treated decellularized wall and leaflets portions demonstrated no calcification within the implanted scaffolds, whereas all the glutaraldehyde treated tissues had heavy calcification within both the leaflet and wall regions (Figure 48).

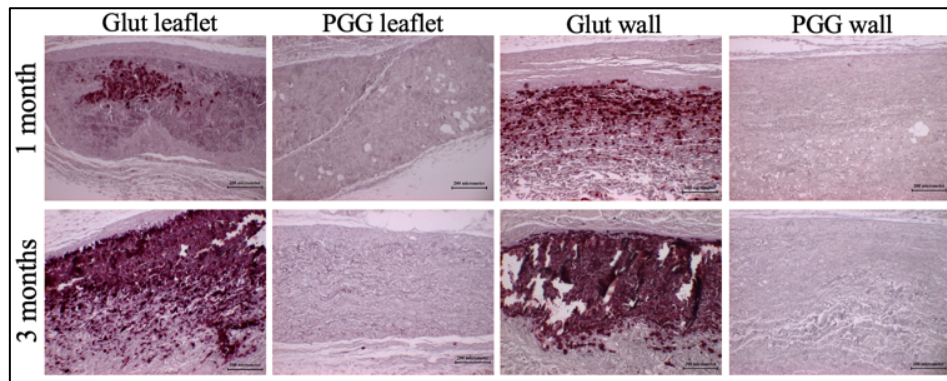


Figure 48: Alizarin red staining of 1-month, and 3-month subcutaneously implanted PGG treated and Glut BJV

ICP analysis of the PGG and glutaraldehyde implants also demonstrated elevated levels of mineral calcium and phosphorous within the glutaraldehyde tissues compared to pre-implant, whereas for the PGG scaffolds, the mineral concentrations did not alter significantly post-implant (Figure 49).

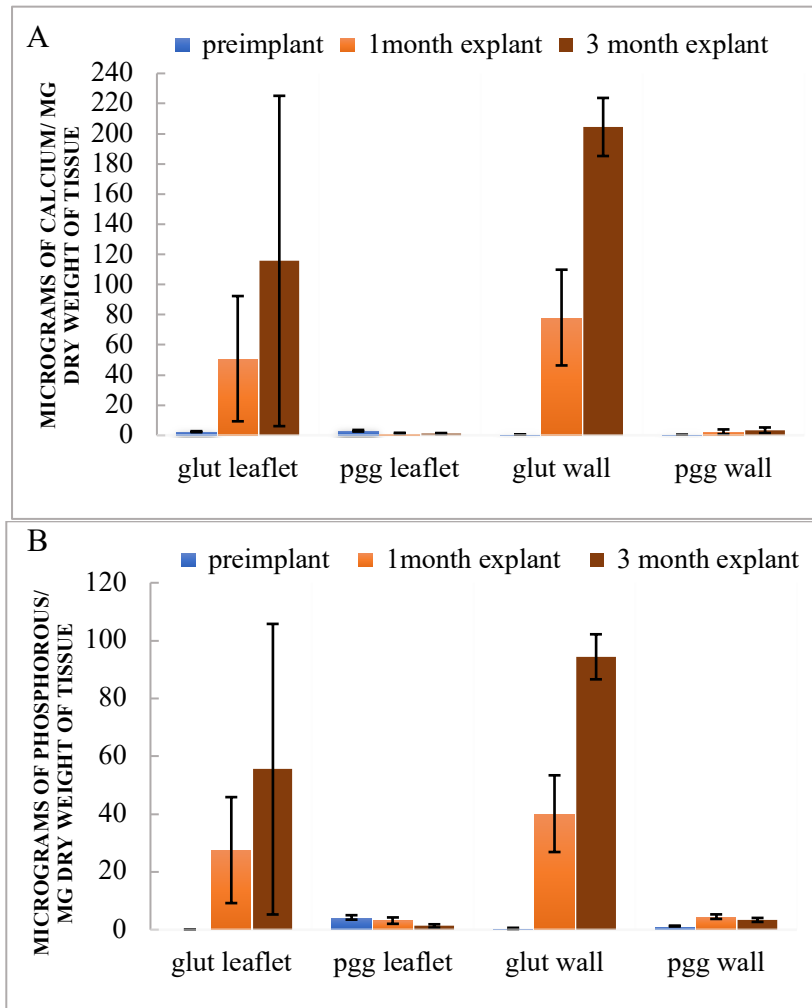


Figure 49: ICP analysis of elemental (A) Calcium and (B) Phosphorous in subcutaneous implanted BJV PGG and Glut walls and leaflets; N=5

H&E staining of glutaraldehyde and PGG treated BJV demonstrated the presence of thick capsules around the glutaraldehyde treated implants, while less or no capsules were present around the PGG implants. Additionally, within the PGG implants, fibroblasts were found within the implant interstice, with the interstice resembling fat or connective tissue, with presence of microvesicles (Figure 50). Table 6 represents the Jansen grading of the

glutaraldehyde and PGG treated implants, demonstrating the superior biocompatibility of PGG scaffolds compared to glutaraldehyde treated tissues.

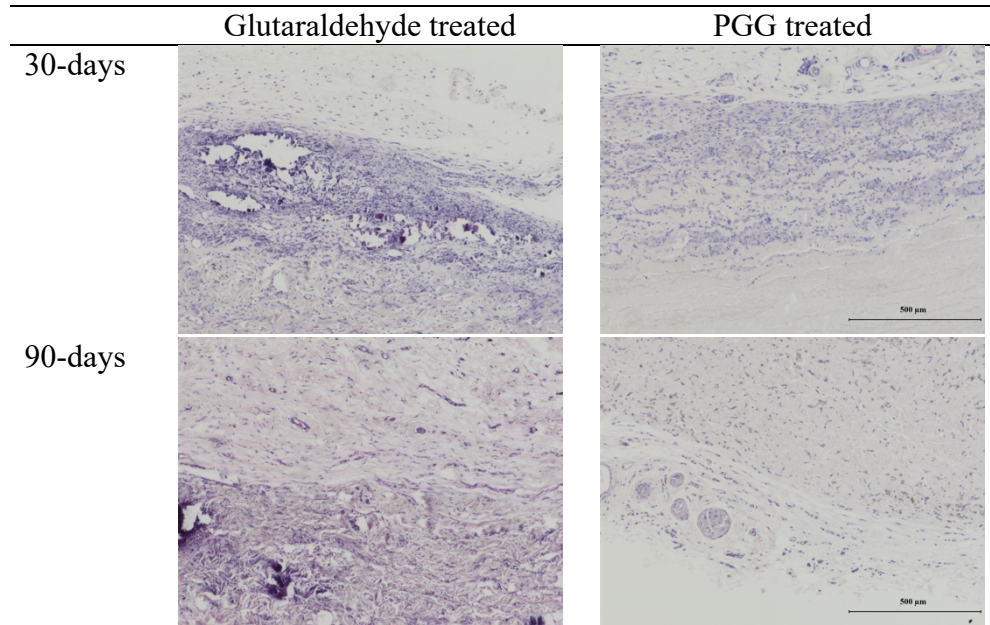


Figure 50: H&E staining of glutaraldehyde and PGG treated BJV subcutaneous explants

	Glut Treated	PGG Treated
Reaction-zone semi-qualitatively	1 (Thick capsule)	4 (1-4 cell layer capsule)
Reaction zone qualitatively	2 (Capsule dense and granulous with fibroblasts and inflammatory cells)	4 (Surrounding tissue not dense, resembling connective or fat tissue)
Interference qualitatively	1 (Multiple layers of macrophages and foreign body cells)	4 (Fibroblasts contact implant surface without foreign body giant cells)
Interstice qualitatively	1 (Tissue in interstitium dense and exclusively inflammatory)	4 (Interstitium tissue fibrous, not dense, resembling fat or connective tissue)
Total Score	5	16

Table 6: Jansen Scoring of Subcutaneously implanted Glutaraldehyde and PGG treated BJV

Hematoxylin and Eosin staining of PGG treated BJV wall implants also demonstrated the infiltration of cells within the scaffolds 30-days and 90-days post implant (Figure 51). Formation of microvesicles were also observed within the 90-day post implant scaffolds.

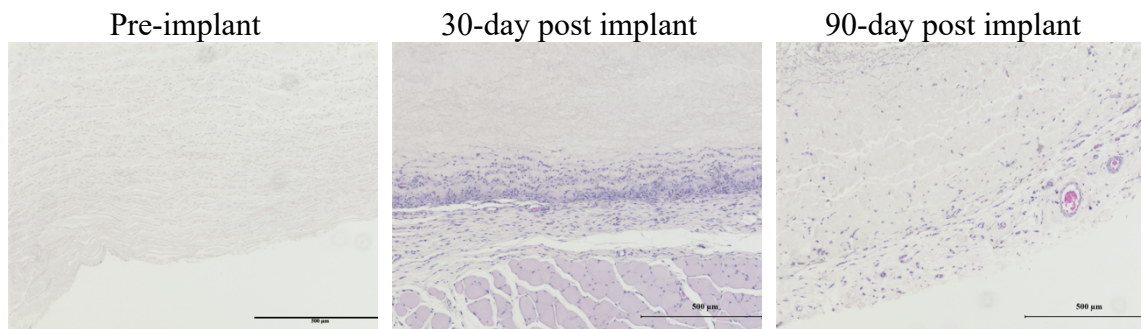
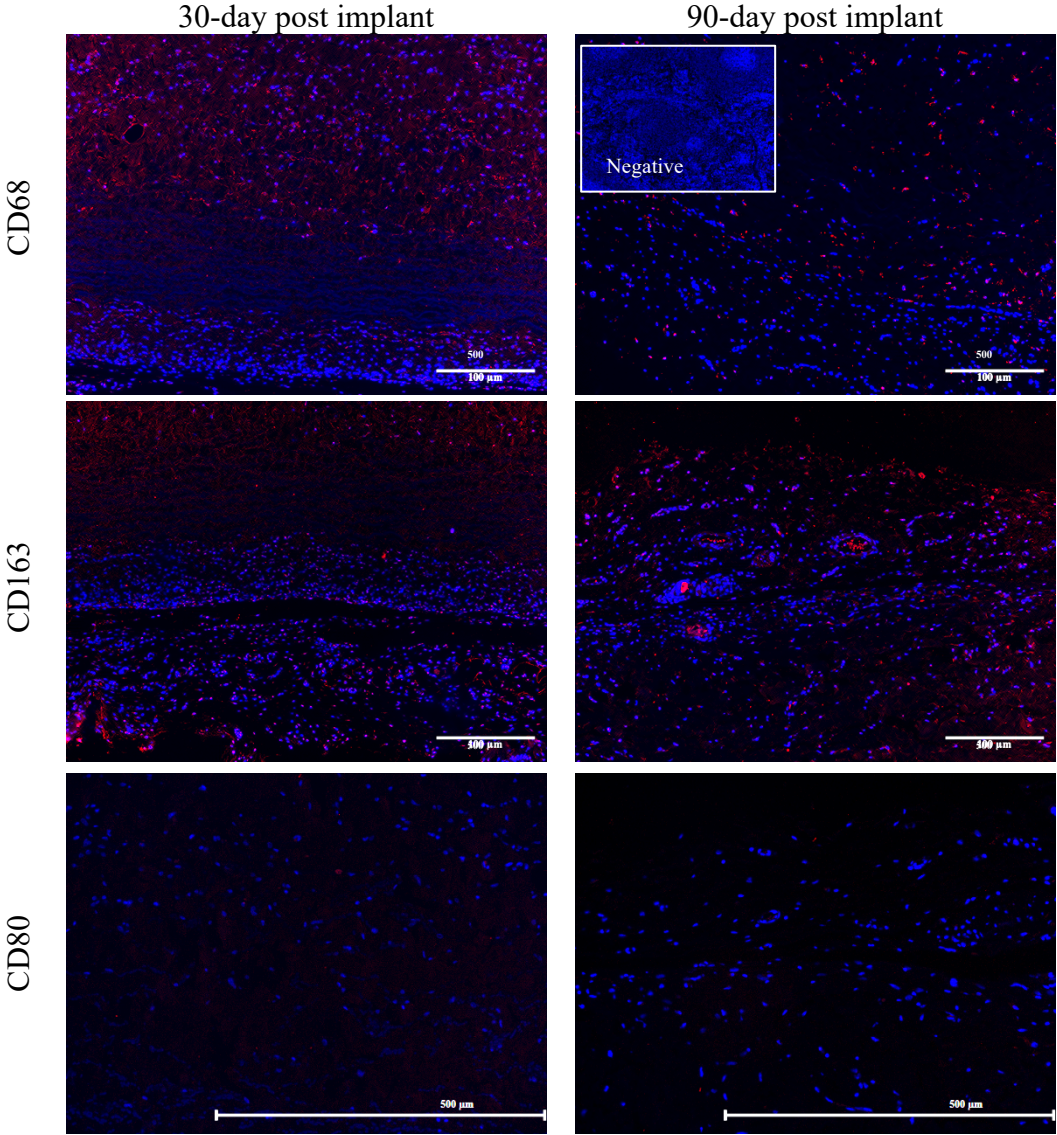


Figure 51: H&E staining of 30-day and 90-day post-implant showing cellular infiltration in subcutaneously implanted BJV

IHC analysis was performed on the explanted BJV walls to determine the types of cells infiltrated within the scaffolds. BJV sections showed the presence of CD68 pan-macrophage antigens. The sections also showed the presence of CD163 anti-inflammatory macrophages, while no CD80 pro-inflammatory macrophage staining was observed. 30-day post-implant scaffolds showed some presence of CD3 T-cells, while the CD3 antigen staining decreased at 90-day post implant. Additionally, no staining was observed for CD11c dendritic cells.

Staining with Vimentin and Alpha-Smooth muscle actin (α -SMA) demonstrated the presence of fibroblast and myofibroblast cells within the subcutaneously implanted scaffolds. The staining was more pronounced at 90-day compared to 30-day post implant.

Representative IHC images of 30-day and 90-day post implant PGG treated decellularized BJV tissues subcutaneously implanted in rats has been shown in Figure 52.



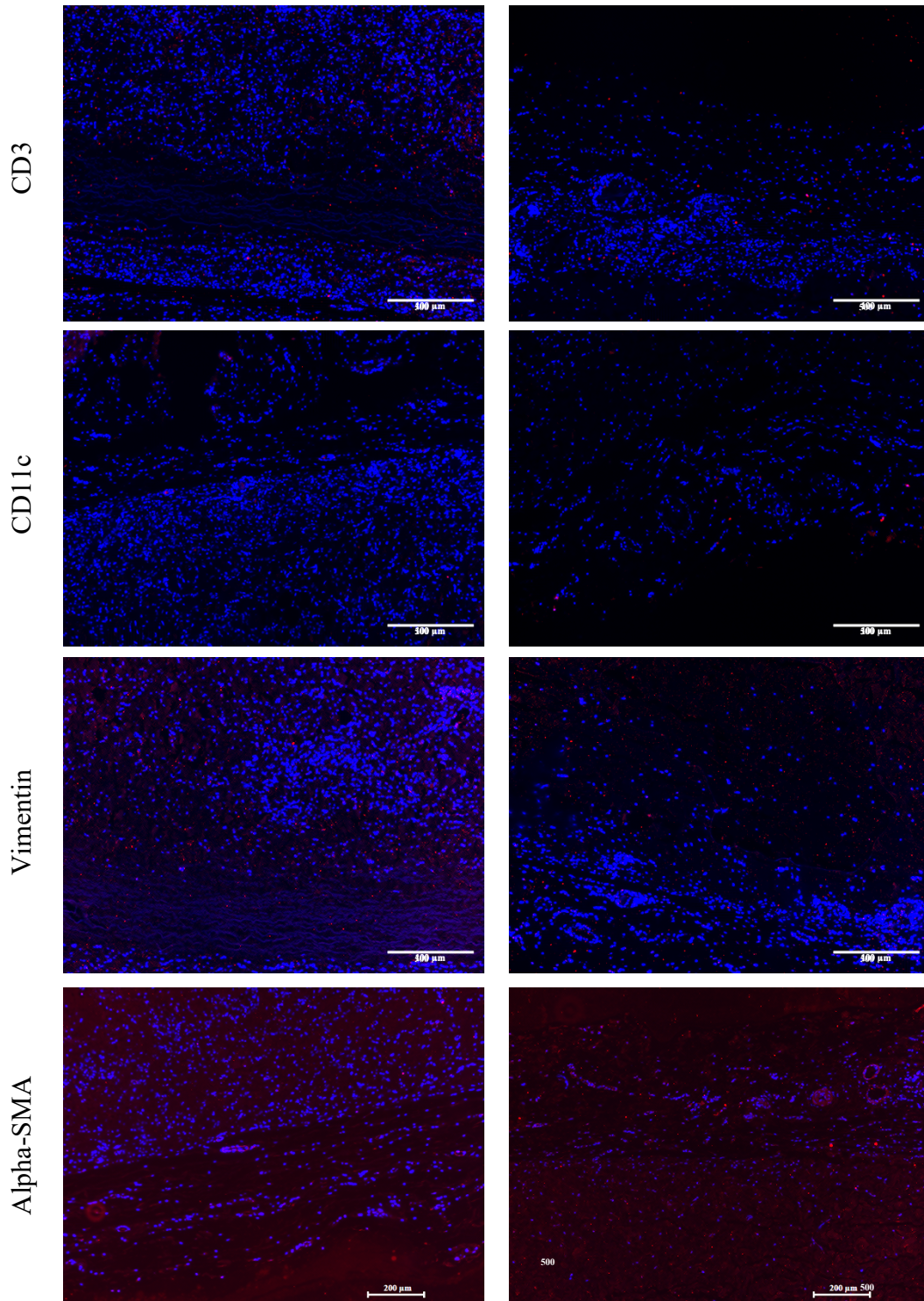


Figure 52: Immunohistological (IHC) staining of subcutaneously implanted BJV Walls

Pulmonary conduit replacement in sheep

PGG treated BJV conduits implanted in sheep as pulmonary conduit replacement units for 1-3 months demonstrated normal functioning of the conduit and valves for the implant period. There was no animal morbidity within the period of the implant. The gross view of the explant showed no thrombus or tissue overgrowth within the implanted conduits. There was no thickening observed in the leaflets within the conduits (Figure 53).

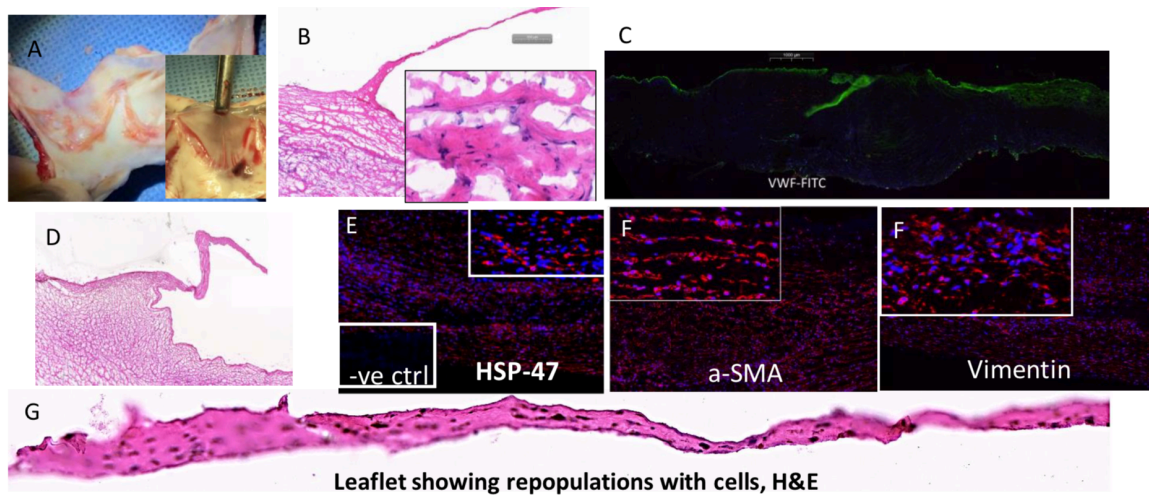


Figure 53: BJV conduits after 3 months of implant showing (A) no tissue overgrowth or thrombosis; (B) cellular infiltration (H&E); (C) Luminal endothelialization shown by VWF staining; (D) No calcification shown by Von Kossa staining; (E) HSP-47 staining for collagen; (F) SMA and (F) Vimentin staining showing infiltration of myofibroblast-like cells in the walls; (G) Leaflet showing cellular infiltration and no thickening

Histological analysis of the explanted conduits demonstrated infiltration of cells within the scaffolds. No calcification was observed by Von Kossa staining of the explants. Immunohistochemistry analysis on the explants showed the presence of endothelial cells along the conduit lumen, as well as fibroblast and myofibroblast-like cells (indicated by

positive staining for Vimentin and α -SMA). The explants also stained positive for HSP-47, indicating collagen remodeling within the tissues (Figure 51).

Additionally, size measurements on the PGG treated conduits done before and after the 3-month implants showed an increase in the size of the outer diameter and length by 10%.

5.4 Discussions

Bioprosthetic pulmonary conduit replacements have been traditionally produced out of native tissues like pericardium, sub intestinal mucosa (SIS), or jugular veins (426). The main advantages of bovine jugular vein valved conduits are the continuity between the valves and conduits and its off-the-shelf availability in pediatric sizes (427). The valved conduits have a structure similar to typical vein tissues, making them adequate to function in a low-pressure system (428). Moreover, the distal and proximal ends of the conduits allow for extended reconstructive procedures (429).

It has been shown that incomplete graft decellularization might result in severe foreign body reaction directed towards graft leaflets (430). Optimum decellularization process of BJV tissues was developed in Chapter IV with final DNA concentrations of <50 ng/ mg tissue dry weight. The PGG concentration for optimum elastin and collagen crosslinking was established in this study. PGG treatment with concentrations > 0.15% demonstrated optimum crosslinking of the ECM components without any significant increase in resistance to enzyme degradation with increasing PGG concentration. The stability of the PGG treatment was also established by the ability of the treated scaffolds to

resist enzyme degradation after extended storage. For the developed scaffolds to be used as easily accessible, off-the-shelf biomaterials, it is important for them to maintain their properties after extended periods of storage. The result from this study indicates even after storage for up to 2 years, there was no significant loss of PGG from the scaffolds, as the enzyme resistance for stored scaffolds was not significantly different from those of freshly prepared scaffolds. Differences in the PGG concentration in methanol extracts obtained from different batches of prepared tissues might be due to the batch-to-batch differences in the tissue characteristics or some un-uniformity in the time used for the PGG crosslinking treatment. The PGG treatment was done for 20 ± 2 hours for all batches, but minor differences in treatment time might have been a contributing factor.

Uniaxial mechanical testing demonstrated no significant difference between the maximum stress and strain at failure between native, decellularized, and PGG treated decellularized tissues. While using a replacement graft, it is desired that the mechanical property of the implanted graft is not different from the native tissue being replaced (426). The tensile strength of the human pulmonary artery demonstrated values of 0.95 ± 0.37 MPa. The strain at failure is reported to be at 1.61 ± 0.52 mm/mm (431). The mechanical characteristics of the PGG treated decellularized tissues satisfy this criterion. It is important to note, however, the mechanical strength of the material is not the sole indicator of implant stability after implantation. Mechanical characteristics of decellularized scaffolds were comparable to the other groups as well. However, they are susceptible to elastase and collagenase degradation (432, 433). Therefore, even though decellularized tissues might have optimum mechanical properties at implantation, due to enzyme degradation, they

might be more susceptible to degradation after implantation compared to PGG treated scaffolds.

Calcification and stenosis in implanted pulmonary valved conduits constitute a significant concern for pediatric patients. Glutaraldehyde fixed xenografts, and allograft tissues have been shown to be prone to calcification upon implantation. Many studies have looked at anti-calcification treatment of glutaraldehyde treated tissues to reduce calcification after implantation (194, 434). However, the long-term results of these treatments remain to be seen. Decellularization has been identified to reduce calcification in both homograft and xenograft tissues (13). Subcutaneous implantation in rats is a standard procedure for the determination of biocompatibility and calcification of biomaterials (434-437). The formation of capsules around subcutaneously implanted materials indicates the ability of the material to be incorporated within the body. Glutaraldehyde-fixed native tissues in this study showed the development of thick capsules around the implants; PGG treated scaffolds, however, did not show extensive capsule formation and demonstrated degradation and re-integration within the surrounding tissues, showing their superior biocompatibility.

Moreover, the PGG treated scaffolds at 30-days, and 90-days post-implant demonstrated little presence of inflammatory cells. CD68 positive cells were present, but most were also stained positive for CD163, indicating most of these macrophages were anti-inflammatory. No dendritic cells or T-cells were observed within the implants. Moreover, the implants showed the presence of fibroblasts and myofibroblasts within the scaffolds. Additionally, no calcification was observed within the PGG treated implants. It

has been established that the principal regions of calcification are the native cells present within the implanted tissues. Glutaraldehyde fixed native tissues, therefore, demonstrated extensive calcification, with an increase in the calcium and phosphorous levels from 30-days to 90-days post-implant.

Sheep implant studies further demonstrated infiltration of cellular components within the decellularized PGG treated scaffolds. More than 90% of the infiltrated cells were determined to be fibroblast and myofibroblast-like cells with very little inflammatory cells. Moreover, endothelial cells were observed along the luminal side of the implanted conduits. This indicates hemocompatibility of the PGG treated decellularized tissues after implantation. Additionally, the explanted tissues demonstrated the presence of HSP-47. HSP-47 is an indicator of collagen remodeling within the implanted scaffolds. Their presence indicates the production of new Type I and type II collagen within the implanted tissues. This would indicate remodeling of the conduits after implantation. Cellular infiltration along with remodeling of the implants are an essential feature of the capacity of the scaffolds to grow along with the patients.

5.5 Conclusions

In this aim, PGG treated decellularized BJV conduits were successfully developed from the native tissues. The concentration of PGG treatment required for imparting resistance against elastase and collagenase enzymes was optimized at 0.15%. The potential of the PGG treated BJV tissues to be stored for extended periods of time was also established. In-vitro mechanical studies demonstrated that the PGG treated

scaffolds were not significantly different from that of the native tissues. Biocompatibility analysis of the PGG treated scaffolds in subcutaneous implant models demonstrated the ability of the scaffolds to resist calcification and allow cellular infiltration. Sheep implant studies of PGG treated BJV conduits demonstrated the potential of these conduits to be used as pulmonary conduit replacement units, allowing cellular infiltration from the host and with a potential to grow along with the patients.

CHAPTER SIX

SPECIFIC AIM 3: DEVELOPMENT OF TISSUE ENGINEERED VALVE LEAFLET PATCH FOR PULMONARY VALVE REPAIR IN PEDIATRIC PATIENTS

6.1 Introduction

Congenital heart diseases (CHD) affect approximately 40,000 new-borns each year in the US. The total number of patients now living with congenital disorders is estimated to be approaching 2 million (1). When the pulmonary valve is affected by congenital disease, specifically resulting in valve stenosis or valve regurgitation, surgery is required to correct the impaired hemodynamics (438-442). Whenever possible, valve repair is preferred over valve replacement for the pediatric population since the available valve devices are far from optimal for young patients. Mechanical valves require the use of life-long anticoagulation therapy while bioprosthetic valves degenerate very rapidly in young patients and are recommended only in patients above 50 years of age (443). The benefits of valve repair over replacement include reduced risk of infection, thrombosis, and lower rate of future reoperations. However, all valves cannot be repaired, and heart valve repair surgery is often more complicated than valve replacement. The benefits of ‘valve-sparing’ surgery, with the ability to preserve the patient’s own native valvular structure, with the elimination of life-long blood thinning medications, outweigh the overall complication of the surgical procedure.

Pulmonary and aortic valve repairs are required for pediatric patients diagnosed with conditions of tetralogy of fallot, which includes malformed pulmonary valve,

pulmonary stenosis, and pulmonary atresia There is an additional group of patients with prior repair of tetralogy of fallot and pulmonary valve regurgitation (also called valve insufficiency or leaky valves). This group, comprising the largest group, currently receive bioprosthetic valves surgically or by catheterization. However, the longevity of these pulmonary valve replacements is limited. All current replacement material has significant limitations, resulting in multiple reoperations throughout the patient's life potential (444). Glutaraldehyde crosslinked pericardium tissue (as used in the Ozaki procedure) or xenograft materials are challenging to prepare and need highly skilled surgeons (188). Glutaraldehyde treated pericardium also lacks the native tri-layer structure of valves, and do not have tissue growth or repair potential since it is not living tissue (acellular) (445, 446). Decellularized tissue material developed from porcine intestinal submucosa (CorMatrix) has been tried as leaflet patch repair material but without much success (447)

To overcome valve calcification, stenosis, and thrombosis, porcine valve leaflet replacement units were prepared from PGG treated porcine aortic or pulmonary valve leaflet with attached wall (Figure 54). The rationale for this was that decellularization would remove the principal sites of immunogenicity and calcification, and treatment with PGG would protect collagen and elastin from rapid degradation. The developed valve replacements also had the valve leaflet attached to the wall. The attached wall would allow easy suturing of the valve unit to the aortic/pulmonary annulus. The functional valve leaflets would not be manipulated since sutures would pass through the attached wall. Furthermore, PGG treatment would provide adequate mechanical properties at the

beginning of the implant, with slow degradation over time, allowing cellular infiltration and from the host tissues and slow remodeling of the grafts.

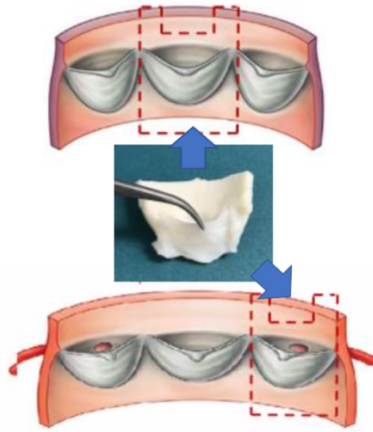


Figure 54: PGG treated leaflet repair patch can be used to repair both defective pulmonary (top) or aortic (bottom) valves

6.2 Materials and methods

Decellularization and PGG treatment of Porcine Aortic Valves and Porcine

Pulmonary Valves

Fresh porcine aortic valves and porcine pulmonary valves harvested from 3–9-month-old pigs were obtained from a commercial supplier (Animal Technologies, Texas). Blood was removed from the native tissues by washing with PBS, and any muscle within the tissue was trimmed. The aortic and pulmonary valves were separated into single valve units comprising of the leaflet with the attached wall. The valve leaflet units were decellularized using the decellularization protocol described in previous chapters. Briefly, tissues were treated with 0.05 M NaOH for 1 hour at room temperature, followed by decellularizing solution composed of 0.25% sodium dodecyl sulfate (SDS), 0.5% sodium

Deoxycholate (DOC), 0.5% Triton X 100, and 0.2% Ethylene Diamine Tetra-Acetic acid (EDTA) in 50 mM TRIS (tris (hydroxymethyl) amino-methane) buffer (pH 7.4 ± 0.05) for six days. DNase and RNase enzymes were used at a concentration of 360 U/mL in Phosphate Buffered Saline (PBS) with 5mM Magnesium Chloride ($MgCl_2$), and 0.02% Sodium azide for four days at 37°C. The scaffolds were sterilized by shaking with sterile 0.1% Peracetic acid (pH 7.4 ± 0.05) for 24 hours at room temperature, treated with sterile 0.15% PGG in 20% Isopropanol in HEPES (pH 5.5) buffer and stored in sterile PBS with 1% Penicillin/ Streptomycin antibiotics.

DNA Quantification

DNA was quantified in native and decellularized valve leaflets and walls using a procedure described in previous chapters. Briefly, tissues were lyophilized, dry weights measured, digested, and DNA was extracted using Qiagen Dneasy Blood and Tissue Kit. The concentration of dsDNA obtained from each sample was quantified with Quant-It Pico green dsDNA Reagent kit. The DNA concentration for each sample was normalized to the dry weight of the tissue initially digested to determine the nanograms (ng) of DNA/ mg of dry weight of the sample.

Histological Analysis

Samples were fixed in formalin, tissue processed, and embedded in paraffin. Paraffin blocks were sectioned at 5 μ m thickness and baked overnight in an oven. For staining, slides were deparaffinized and stained with hematoxylin and eosin to determine

cellular and nuclear remains within the scaffolds. The structure of the scaffold ECM was also visualized using Masson's Trichrome, VVG, and Alcian Blue staining.

Enzyme (Elastase and Collagenase) Treatment of Valves

Native, decellularized and PGG treated decellularized leaflets and walls of valves were challenged with elastase and collagenase to determine the resistance of the scaffolds to enzymatic degradation. As described previously, elastase treatment was done in Calcium Chloride (CaCl_2) and Sodium Azide (NaN_3) in TRIS buffer ($\text{pH } 7.8 \pm 0.05$) for 24 hours. For collagenase treatment, type VII Collagenase was used in CaCl_2 and NaN_3 in TRIS buffer ($\text{pH } 8 \pm 0.05$) for 48 hours. Samples were lyophilized after the treatment and the % loss in dry weight calculated.

Biaxial mechanical testing of tissue-engineered valves

Biaxial testing was performed with the native, decellularized and PGG treated valve leaflets to determine their mechanical strength. The biaxial testing procedure was used as described in the literature for biaxial testing of bovine jugular vein valves (448). The central belly regions of the valve leaflets were trimmed into 7 mm x 7 mm sections. The testing was performed using the BioTester 5000 (CellScale, Waterloo, Ontario, Canada), equipped with two load cells and real-time monitoring capabilities with a charged coupled device (CCD) camera. The 7mm x 7mm leaflet sections were mounted and secured by gripping with BioRake 'tines' on all four edges, preventing sample shear and deformation (449).

After the initial set-up, samples were pre-loaded to 0.01N to generate repeatable and reliable results. Equibiaxial stretching was applied at a rate of 1%/sec to a strain of 60% of initial dimensions and recovered back to 0% strain, for three cycles. The stretching to 60% strain was calculated by initial testing, which did not result in tissue failure at that strain rate. Displacement and force data was collected during the stretching-relaxation cycles. Based on the measured dimensions of the sample and the output data, corresponding nominal stress (i.e., first Piola–Kirchhoff stress) and true strain values were calculated, using equations described below, and stress-strain curves were plotted. The peak tangent modulus was calculated from the stress-strain curve of each sample between the relatively linear region of 45% and 60% strain. The stress at 45% strain was subtracted from the stress at 60% strain, and the value was divided by the difference in strain % (15%). Peak stress was defined as the stress values measured at 60% strain rate.

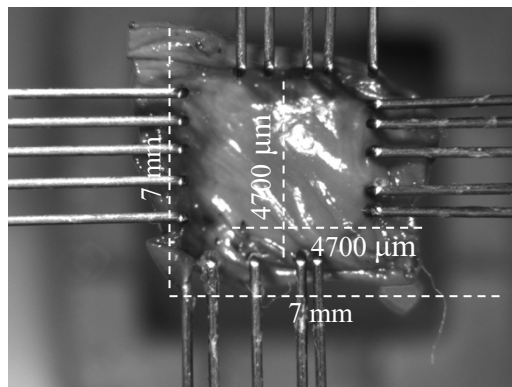


Figure 55: Biaxial testing set-up for porcine aortic valve leaflets

Maximum Stress at 60% strain (MPa)

$$= \frac{\text{Load at 60\% strain (mN)}}{\text{Tissue thickness (mm)} \times \text{tissue width (cm)}}$$

Peak tangent modulus (MPa)

$$= \frac{(\text{Stress at 60\% strain (MPa)}) - (\text{Stress at 45\% strain (MPa)})}{15\%}$$

Suture retention strength of tissue engineered valves

Wall portions of the PGG treated porcine aortic valves were compared to native glutaraldehyde (glut) fixed aortic walls to determine the ability of the tissues to resist suture failure.

Rectangular sections of 1 cm x 0.5 cm were excised from PGG treated and glutaraldehyde treated walls in both the circumferential and longitudinal directions. The bottom 0.5 cm section of each sample was secured in the lower clamp of a uniaxial tester (Instron, Norwood, Massachusetts, USA). A 4-0 Prolene suture was inserted through the center of the section 0.2 cm from the top. The top of the suture was secured and attached to the upper clamp of the uniaxial tester. Samples were pre-loaded to 0.01 N and then stretched at a rate of 1mm/sec. The maximum load for tissue failure was recorded, and the maximum stress at failure was calculated by dividing the maximum load by the cross-sectional area of the hole (Tissue thickness x suture diameter)

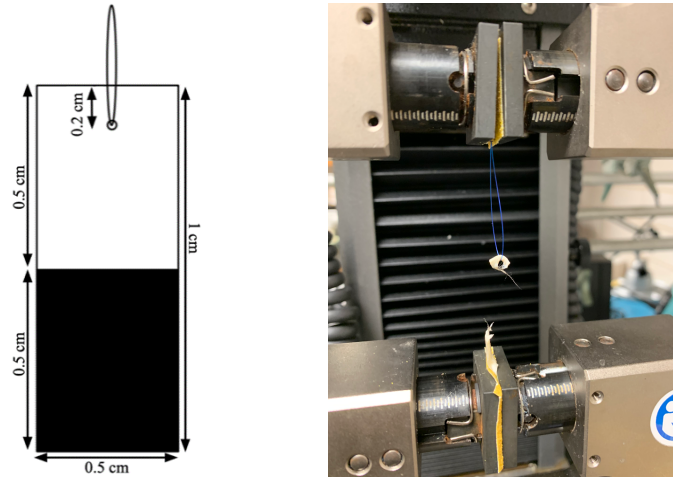


Figure 56: Suture retention strength measurement sample preparation and experiment set-up

Maximum Stress at failure (MPa)

$$= \frac{\text{Load at failure (N)}}{\text{Tissue thickness (mm)} \times \text{Diameter of the suture (mm)}}$$

Subcutaneous implantation of PGG treated porcine aortic valves

PGG treated decellularized and glutaraldehyde fixed native porcine aortic valve leaflets and walls were implanted subcutaneously in 3-4-week-old Sprague Dawley (SD) rats to determine the biocompatibility of the scaffolds (450, 451). Subcutaneous implantation was done as described previously in *Chapter Five*.

Pre-prepared implants (PGG treated decellularized/ glutaraldehyde treated native leaflets or walls) were placed into pouches created surgically at the back of SD rats to study the effects of *in-vivo* calcification. One valve and one wall were implanted in each rat. The

wound was closed with surgical staples and the animals were allowed to recover and housed in animal quarters. At the designated time interval, rats were euthanized, and implants were retrieved.

Gross view of the explants was observed for any capsule formation, and implant degradation. The implant periods used were 30 days, 60 days, and 90 days. 10 animals were used for PGG tissue implant at each time point, and 5 animals at each time point had glutaraldehyde treated aortic valve and wall implants. The subcutaneous implantation procedure has been demonstrated schematically in Figure 57.

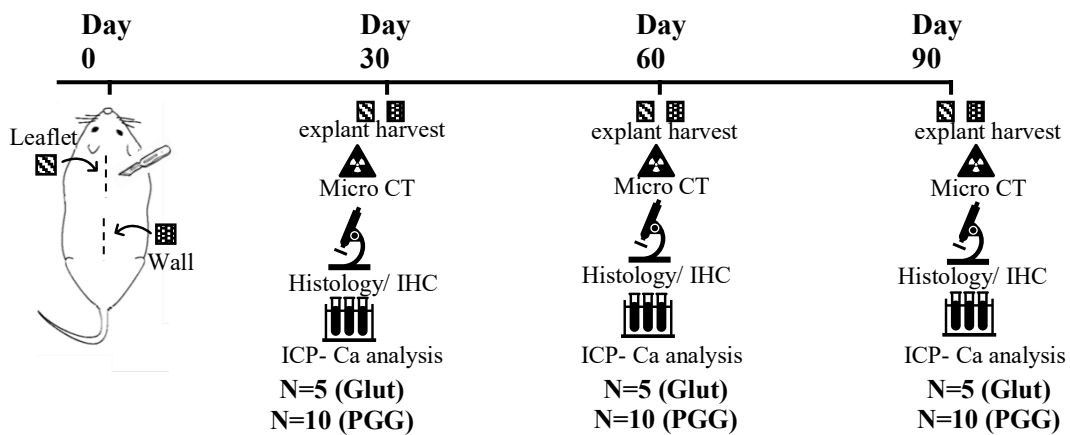


Figure 57: Schematic representation of subcutaneous study in rats

Micro-Computed Tomography (Micro-CT) analysis of subcutaneous explants

Subcutaneous valve leaflets and walls explanted from rats were scanned using Micro-CT (Bruker Micro CT 1176) to identify any calcification within the explants. A voltage of 65 kV was used with the current of 296 μ A, for 60 ms, and 0.2 Al filter. 3-D

models of the scanned images were reconstructed using NRecon (Micro Photonics Inc.) and visualized with CTvox (Bruker MicroCT) Software.

Histological analysis of subcutaneous implants

Harvested explants were fixed in formalin, tissue processed, embedded in paraffin, sectioned to 5 μm sections, and were mounted on glass slides and heated for 30 mins to adhere the sections to the slides. Slides were deparaffinized and stained with hematoxylin and eosin for cellular infiltration. Explant sections were also stained with Alizarin red to determine any calcification within the explants.

ICP (Inductively Coupled Plasma) analysis of subcutaneous explants

The subcutaneously explanted samples, after removal of capsules, were lyophilized, acid hydrolyzed, and dried under nitrogen gas. The residue was resuspended in DI water and filtered to remove any solid particles. Calcium and phosphorous content within the samples were analyzed using the Spectro Acros ICP Spectrometer (SPECTRO Analytical Instruments, Kleve, Germany). Element concentration values were normalized to the dry sample weights. (452)

Immuno-histochemical (IHC) Analysis

Histological tissue sections were deparaffinized, boiled in Citrate buffer, blocked, and incubated with primary antibodies at 1:100 dilution overnight. Secondary fluorescent antibody incubation was done for 1 hour, followed by DAPI nuclear staining, mounting,

and imaging (Keyence BZ-X810). Inflammatory responses in the explants were evaluated using immunohistochemistry for CD 3-T cells, CD 11c dendritic cells, and macrophage marker CD 68. Sectioned were also stained for Vimentin and α -Smooth Muscle Actin (α SMA) to determine infiltration of fibroblasts and myofibroblasts. Collagen remodeling and new collagen formation was determined using Heat Shock Protein 47 (HSP-47) staining.

Flow Cytometry analysis of subcutaneous explants

Freshly explanted valve leaflets and walls from the 90-day explants were used for flow cytometry analysis. For the PGG treated scaffolds, the leaflets/ walls along with the surrounding tissue were digested. Since no cellular infiltration was expected within the glutaraldehyde treated explants, the capsules formed around the glutaraldehyde tissues were separated from the implants and used for the analysis.

Samples were digested using a cell dispersion procedure for subcutaneous tissues (453, 454). Briefly, freshly explanted samples were placed in PBS containing Dispase I, 3% FBS (Fetal Bovine Serum), and 1% Pen/Strep at 4°C overnight with shaking. The next day, remaining samples were removed, minced, and incubated in RPMI (Roswell Park Memorial Institute media 1640, Lonza) media with 1 mg/ml collagenase, 1 mg/ml hyaluronidase, 150 U/ml DNase, and 1% Pen/Strep at 37°C for 2 hours with shaking. After digestion, both solutions were passed through 40 μ m nylon mesh sterile cell strainers (Fisher scientific), and any remaining tissue was mashed and washed with PBS. The cell suspension obtained after filtering was centrifuged, resuspended in Cell staining Buffer,

washed, blocked with F_c block, and incubated with 1:100 diluted fluorescent labeled primary antibody cocktail for extracellular antigens (CD45 and CD31) for 30 minutes at 4°C. After primary antibody incubation, cells were treated with fixation buffer, permeabilized using permeabilization buffer, and incubated with 1:50 diluted fluorescent labeled primary antibody cocktail for intracellular staining (Vimentin and αSMA) for 1 hour at room temperature. Subsequently, the cell suspension was washed to remove any unbound antibodies, resuspended in cell staining buffer, and analyzed using Attune NxT flow cytometer (Thermofisher Scientific).

Implantation of tissue-engineered valves as pulmonary valve repair unit in sheep²

PGG treated porcine aortic valves and porcine pulmonary valves were implanted in sheep as pulmonary valve repair units for up to three months. For the surgery, the main pulmonary artery was partially transected at 1 cm above the level of the sino-tubular junction, and one pulmonary valve leaflet was excised. An appropriately sized PGG treated valve repair patch with the attached wall was trimmed to an appropriate geometry and sutured to repair the excised leaflet. After pulmonary arteriotomy closure, the animals were weaned from cardiopulmonary bypass and when hemodynamically stable, the function of the implanted valve leaflet was assessed with epicardial 2-D and 3-D echocardiography. At three months after the implant procedure, the left thoracotomy incision was reopened under general anesthesia, and 2-D and 3-D echocardiography images were acquired. The

² Sheep Implant surgeries done by Dr. John E. Mayer at Boston Children's Hospital

animals were heparinized to prevent post-mortem thrombosis, and then euthanized with pentobarbital sodium (80-100 mg/kg, IV). Pulmonary valve explanted were obtained and analyzed by their gross view, histologically, and immunohistochemically.

Statistical analysis

The data was reported as the Mean \pm Standard Deviation. Data from different groups were analyzed by one-way analysis of variance (ANOVA) followed by Tukey's HSD. All statistical analysis was done using JMP[®] Pro 15.2.0. Significance was reported at three different significance levels: *** $p \leq 0.001$, ** $p \leq 0.01$, * $p \leq 0.05$.

6.3 Results

DNA Quantification:

Native porcine aortic valve leaflets and walls had average DNA concentrations of 2986.2 ± 1017 ng DNA/ mg tissue weight and 4057.4 ± 1583 ng DNA/ mg dry weight of tissue, respectively. After decellularization, this value decreased to 38.2 ± 33 ng DNA/ mg tissue and 34.7 ± 18.9 ng DNA/ mg tissue (Figure 58). This represented a 98.7% decrease in DNA content in the leaflets and 99.1% decrease in the walls. The difference in DNA content between the native and decellularized scaffolds was statistically significant.

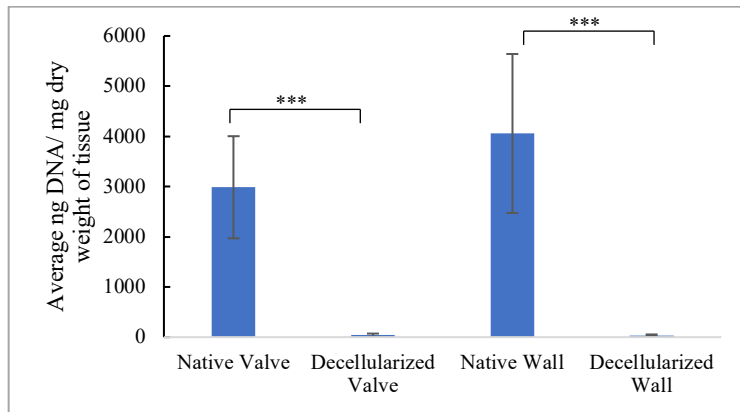


Figure 58: DNA quantification in porcine aortic valve leaflets and walls before and after decellularization; N=6; *** $p \leq 0.001$

Native porcine pulmonary valve leaflets had average DNA concentrations of 11317.9 ± 864 ng/ mg tissue weight and 4697.6 ± 1076 ng DNA/ mg tissue weight for the leaflets and walls, respectively. In decellularized leaflets and valves, the DNA concentration decreased to averages of 87.82 ± 11.8 ng/ mg dry weight and 63.9 ± 24.4 ng DNA/ mg dry weight (Figure 59). This represented a 99.2% and 98.6% decrease in DNA content in the pulmonary leaflets and walls, respectively.

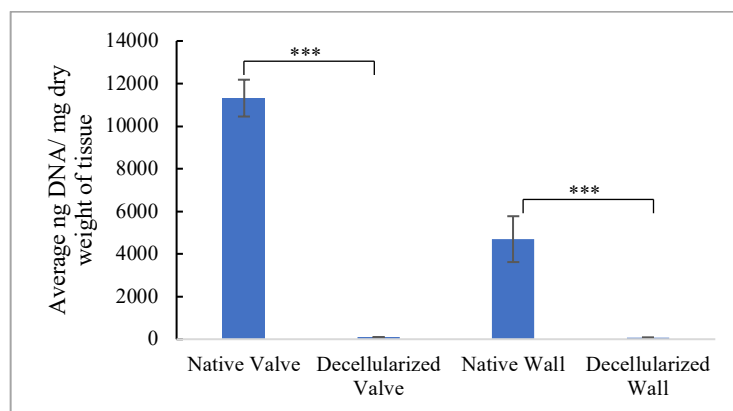


Figure 59: DNA quantification in porcine pulmonary valve leaflets and walls before and after decellularization; N=6; *** $p \leq 0.001$

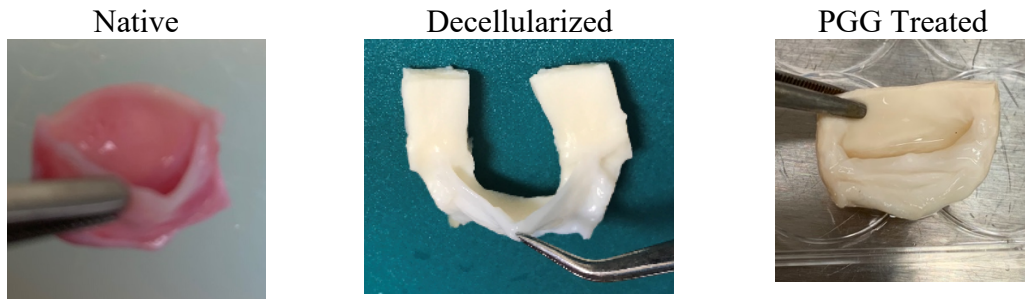
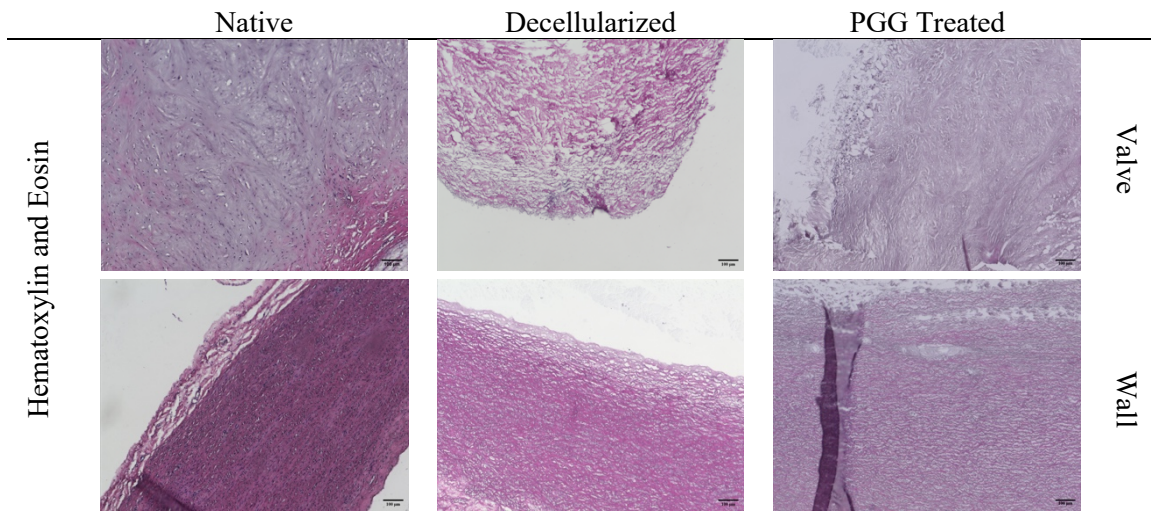


Figure 60: Gross View of native, decellularized and PGG treated valve leaflets

Histologically, H&E staining of the decellularized and PGG treated aortic and pulmonary valves did not show the presence of any cellular or nuclear material. Masson's trichrome and VVG staining of the native, decellularized, and PGG treated scaffolds showed the presence of collagen and elastin within the extracellular matrix of the scaffolds. There was no difference observed histologically between the arrangement of these fibers within the ECM. Alcian blue staining also confirmed the presence of glycosaminoglycans (GAGs) within the scaffolds after decellularization and PGG treatment (Figures 61 and 62).



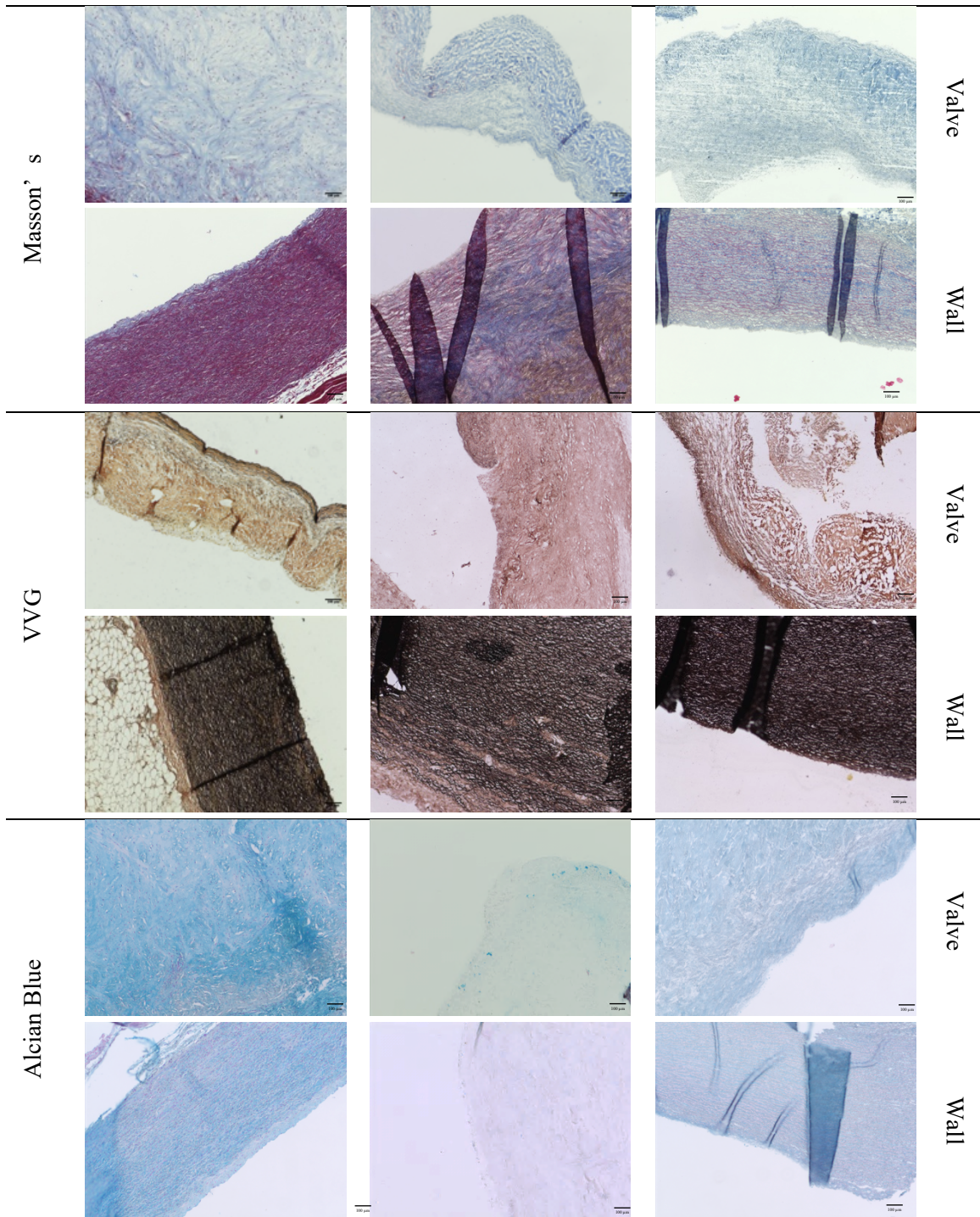
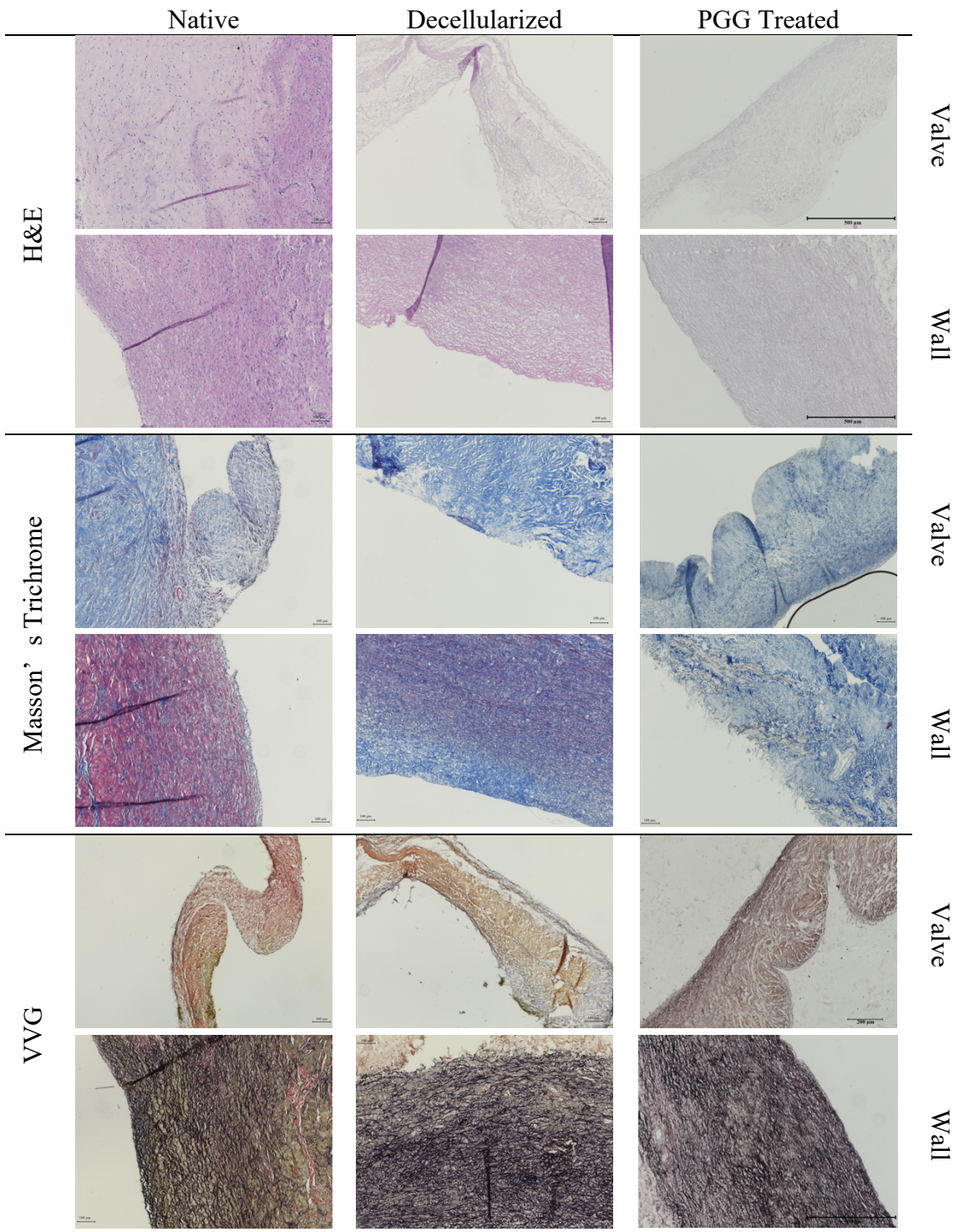


Figure 61: Porcine Aortic Valves Histology



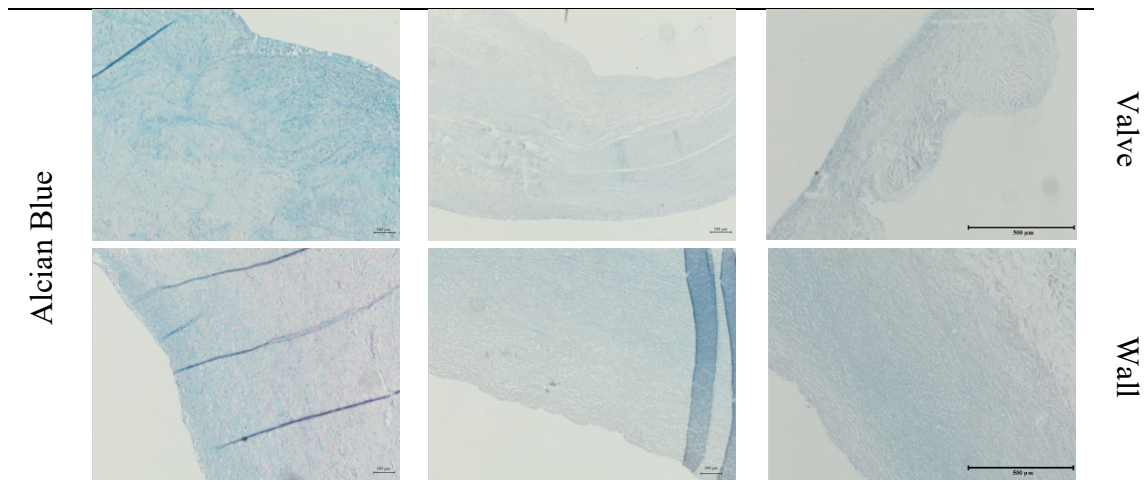


Figure 62: Porcine pulmonary valves histology

Resistance to elastase and collagenase enzymes

PGG treated decellularized porcine aortic valve and wall tissues treated separately with elastase and collagenase enzymes demonstrated a decrease in weight loss after the enzyme treatments compared to decellularized valves and walls. The % loss in dry weight for the decellularized valve leaflets and walls were 41.3 ± 13.2 % and 77.2 ± 7.9 %, respectively, after elastase treatment. PGG treatment of the decellularized tissues decreased this weight loss to 19.7 ± 2 % and 54.7 ± 2.1 % for the valves and walls, respectively (Figure 63.A). Collagenase treatment of decellularized valves and walls resulted in weight losses of 95.1 ± 7.8 % and 46.2 ± 11.6 % respectively, while PGG crosslinking of the tissues decreased the weight loss to 10.9 ± 5 % and 9.7 ± 4.1 %, respectively (Figure 63.B). All the reductions in weight loss from enzyme treatments were statistically significant, as indicated below.

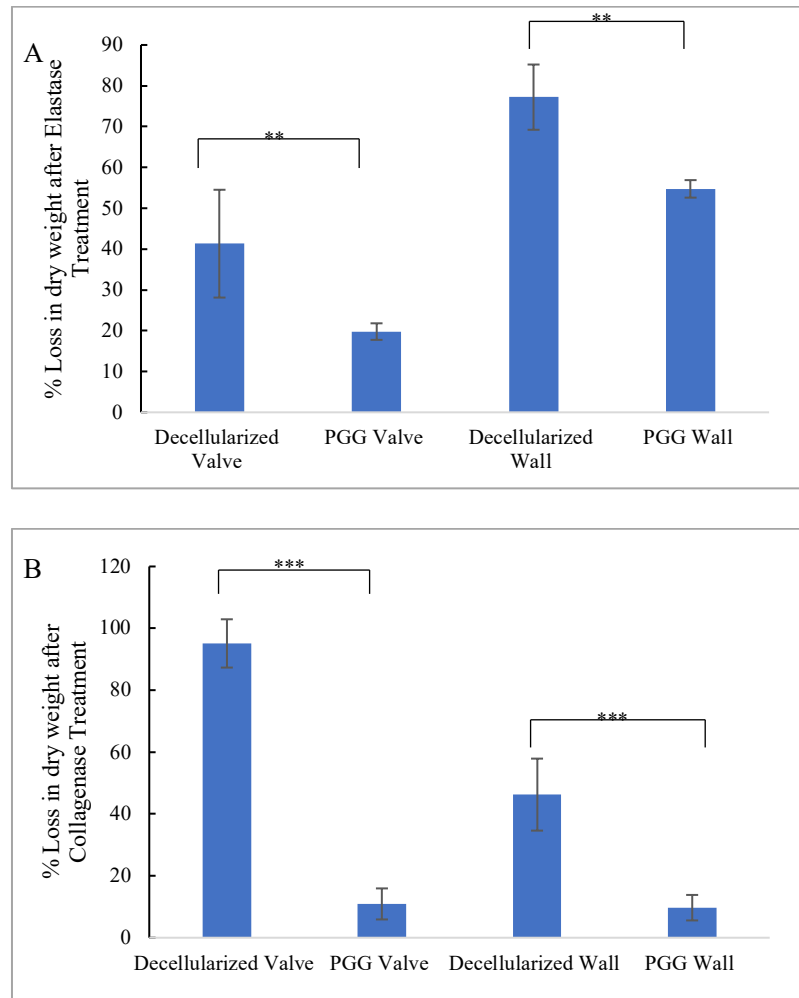


Figure 63: A. Elastase and B. Collagenase Enzyme treatment of Native, Decellularized, and PGG treated decellularized Porcine Aortic Valves and Walls; N=8 (**, ***: Statistically significant difference in % weight loss after enzyme treatment)

Native pulmonary valve leaflets and walls demonstrated weight losses of $40 \pm 2.5\%$ and $63.7 \pm 14.8\%$ when treated with elastase enzyme. For decellularized scaffolds, the values were $30.6 \pm 2.5\%$ $63.3 \pm 18.3\%$ respectively. In PGG treated scaffolds, the % weight loss from elastase treatment decreased to $2.7 \pm 0.7\%$ and $9.2 \pm 3.4\%$ in the leaflets and walls, respectively. For collagenase treatment, native pulmonary valve leaflets and walls

demonstrated loss in dry weight of $90.7 \pm 4.8\%$ and $38.8 \pm 13.6\%$, respectively. In decellularized valves, the weight loss was $79.6 \pm 11.7\%$ for leaflets and $33.5 \pm 20.4\%$ for walls. PGG treated scaffolds had weight losses of $7.9 \pm 0.6\%$ and $2.9 \pm 0.9\%$ respectively in the leaflets and walls. The difference in weight loss was statistically significant between the PGG scaffolds and the native and decellularized valves (Figure 64).

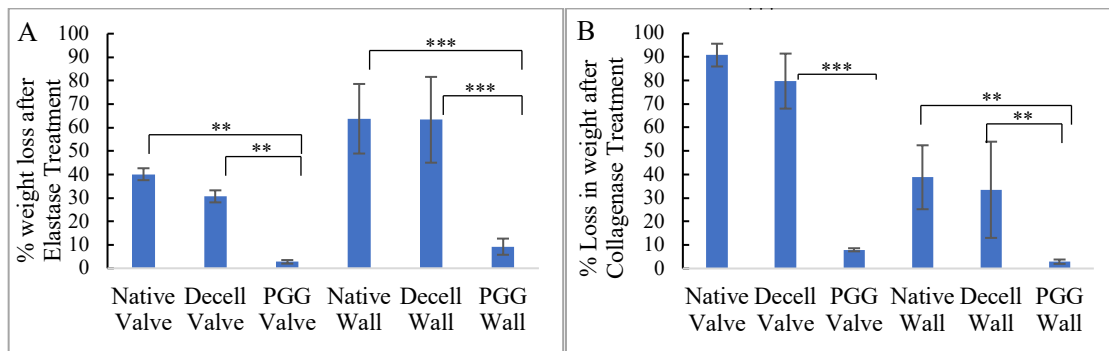


Figure 64: (A) Elastase and (B) Collagenase Enzyme treatment of Native, Decellularized, and PGG treated decellularized Porcine Pulmonary Valves and Walls; N=8 (**, ***: Statistically significant difference in % weight loss after enzyme treatment)

Biaxial testing

Equibiaxial stretching and relaxing of native, decellularized, and PGG treated porcine aortic valve leaflets demonstrated the ability of the leaflets to withstand cyclical stretching and relaxation cycles without tissue deformation (Figure 65).

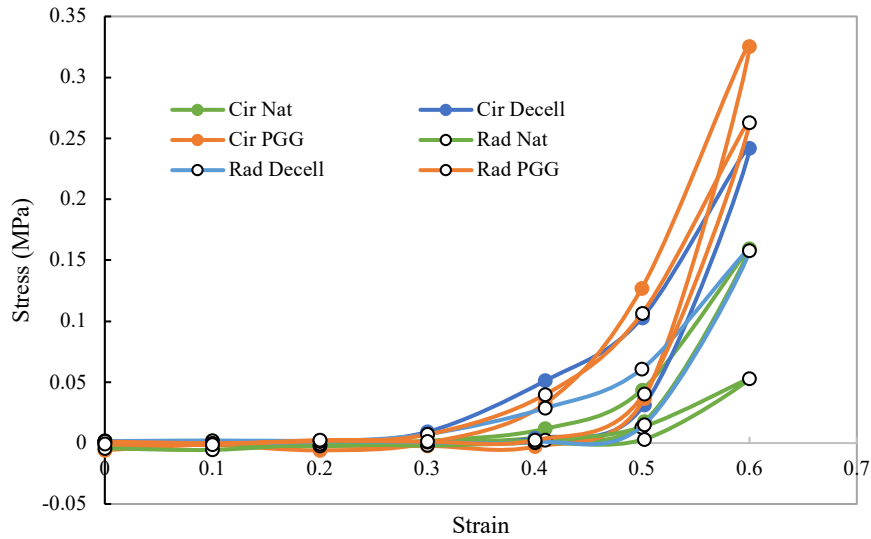


Figure 65: Stress-strain biaxial curves for native, decellularized, and PGG treated porcine aortic valve leaflets

The maximum peak stress at 60% strain for native, decellularized, and PGG treated aortic valve leaflets revealed higher average maximum peak stress in the circumferential direction compared to the radial direction for all three kinds of tissues. The maximum peak stress for native PAV was 0.23 ± 0.08 MPa in the circumferential direction, compared to 0.05 ± 0.03 MPa in the radial direction. In decellularized leaflets, the peak stress in the circumferential direction was 0.27 ± 0.16 MPa compared to 0.15 ± 0.11 MPa in the radial direction. PGG treated PAV leaflets had 0.32 ± 0.17 MPa peak stress in the circumferential direction compared to 0.26 ± 0.16 MPa in the radial direction (Figure 66).

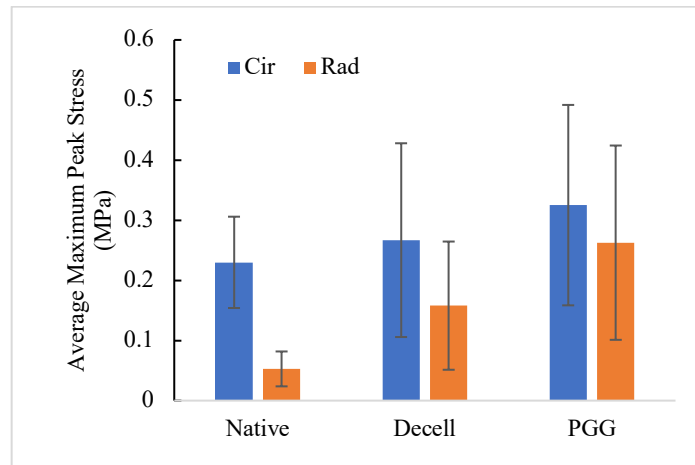


Figure 66: Average maximum peak stress at 60% strain from biaxial testing in porcine aortic valve leaflets; N=6

The peak tangent modulus for the native PAV leaflets was 0.15 ± 0.09 in the circumferential direction and 0.04 ± 0.03 in the radial direction. For the decellularized leaflets, the tangent modulus was 0.15 ± 0.11 in the circumferential direction and 0.09 ± 0.05 in the radial direction. In PGG treated leaflets, the values were 0.19 ± 0.12 and 0.16 ± 0.11 in the circumferential and radial directions, respectively (Figure 67).

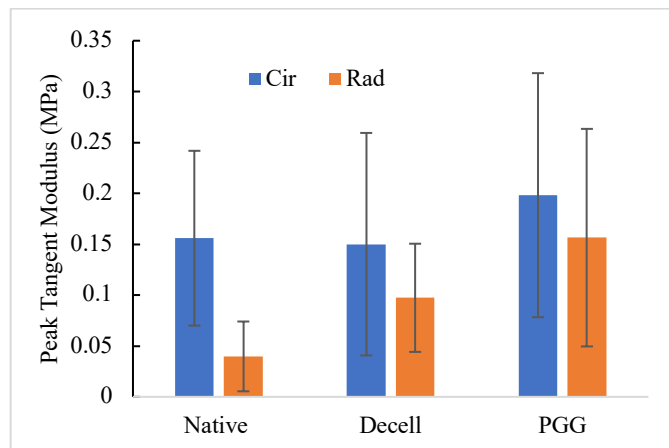


Figure 67: Peak tangent modulus for biaxial testing in porcine aortic valve leaflets; N=6

The thickness of the native, decellularized, and PGG treated porcine pulmonary valves was measured prior to biaxial testing. The average thickness of the tissues was 0.26 ± 0.03 mm, 0.24 ± 0.02 mm, and 0.29 ± 0.04 mm, for the native, decellularized, PGG treated, and glutaraldehyde fixed valve leaflets, respectively (Figure 68). No significant difference was observed within the tissue thickness of the different groups.

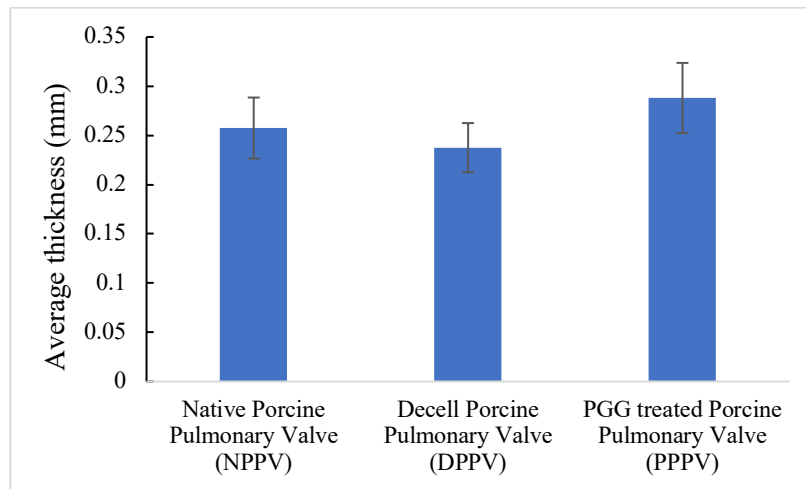


Figure 68: Average thickness of native, decellularized, and treated porcine pulmonary valves; N=5

Biaxial testing of the native, decellularized, and PGG treated decellularized porcine pulmonary valve leaflets demonstrated the ability of the leaflets to stretch and recoil with cyclical applied forces in both the circumferential and radial directions (Figure 69).

The maximum stress at 60% strain for native PPV was 0.81 ± 0.4 MPa in the circumferential direction and 0.59 ± 0.55 MPa in the radial direction. For the decellularized PPV, circumferential and radial stresses were 0.98 ± 0.09 MPa and 0.72 ± 0.24 MPa, respectively. PGG treated decellularized PPV leaflets demonstrated maximum stress values at 60% strain at 0.99 ± 0.19 MPa and 0.57 ± 0.49 MPa in the circumferential and

radial directions, respectively (Figure 70.A). There was no statistical difference observed between the maximum stresses among the three groups. The anisotropic trend in maximum stresses was preserved after decellularization and PGG treatment of the PPV leaflets.

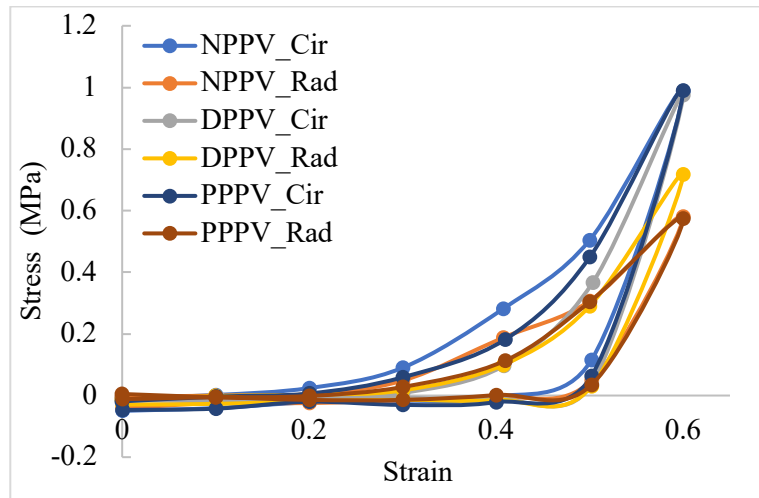


Figure 69: Stress-Strain biaxial analysis of porcine pulmonary valve leaflets; Cir: Circumferential direction; Rad: Radial direction; NPPV: Native pulmonary valves; DPPV: Decellularized pulmonary valves; PPPV: PGG treated pulmonary valves

Peak tangent modulus, calculated from the relatively linear region of 45% to 60% strain was similar in the three groups of PPV. The average peak tangent modulus for the native tissues were 3.53 ± 1.91 MPa in the circumferential direction, and 2.5 ± 1.59 MPa in the radial direction. For decellularized scaffolds, the tangent modulus values were 4.39 ± 0.62 MPa in the circumferential direction, and 3.09 ± 1.78 MPa in the radial direction. PGG treated decellularized leaflet scaffolds demonstrated maximum peak tangent modulus values of 4.04 ± 0.55 MPa in the circumferential direction and 2.3 ± 4.13 in the radial

direction (Figure 70.B). No significant differences were observed in the tangent modulus values between the groups.

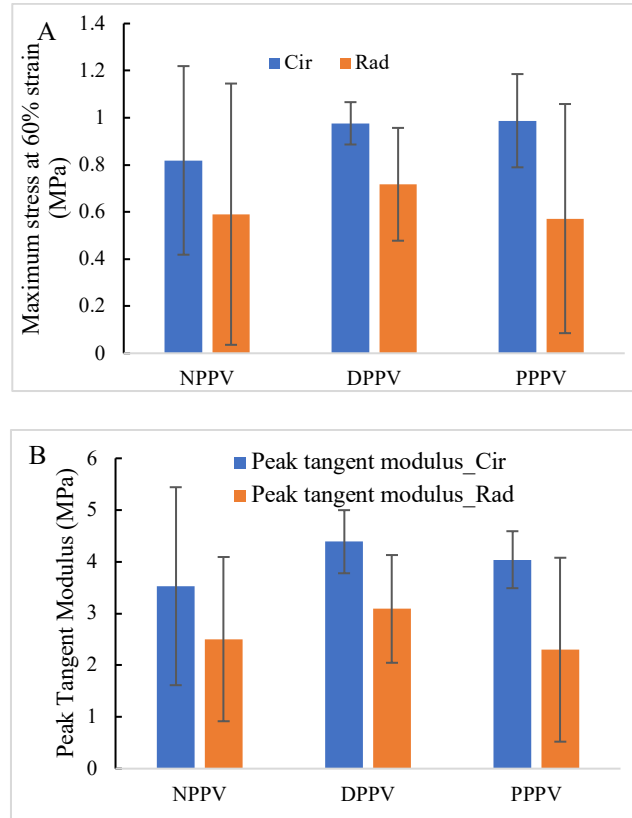


Figure 70: (A) Maximum stress at 60% strain (MPa) for native (NPPV), decellularized (DPPV), and PGG treated (PPPV) porcine pulmonary valve leaflets; (B) Peak Tangent Modulus (MPa) for native, decellularized, and PGG treated porcine pulmonary valve leaflets; Cir: Circumferential direction, Rad: Radial direction; N=5

Suture retention testing

PGG and glut treated aortic valve walls, with inserted suture, were stretched in a uniaxial tester until tissue failure. The average maximum force required for tissue failure

in PGG treated scaffolds was 73.59 ± 15.34 MPa in the circumferential direction, and 17.21 ± 4.29 MPa in the longitudinal direction. The corresponding values for the glutaraldehyde treated walls were 7.97 ± 2.03 MPa in the circumferential direction and 14.96 ± 9.17 MPa in the longitudinal direction. The maximum force required for suture failure was significantly higher in PGG treated walls compared to glutaraldehyde fixed walls in the circumferential direction, whereas the difference in the required force was not significantly different between the two treatments in the longitudinal direction (Figure 71).

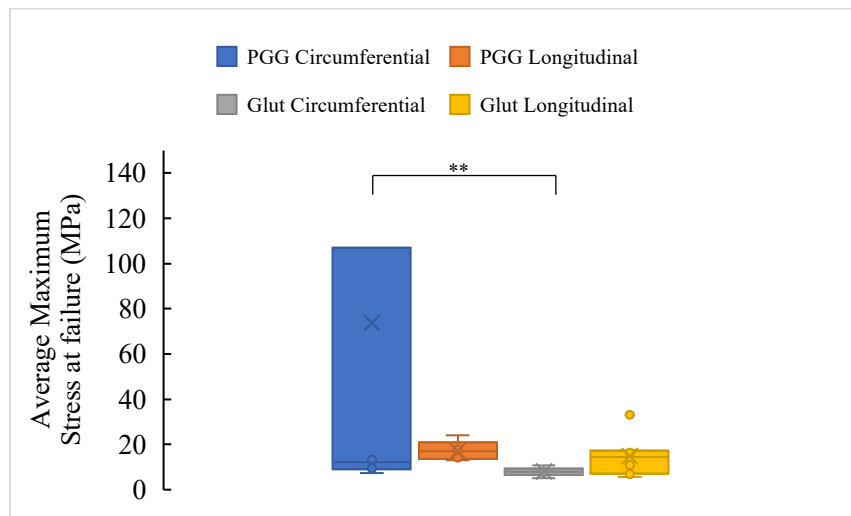


Figure 71: Maximum stress required for failure in suture pull-through test for PGG and glut aortic walls; N=8

Glutaraldehyde and PGG treated pulmonary walls stretched at a constant rate with suture insertion did not result in a significant difference in the maximum force and stress at failure. Glutaraldehyde treated walls had a maximum stress at tissue failure of 36.1 ± 8.75 MPa in the circumferential direction and 27.36 ± 3.76 MPa in the radial direction. The stresses calculated at failure for the glutaraldehyde treated group were 14.99 ± 7.9 MPa

and 16.9 ± 8.2 MPa in the circumferential and radial directions, respectively. Although the average values for the force and stress were higher for the PGG tissues, no significant difference was observed between glutaraldehyde and PGG treated groups (Figure 72).

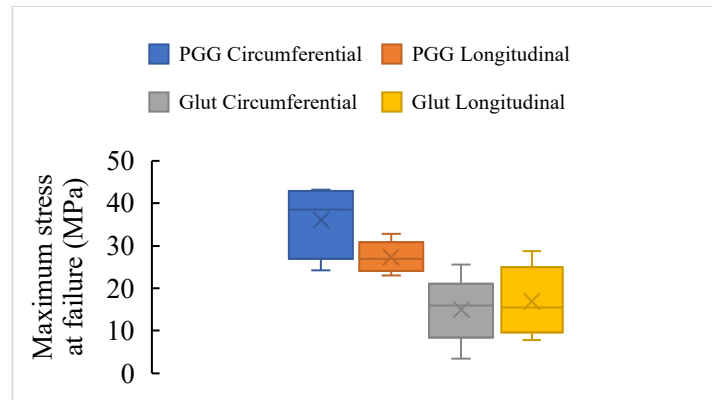


Figure 72: Suture pull-through testing of native, decellularized, and PGG treated porcine pulmonary valves; Cir: circumferential direction; Rad: Radial direction; No significant difference between groups; N=5

Subcutaneous implantation

All rats with subcutaneous implants, both glut valves and PGG treated valves, healed after the implantation procedure without any infection or morbidity. The gross view of the subcutaneously implanted glut treated native porcine aortic valves demonstrated thick capsule formation around all the leaflet and wall implants for all time points. There was no degradation of any of the glut implants. PGG treated decellularized aortic valve implants, on the other hand, did not show any extensive capsule formation. The PGG treated implants also demonstrated degradation of the tissues after implantation; the degradation rate increased with the time of implantation. At the end of the 90-day implant

period, the PGG treated decellularized leaflets implants had been mostly absorbed into the surrounding tissue, without any visible signs of inflammation (Figure 73).

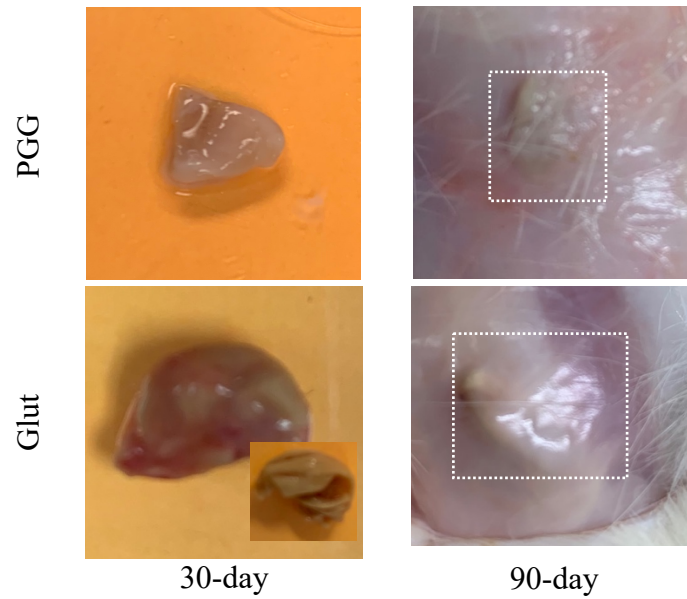


Figure 73: Gross view of 30-day and 90-day glut and PGG subcutaneous implants

Micro CT imaging of glut and PGG implants demonstrated the presence of heavy calcification within the glut leaflets and walls. All glut implants at 30, 60, and 90-days showed calcification within the tissues. None of the PGG implants showed the presence of any calcification by micro-CT imaging. Calcification within the tissues or scaffolds were identified as mineralized densities with an attenuation coefficient higher than surrounding soft tissues (Figure 74).

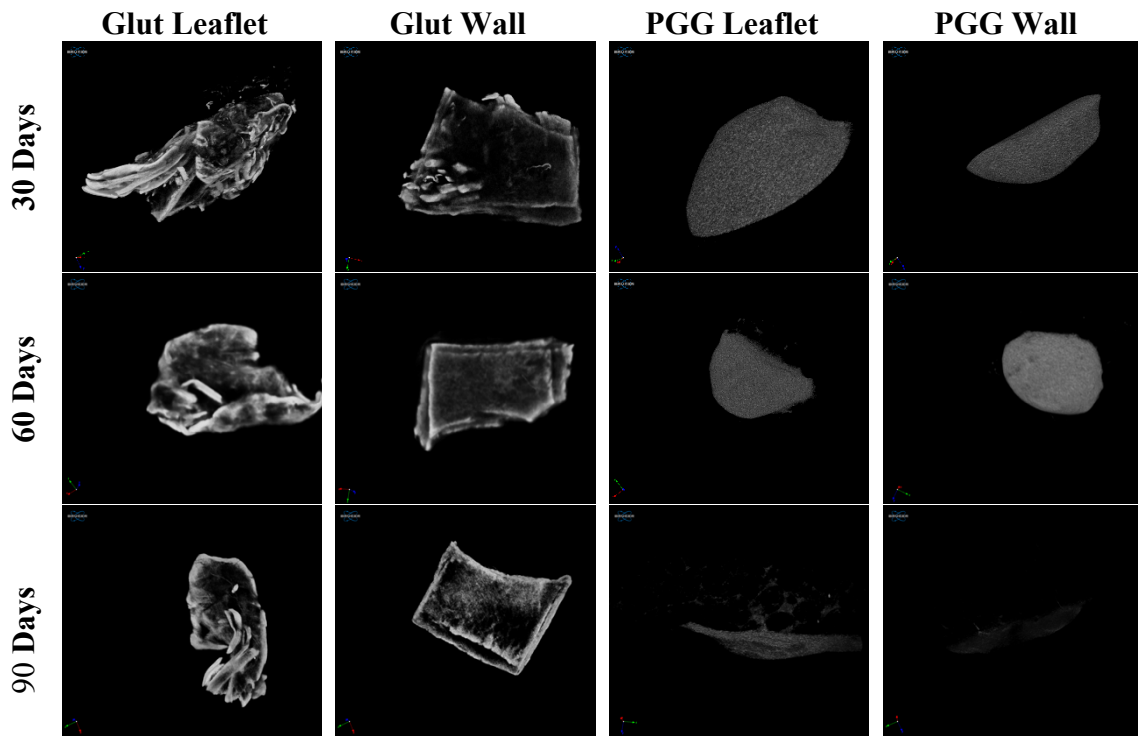
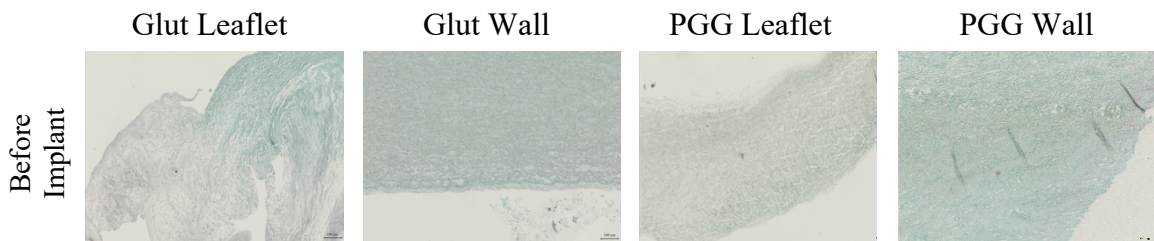


Figure 74: Micro CT imaging of subcutaneous porcine aortic valve explants after 30, 60, and 90 days of implantation

Alizarin red staining of the glut and PGG explants confirmed calcification within the glut valves. Dark red staining by alizarin red indicates presence of calcium within the tissues. All the glut explant sections demonstrated staining with alizarin red, while none of the PGG explant sections demonstrated any calcification (Figure 75).



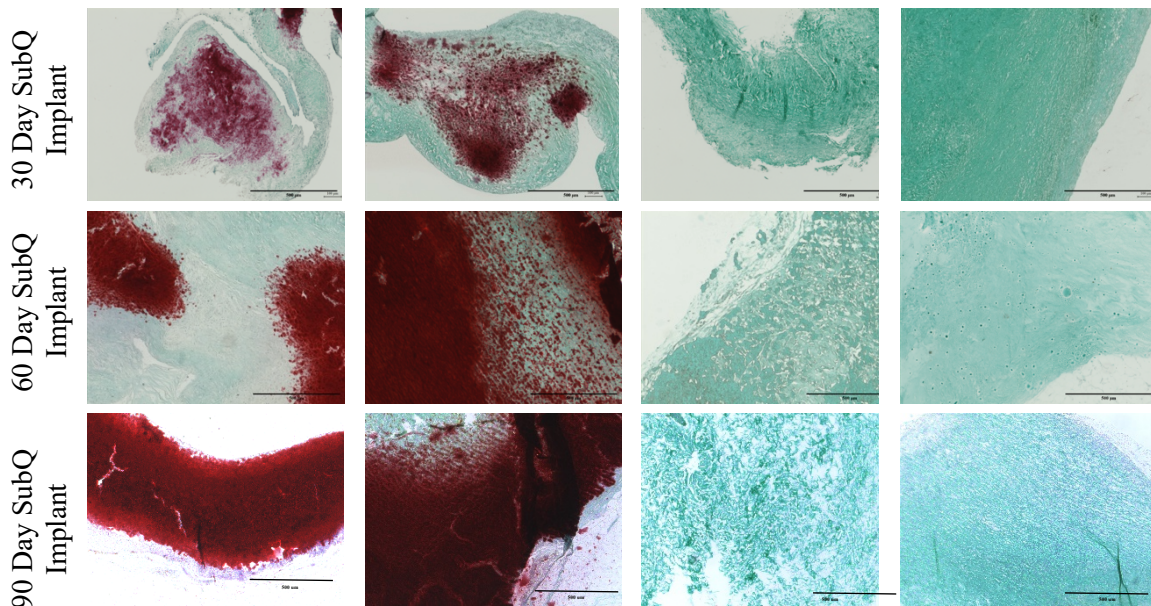


Figure 75: Alizarin red staining of porcine aortic valve subcutaneous explants after 30, 60, and 90 days of implant

ICP calcium (Ca) and phosphorous (P) mineral analysis within the subcutaneously explanted porcine aortic valves demonstrated increase in average Ca and P content in glut leaflets and walls. Pre-implant glut leaflets had Ca and P concentrations of $2.3 \pm 1.4 \mu\text{g}/\text{mg}$ tissue weight and $1.7 \pm 0.21 \mu\text{g}/\text{mg}$ tissue, which increased to $124.7 \pm 66.8 \mu\text{g}/\text{mg}$ and $60.6 \pm 30.5 \mu\text{g}/\text{mg}$ respectively at 30 days, $129.8 \pm 50.4 \mu\text{g}/\text{mg}$ and $64.1 \pm 24.4 \mu\text{g}/\text{mg}$ at 60 days, and $460.9 \pm 608.9 \mu\text{g}/\text{mg}$ and $214.7 \pm 290.4 \mu\text{g}/\text{mg}$ at 90 days respectively. In the glut walls, the Ca and P concentrations increased from $0.86 \pm 0.3 \mu\text{g}/\text{mg}$ and $1.2 \pm 0.1 \mu\text{g}/\text{mg}$ pre implant to $76.5 \pm 7.9 \mu\text{g}/\text{mg}$ and $37.7 \pm 4.4 \mu\text{g}/\text{mg}$ at 30 days, $100 \pm 19.5 \mu\text{g}/\text{mg}$ and $47.4 \pm 9.2 \mu\text{g}/\text{mg}$ at 60 days, and $149.2 \pm 32 \mu\text{g}/\text{mg}$ and $66.7 \pm 13.6 \mu\text{g}/\text{mg}$ respectively at 90 days. PGG treated valve leaflets and implants, on the other hand, had Ca and P concentrations ranging from $0.76 \pm 0.32 \mu\text{g}/\text{mg}$ to $8.57 \pm 4.1 \mu\text{g}/\text{mg}$ of tissue for

the pre-implant and post implant tissues. No significant increase in Ca or P concentrations were seen (Figure 76).

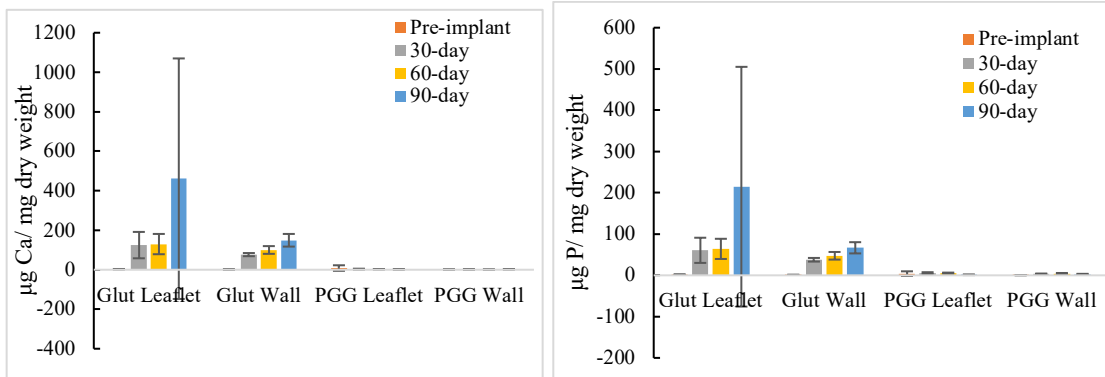
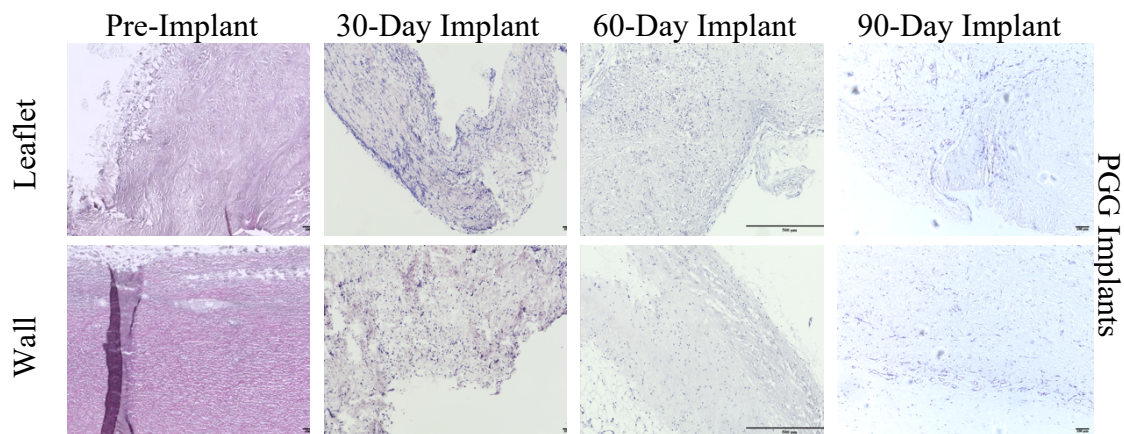


Figure 76: Calcium and phosphorous mineral analysis in explanted aortic valves; N=5

H&E staining of the PGG treated aortic valve and leaflets showed cellular infiltration post-implant. Moreover, no significant capsule formation was seen around the PGG implants. Most of the tissues were surrounded by subcutaneous tissue. At 90-days, most of the explanted valves had been absorbed into the surrounding tissue (Figure 77). Jansen grading of the subcutaneous implants (Table 7) demonstrated superior biocompatibility of PGG treated scaffolds compared to glutaraldehyde treated tissues.



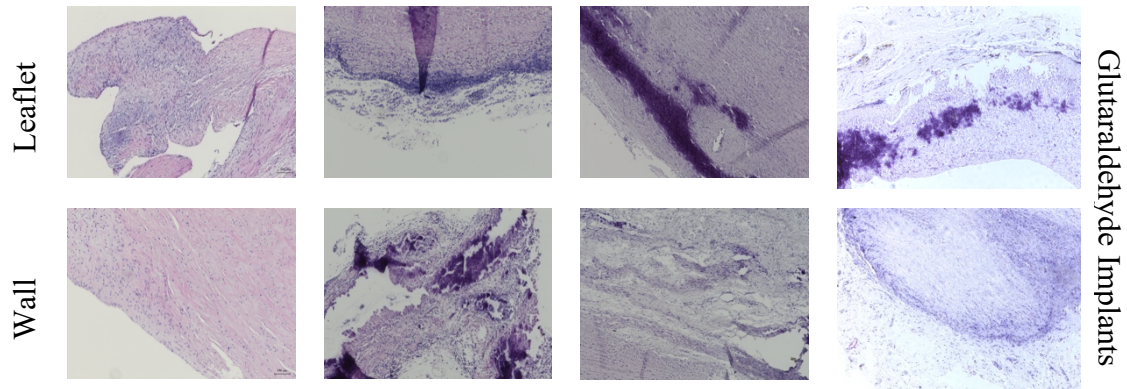


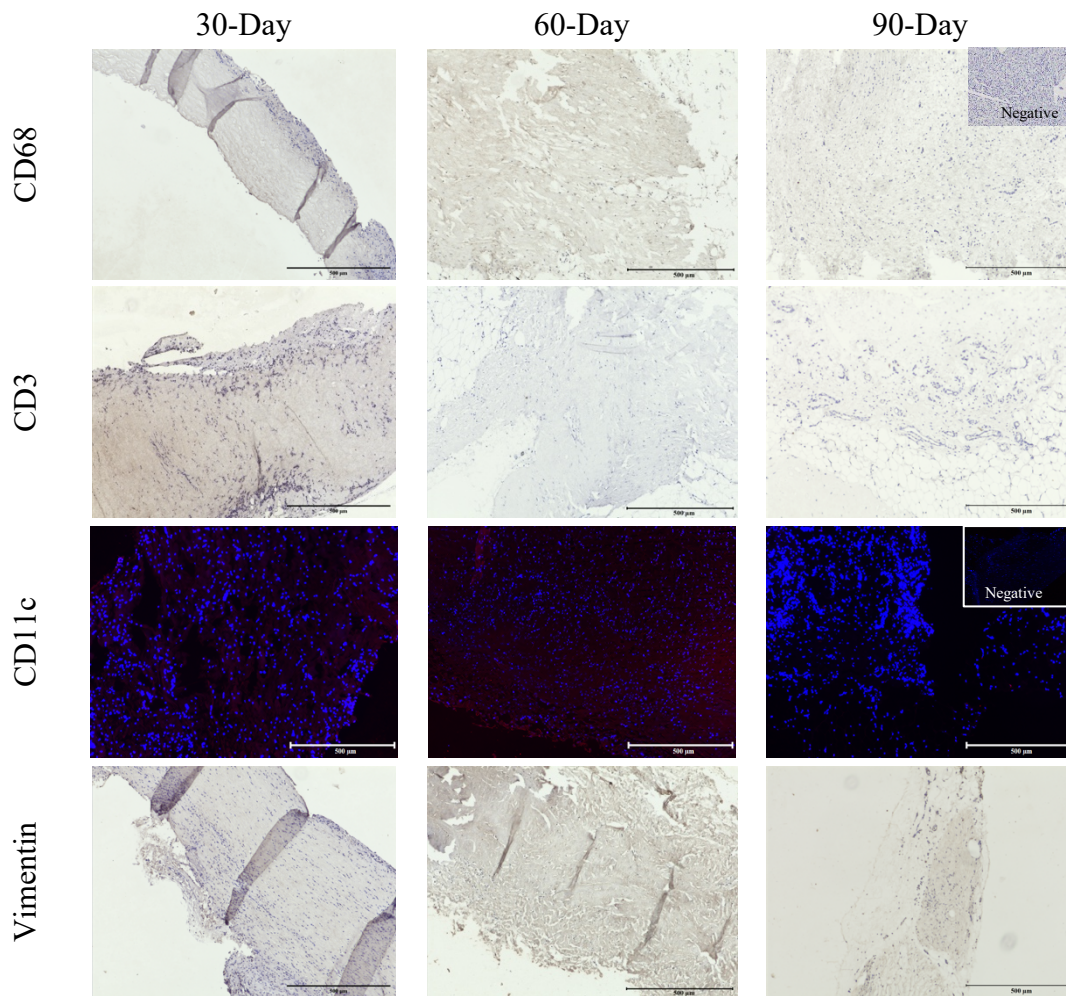
Figure 77: Hematoxylin and eosin staining of 30-, 60-, and 90-day aortic valve subcutaneous explants

	Glut Treated	PGG Treated
Reaction-zone semi-qualitatively	1 (Thick capsule)	4 (1-4 cell layer capsule)
Reaction zone qualitatively	2 (Capsule dense and granulous with fibroblasts and inflammatory cells)	4 (Surrounding tissue not dense, resembling connective or fat tissue)
Interference qualitatively	1 (Multiple layers of macrophages and foreign body cells)	4 (Fibroblasts contact implant surface without presence of foreign body giant cells)
Interstice qualitatively	1 (Tissue in interstitium dense and exclusively inflammatory)	4 (Interstitium tissue fibrous, not dense, resembling connective or fat tissue)
Total Score	5	16

Table 7: Jansen grading of glutaraldehyde and PGG treated aortic valve subcutaneous implants

Immunohistochemical staining of PGG treated decellularized aortic leaflet subcutaneous implants demonstrated the presence of CD68 macrophages at 30 days and 60 days, but at 90 days, there was no significant staining of CD68. Leaflets also demonstrated

some CD3 T cell staining at 30 days, but at 60 and 90 days, no CD3 staining was observed. No CD11c dendritic cell staining was observed in any of the PGG treated leaflets. In comparison to inflammatory cells, vimentin, α Smooth muscle actin, and HSP-47 positive staining was observed in all PGG implants, with more prominent HSP-47 staining at 90 days post implant (Figure 78).



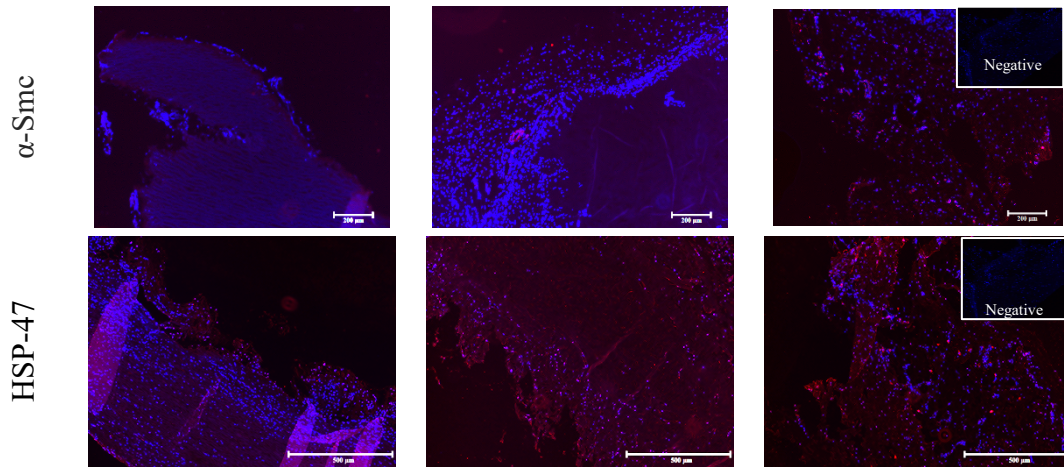


Figure 78: IHC staining of subcutaneously explanted 30-, 60-, and 90-day aortic valve leaflet implants

Flow Cytometry

Flow cytometry analysis of the PGG treated decellularized valves and walls subcutaneously explanted from rats demonstrated <27% and <36% of the cells were inflammatory within the leaflets and walls, respectively. More than 60% of the infiltrated cells were fibroblasts and myofibroblasts as well, as some infiltration of endothelial CD31 cells were also observed (Table 8).

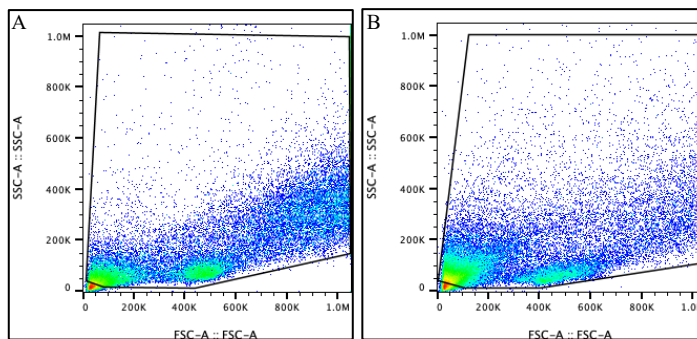


Figure 79: Representative dot plots from flow cytometry (A) PGG valve leaflets (B) PGG valve walls subcutaneous explants from rats

Cell Type	PGG Valve Leaflets				PGG Valve Walls			
	Pan-inflammatory	Endothelial	Fibroblasts	Myofibroblasts	Pan-inflammatory	Endothelial	Fibroblasts	Myofibroblasts
Antigen	CD45	CD31	Vimentin	α -SMA	CD45	CD31	Vimentin	α -SMA
Mean (%)	26.81	4.04	22.35	56.12	35.44	10.87	16.85	44.47
SD	12.39	1.22	3.12	21.91	5.9	4.01	2.07	14.15

Table 8: Statistics of cells stained positive for different antigens; Mean and Standard deviation of the % of cells; N=3

Implantation of PGG treated porcine aortic valves in sheep

PGG treated decellularized porcine aortic and pulmonary valves implanted in juvenile sheep as pulmonary valve replacement units for up to 6 weeks demonstrated thickening of the valve replacements after explanting 4-weeks and 6-weeks post implantation. Figure 80 represents thickening observed within PGG treated aortic valve explant after 4 weeks in the pulmonary position.

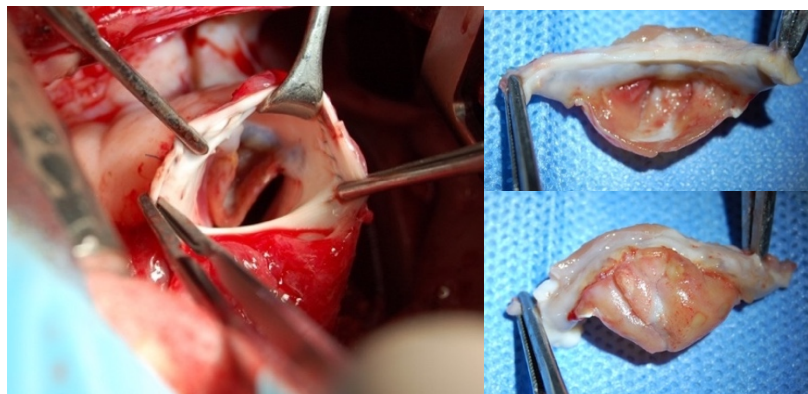


Figure 80: PGG treated decellularized porcine aortic valves explanted from sheep as pulmonary valve implants

6.4 Discussions

The current gold standard for valve replacement in pediatric patients is the use of cryopreserved allograft valves (455). There is, however, a shortage of available allografts as well as patient-valve size mismatch (456). Mechanical and synthetic valves, as discussed before, have their own limitations. Moreover, none of the currently available valve replacement strategies allow the somatic growth of cells within the valves. Therefore, multiple reoperations are required for pediatric patients.

Tissue-engineered heart valves are a promising approach to overcoming the limitations of current heart valves. Tissue-engineered valves are composed of a porous scaffold, cell population, and signaling factors (11, 457, 458). Ideally, tissue engineered valves should provide sufficient hemodynamics, thereby eliminating the need for reoperations; active tissue remodeling prevents degeneration and growth characteristics, preventing the need for multiple reoperations. To achieve these characteristics, the scaffolds of tissue-engineered valves are composed either from natural scaffolds or from degradable polymers (5). Recreation of the macro- and micro- valve anatomy and mechanical anisotropy might be challenging to achieve with degradable polymers (459). Decellularized valves, on the other hand, are composed of biological materials that can positively impact cellular differentiation and remodeling (460, 461). Moreover, complete degradation is not necessary with decellularized valves, and the mechanical anisotropic characteristics are maintained (462-466). Although some polymer valves have recently been used for valve replacement strategies, the long term performance of these remain to

be evaluated (467-471). Decellularized valve replacements have therefore been more widely used in clinical applications (472-478).

The detergent-based decellularization procedure utilized in this study was successful in removing most of the nuclear material from the scaffolds. The presence of nuclear and cellular material within the implanted scaffolds has been identified as the foci for the development of calcification within the tissues (374). Moreover, the absence of xenogeneic cellular material removes the possibility of the inflammatory response to the implanted tissue (369). The final DNA concentration within the porcine leaflets and walls was less than 50 ng/ mg tissue dry weight, which has been identified as an optimum level of remaining DNA (479).

Crosslinking of decellularized aortic and pulmonary valves with PGG was demonstrated to have significantly lower weight loss compared to decellularized and native tissues. This indicates the PGG treated scaffolds would be less susceptible to enzymatic degradation upon implantation, potentially prolonging the degradation time of the scaffolds. Early degradation of implanted valves is a major issue in bioprosthetic heart valves. Commercially, glutaraldehyde is the most widely used crosslinker to prevent rapid degradation of implanted valves. Glutaraldehyde crosslinking, however, does not effectively protect elastin from enzymatic degradation (14, 15).

Biaxial mechanical testing on the native, decellularized, and PGG treated aortic and pulmonary valve leaflets demonstrated the leaflets had comparable mechanical strength even after decellularization and PGG treatment procedures. Moreover, cyclical stretching and relaxation of the PGG treated tissues demonstrated they were capable of withstanding

cyclical forces. Suture pull-through testing performed on the aortic and pulmonary walls also demonstrated that the suture retention strength of the wall portions was comparable or higher than those of the glutaraldehyde treated tissues. This indicates the PGG treated tissues are comparable or more resistant to suture tearing compared to glutaraldehyde tissues.

Subcutaneous implantation of PGG decellularized treated porcine aortic valves demonstrated no calcification within both the leaflet and wall portions. The glutaraldehyde treated implants, on the other hand, demonstrated extensive calcification. Additionally, unlike glutaraldehyde implants, PGG treated implants did not have extensive capsule formation around the tissues. The thickness and nature of the surrounding capsule are an indication of the biocompatibility of the material. The PGG implants also demonstrated degradation of the scaffolds after 90-days of subcutaneous implantation indicating the potential of the scaffolds to integrate with the surrounding tissue. Flow cytometry and IHC analysis of the 90-day implants showed the presence of endothelial cells, fibroblasts, and myofibroblasts, with very few inflammatory cells. The glutaraldehyde treated implants, on the other hand, had more inflammatory cells within the surrounding capsules.

Sheep implants of the porcine aortic and pulmonary valves demonstrated some thickening of the valves after 4-weeks. Analysis of the explanted valves indicates this might have been due to the mismatch of the aortic tissue implanted at the pulmonary position. Aortic valves are more robust than pulmonary valves and are equipped to handle more shear stress. The absence of this might have led to the deposition of cellular material within the valves. Additionally, porcine tissues contain alpha-galactose epitopes and their

insufficient removal by the decellularization procedure might have been a cause for the thickening of the implanted valves. Alpha galactose, or Galactose-alpha-1,3-galactose is a carbohydrate found in most mammalian cell membranes. It is not found in humans and most primates. Presence of xenogeneic alpha-gal might illicit immune responses leading to graft failure. The alpha-galactose content within the tissues were not measured in this experiment. Further investigations need to be conducted regarding the failure of the PGG treated aortic and pulmonary valves in sheep. Moreover, for a more effective analysis of the failure of the valve replacements as a pulmonary valve, in vitro bioreactor studies can be performed. Evaluation of the functioning of the valves in a controlled hemodynamic environment might be able to effectively point out the reason for leaflet thickening.

Additionally, alternate tissue sources, not containing alpha-galactose can be investigated for pulmonary valve replacements. Since the decellularization and PGG treatment process was shown to produce optimal in vitro results in both porcine aortic and pulmonary valves, the same treatment might be beneficial in the production of functional valves from a more suitable donor source.

6.5 Conclusions

In this aim, tissue-engineered valve replacements were developed from porcine aortic valves and porcine pulmonary valves. The valve units demonstrated sufficient mechanical strength and resistance against enzyme degradation. Subcutaneous implantation of porcine aortic valves demonstrated the ability of the PGG treated decellularized valve leaflets and walls to resist calcification upon implantation. Cellular

analysis of infiltrated cells within the subcutaneous PGG implants demonstrated most of the cells were endothelial and myofibroblast-like cells, with very few inflammatory cells. Implantation of PGG treated decellularized porcine aortic and pulmonary valves in sheep as pulmonary valve repair units demonstrated some tissue thickening, probably due to tissue mismatch and presence of alpha galactose epitopes within the porcine tissue.

CHAPTER SEVEN

SPECIFIC AIM 4: EVALUATION OF PGG TREATED BOVINE PERICARDIUM SCAFFOLDS AS INTRA-MUSCULAR IMPLANTS IN DIABETIC CONDITIONS

7.1 Introduction

Biomaterials are increasingly being used for the repair of tissue defects. Muscular defects such as that of the abdominal wall result from surgery or tissue loss from traumatic injuries (480, 481). The use of synthetic materials for such tissue construction involves polypropylene or polytetrafluorethylene meshes, which are prone to infections and adhesions leading to severe bowel obstruction and herniation (482). Tissue substitutes such as acellular dermal matrices or small intestine submucosa are considered to be more favorable to promote tissue regeneration.

Decellularized pericardium tissues are rich in collagen, which is able to provide mechanical stability as well as structural guidance to cells, along with providing a matrix for cellular attachment (483). PGG treatment of decellularized pericardium scaffolds would further enhance the mechanical stability of the biomaterial and provide protection against enzymatic degradation, thus allowing more time for cellular infiltration and remodeling. Decellularized bovine pericardium and PGG treated bovine pericardium scaffolds were used as intra-muscular implants to repair abdominal wall defects.

Moreover, the repair and regeneration potential of abdominal defects is reduced with the incidence of diabetes due to an increase in pro-inflammatory cell response and

reduced anti-inflammatory cytokines (484). This impairs the healing of chronic wounds and might lead to herniation in abdominal defects. Diabetic rats with abdominal wall defects will also be implanted with intra-muscular decellularized and PGG treated pericardium to determine the adhesion of the tissues, the ability of the biomaterials to repair the wound and prevent herniation, as well as cellular infiltration within the decellularized and PGG treated implants.

PGG as a therapeutic reagent has been reported to have antimicrobial properties (18). The Minimum Inhibitory Concentration (MIC) of PGG with anti-microbial properties against *Staphylococcus aureus* is 0.13 ± 0.00 mg/ml (485). PGG added to cultures at concentrations of 12.5 μ M, PGG has also been reported to prevent biofilm formation by *S aureus* on polycarbonate membranes (486). In this study, it was determined if the PGG bound within the tissue ECM still possesses this antimicrobial property and if it renders resistance to the bacterial attachment to the PGG treated tissues.

7.2 Materials and Methods

Development of PGG treated decellularized scaffolds from bovine pericardium

Native Bovine Pericardium was obtained from Animal Technologies, Inc. The tissues after washing and removal of fat were decellularized as described in previous chapters. The tissues were treated with a decellularizing solution composed of 0.25% sodium dodecyl sulfate (SDS), 0.5% sodium Deoxycholate (DOC), 0.5% Triton X 100, and 0.2% Ethylene Diamine Tetra-Acetic acid (EDTA) in 50 mM TRIS buffer (pH $7.4 \pm$

0.05) for three days. Decellularization solution was replaced with fresh solution every day. The pericardium sheets were cut into 10 cm x 10 cm patches prior to the decellularization process to ensure the effective removal of nuclear material. DNase and RNase solutions were used at a concentration of 360 U/mL (for both DNase and RNase) to remove bovine nucleic acid components from the pericardium tissue. The DNase/ RNase treatment was done for four days at 37°C, and the solution was replaced with fresh DNase/RNase every 24 hours. The decellularized scaffolds were sterilized by shaking with sterile 0.1% Peracetic acid (pH 7.4 ± 0.05) at room temperature for 24 hours. Sterilized Decellularized Pericardium was crosslinked by treatment with sterile 0.15% PGG solution in 50 mM HEPES (4-(2-hydroxyethyl)-1-piperazineethanesulfonic acid) solution (pH 5.5) for 20 ± 2 hours. After PGG crosslinking, pericardium scaffolds were washed with PBS, and stored in sterile PBS with 1% Penicillin/Streptomycin Antibiotics.

DNA Extraction and Quantification

DNA was extracted from lyophilized native and decellularized pericardium tissues using Qiagen Dneasy Blood and Tissue Kit (Cat. No. 69504). The amount of DNA obtained from each sample was quantified with Quant-It Pico green dsDNA Reagent kit. DNA concentrations were normalized to the dry weight of tissue used for extraction.

Histology:

Native, Decellularized, and PGG treated decellularized scaffolds were fixed in 10% Neutral Buffered Formalin (NBF) Solution and processed by a series of changes through

formalin, ethanol, and paraffin to prepare the samples for histological analyses. Paraffin embedded samples were cut into 5 Micrometer sections using a microtome and stained to determine the presence of cellular material in the scaffolds as well as to determine the composition of the extracellular matrix of the scaffolds after each step.

Enzyme Treatment (Elastase and Collagenase):

Enzyme treatment was done on the native, decellularized, and PGG treated bovine pericardium scaffolds as described previously. Briefly, lyophilized tissues were treated with elastase and collagenase enzymes in TRIS buffer with CaCl_2 and NaN_3 for 24 hours and 48 hours respectively. The digested samples were lyophilized, and the percent (%) weight loss calculated for each sample.

Antimicrobial properties of PGG:

PGG as a therapeutic reagent has been reported to have antimicrobial properties. The antimicrobial property of PGG was analyzed by using free PGG in the bacterial culture media as well as after being integrated within the tissue as a crosslinking reagent.

An overnight culture in Lysogeny Broth (LB) media of *Staphylococcus aureus* was diluted to a concentration of 64×10^5 Colony Forming Units (CFU)/mL. Lyophilized decellularized and PGG treated decellularized scaffolds were soaked in 5 mL of LB media overnight. Free PGG control samples were prepared by adding PGG to LB media at concentrations of 2 mM/mL and 0.4 mM/mL. Antibiotic controls were prepared by adding

0.2 mM/mL of Penicillin/ Streptomycin and 1.7 mM/mL of Cefalexin. Positive control was used with no addition of scaffolds, PGG or antibiotics. Each of the 5 mL media samples were inoculated with 20 μ L of the diluted *S aureus* culture. A negative control was also used with no addition of bacterial culture. All of the samples were put on a shaker in an incubator at 37°C The bacterial growth in each sample was measured at time points of 3-hour, 6-hour, 12-hour, and 24-hour from the time of incubation. The CFU/mL of each sample was analyzed at each of the time points by plating on LB-Agar. At the end of 24 hours, the decellularized and PGG treated decellularized samples were removed from the bacterial culture and washed in sterile PBS to remove any bacteria that might not have adhered to the scaffolds. Each of the sample scaffolds were divided into two equal halves. The first half of the scaffolds were placed in fresh 5mL of LB Media after washing with sterile media. These samples in fresh media were placed in a shaker at 37°C for 24 hours. Bacterial growth after 24-hour from the time of incubation was measured by plating the samples after 24-hours on LB-agar plates.

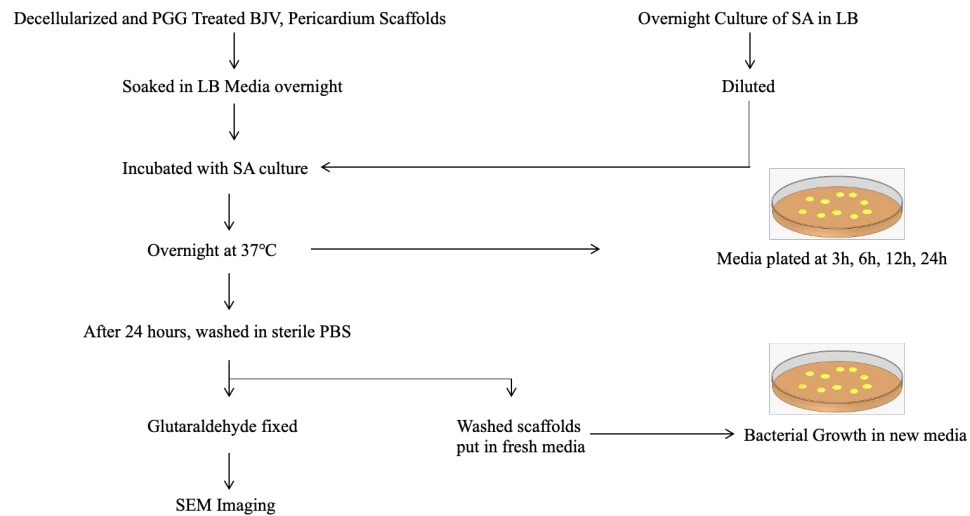


Figure 81: Experimental design for the study of antimicrobial properties of PGG treated decellularized pericardium

The second halves of the scaffolds were fixed with glutaraldehyde; the scaffolds were treated with 0.6% glutaraldehyde in 50 mM 4-(2-hydroxyethyl)-1-piperazineethanesulfonic acid (HEPES) buffered saline (pH 7.4) at room temperature with gentle shaking for 24 hours, solution decanted, and replaced with 0.2% glutaraldehyde in 50 mM HEPES buffered saline (pH 7.4) for another 24 hours (452). The Glutaraldehyde treated samples were lyophilized and sputter-coated with Platinum to be analyzed under a Scanning Electron Microscope (SEM). An electron beam with a voltage of 3 kV was used with an SE Lower Detector to visualize the surface of the scaffolds and determine bacterial attachment to the scaffolds.

Bacterial culture was also done with the extracts from the enzyme (Elastase and Collagenase) treatment. The enzyme challenge extracts were added to LB media at concentrations of 20%, 2%, and 0.2% of the total media volume. The solutions were

incubated with an incubation culture of 24×10^5 CFU/ml, and incubated overnight at 37°C. The bacterial growth within the samples were observed the next day by plating the samples and determining the CFU/ml counts.

Development of Type 2 Diabetes Model in Sprague Dawley Rats:

Type II diabetes was developed in 6-week-old SD rats using a High Fat Diet/Streptozotocin (HFD/STZ) model (487-489). The animals were allowed a week of acclimatization after obtaining from a commercial vendor. They were fed a high-fat diet consisting of 10% lard, 20% sucrose, 2.5% cholesterol and 1.0% cholate for two weeks.

After two weeks, the animals were subjected to overnight fast, and injected with Streptozotocin (55 mg/kg body weight in 0.1 M citrate buffer, pH 4.5) by tail vein injection. Animals had free access to food and water after STZ injection. A small amount of blood (~0.3 ml) was collected after three days from the tail vein, and blood glucose level was assayed using Alpha TRAK (Gen II) test strips on the Alpha TRAK Blood Glucose Monitoring System, designed specifically for animals. A blood glucose level >200 mg glucose/dL blood was considered as an establishment of Diabetes in the animals. Levels of blood glucose were monitored 3-4 times per week. Diabetic rats were given subcutaneous injections of long-lasting insulin (2-4 U Isophane) every other day to maintain blood glucose levels in a desirable range (300-500 mg glucose/dL blood) and to prevent the development of ketonuria and weight loss. Glucose levels, individual weights, hydration status, and food and water consumption were monitored closely. Animals were provided with food and water *ad libitum*.

The healthy animal group consisted of SD rats fed on a normal diet without any STZ injection.

Intra-muscular implantation surgery:

Decellularized and PGG treated decellularized pericardium patches were implanted in healthy and diabetic Sprague Dawley (SD) rats as an abdominal intra-muscular implant.

Before the full-thickness wound surgery, 1.1 -1.2 mg/kg of buprenorphine SR was administered subcutaneously to the rats at the time of surgery for analgesia. Anesthesia was induced using isoflurane in a chamber. Each animal was administered ophthalmic ointment to prevent corneal desiccation. Once the animal had reached an acceptable level of anesthesia sufficient for surgery, the ventral abdomen was shaved using clippers from the pubis to the sternum and from the lateral margins on the ventrum. The shaved area was prepared for surgery by scrubbing with an iodophor antiseptic and 70% ethanol wipe. A vertical incision, approximately 3-4 cm, was made along the ventral midline to the abdominal musculature. The abdominal wall was gently lifted, and a small opening was made through the linea alba. Incision was made into the muscle to create an approximately 2 cm x 2 cm full-thickness defect, cutting approximately 1 cm lateral from each side of the midline on both sides of the linea alba incision. A pre-cut section of mechanical bridging material (implant) was laid over the defect, the four corners of which were sutured to the abdominal wall muscle using non-absorbable suture in a simple interrupted suture pattern. Each edge of the material was secured using three additional sutures spaced equally. If significant gaps existed, which might allow passage of viscera through the abdominal wall,

they were secured using additional sutures. The subcutaneous tissue was closed using 4-0 absorbable sutures in a simple interrupted pattern (490, 491). Additionally, if the linea alba's surgical incision extended beyond the defect's margins, the remaining linea alba was closed with 4-0 absorbable sutures, also in an interrupted pattern. The skin was closed using surgical staples. Animals were allowed to recover and closely monitored until complete recovery. The skin staples were removed 7-10 days following surgery.

Animals from each group were euthanized at time points of 2 weeks, four weeks and six weeks after implantation and the implanted material was harvested. After euthanizing the animals, the skin and abdominal wall were opened to expose the area of the implant. The adhesion of the implanted material to the underlying viscera, if any, was observed. Gross pathology observations were made, and the implant was removed by cutting a wide section of the tissue, including the implant. In vitro analysis of the implant along with the surrounding tissue was done to determine the comparative ability and effectiveness of the implants incorporated into the host tissues. (Figure 82)

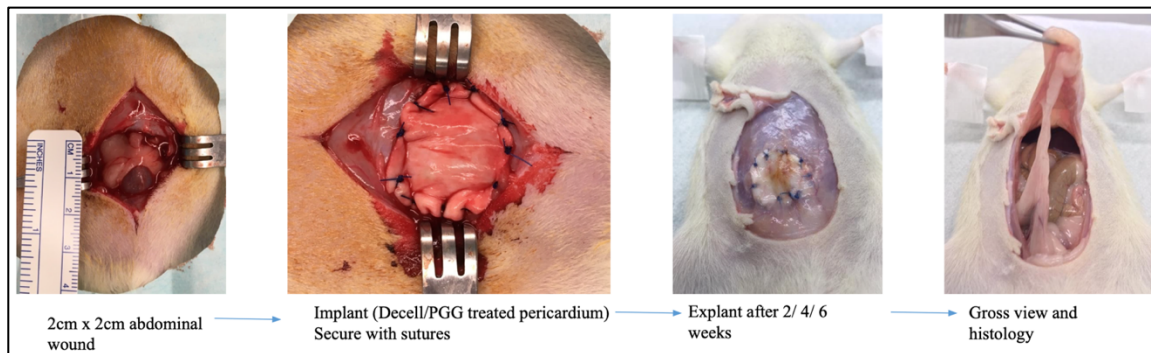


Figure 82: Intra-muscular abdominal implant surgery

In vitro analysis of explants:

The explants were analyzed in vitro to determine the cellular infiltration within the implants as well as the nature of the cellular infiltrates. Each implant was analyzed at two areas- the center of the implant and the intersection area between the implant and the abdominal muscle of the rat. Histological staining, including Hematoxylin and Eosin (H&E), Verhoeff's Elastic Stain (VVG), Alcian Blue and Masson's trichrome staining was done to determine the cellular infiltration of cells, as well as the composition of the extracellular matrix (relative distribution and structure of elastin and collagen) of the scaffolds after the implant period. Alizarin red staining was also done to determine any development of calcification within the implants.

The center and intersection areas of the implants were also analyzed immunohistochemically (IHC) to determine the relative infiltration of polarized macrophages as well as fibroblasts within the scaffolds. CD68, iNOS, and CD163 antibodies were used to look at the relative distribution of pro-inflammatory and anti-inflammatory macrophages. Vimentin and alpha-Smooth Muscle Cell staining was performed to identify the fibroblast distribution, and the implants were also stained for TNF- α to determine the presence of the inflammatory cytokine within the implant tissue. Sections were additionally stained with MMP-9 to determine the presence of this matrix metalloprotease within the decellularized and PGG treated explants. IHC images were semi-quantitatively analyzed using ImageJ software, the amount of DAB staining in each section was normalized to the cell count in the particular sample for the analysis (492).

7.3 Results

DNA Analysis:

The nanograms of DNA obtained from each sample were normalized to the initial dry weight of the sample to obtain the ng DNA/ mg dry weight of tissue. The DNA concentration obtained from the Native tissue averaged 2862.05 ± 2117.28 ng DNA/mg Dry tissue weight, and the decellularized tissues had an average DNA content of 270.03 ± 28.94 ng DNA/ mg dry weight of tissue. The DNA quantification indicated a 90.5% decrease in the DNA content of the tissues after decellularization (Figure 83).

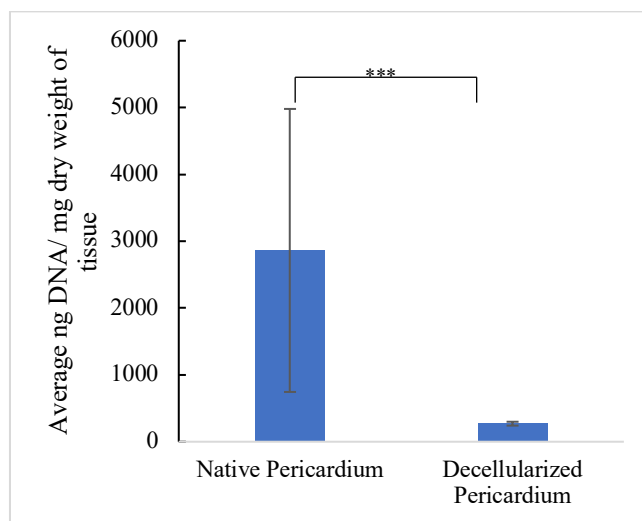


Figure 83: Pico-green dsDNA quantification in native and decellularized bovine pericardium; N=6

Histology:

Hematoxylin and Eosin (H&E) staining of the Native tissue sections indicated the presence of cell nuclei within the scaffolds (indicated by blue staining). The scaffolds after decellularization did not show the presence of any nuclear material indicating the

successful removal of Bovine nuclear material from within the scaffolds. Since the PGG crosslinking of the scaffolds was done after the decellularization step, no nuclear material was observed in the PGG treated Decellularized Pericardium scaffolds (Figure 84).

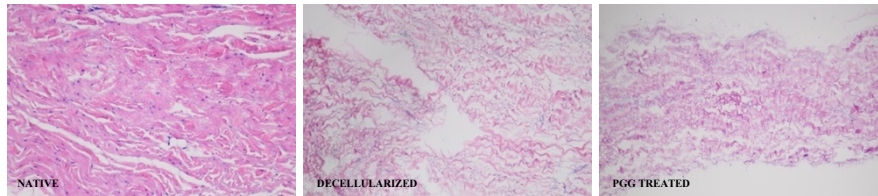


Figure 84: Hematoxylin and eosin staining of native, decellularized, and PGG treated decellularized bovine pericardium

PGG treated decellularized bovine pericardium tissues showed the presence of elastic fibers within the extracellular matrix was confirmed by the presence of dark brown staining in VVG. Masson's Trichrome staining showed the presence of collagen fibers (blue staining) within the ECM. The relative distribution and arrangement of the elastin and collagen fibers remained constant throughout the decellularization and PGG treatment processes, indicating that the processing of the native tissues to produce PGG crosslinked decellularized tissues do not affect the structure and distribution of elastin and collagen in the ECM.

Antimicrobial properties of PGG:

Incubation of decellularized and PGG treated decellularized bovine pericardium scaffolds in staphylococcus aureus cultures overnight did not affect bacterial growth in the cultures compared to control (media without any scaffolds) over a period of 24 hours. The

addition of PGG to bacterial culture media, at concentrations of 2 mg/ml and 0.4 mg/ml, however, did not show any bacterial growth, indicating PGG as a free compound was capable of inhibiting the growth of bacteria in cultures (Figure 85).

The scaffolds from the above bacterial cultures washed with PBS to remove any unattached bacterial cells when put into fresh media for 24 hours and incubated at 37°C showed growths of bacterial cells within both the decellularized and PGG treated decellularized scaffolds. There was no difference observed between the CFU/ml concentrations between the decellularized and PGG treated groups (Figure 86).

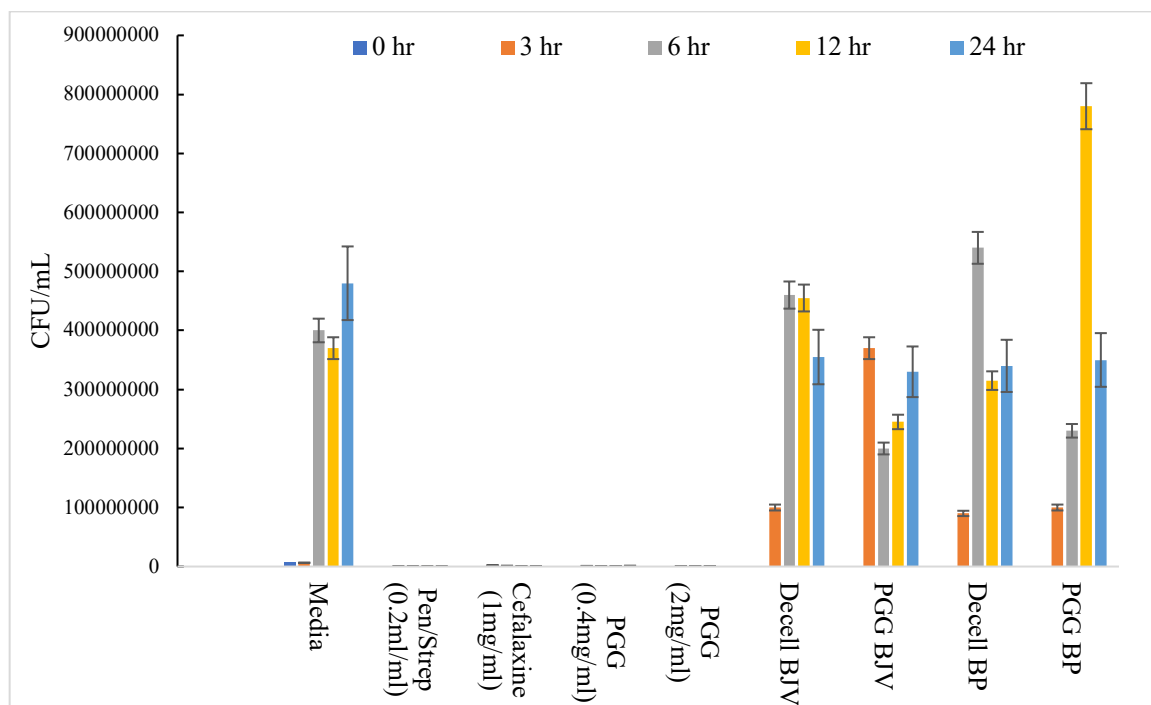


Figure 85: Decellularized and PGG treated decellularized bovine pericardium scaffolds in *S aureus* cultures (Samples in media Day-1); Decell BJV: Decellularized bovine jugular vein; PGG BJV: PGG treated Bovine jugular vein; Decell BP: Decellularized Bovine Pericardium; PGG BP: PGG treated bovine pericardium; N=4

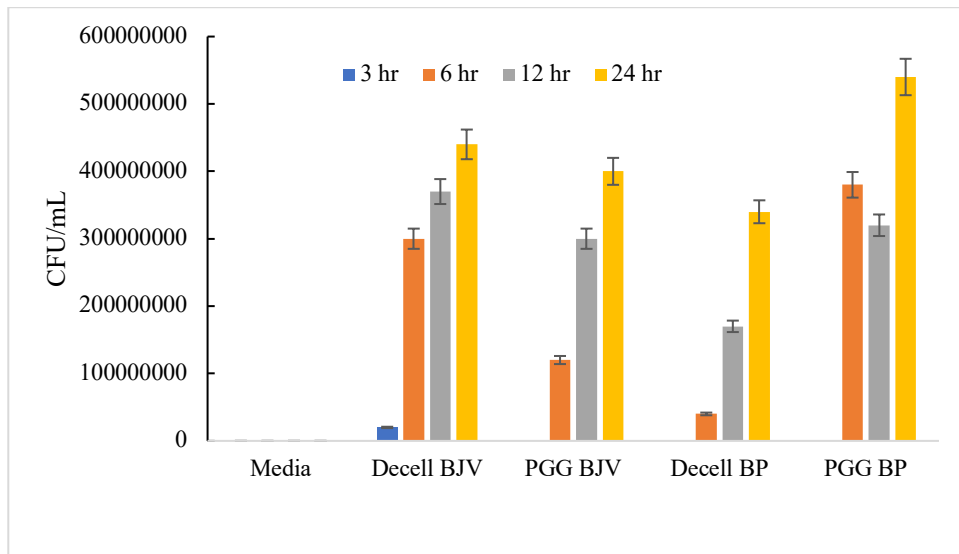


Figure 86: Growth of bacteria in *S aureus* cultures with the addition of scaffolds incubated in culture from day1; Decell BJV: Decellularized bovine jugular vein; PGG BJV: PGG treated Bovine jugular vein; Decell BP: Decellularized Bovine Pericardium; PGG BP: PGG treated bovine pericardium; N=4

Decellularized and PGG treated decellularized scaffolds after the first day in bacterial cultures were washed to remove any unattached bacterial cells and fixed in glutaraldehyde to be subsequently visualized under Scanning electron microscopy. SEM imaging of the scaffolds did not show any resistance to bacterial attachment by the PGG treated scaffolds. Figures 87, 88 and 89 represent the surface structures of decellularized and PGG treated pericardium scaffolds before and after incubation in bacterial cultures.

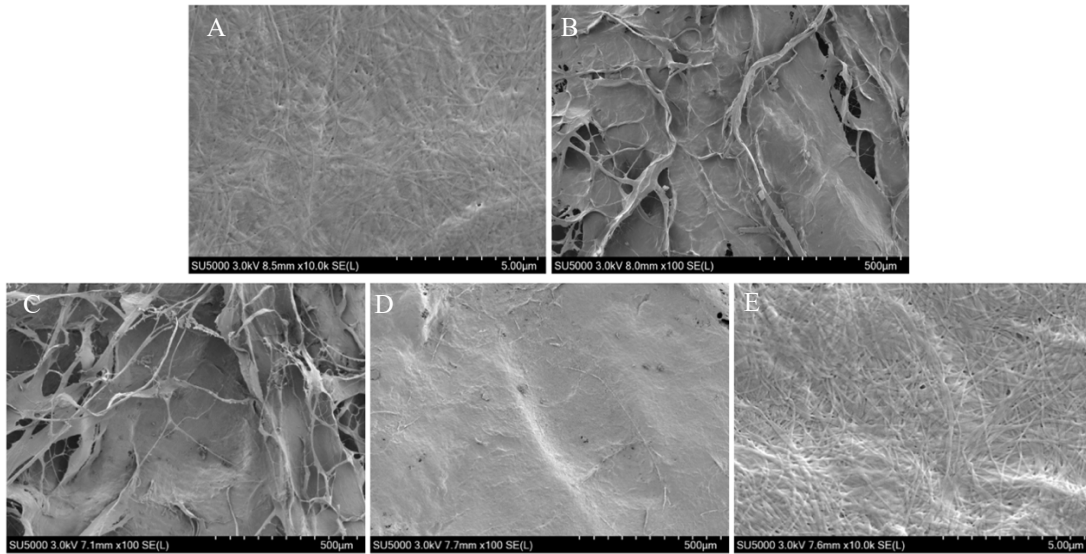


Figure 87: SEM imaging of (A,B) Decellularized and (C-E) PGG treated decellularized bovine pericardium scaffolds without bacterial incubation

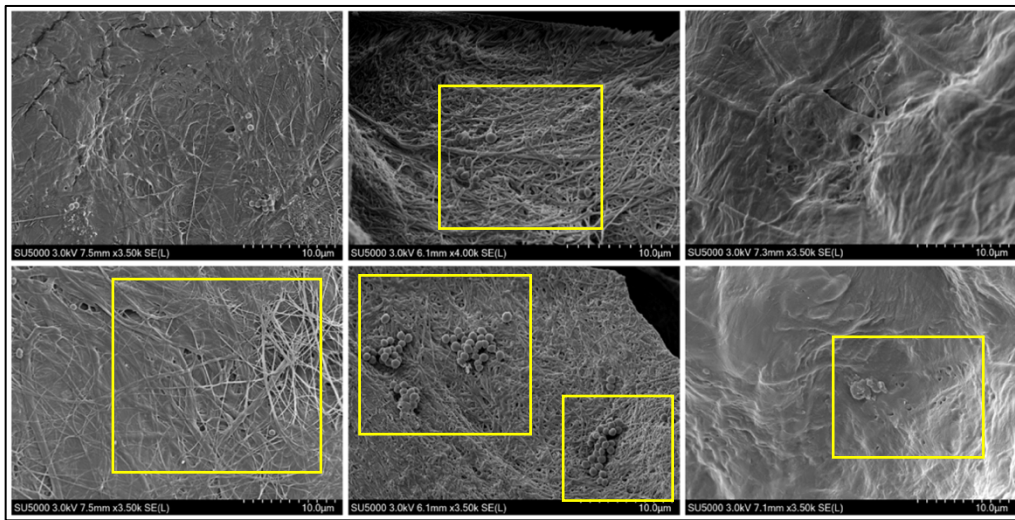


Figure 88: SEM images of decellularized bovine pericardium incubated with *Staphylococcus aureus* cultures

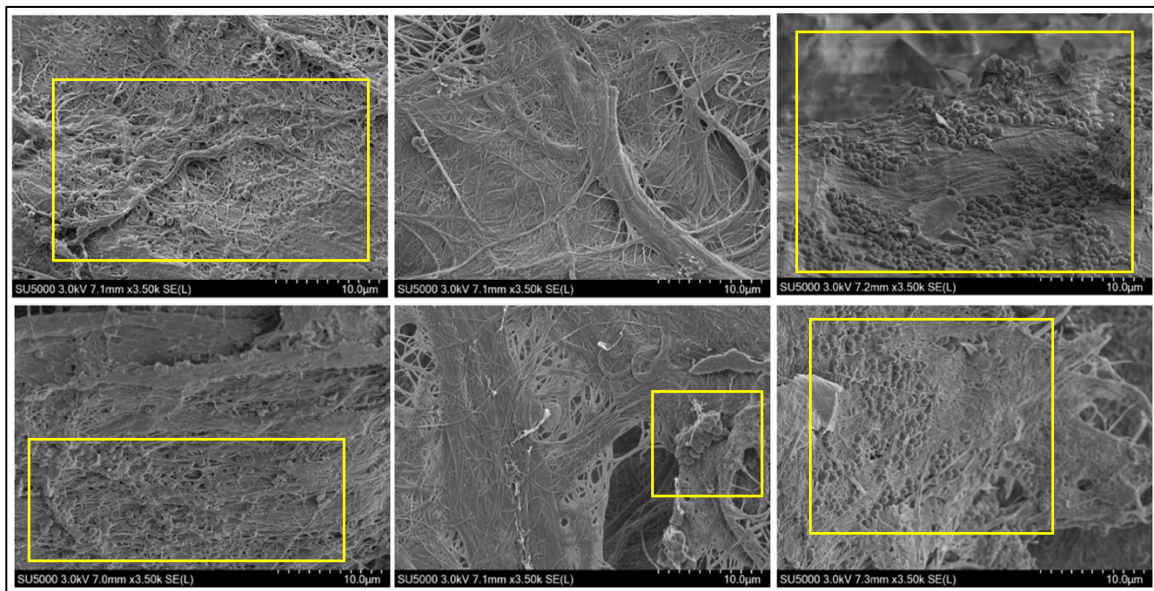


Figure 89: SEM images of PGG treated decellularized bovine pericardium incubated with *Staphylococcus aureus* cultures

Additionally, extracts from elastase and collagenase enzyme challenge of decellularized and PGG treated decellularized bovine pericardium scaffolds incubated with bacterial culture media at 20%, 2%, and 0.2% of the total media volume demonstrated a reduction in bacterial growth within the PGG group compared to decellularized extracts at a concentration of 20% for elastase treatment, and 2% for collagenase treatment. Free PGG added to bacterial cultures were capable of reducing bacterial growth at concentrations up to 50 micro-grams/ml (Figure 90).

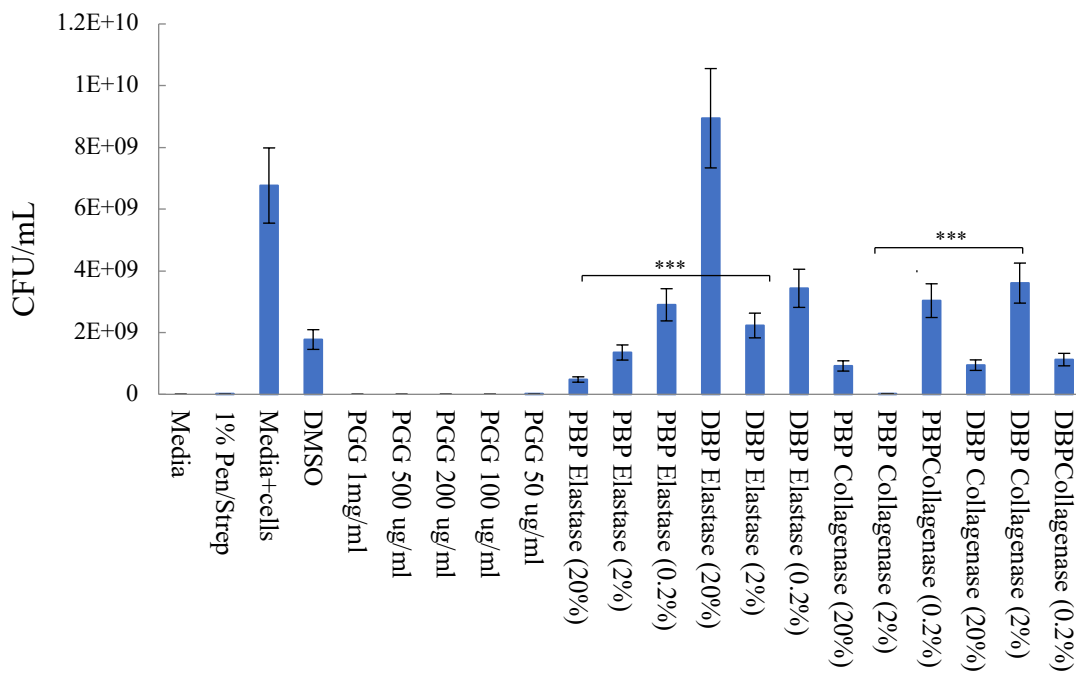


Figure 90: Bacterial growth in cultures after addition of elastase and collagenase enzyme digestion extracts from decellularized and PGG treated decellularized bovine pericardium scaffolds. PGG dissolved in DMSO was used as control; DBP: Decellularized Bovine pericardium PBP: PGG treated Bovine pericardium; N=4

High Fat Diet-Streptozotocin induced Type 2 Diabetes model in SD rats:

Diabetes was successfully induced in SD rats using the 14-day High Fat Diet followed by a single injection of STZ. The blood glucose levels of the rats were consistently maintained above 200 mg glucose/ dL blood over the time period of the implants. The weights of the individual rats were maintained at a constant level throughout the implant period. The average weights of the female diabetic rats were significantly lower than the

average weights of the male diabetic rats. The weights and blood glucose levels of the diabetic rats over the time period of the implants have been depicted in Figure 91 below.

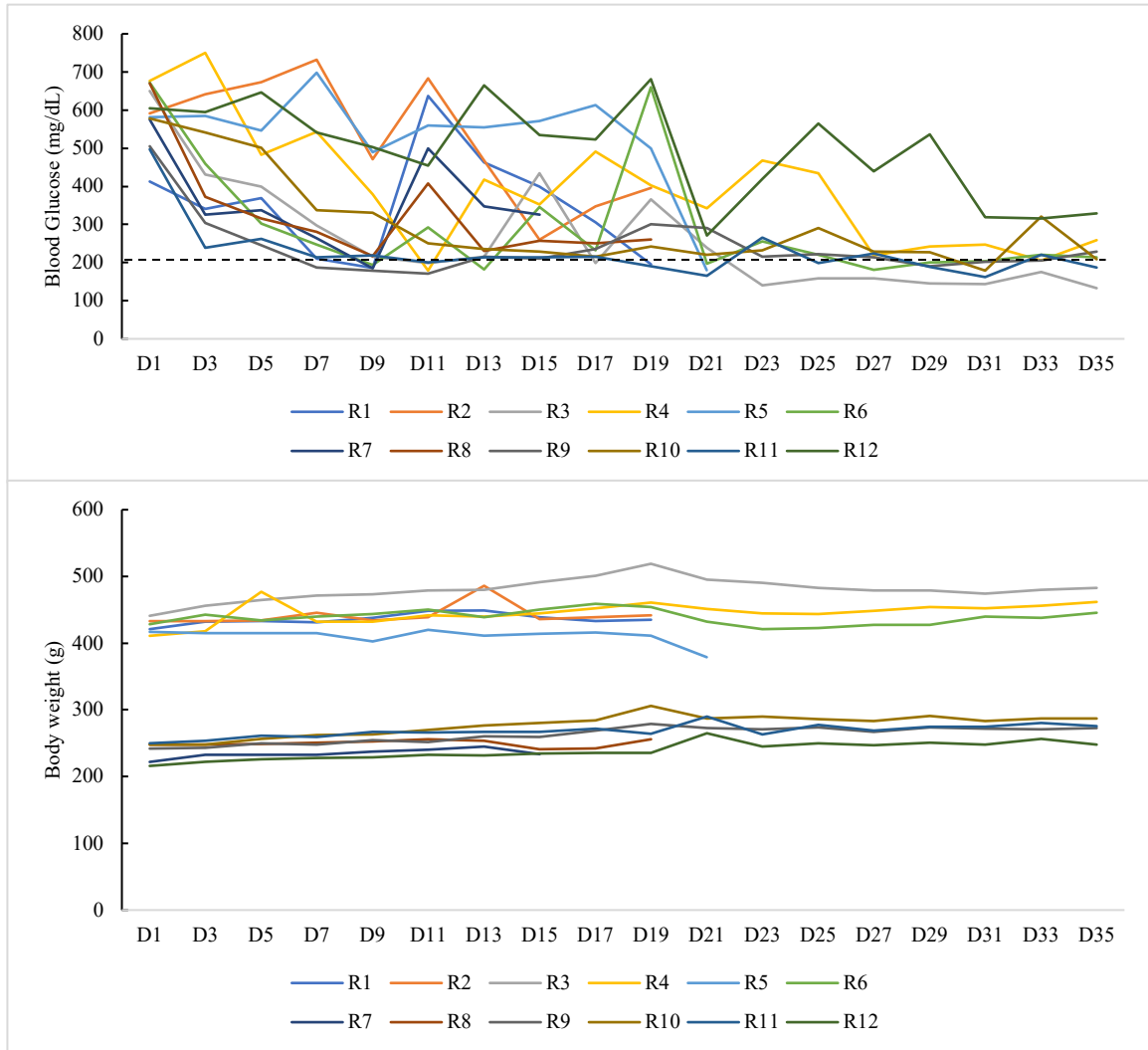


Figure 91: Weight and Blood Glucose Levels of HFD/STZ induced diabetic rats (Day 1 to Day 35); Rat 1-Rat 6: Males; Rat 7-Rat 12: Females

Gross view analysis of explants

The gross view of the implants was analysis after euthanizing the animals. One out of 10 of the non-diabetic SD rats implanted with decellularized pericardium, showed the

presence of herniation and attachment of the intestines to the implant after 4 weeks. None of the animals with PGG treated implants displayed any herniation or implant adhesion to the underlying intestines (Figure 92).

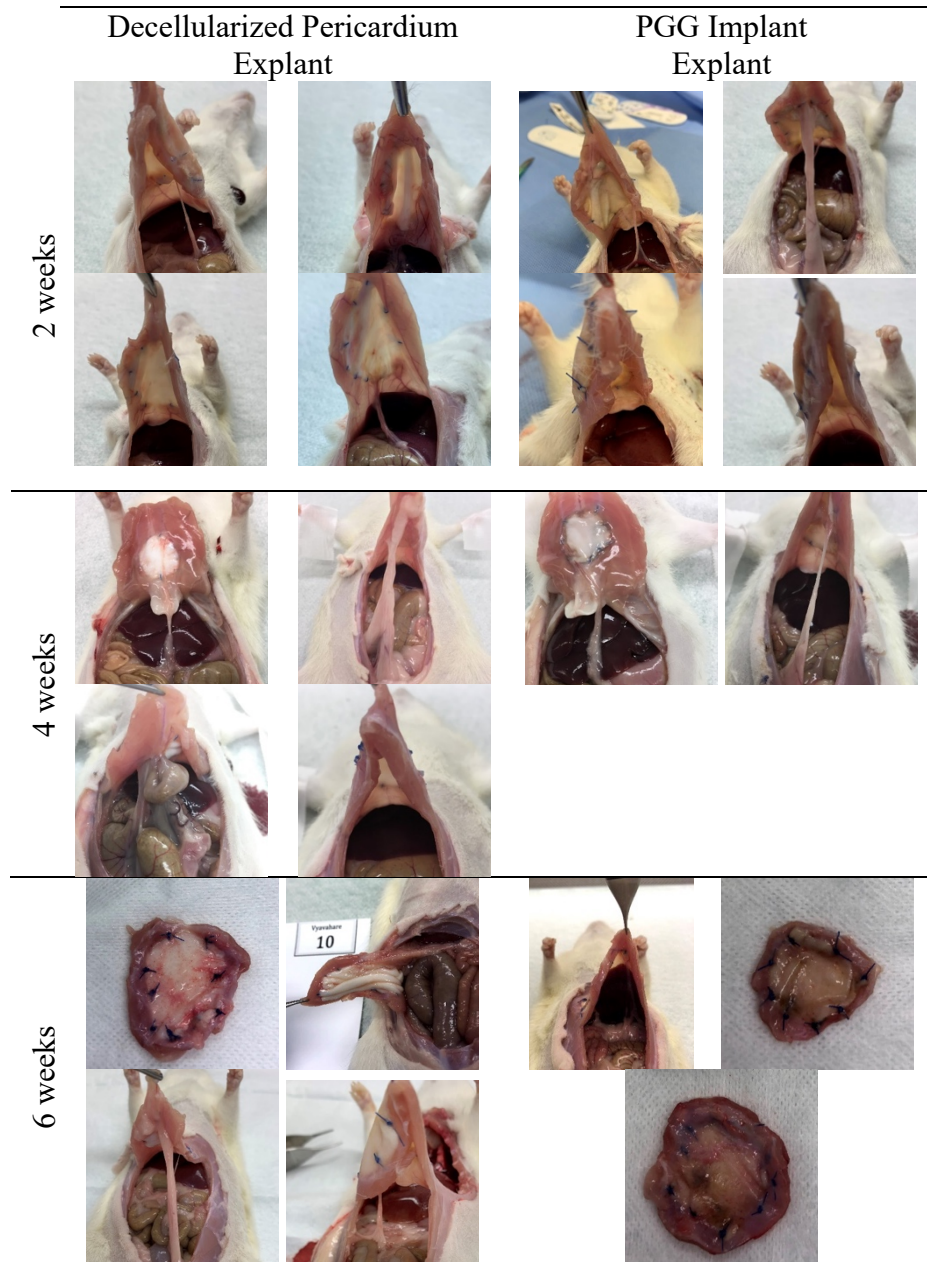


Figure 92: Gross view analysis of decellularized and PGG treated pericardium as intra-muscular implants in healthy rats

Induction of diabetes in the SD rats reduced their rate of wound healing compared to the normal rats. After two weeks of pericardium implantation, all of the diabetic rats developed herniation. To counteract the lower rate of healing, the number of sutures used to secure the implant was increased in the diabetic rats for the 4-week and 6-week time points. The addition of extra sutures prevented any further incidence of herniation, and after 4/6 weeks of implant, no adhesion was observed in any of the implants (Figure 93)

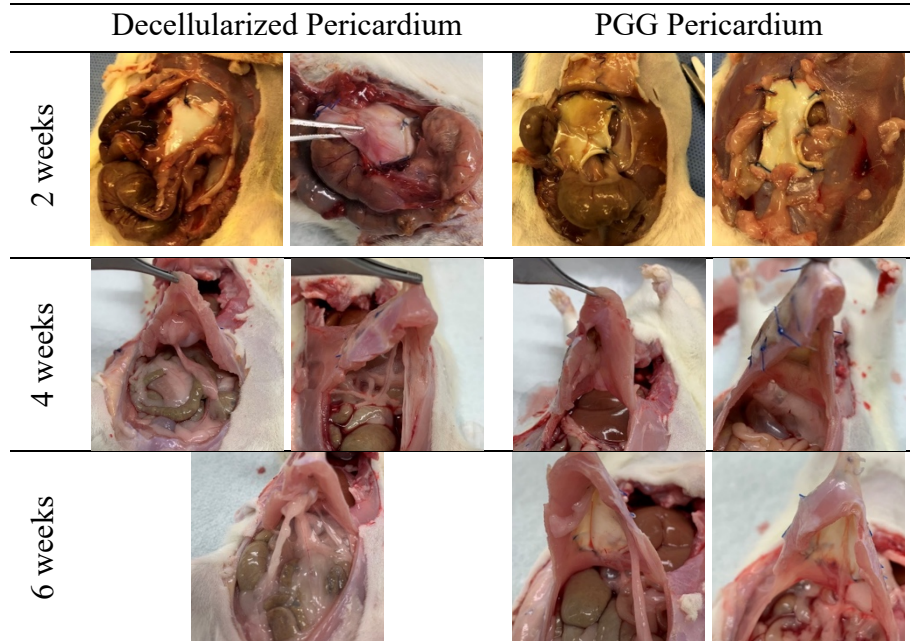


Figure 93: Gross view analysis of decellularized and PGG treated decellularized pericardium intra-muscular implants in diabetic rats

Histological analysis of intra-muscular implants

Hematoxylin and eosin staining of decellularized and PGG treated explants from intra-muscular implants in healthy and diabetic rats demonstrated infiltration of cells within

the implants after 2-, 4-, and 6- weeks of implantation. Higher number of cells were seen at the intersection of the implant and muscle compared to the center of the implants for both decellularized and PGG treated pericardium. There was no extensive inflammation observed within the explants with H&E staining.

Masson's trichrome, VVG, and Alcian blue staining of the explants demonstrated the presence of collagen, elastin, and some GAGs within the explants. No calcification was seen, as demonstrated by Alizarin red staining. The histology images of explants from healthy and diabetic rats have been demonstrated in the Figures 94-98 below.

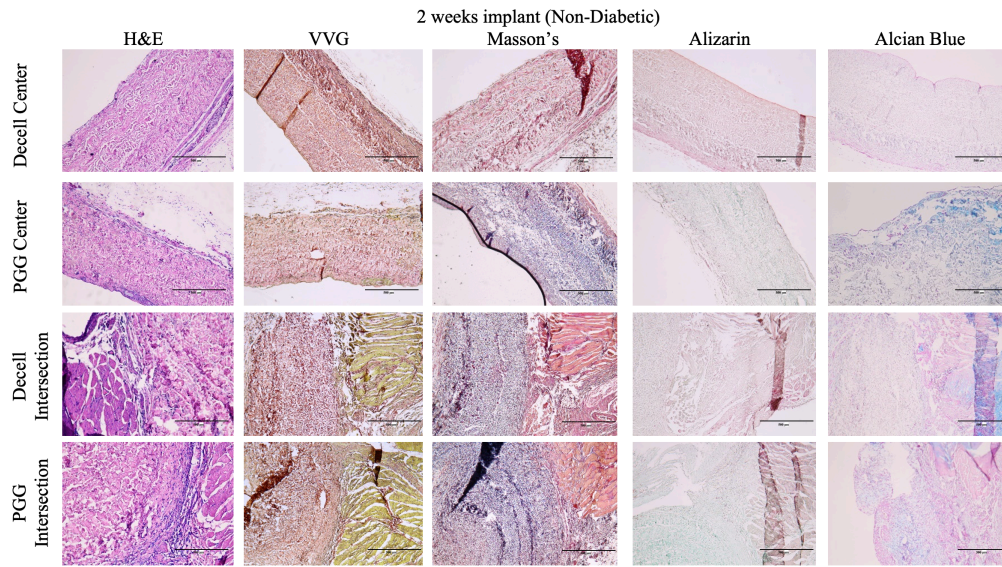


Figure 94: Histology of decellularized and PGG treated decellularized pericardium intramuscular implants in healthy rats for 2 weeks

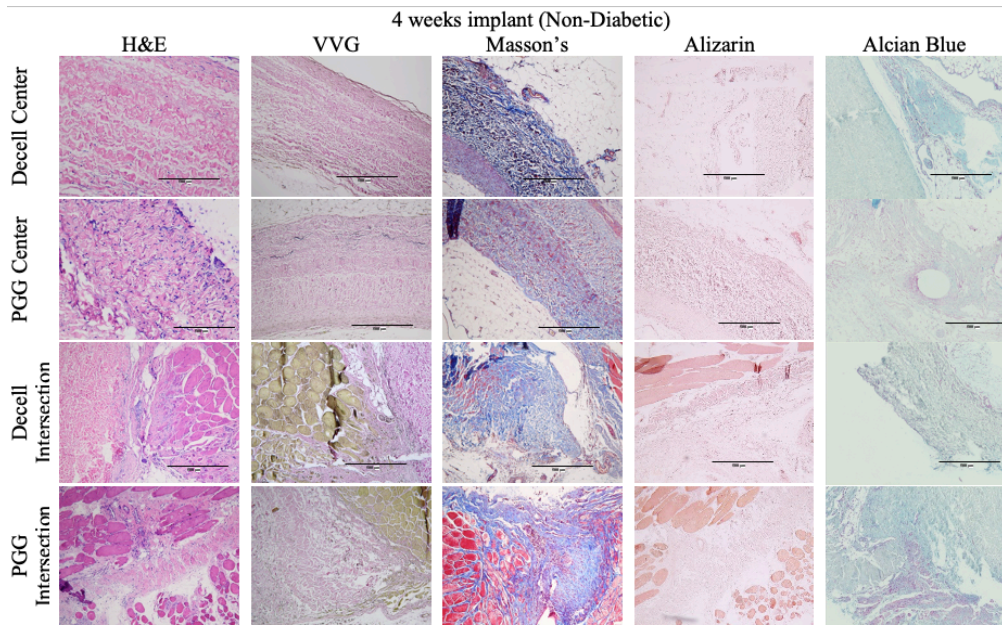


Figure 95: Histology of decellularized and PGG treated decellularized pericardium intramuscular implants in healthy rats for 4 weeks

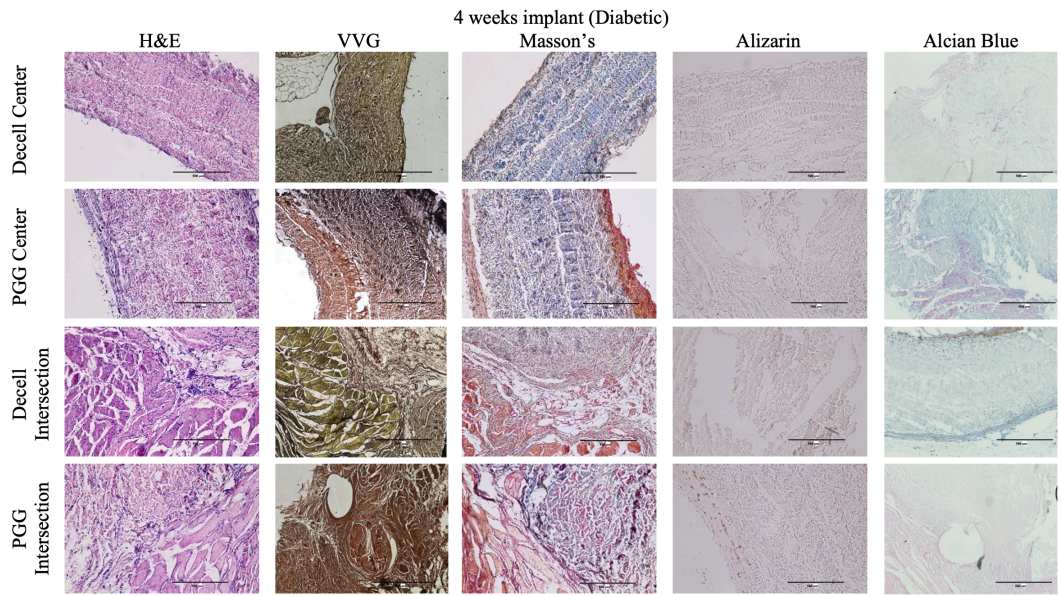


Figure 96: Histology of decellularized and PGG treated decellularized pericardium intramuscular implants in diabetic rats for 4 weeks

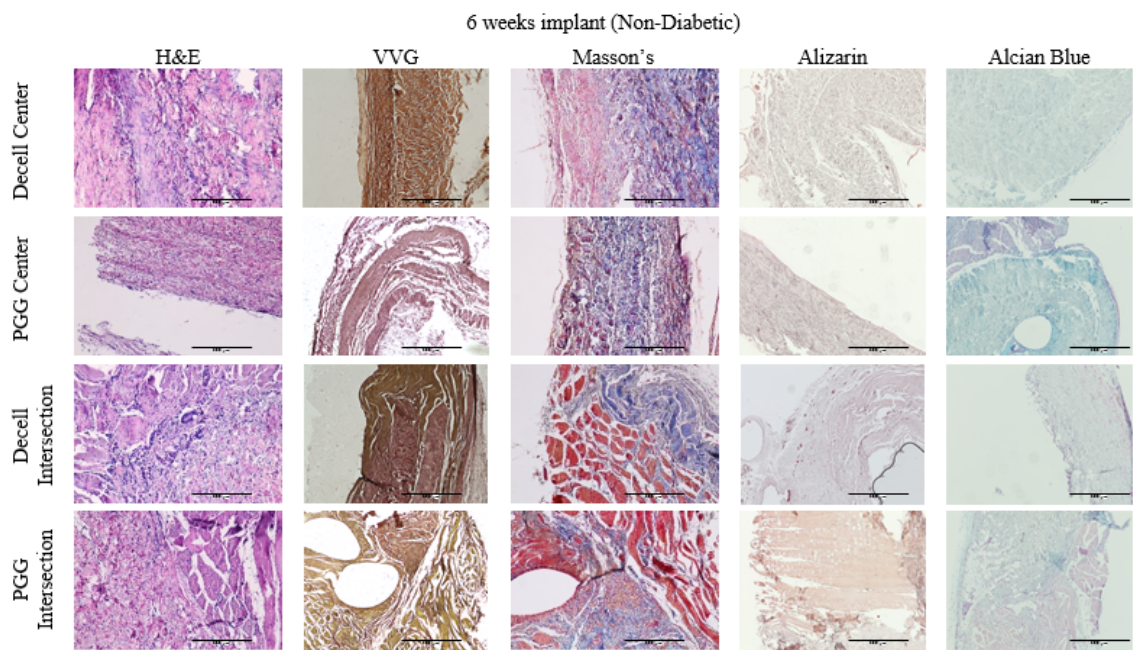


Figure 97: Histology of decellularized and PGG treated decellularized pericardium intramuscular implants in healthy rats

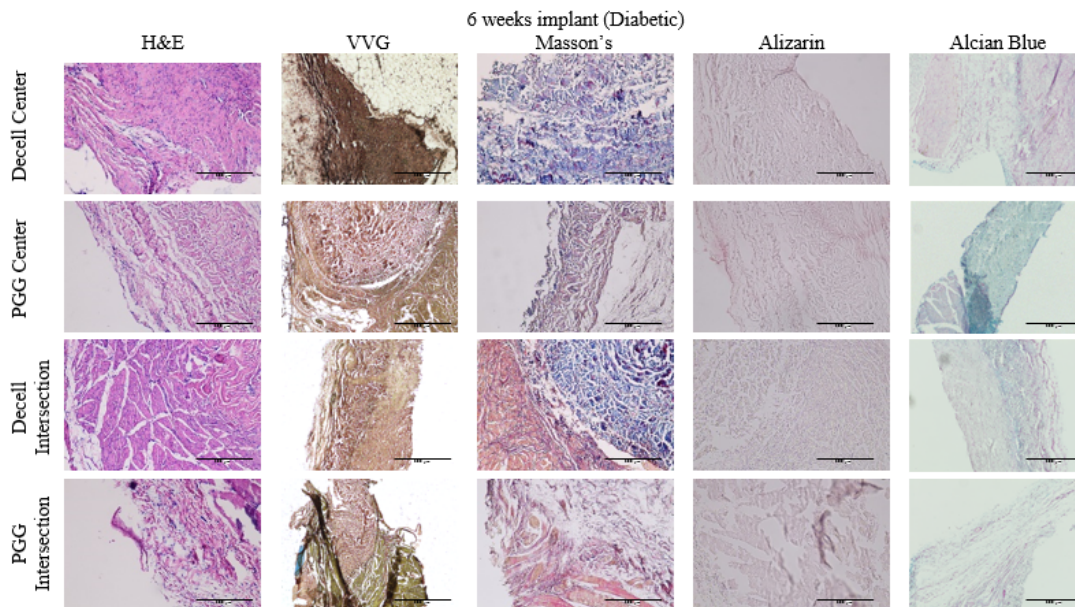


Figure 98: Histology of decellularized and PGG treated decellularized pericardium intra-muscular implants in diabetic rats

IHC Analysis of explants

To determine the infiltration of inflammatory cells within the decellularized and PGG treated bovine pericardium intra-muscular implants, explants were stained with CD68 and CD3 primary cells. M1 and M2 macrophage infiltration were also observed using iNOS and CD163 markers. TNF-alpha staining within the tissues was done to determine the presence of this pro-inflammatory cytokine in the tissues. Additionally, vimentin staining was also performed to determine the infiltration of fibroblast cells within the intra-muscular explants.

CD68 staining

Higher CD68 staining was observed in the 2-week diabetic explants compared to the healthy explants. This increase in macrophage concentration might be because of the herniation within the 2-week diabetic rats. At 4 and 6 weeks, no difference was observed between the healthy and diabetic rats for the decellularized and PGG treated groups. Furthermore, within non-diabetic animals, CD68 showed an increase in staining from 2-week to 6-week (Figure 99)

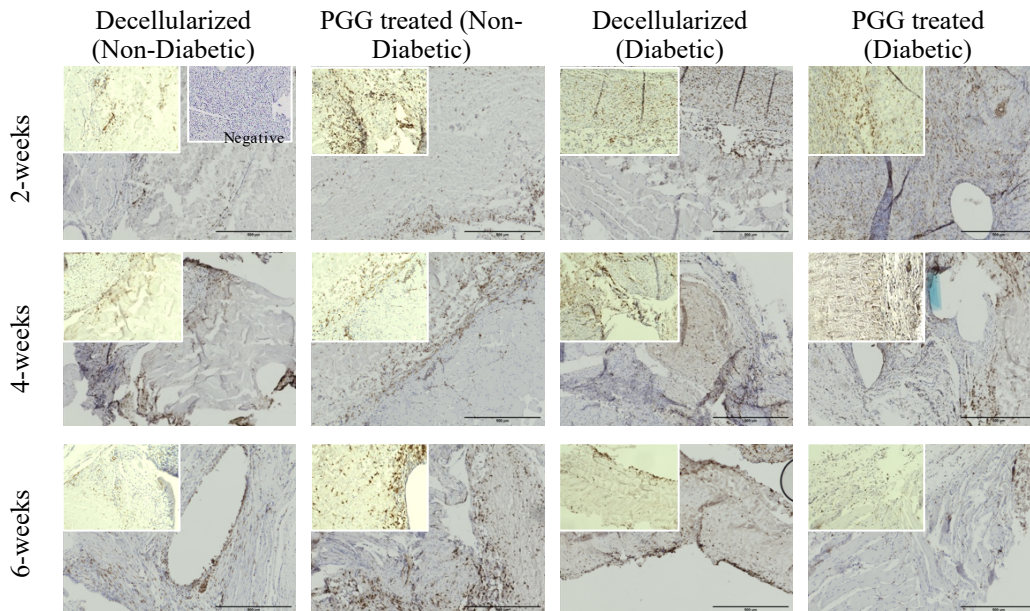


Figure 99: Representative IHC images for CD68 staining for decellularized and PGG treated decellularized bovine pericardium intra-muscular implants

	Decellularized (Non-Diabetic)	PGG treated (Non-Diabetic)	Decellularized (Diabetic)	PGG treated (Diabetic)
2-weeks	0.70	0.72	1.65	2.12
4-weeks	4.61	1.68	5.75	2.81
6-weeks	1.10	2.85	1.71	1.13

Table 9: IHC semi-quantification for CD68 DAB staining: DAB staining: number of nuclei

x 1000

CD80- Pro-inflammatory macrophages

For CD80 pro-inflammatory macrophage staining, higher CD80 positive cells were observed at 2-weeks in diabetic rats. Subsequently, at 4-week and 6-week lower CD80 staining was observed in both healthy and diabetic rats, indicating no severe inflammatory response to the implanted scaffolds. No significant difference was observed between decellularized and PGG treated implants. Moreover, diabetic implants showed an increased inflammatory response at 4- and 6- weeks compared to healthy implants (Figure 100).

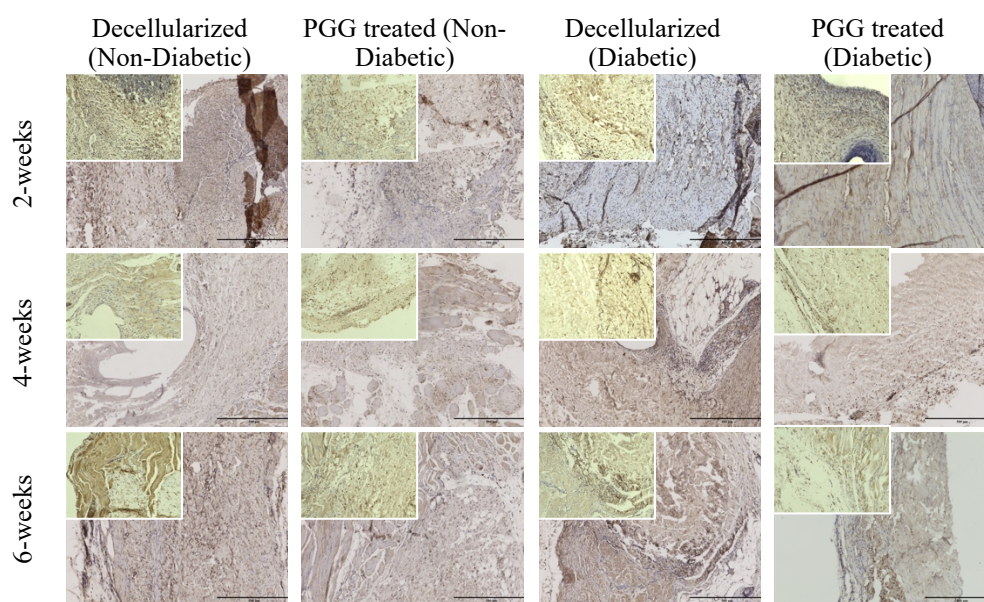


Figure 100: Representative IHC images for CD80 staining for decellularized and PGG treated decellularized bovine pericardium intra-muscular implants

	Decellularized (Non-Diabetic)	PGG treated (Non-Diabetic)	Decellularized (Diabetic)	PGG treated (Diabetic)
2-weeks	1.58	0.72	1.74	2.53
4-weeks	0.79	2.74	2.7	1.52
6-weeks	2.34	1.27	1.30	2.11

Table 10:IHC semi-quantification for CD80 DAB staining: DAB staining: number of nuclei x 1000

CD163 – anti-inflammatory Macrophages

Significant infiltration of anti-inflammatory macrophages was observed within the implanted decellularized and PGG treated implants. The staining of M2 macrophages increased from 2-week to 6-weeks. No significant difference was observed between the decellularized and PGG groups. Moreover, significant CD163 staining was observed within the diabetic implants at 4 and week time points (Figure 101).

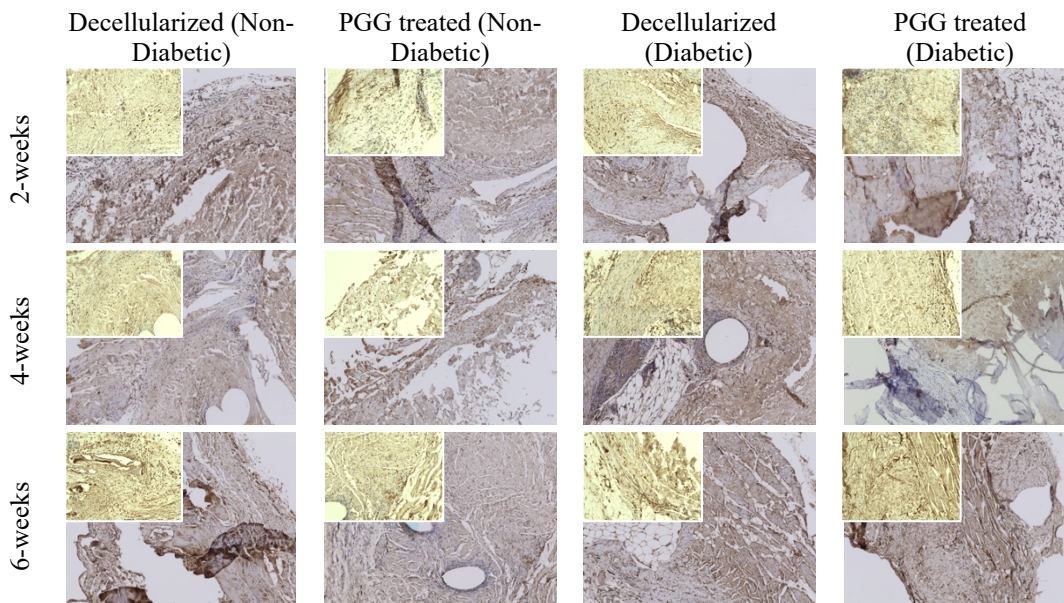


Figure 101: Representative IHC images for CD163 staining for decellularized and PGG treated decellularized bovine pericardium intra-muscular implants

	Decellularized (Non-Diabetic)	PGG treated (Non-Diabetic)	Decellularized (Diabetic)	PGG treated (Diabetic)
2-weeks	5.23	7.44	9.61	7.72
4-weeks	16.21	9.91	2.32	6.36
6-weeks	9.77	11.56	5.51	6.47

Table 11: IHC semi-quantification for CD163 DAB staining: DAB staining: number of nuclei x 1000

CD3 – T cells

CD3 T-cell infiltration was less compared to macrophages seen previously. For healthy rats, some CD3 was observed at 2-weeks for decellularized implants. However, PGG treatment demonstrated less CD3 cell infiltration. At 4-week and 6-weeks, the CD3 staining was less for both decellularized and PGG implants, with no significant difference. It is important to note that for the diabetic implants, no elevated CD3 presence was observed at 2-, 4-, or 6- week time points (Figure 102).

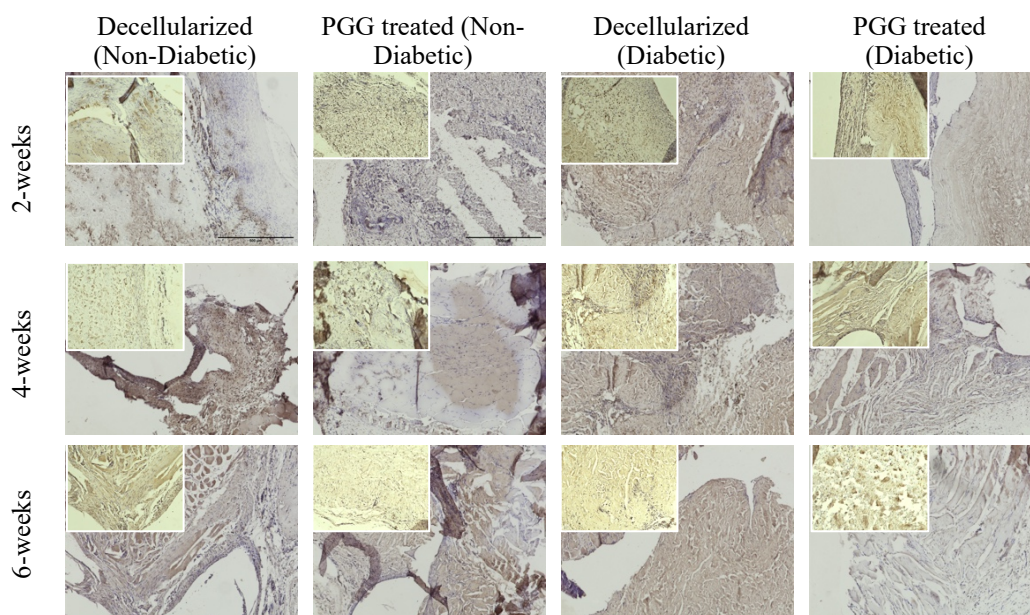


Figure 102: Representative IHC images for CD3 staining for decellularized and PGG treated decellularized bovine pericardium intra-muscular implants

	Decellularized (Non-Diabetic)	PGG treated (Non-Diabetic)	Decellularized (Diabetic)	PGG treated (Diabetic)
2-weeks	0.15	0.01	0.02	0.006
4-weeks	0.009	0.01	0.04	0.04
6-weeks	0.01	0.01	0.02	0.01

Table 12: IHC semi-quantification for CD3 DAB staining: DAB staining: number of nuclei

TNF-alpha pro-inflammatory cytokine

Less TNF-alpha staining was observed within all explants. This might be because most of the pro-inflammatory cytokine is found within the blood, and very less within tissues. Moreover, staining was less pronounced in healthy rats at 4-, and 6- weeks for both decellularized and PGG implants. Diabetic rats demonstrated an increased level of the cytokine as is observed in diabetic conditions. There was, however, no difference observed between decellularized and PGG implants in diabetic conditions (Figure 103).

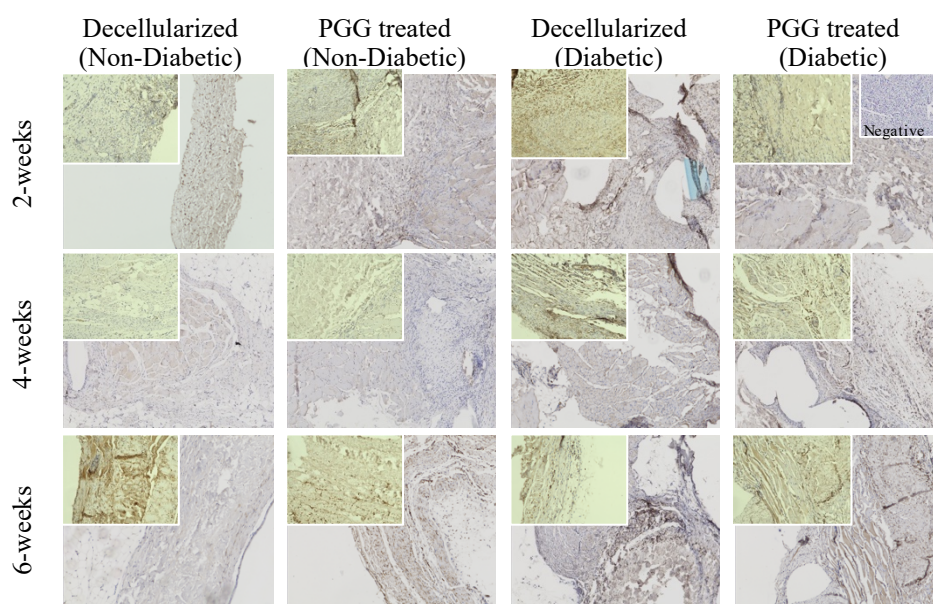


Figure 103: Representative IHC images for TNF - Alpha staining for decellularized and PGG treated decellularized bovine pericardium intra-muscular implants

	Decellularized (Non-Diabetic)	PGG treated (Non-Diabetic)	Decellularized (Diabetic)	PGG treated (Diabetic)
2-weeks	2.73	2.14	6.78	1.30
4-weeks	3.79	5.75	5.92	4.10
6-weeks	1.64	8.52	1.65	2.62

Table 13: IHC semi-quantification for TNF-alpha DAB staining: DAB staining: number of nuclei x1000

iNOS- Nitric Oxide Synthase

i-NOS (inducible Nitric Oxide Synthase) staining of the intra-muscular explants demonstrated significantly less presence of nitric oxide species within the PGG treated implants. Presence of iNOS might be an indication of the production of inflammatory macrophages and cytokines. Moreover, PGG implants demonstrated less iNOS expression compared to decellularized explants in both healthy and diabetic conditions (Figure 104).

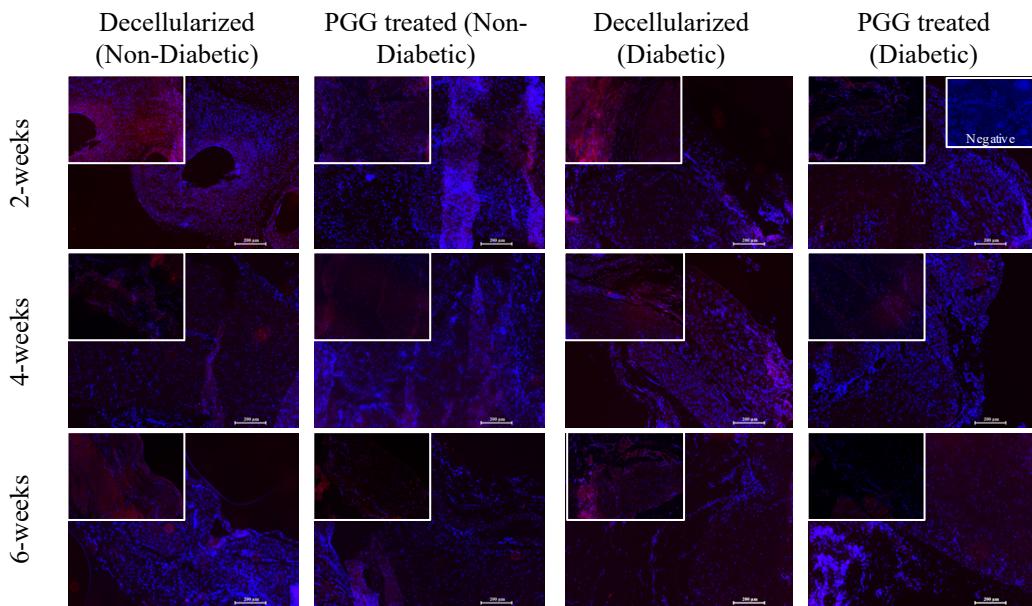


Figure 104: Representative IHC images for i-NOS staining for decellularized and PGG treated decellularized bovine pericardium intra-muscular implants

	Decellularized (Non-Diabetic)	PGG treated (Non-Diabetic)	Decellularized (Diabetic)	PGG treated (Diabetic)
2-weeks	0.9	0.35	1.11	0.68
4-weeks	0.67	0.41	0.81	0.40
6-weeks	0.41	0.47	0.93	0.58

Table 14: IHC semi-quantification for i-NOS staining: Immunofluorescence staining: area of nuclei

MMP-9

MMP-9 is a matrix metalloproteinase that regulates pathological remodeling of tissues associated with inflammation and fibrosis in cardiovascular diseases. While the presence of some MMPs like MMP-1 is normal in wound healing sites, excessive MMP-9 indicates chronic inflammation. The PGG treated explants demonstrated lesser expression of MMP for 4- and 6- weeks in both healthy and diabetic conditions indicating lower incidence of chronic inflammation (Figure 105).

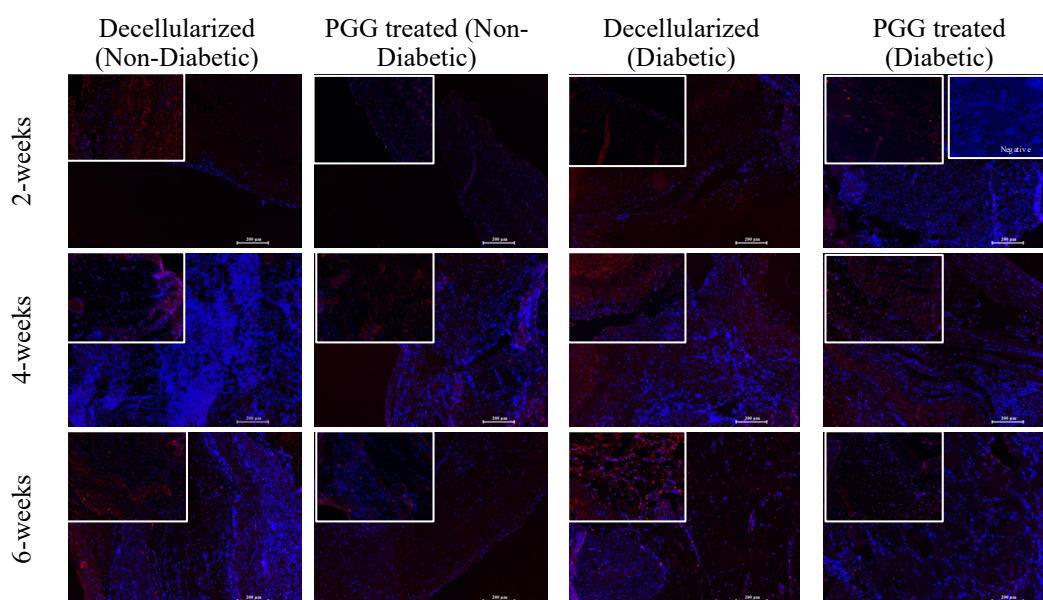


Figure 105: Representative IHC images for MMP-9 staining for decellularized and PGG treated decellularized bovine pericardium intra-muscular implants

	Decellularized (Non-Diabetic)	PGG treated (Non-Diabetic)	Decellularized (Diabetic)	PGG treated (Diabetic)
2-weeks	1.72	1.02	0.77	0.25
4-weeks	1.04	0.51	0.63	0.57
6-weeks	1.14	0.68	1.74	0.81

Table 15: IHC semi-quantification for MMP-9 staining: Immunofluorescence staining: area of nuclei

Vimentin - Fibroblasts

Infiltration of vimentin-positive fibroblasts within healthy implants increased with an increase in time of implant. At 2-weeks, significantly less cells were observed, which increased at 4-, and 6- weeks. No difference was observed between decellularized and PGG implants. More spindle-shaped fibroblasts were observed in PGG implants. Diabetic implants showed more fibroblast infiltration. Additionally, more vimentin staining was seen in PGG implants in diabetic rats compared to decellularized implants (Figure 106).

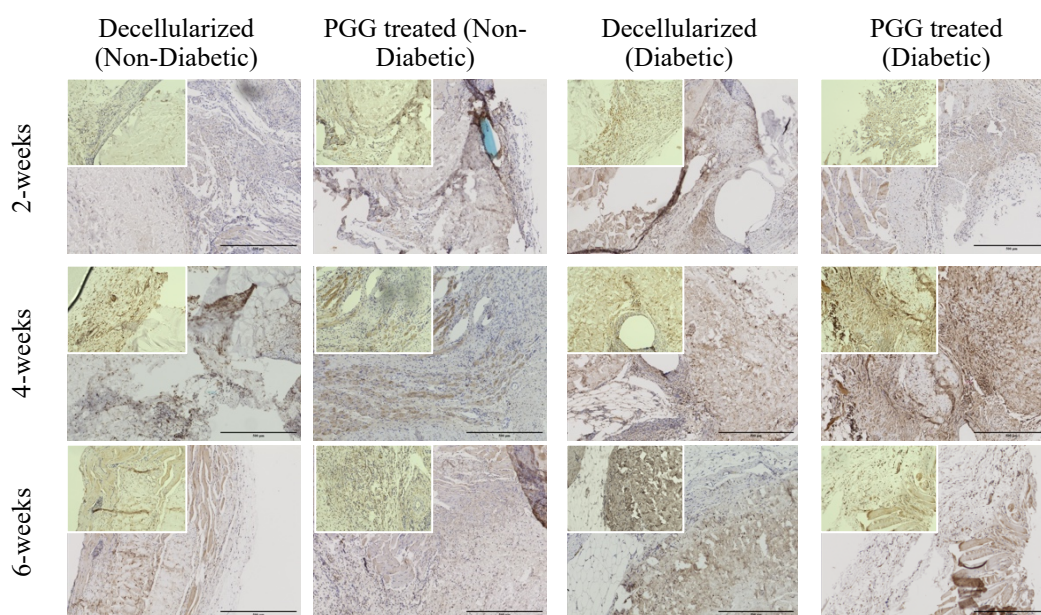


Figure 106: Representative IHC images for Vimentin staining for decellularized and PGG treated decellularized bovine pericardium intra-muscular implants

	Decellularized (Non-Diabetic)	PGG treated (Non-Diabetic)	Decellularized (Diabetic)	PGG treated (Diabetic)
2-weeks	0.20	2.27	5.16	4.04
4-weeks	3.57	2.19	2.69	5.58
6-weeks	2.79	1.78	5.04	3.32

Table 16: IHC semi-quantification for Vimentin DAB staining: DAB staining: number of nuclei

Alpha-Smooth Muscle Actin (SMA)

Both decellularized and PGG treated decellularized explants demonstrated the expression of Smooth Muscle actin in lower concentrations, indicating some infiltration of myofibroblast cells. The infiltration of SMA increased with increase in implantation time. No significant difference was observed between the decellularized and PGG implants with respect to myofibroblast infiltration (Figure 107).

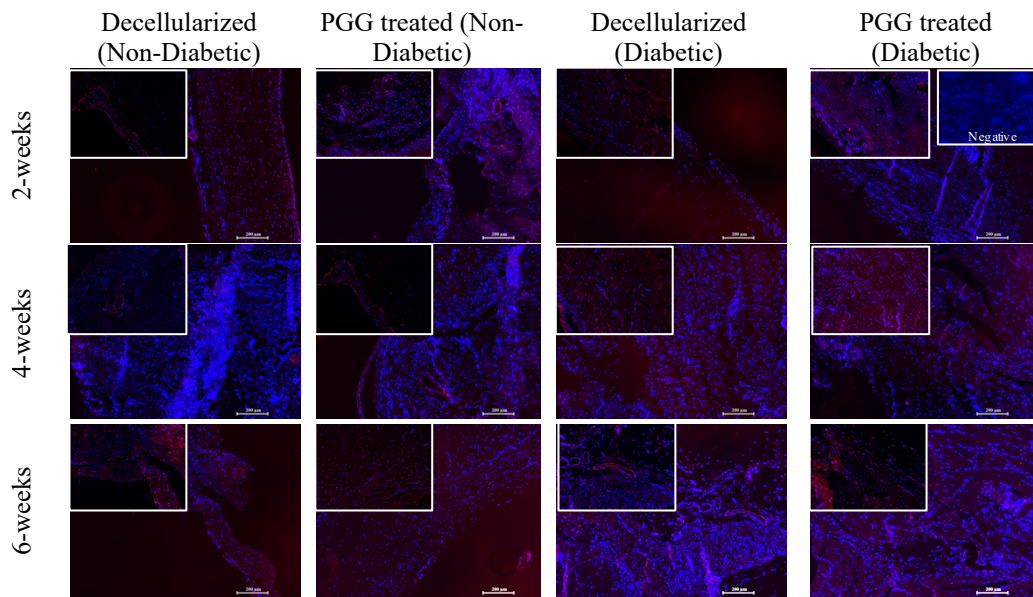


Figure 107: Representative IHC images for Alpha-Smooth muscle cell staining for decellularized and PGG treated decellularized bovine pericardium intra-muscular implants

	Decellularized (Non-Diabetic)	PGG treated (Non-Diabetic)	Decellularized (Diabetic)	PGG treated (Diabetic)
2-weeks	0.95	1.19	0.68	1.89
4-weeks	0.59	1.21	0.73	1.27
6-weeks	2.79	1.48	0.46	1.06

Table 17: IHC semi-quantification for Alpha-SMC staining: Immunofluorescence staining:

area of nuclei

7.4 Discussions

Wound healing in diabetic conditions is a major issue resulting from a prolonged inflammatory phase and delayed regeneration of tissues. It results in various complications, including the susceptibility of the wound to infection. Moreover, delayed abdominal wound healing in diabetic conditions leads to herniation and bowel obstruction in patients.

In this study, PGG and decellularized pericardium scaffolds were initially analyzed for their antibacterial properties. PGG has been observed to inhibit the growth of bacterial cells in cultures, as well as the adhesion of bacterial cells to surfaces. The addition of free PGG to media resulted in inhibition of growth of *Staphylococcus aureus* in cultures for up to concentrations of 50 ug/ ml. However, when PGG was used to crosslink decellularized scaffolds, there was no inhibition to bacterial growth observed. The PGG treated decellularized scaffolds further failed to prevent attachment by bacterial cells as observed with Scanning electron microscopy. Extracts obtained from enzyme degradation of PGG treated decellularized scaffolds were able to inhibit bacterial growth at higher concentrations, however at lower concentrations, owing to the very less concentration of PGG present in the extracts, no significant inhibition to bacterial growth was observed. It would therefore be more beneficial to treat PGG treated decellularized scaffolds with antibiotics to render them anti-microbial properties.

The type II diabetic model developed in this study using a high-fat diet and STZ injection was capable of developing and maintaining elevated blood glucose levels within the rats. The elevated glucose levels were maintained for at least 7-weeks after the STZ injections, covering the whole time of the intra-muscular implant experiments.

Decellularized and PGG treated decellularized pericardium scaffolds implanted in rats as intra-muscular implants demonstrated effective closure of the wound in healthy and diabetic rats. In diabetic conditions, however, owing to the delayed wound healing in the rats, with the same number of sutures for patch securing, herniation of the intestines was observed after the surgery. Corrective measures using a higher number of the non-continuous suture securing were successful in counteracting the adverse reactions. No herniation was observed in the diabetic rats with an increased number of sutures. Additionally, decellularized implants, due to their higher susceptibility to enzymes degrading the ECM components, demonstrated a higher degree of absorption into the surrounding tissues. While the integration of implants is desired, a speedy rate of degradation might lead to implant failure and herniation or intestinal adhesion in the case of intra-muscular implants. Adhesion to underlying organs was observed in two of the decellularized implants in healthy rats. The PGG treated decellularized pericardium scaffolds did not show any adhesion to the underlying organs for any of the rats. This property of PGG treated implants should be further studied and utilized for abdominal wound healing patch developments.

Histologically, no increased inflammatory response was observed to the PGG treated implants compared to the decellularized implants. Even under diabetic conditions, the PGG treated implants did not induce any higher inflammatory response. There was, however, no reduction in infiltration of inflammatory cells observed with PGG treated implants. Moreover, a higher number of fibroblasts were seen in PGG treated diabetic implants compared to decellularized scaffolds. It has been observed in studies, however,

that fibroblast morphology in diabetic conditions is altered. Additionally, lesser expression of i-NOS and MMP-9 was observed in the PGG treated implants for both healthy and diabetic rats. Lower nitric oxide synthase as well as MMP-9 within the PGG treated implants might be an indication of the ability of these scaffolds to prevent chronic inflammation. More investigation is required in understanding the effect of altered fibroblast morphology, number, and wound healing potential in diabetic conditions.

7.8 Conclusions

PGG treated decellularized bovine pericardium scaffolds did not demonstrate antibacterial properties, although free PGG is capable of inhibiting bacterial growth at concentrations up to 50 ug/ml. PGG treated decellularized implants in healthy and diabetic rats as intra-muscular implants did not show any extensive inflammatory response in diabetic conditions. Both decellularized and PGG treated bovine pericardium implants showed optimum performance as intra-muscular patches. PGG treated implants degraded and reintegrated slower to decellularized scaffolds. Moreover, PGG treatment of implants encouraged more fibroblast infiltration in diabetic conditions, as well as reduced i-NOS and MMP-9 expression within the scaffolds. PGG treated decellularized pericardium implants can therefore be a suitable patch material for diabetic conditions.

CHAPTER EIGHT

CONCLUSIONS AND FUTURE RECOMMENDATIONS

8.1 Conclusions

Treatment of congenital heart diseases requiring replacement conduit and valves has always been challenging owing to the failure of these grafts in the long run. Use of synthetically derived or bioprosthetic scaffolds that do not grow along with pediatric patients lead to multiple surgeries throughout their lifetime leading to increased risk of infection, thrombosis, calcification, and implant failure. This research aimed at developing conduit and valve replacements for pediatric patients that allow cellular infiltration and have a growth potential.

The first part of this research aimed at developing a decellularization protocol and optimizing its efficiency in different tissue types. The Ethanol- NaOH- detergent based decellularization protocol developed was successful in decellularizing most of the cellular and nuclear components from bovine jugular veins, bovine pericardium, and porcine fascia tissues. The process maintained the structure of the extracellular matrix within the native tissues while successfully reducing the ng DNA/mg dry weight of tissue concentrations. Decellularized scaffolds were then crosslinked to prevent rapid degradation of elastin and collagen within the extracellular matrix of the tissues. Different polyphenols were compared for their efficiency in the crosslinking procedure. Among polyphenols, Quercetin, Hesperidin, PGG, D-Salicin, and ATRA; Quercetin, PGG and ATRA showed crosslinking capabilities to various degrees in different tissues. PGG however was

determined as the most effective in protecting elastin and collagen from enzymatic degradation. Additionally, addition of 10 ug/ml of each of the polyphenols to HAoSMC cultures demonstrated that quercetin and PGG substantially increased the deposition of insoluble elastin as well as Fibrillin I within the cell culture matrix. PGG, therefore was the most effective in protecting extracellular components from enzyme degradation and was used for studies in the next aims.

The second part of the research aimed at developing pediatric conduit and valve replacements from decellularized scaffolds crosslinked with PGG. The concentration of PGG required for optimal crosslinking was determined, and PGG crosslinked BJV demonstrated superior resistance to enzyme degradation compared to decellularized scaffolds. PGG treated scaffolds also demonstrated mechanical properties comparable to that of native tissues, and when implanted subcutaneously in rats showed resistance to calcification as well as cellular infiltration. PGG treated decellularized BJV conduits implanted in juvenile sheep as pulmonary conduit replacements also demonstrated no calcification, stenosis, no leaflet thickening, as well as significant cellular infiltration of fibroblasts, myo-fibroblasts, endothelial luminization, collagen remodeling, and an increase in size explanted after 3 months. Valve replacements developed from porcine aortic valves and porcine aortic valves also demonstrated resistance to enzyme degradation and had mechanical characteristics not significantly different from native tissues. PGG treated porcine aortic valves also resisted calcification in subcutaneous implantations, unlike glutaraldehyde tissues, and showed infiltration of >60% non-inflammatory cells.

However, pulmonary valve repairs in sheep using porcine aortic and pulmonary valves showed some thickening within the leaflet walls due to tissue mismatch

Finally, in the last section of this research, PGG treated decellularized bovine pericardium scaffolds were evaluated as intra-muscular implants in healthy and diabetic rats to look at the inflammatory responses induced by the implants. The infiltration of inflammatory cells in PGG treated scaffolds was not different from decellularized scaffolds. PGG treated decellularized scaffolds demonstrated lesser expression of nitric oxide synthase and MMP-9. Additionally, PGG treated tissues in-vitro showed reduced degradation compared to decellularized scaffolds and prevented herniation within the animals.

8.2 Recommendations for future work

- In aim 1, the ability of different polyphenols to crosslink components of the extracellular matrix was studied. All the polyphenol treatments were done at the same concentrations. At the used concentrations and buffering solutions, PGG was identified as the most effective crosslinker. However, ATRA, Hesperidin and Quercetin also demonstrated some degree of collagen and crosslinking in some of the tissues. It would be useful to study the individual polyphenols at different concentrations and under optimal buffering solutions. Even though these polyphenols did not show optimal crosslinking at the used concentrations, a different buffering solution or concentration would be more suitable for them.

- The effect of polyphenols PGG, quercetin, hesperidin, D-salicin, and ATRA on elastin synthesis was studied in human aortic smooth muscle cell cultures. However, only the amount of insoluble elastin deposited and the effect of treatment on Fibrillin I protein were analyzed. To better understand the effect of the specific polyphenol on cell cultures, proteins affecting the elastin synthesis process, like LOX, can also be studied. Additionally, it would also be interesting to look at the effect of polyphenol treatments on the production of tropoelastin within the cell culture.
- The decellularization procedure using Ethanol-NaOH and detergents could be optimized for the different tissue types used. In this study, the efficiency of the decellularization treatment was optimized in bovine jugular vein tissues, and subsequently, the same treatment was used for all the other tissue types. Although no destruction of the extracellular matrix was seen within any of the tissue types decellularized, optimization of the procedure for each tissue might result in a reduction of the decellularization steps and optimize time as well as the use of reagents.
- Determination of the efficiency of the decellularization procedure in this research was done by quantifying the amount of dsDNA within the native and decellularized tissues. For a more effective evaluation, lengths of the

remaining DNA base pairs must also be analyzed (<200 bp), as well as the effective removal of alpha-galactose within the scaffolds should also be analyzed.

- Additionally, the decellularization process was carried out in a laboratory setup for this research. To standardize the procedure and use the decellularization process for commercial applications, it is necessary to develop a bioreactor set-up for the process. The set-up should ensure the uniform time of treatments for different batches, as well as optimum hemodynamics during the decellularization process. Sub-standard decellularization or insufficient shaking during the process might leave out patches of native cellular and DNA material in regions less accessible. A bioreactor setup would help in ensuring uniform decellularization of the complete tissue.
- In this research, the development of PGG treated conduits and valves were discussed for congenital disease disorders. However, in addition to valved conduits and patches, repair of congenital abnormalities also requires replacement patches. Developed decellularized PGG treated bovine jugular veins could also be evaluated as patch replacements. Since the scaffolds showed optimal biocompatibility, cellular infiltration, and remodeling as in vivo implants, the same advantages might also be helpful when used as patch repairs.

- *In vivo* sheep implant studies with PGG treated bovine jugular vein conduits were conducted for a maximum of three months. Although the conduits showed excellent biocompatibility, functionality, cellular infiltration, and hemodynamics within this period, longer animal studies are required before these conduits can be used for clinical applications.
- PGG treated decellularized porcine aortic valve leaflets used as pulmonary valve repair units in this study demonstrated leaflet thickenings after 4-weeks of the implant. To effectively understand the reason for the failure of these valves, as well as to get a deeper understanding of the biomechanics and hemodynamic characteristics in a circulatory environment leading to graft or valve failures, *in-vitro* bioreactor studies can be more helpful.
- Additionally, it is hypothesized that the failure of the PGG treated decellularized porcine aortic valve leaflets in the pulmonary position might have been because of the difference in the thickness of the leaflet materials, which might have led to altered hemodynamics leading to thickening. Since the decellularization and PGG treatment process showed optimal *in vitro* properties of the scaffolds, alternate tissue material could be investigated with the same treatment procedure for development of more suitable valve repair units.

- Furthermore, the cause of leaflet thickening within the porcine aortic and pulmonary valve implants might be the presence of alpha-galactose within the porcine tissues. The quantification of this epitope was not done in this study. Further investigations need to be made into whether alpha galactose was the cause of leaflet thickening and valve failure.
- A lot of the strategies developed in this study aims at the reduction or elimination of calcification within vascular grafts and valve implants. The complexities of the development of calcification within vascular implants is still unclear; however, since the PGG treated decellularized scaffolds were able to resist calcification, it would be helpful to study the effects of these scaffolds in cell cultures and compared to glutaraldehyde treated tissues to get a better understanding of the mechanism of formation of calcification within the commercially available glutaraldehyde treated tissues.
- Furthermore, although the replacement strategies developed in this research were aimed at pediatric patients, the same strategies can be applied to adult patients as well. Valved conduit and valve replacements in children pose more significant risk factors owing to the smaller size of the required implants and the change in their sizes with growth in patients. Although there should not be many alterations in implanted graft sizes in adults, the use of the replacements developed with these strategies might be more

effective in reducing valve and conduit stenosis as well as calcification within adult patients.

- Flow cytometry studies performed in this research for the subcutaneously implanted decellularized PGG treated porcine aortic valves analyzed inflammatory and non-inflammatory cells. The pan-inflammatory marker CD45 was used for inflammatory cells. To study the concentrations of different inflammatory cell infiltrations within the explants, studies can be performed with a wider range of inflammatory cell markers (M1 and M2 macrophages, Cytotoxic and Helper T-cells, dendritic cells).
- Anti-microbial studies were done on decellularized and PGG treated bovine pericardium tissues in this research failed to show the resistance of the scaffolds to bacterial attachment. For conduit and valve replacements, as well as in wound healing applications, infection of the implants is a major concern. Although PGG possesses anti-bacterial properties in its free form, when crosslinked to extracellular matrix components, the anti-microbial properties of PGG were not preserved. It would therefore be helpful to treat these prepared scaffolds with antibiotics to impart antibacterial properties to the scaffolds. Moreover, treatment with a higher concentration of PGG (>0.15%) might be helpful in utilizing the properties of PGG. Cell culture studies done with spent solutions from elastase and collagenase enzymes did not show any bacterial resistance due to the low concentrations of PGG

within the solutions. Concentration optimization done in Chapter V demonstrated 0.55% PGG treated bovine jugular vein conduits demonstrated the highest average concentration of extracted PGG. Perhaps treatment of scaffolds with this concentration might be able to produce significant amounts of PGG after degradation to be effective anti-microbial agents (Appendix).

- In aim 4, the PGG treated decellularized pericardium tissues were analyzed histochemically for their responses in healthy and diabetic intra-muscular implants. The PGG treated scaffolds did not show significantly different tissue response compared to decellularized tissues immunohistochemically. To obtain a more quantitative estimation of cellular responses to PGG treated scaffolds in intra-muscular implants, it might be helpful to perform flow-cytometric analysis within the implants. Moreover, the systemic response of these implants can be studied by analyzing spleen samples from the implanted animals.

APPENDIX

Enzyme treatment solutions BJV quantification

PGG was quantified within the extracts obtained from elastase and collagenase treatments of decellularized BJV scaffolds treated with different concentrations of PGG. PGG concentrations of 0.55% and higher demonstrated a higher concentration of PGG compared to 0.15% within the extracts after enzyme treatment (Figure 108).

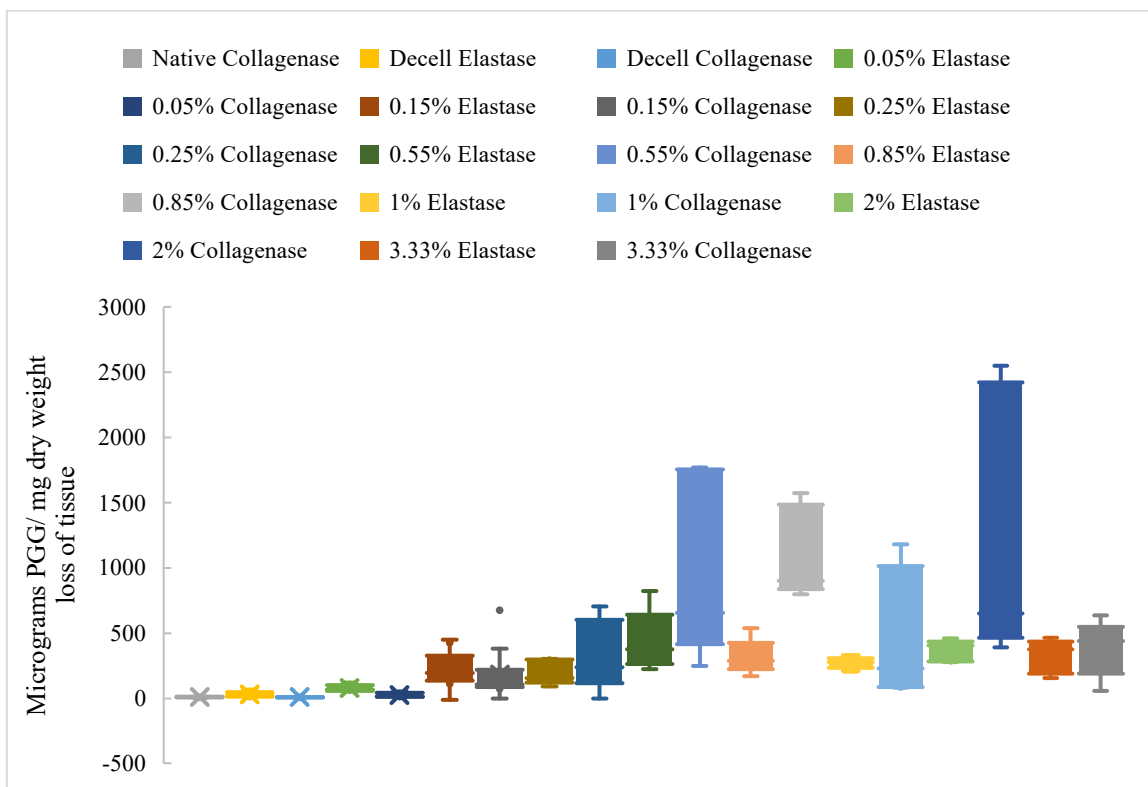


Figure 108: PGG quantification in enzyme treatment extracts of BJV treated with different PGG concentration; N=4

A higher PGG concentration within extracts could potentially inhibit the growth of bacteria within cultures after incubation. Within experiments in this study, bacterial culture studies were performed with 0.15% PGG treated scaffolds, with an average PGG concentration ~100 micrograms/mg dry weight of tissue, which demonstrated no significant decrease in bacterial growth. However, with PGG treatments of 0.55% or higher, since the PGG concentration within the extracts increase, it might be sufficient to demonstrate significant reduction of bacterial growth.

REFERENCES

1. Wu W, He J, Shao X. Incidence and mortality trend of congenital heart disease at the global, regional, and national level, 1990-2017. *Medicine (Baltimore)*. 2020 Jun 05;; 99(23): e20593.
2. Silke Rickert-Sperling, Robert G Kelley, David J Driscoll. Congenital heart diseases: The broken heart. Springer; 2016.
3. Elaine N. Marieb, Katja Hoehn. Human anatomy & physiology. 8th ed. ; 2010.
4. Lacour-Gayet F, Gouton M, Bical O, Lucet V, Roussin R, Leca F. Surgery for severe congenital heart diseases in children from developing nations. *The Journal of thoracic and cardiovascular surgery*. 2021 May.
5. Brody S, Pandit A. Approaches to heart valve tissue engineering scaffold design. *Journal of Biomedical Materials Research Part B: Applied Biomaterials*. 2007 Oct; 83B(1): 16-43.
6. Saxena AK. Congenital anomalies of soft tissues: Birth defects depending on tissue engineering solutions and present advances in regenerative medicine. *Tissue engineering. Part B, Reviews*. 2010 Oct; 16(5): 455-466.
7. Torok RD, Campbell MJ, Fleming GA, Hill KD. Coarctation of the aorta:Management from infancy to adulthood. *World journal of cardiology*. 2015; 7(11): 765-775.
8. van Brakel, Thomas J., MD, PhD, Schoof, Paul H., MD, PhD, de Roo F, MPA, Nikkels, Peter G.J., MD, PhD, Evens FCM, MD, Haas F, MD. High incidence of dacron conduit stenosis for extracardiac fontan procedure. *The Journal of thoracic and cardiovascular surgery*. 2014; 147(5): 1568-1572.
9. Mayer J, Shin'oka T, Shum-Tim D. Tissue engineering of cardiovascular structures. *Current opinion in cardiology*. 1997 Nov; 12(6): 528-532.
10. Vesely I. The evolution of bioprosthetic heart valve design and its impact on durability. *Cardiovascular pathology*. 2003; 12(5): 277-286.
11. Maxfield MW, Cleary MA, Breuer CK. Chapter 40 - tissue-engineering heart valves. In: Lanza R, Langer R, Vacanti J, editors. Principles of Tissue Engineering (Fourth Edition). Boston: Academic Press; 2014. p. 813-833.

12. Mantakaki A, Fakoya AOJ, Sharifpanah F. Recent advances and challenges on application of tissue engineering for treatment of congenital heart disease. *PeerJ (San Francisco, CA)*. 2018; 6: e5805.
13. Hopkins RA, Jones AL, Wolfinbarger L, Moore MA, Bert AA, Lofland GK. Decellularization reduces calcification while improving both durability and 1-year functional results of pulmonary homograft valves in juvenile sheep. *J Thorac Cardiovasc Surg*. 2009 Apr; 137(4): 907-4.
14. Ma B, Wang X, Wu C, Chang J. Crosslinking strategies for preparation of extracellular matrix-derived cardiovascular scaffolds. *Regenerative biomaterials*. 2014 Nov; 1(1): 81-89.
15. Isenburg JC, Simionescu DT, Vyavahare NR. Tannic acid treatment enhances biostability and reduces calcification of glutaraldehyde fixed aortic wall. *Biomaterials*. 2005; 26(11): 1237-1245.
16. Isenburg JC, Karamchandani NV, Simionescu DT, Vyavahare NR. Structural requirements for stabilization of vascular elastin by polyphenolic tannins. *Biomaterials*. 2006; 27(19): 3645-3651.
17. Isenburg JC, Simionescu DT, Vyavahare NR. Elastin stabilization in cardiovascular implants: Improved resistance to enzymatic degradation by treatment with tannic acid. *Biomaterials*. 2004; 25(16): 3293-3302.
18. Torres-León C, Ventura-Sobrevilla J, Serna-Cock L, Ascacio-Valdés JA, Contreras-Esquivel J, Aguilar CN. Pentagalloylglucose (PGG): A valuable phenolic compound with functional properties. *Journal of functional foods*. 2017 Oct; 37: 176-189.
19. Humphrey JD. Cardiovascular solid mechanics: Cells, tissues, and organs. Springer; 2002.
20. Hamilton WJ. Textbook of human anatomy. Second Edition. ed. London: Palgrave Macmillan Limited; 1982.
21. Kara Rogers, and Britannica Educational Publishing Staff. The cardiovascular system. Rosen Publishing Group; 2010.
22. Cardiovascular system [homepage on the Internet]. . 2016 October 8,. Available from: https://sphweb.bumc.bu.edu/otlt/mph-modules/ph/ph709_heart/ph709_heart2.html.
23. Kassab GS. Biomechanics of the cardiovascular system: The aorta as an illustratory example. *Journal of the Royal Society interface*. 2006 Dec 22,; 3(11): 719-740.

24. Human cardiovascular system [homepage on the Internet]. . Available from: <https://www.britannica.com/science/human-cardiovascular-system/additional-info#contributors>.
25. Anatomy and physiology [homepage on the Internet]. . 2013 Apr 25,. Available from: <https://openstax.org/books/anatomy-and-physiology/pages/1-introduction>.
26. Kevin Patton, Gary Thibodeau. Anthony's textbook of anatomy & physiology. 20th ed. ; 2012.
27. Hinton RB, Yutzey KE. Heart valve structure and function in development and disease. *Annual review of physiology*. 2011; 73(1): 29-46.
28. Anderson RH. ANATOMY: Clinical anatomy of the aortic root. *British heart journal*. 2000 Dec 01,; 84(6): 670-673.
29. Anderson RH, Ho SY, Becker AE. Anatomy of the human atrioventricular junctions revisited. *Anat Rec*. 2000; 260(1): 81.
30. Brazile B, Wang B, Wang G, Bertucci R, Prabhu R, Patnaik SS, Butler JR, Claude A, Brinkman-Ferguson E, Williams LN, Liao J. On the bending properties of porcine mitral, tricuspid, aortic, and pulmonary valve leaflets. *Journal of long-term effects of medical implants*. 2015; 25(1-2): 41-53.
31. Sacks MS, David Merryman W, Schmidt DE. On the biomechanics of heart valve function. *Journal of biomechanics*. 2009; 42(12): 1804-1824.
32. del Monte-Nieto G, Fischer JW, Gorski DJ, Harvey RP, Kovacic JC. Basic biology of extracellular matrix in the cardiovascular system, part 1/4. *Journal of the American College of Cardiology*. 2020 May 05,; 75(17): 2169-2188.
33. Wagenseil JE, Mecham RP. Vascular extracellular matrix and arterial mechanics. *Physiological Reviews*. 2009 Jul 01,; 89(3): 957-989.
34. Dingemans KP, Teeling, Peter, Lagendijk, Jaap H, Becker AE. Extracellular matrix of the human aortic media: An ultrastructural histochemical and immunohistochemical study of the adult aortic media. *Anat Rec*. 2000; 258(1): 1.
35. Wiltz D. Extracellular matrix organization, structure, and function. In: IntechOpen; 2013.
36. Canty EG, Kadler KE. Procollagen trafficking, processing and fibrillogenesis. *Journal of Cell Science*. 2005 Apr 01,; 118(7): 1341-1353.

37. Xu J, Shi G. Vascular wall extracellular matrix proteins and vascular diseases. *Biochimica et biophysica acta. Molecular basis of disease*. 2014 Nov; 1842(11): 2106-2119.
38. Kuivaniemi H, Tromp G, Prockop DJ. Mutations in fibrillar collagens (types I, II, III, and XI), fibril-associated collagen (type IX), and network-forming collagen (type X) cause a spectrum of diseases of bone, cartilage, and blood vessels. *Hum Mutat*. 1997; 9(4): 300.
39. Paepe AD, Malfait F. Bleeding and bruising in patients with ehlers-danlos syndrome and other collagen vascular disorders. *British journal of haematology*. 2004 Dec; 127(5): 491-500.
40. Clinical and genetic features of ehlers-danlos syndrome type IV, the vascular type. *The New England Journal of Medicine*. 2001 Feb 1; 344(5): 392.
41. You W, Bonaldo P, Stallcup WB. Collagen VI ablation retards brain tumor progression due to deficits in assembly of the vascular basal lamina. *The American journal of pathology*. 2012; 180(3): 1145-1158.
42. Sherratt M. Tissue elasticity and the ageing elastic fibre. *AGE*. 2009 Dec; 31(4): 305-325.
43. J Rosenbloom, W R Abrams, R Mecham. Extracellular matrix 4: The elastic fiber. *FASEB journal : official publication of the Federation of American Societies for Experimental Biology*. 1993(7(13)): 1208–1218.
44. Rosenbloom J, Bashir M, Yeh H, Rosenbloom J, Ornstein-Goldstein N, Fazio M, Kahari V, Uitto J. Regulation of elastin gene expression. *Annals of the New York Academy of Sciences*. 1991 May; 624(1): 116-136.
45. Xiaoying Wang. Diagnosis, rupture risk evaluation and therapeutic intervention of abdominal aortic aneurysms using targeted nanoparticles [dissertation]. Clemson University; 2020.
46. Tsamis A, Krawiec JT, Vorp DA. Elastin and collagen fibre microstructure of the human aorta in ageing and disease: A review. *Journal of the Royal Society interface*. 2013 Jun 06; 10(83): 20121004.
47. Vesely I. The role of elastin in aortic valve mechanics. *Journal of Biomechanics*. 1998; 31(2): 115.
48. Clark RE, Finke EH. Scanning and light microscopy of human aortic leaflets in stressed and relaxed states. *J Thorac Cardiovasc Surg*. 1974; 67(5): 792-804.

49. Vesely I, Scott MJ. Morphology of porcine aortic valve cusp elastin. *The Journal of Heart Valve Disease*. 1996 01 Sep; 5(5): 464-471.
50. Clark RE, Finke EH. The morphology of stressed and relaxed human aortic leaflets. *Transactions - American Society for Artificial Internal Organs*. 1974; 20 B: 437-448.
51. SchoenFJ, LevyRJ. Tissue heart valves: Current challenges and future research perspectives. *Journal of Biomedical Materials Research*. 1999 April 28-May 2,.
52. Extracellular matrix [homepage on the Internet]. . Available from: http://medcell.org/scientific_foundations/extracellular_matrix.php.
53. Congenital heart defects [homepage on the Internet]. . Available from: <https://www.nhlbi.nih.gov/health-topics/congenital-heart-defects>.
54. Congenital heart defects (CHDs) [homepage on the Internet]. . 2020 November 17,. Available from: <https://www.cdc.gov/ncbddd/heartdefects/facts.html>.
55. van der Linde, Denise, MSc, Konings EEM, BSc, Slager MA, BSc, Witsenburg, Maarten, MD, PhD, Helbing, Willem A., MD, PhD, Takkenberg, Johanna J.M., MD, PhD, Roos-Hesselink, Jolien W., MD, PhD. Birth prevalence of congenital heart disease worldwide. *Journal of the American College of Cardiology*. 2011; 58(21): 2241-2247.
56. Liu Y, Chen S, Zühlke L, Black GC, Choy M, Li N, Keavney BD. Global birth prevalence of congenital heart defects 1970–2017: Updated systematic review and meta-analysis of 260 studies. *International journal of epidemiology*. 2019 Apr 01; 48(2): 455-463.
57. van der Bom T, Zomer AC, Zwinderman AH, Meijboom FJ, Bouma BJ, Mulder BJM. The changing epidemiology of congenital heart disease. *Nature reviews cardiology*. 2011; 8(1): 50-60.
58. Go AS, Mozaffarian D, Roger VL, Benjamin EJ, Berry JD, Blaha MJ, Dai S, Ford ES, Fox CS, Franco S, Fullerton HJ, Gillespie C, Hailpern SM, Heit JA, Howard VJ, Huffman MD, Judd SE, Kissela BM, Kittner SJ, Lackland DT, Lichtman JH, Lisabeth LD, Mackey RH, Magid DJ, Marcus GM, Marelli A, Matchar DB, McGuire DK, Mohler ER,3rd, Moy CS, Mussolino ME, Neumar RW, Nichol G, Pandey DK, Paynter NP, Reeves MJ, Sorlie PD, Stein J, Towfighi A, Turan TN, Virani SS, Wong ND, Woo D, Turner MB, American Heart Association Statistics Committee and Stroke Statistics Subcommittee. Executive summary: Heart disease and stroke statistics--2014 update: A report from the american heart association. *Circulation*. 2014 Jan 21; 129(3): 399-410.
59. Kerstjens-Frederikse WS. Genetic aspects of congenital heart defects. . 2014.

60. P. Engelfriet, B. J. M. Mulder. Gender differences in adult congenital heart disease. *Neth Heart J*. 2009; 17: 414-7.
61. Berto J. Bouma, Barbara J.M. Mulder. Changing landscape of congenital heart disease. *Circ Res*. 2017; 120: 908-922.
62. Congenital heart disease in adults [homepage on the Internet]. . Available from: <https://www.mayoclinic.org/diseases-conditions/adult-congenital-heart-disease/symptoms-causes/syc-20355456>.
63. Congenital heart disease [homepage on the Internet]. . 2021 07 September. Available from: <https://www.nhs.uk/conditions/congenital-heart-disease/types/>.
64. What are the types of congenital heart defects?[homepage on the Internet]. . 2020 November 07,. Available from: <https://www.webmd.com/heart-disease/types-congenital-heart-defects>.
65. Congenital heart defects (CHDs) [homepage on the Internet]. . 2020 November 17,. Available from: <https://www.cdc.gov/ncbddd/heartdefects/truncusarteriosus.html>.
66. Common types of heart defects [homepage on the Internet]. . 2021. Available from: <https://www.heart.org/en/health-topics/congenital-heart-defects/about-congenital-heart-defects/common-types-of-heart-defects>.
67. Congenital heart disease [homepage on the Internet]. . Available from: <https://childrenswi.org/medical-care/herma-heart/conditions/congenital-heart-disease>.
68. Congenital heart defects [homepage on the Internet]. . Available from: <https://www.nhlbi.nih.gov/health-topics/congenital-heart-defects>.
69. Cardiac catheterization [homepage on the Internet]. . 2021. Available from: <https://www.hopkinsmedicine.org/health/treatment-tests-and-therapies/cardiac-catheterization>.
70. Rashkind WJ, Tait S, Gibson RJ. Interventional cardiac catheterization in congenital heart disease. *International Journal of Cardiology*. 1985; 7(1): 1.
71. Eilers, L. F., Gowda, S. T., Gowda, S., Lahiri, S., Aggarwal, V., Stapleton, G. E., Gillespie, M. J., & Qureshi, A. M. Mullins-sheath facilitated delivery of gore cardioform ASD occluder devices for closure of large or challenging secundum atrial septal defects. *The Journal of invasive cardiology*. 2021; 33(6): E425–E430.
72. Congenital heart disease [homepage on the Internet]. . 2020 December 07. Available from: <http://www.pted.org/?id=surgery>.

73. Fontan F, Baudet E. Surgical repair of tricuspid atresia. *Thorax*. 1971; 26(3): 240-248.
74. Fredenburg TB, Johnson TR, Cohen MD. The fontan procedure : Anatomy complications and manifestations of failure. *Radiographics*. 2011 Mar; 31(2): 453-463.
75. de Leval MR, Kilner P, Gewillig M, Bull C. Total cavopulmonary connection: A logical alternative to atriopulmonary connection for complex fontan operations. experimental studies and early clinical experience. *J Thorac Cardiovasc Surg*. 1988 Nov; 96(5): 682-695.
76. Alsoufi B, Awan A, Al-Omrani A, Al-Ahmadi M, Canver CC, Bulbul Z, Kalloghlian A, Al-Halees Z. The rastelli procedure for transposition of the great arteries: Resection of the infundibular septum diminishes recurrent left ventricular outflow tract obstruction risk. *Ann Thorac Surg*. 2009 Jul; 88(1): 137-3.
77. Okabe H, Furuse A. Rastelli's procedure. *Rinsho Kyobu Geka*. 1989 Apr; 9(2): 125-132.
78. Martins P, Tran V, Price G, Tsang V, Cook AC. Extending the surgical boundaries in the management of the left ventricular outflow tract obstruction in discordant ventriculo-arterial connections--a surgical and morphological study. *Cardiol Young*. 2008 Apr; 18(2): 124-134.
79. Al-Halees Z, Pieters F, Qadoura F, Shahid M, Al-Amri M, Al-Fadley F. The ross procedure is the procedure of choice for congenital aortic valve disease. *J Thorac Cardiovasc Surg*. 2002; 123(3): 437-442.
80. Stelzer P. The ross procedure: State of the art 2011. *Semin Thorac Cardiovasc Surg*. 2011; 23(2): 115-123.
81. Peter Pastuszko, Thomas L. Spray. Operative techniques in thoracic and cardiovascular surgery. Elsevier; 2002.
82. Tetralogy of fallot [homepage on the Internet]. . 2021. Available from: <https://www.mayoclinic.org/diseases-conditions/tetralogy-of-fallot/diagnosis-treatment/drc-20353482>.
83. Fallots tetralogy [homepage on the Internet]. . Available from: https://www.rch.org.au/cardiology/heart_defects/Fallots_Tetralogy/.
84. Dhulekar J. Development of tissue engineered vascular grafts resistant to diabetes mellitus [dissertation]. Clemson University Libraries.

85. Villalona GA, Udelsman B, Duncan DR, McGillicuddy E, Sawh-Martinez RF, Hibino N, Painter C, Mirensky T, Erickson B, Shinoka T, Breuer CK. Cell-seeding techniques in vascular tissue engineering. *Tissue engineering. Part B, Reviews*. 2010 Jun; 16(3): 341-350.
86. El Oakley RM, Ooi OC, Bongso A, Yacoub MH. Myocyte transplantation for myocardial repair: A few good cells can mend a broken heart. *The Annals of thoracic surgery*. 2001 May; 71(5): 1724-1733.
87. Reinecke H, Zhang M, Bartosek T, Murry CE. Survival, integration, and differentiation of cardiomyocyte grafts : A study in normal and injured rat hearts. *Circulation*. 1999 Jul 13;; 100(2): 193-202.
88. Taylor DA. Cellular cardiomyoplasty with autologous skeletal myoblasts for ischemic heart disease and heart failure. *Current controlled trials in cardiovascular medicine*. 2001; 2(5): 208-210.
89. Starnecker F, König F, Hagl C, Thierfelder N. Tissue-engineering acellular scaffolds-the significant influence of physical and procedural decellularization factors. *Journal of biomedical materials research. Part B, Applied biomaterials*. 2018 Jan; 106(1): 153-162.
90. Walles T, Puschmann C, Haverich A, Mertsching H. Acellular scaffold implantation - no alternative to tissue engineering. *International journal of artificial organs*. 2003 Mar; 26(3): 225-234.
91. Scarritt ME, Pashos NC, Bunnell BA. A review of cellularization strategies for tissue engineering of whole organs. *Frontiers in bioengineering and biotechnology*. 2015; 3: 43.
92. Zhang X, Chen X, Hong H, Hu R, Liu J, Liu C. Decellularized extracellular matrix scaffolds: Recent trends and emerging strategies in tissue engineering. *Bioactive materials*. 2021 Sep.
93. Ma B, Wang X, Wu C, Chang J. Crosslinking strategies for preparation of extracellular matrix-derived cardiovascular scaffolds. *Regenerative biomaterials*. 2014 Nov; 1(1): 81-89.
94. Dar A, Shachar M, Leor J, Cohen S. Optimization of cardiac cell seeding and distribution in 3D porous alginate scaffolds. *Biotechnology and bioengineering*. 2002 Nov 5;; 80(3): 305-312.
95. Brutsaert DL, De Keulenaer GW, Franssen P, Mohan P, Kaluza GL, Andries LJ, Rouleau J, Sys SU. The cardiac endothelium: Functional morphology, development, and physiology. *Progress in cardiovascular diseases*. 1996; 39(3): 239-262.

96. Taylor PM, Batten P, Brand NJ, Thomas PS, Yacoub MH. The cardiac valve interstitial cell. *The international journal of biochemistry & cell biology*. 2003; 35(2): 113-118.
97. Fukuda K. Development of regenerative cardiomyocytes from mesenchymal stem cells for cardiovascular Tissue Engineering. *Artificial organs*. 2001 Mar 1; 25(3): 187-193.
98. Advances in the research of stem cell tissue-engineering. *Zhonghua shao shang za zhi*. 2020 Jun 20; 36(6): 510-515.
99. Mertsching H, Hansmann J. Bioreactor technology in cardiovascular tissue engineering. *Advances in biochemical engineering, biotechnology*. 2009; 112: 29-37.
100. Hansmann J, Groeber F, Kahlig A, Kleinhans C, Walles H. Bioreactors in tissue engineering-principles, applications and commercial constraints. *Biotechnology journal*. 2013 Mar; 8(3): 298-307.
101. Carrier RL, Papadaki M, Rupnick M, Schoen FJ, Bursac N, Langer R, Freed LE, Vunjak-Novakovic G. Cardiac tissue engineering: Cell seeding, cultivation parameters, and tissue construct characterization. *Biotechnology and bioengineering*. 1999 Sep 5; 64(5): 580-589.
102. Kofidis T, Lenz A, Boublik J, Akhyari P, Wachsmann B, Mueller-Stahl K, Hofmann M, Haverich A. Pulsatile perfusion and cardiomyocyte viability in a solid three-dimensional matrix. *Biomaterials*. 2003; 24(27): 5009-5014.
103. Sacks MS, Engelmayer GC, Hildebrand DK, Mayer JE. Biomechanical considerations for tissue engineered heart valve bioreactors. In: *Bioreactors for Tissue Engineering*. Dordrecht: Springer Netherlands. 235-267.
104. Roll S, Müller-Nordhorn J, Keil T, Scholz H, Eidt D, Greiner W, Willich SN. Dacron® vs. PTFE as bypass materials in peripheral vascular surgery — systematic review and meta-analysis. *BMC surgery*. 2008 Dec 19; 8(1): 22.
105. Mooney DJ, Organ G, Vacanti JP, Langer R. Design and fabrication of biodegradable polymer devices to engineer tubular tissues. *Cell transplantation*. 1994 Mar; 3(2): 203-210.
106. Makadia HK, Siegel SJ. Poly lactic-co-glycolic acid (PLGA) as biodegradable controlled drug delivery carrier. *Polymers*. 2011 Sep 1; 3(3): 1377-1397.
107. Liu Y, Wang S, Zhang R. Composite poly(lactic acid)/chitosan nanofibrous scaffolds for cardiac tissue engineering. *International journal of biological macromolecules*. 2017 Oct; 103: 1130-1137.

108. Castro-Aguirre E, Iñiguez-Franco F, Samsudin H, Fang X, Auras R. Poly(lactic acid)—Mass production, processing, industrial applications, and end of life. *Advanced drug delivery reviews*. 2016 Dec 15; 107: 333-366.
109. Pant HR, Neupane MP, Pant B, Panthi G, Oh H, Lee MH, Kim HY. Fabrication of highly porous poly (ϵ -caprolactone) fibers for novel tissue scaffold via water-bath electrospinning. *Colloids and surfaces, B, Biointerfaces*. 2011; 88(2): 587-592.
110. Ye S, Hong Y, Sakaguchi H, Shankarraman V, Luketich SK, D'Amore A, Wagner WR. Nonthrombogenic, biodegradable elastomeric polyurethanes with variable sulfobetaine content. *ACS applied materials & interfaces*. 2014 Dec 24; 6(24): 22796-22806.
111. Hong Y, Ye S, Pelinescu AL, Wagner WR. Synthesis, characterization, and paclitaxel release from a biodegradable, elastomeric, poly(ester urethane)urea bearing phosphorylcholine groups for reduced thrombogenicity. *Biomacromolecules*. 2012 Nov 12; 13(11): 3686-3694.
112. Rai R, Tallawi M, Grigore A, Boccaccini AR. Synthesis, properties and biomedical applications of poly(glycerol sebacate) (PGS): A review. *Progress in polymer science*. 2012 Aug; 37(8): 1051-1078.
113. Langer R, Wang Y, Ameer GA, Sheppard BJ. A tough biodegradable elastomer. *Nature biotechnology*. 2002 Jun; 20(6): 602-606.
114. Gaharwar AK, Nikkhah M, Sant S, Khademhosseini A. Anisotropic poly (glycerol sebacate)-poly (ϵ -caprolactone) electrospun fibers promote endothelial cell guidance. *BF*. 2014 Dec 17; 7(1): 015001.
115. Pektok E, Nottelet B, Tille J, Gurny R, Kalangos A, Moeller M, Walpoth BH. Degradation and healing characteristics of small-diameter poly(ϵ -caprolactone) vascular grafts in the rat systemic arterial circulation. *Circulation*. 2008 Dec 9; 118(24): 2563-2570.
116. Fukunishi T, Best CA, Sugiura T, Shoji T, Yi T, Udelsman B, Ohst D, Ong CS, Zhang H, Shinoka T, Breuer CK, Johnson J, Hibino N. Tissue-engineered small diameter arterial vascular grafts from cell-free nanofiber PCL/chitosan scaffolds in a sheep model. *PloS one*. 2016; 11(7): e0158555.
117. Cellular and molecular life sciences. *Cellular and molecular life sciences*. 1997.
118. Liu X, Holzwarth JM, Ma PX. Functionalized synthetic biodegradable polymer scaffolds for tissue engineering. *Macromolecular bioscience*. 2012 Jul; 12(7): 911-919.

119. Sodian R, Hoerstrup SP, Sperling JS, Daebritz S, Martin DP, Moran AM, Kim BS, Schoen FJ, Vacanti JP, Mayer JE, Jr. Early in vivo experience with tissue-engineered trileaflet heart valves. *Circulation*. 2000 Nov 7;; 102(90003): III-29.
120. Morales DL, Herrington C, Bacha EA, Morell VO, Prodán Z, Mroczek T, Sivalingam S, Cox M, Bennink G, Asch FM. A novel restorative pulmonary valve conduit: Early outcomes of two clinical trials. *Frontiers in Cardiovascular Medicine*. 2021; 7: 367.
121. Theus AS, Tomov ML, Cetnar A, Lima B, Nish J, McCoy K, Mahmoudi M, Serpooshan V. Biomaterial approaches for cardiovascular tissue engineering. *emergent mater*. 2019 Jul 29;; 2(2): 193-207.
122. Weinberg CB, Bell E. A blood vessel model constructed from collagen and cultured vascular cells. *Science*. 1986 Jan 24;; 231(4736): 397-400.
123. Seliktar D, Black R, Vito R, Nerem R. Dynamic mechanical conditioning of collagen-gel blood vessel constructs induces remodeling in vitro. *Annals of Biomedical Engineering*. 2000 Apr; 28(4): 351-362.
124. Seliktar D, Nerem RM, Galis ZS. Mechanical strain-stimulated remodeling of tissue-engineered blood vessel constructs. *Tissue engineering*. 2003 Aug; 9(4): 657-666.
125. Liu Y, Wang S, Zhang R. Composite poly(lactic acid)/chitosan nanofibrous scaffolds for cardiac tissue engineering. *International journal of biological macromolecules*. 2017 Oct; 103: 1130-1137.
126. Pok S, Myers JD, Madihally SV, Jacot JG. A multilayered scaffold of a chitosan and gelatin hydrogel supported by a PCL core for cardiac tissue engineering. *Acta biomaterialia*. 2013 Mar; 9(3): 5630-5642.
127. Kharaziha M, Nikkhah M, Shin S, Annabi N, Masoumi N, Gaharwar AK, Camci-Unal G, Khademhosseini A. PGS:Gelatin nanofibrous scaffolds with tunable mechanical and structural properties for engineering cardiac tissues. *Biomaterials*. 2013; 34(27): 6355-6366.
128. Vanderhooft JL, Alcoutlabi M, Magda JJ, Prestwich GD. Rheological properties of cross-linked hyaluronan-gelatin hydrogels for tissue engineering. *Macromolecular bioscience*. 2009 Jan 9;; 9(1): 20-28.
129. Dar A, Shachar M, Leor J, Cohen S. Optimization of cardiac cell seeding and distribution in 3D porous alginate scaffolds. *Biotechnology and bioengineering*. 2002 Nov 5;; 80(3): 305-312.

130. Zhang Y, Liu J, Huang L, Wang Z, Wang L. Design and performance of a sericin-alginate interpenetrating network hydrogel for cell and drug delivery. *Scientific reports*. 2015 Jul 24; 5(1): 12374.
131. Shachar M, Tsur-Gang O, Dvir T, Leor J, Cohen S. The effect of immobilized RGD peptide in alginate scaffolds on cardiac tissue engineering. *Acta biomaterialia*. 2011; 7(1): 152-162.
132. Zhang L, Ao Q, Wang A, Lu G, Kong L, Gong Y, Zhao N, Zhang X. A sandwich tubular scaffold derived from chitosan for blood vessel tissue engineering. *Journal of Biomedical Materials Research Part A*. 2006 May; 77A(2): 277-284.
133. Hongu H, Yamagishi M, Maeda Y, Itatani K, Fujita S, Nakatsuji H, Yaku H. Expanded polytetrafluoroethylene conduits with bulging sinuses and a fan-shaped valve in right ventricular outflow tract reconstruction. *Semin Thorac Cardiovasc Surg*. 2021.
134. Belli E, MD, Salihoğlu E, MD, Leobon B, MD, Roubertie F, MD, Ly M, MD, Roussin R, MD, Serraf A, MD. The performance of hancock porcine-valved dacron conduit for right ventricular outflow tract reconstruction. *The Annals of thoracic surgery*. 2010; 89(1): 152-158.
135. Gonzalez-Lavin L, Sparrow AW. Dacron conduit with a stented porcine xenograft valve in the anatomic correction of transposition of the great arteries and subpulmonary stenosis. *Thorax*. 1975 Dec; 30(6): 644-649.
136. Ruffer A, Wittmann J, Potapov S, Purbojo A, Glöckler M, Koch AM, Dittrich S, Cesnjevar RA. Mid-term experience with the hancock porcine-valved dacron conduit for right ventricular outflow tract reconstruction. *Eur J Cardiothorac Surg*. 2012 Dec; 42(6): 988-995.
137. Belli E, Salihoğlu E, Leobon B, Roubertie F, Ly M, Roussin R, Serraf A. The performance of hancock porcine-valved dacron conduit for right ventricular outflow tract reconstruction. *Ann Thorac Surg*. 2010 Jan; 89(1): 152-8.
138. Prodan Z, Mroczek T, Sivalingam S, Bennink G, Asch FM, Cox M, Carrel T, Yakub MA, Nagy Z, Skalski J, Svanidze O, Schutte E, Verhees L, Klersy C, Virmani R, Sreeram N. Initial clinical trial of a novel pulmonary valved conduit. *Semin Thorac Cardiovasc Surg*. 2021.
139. Stentless valved pulmonary conduit [homepage on the Internet]. . Available from: <http://www.labcor.com.br/pdf/54.pdf>.

140. Shaker R, Arabi M, Khafaja S, Fayad D, Casals AA, Lteif M, Shamseddine S, Taqa MA, Charafeddine F, Rassi IE, Al-Halees Z, Bitar F, Hanna-Wakim R, Dbaibo G. Placement of labcor pulmonary conduit results in a high incidence of postoperative fever. *World J Pediatr Congenit Heart Surg.* 2021; 12(1): 55-60.
141. Jussli-Melchers J, Scheewe J, Hansen JH, Grothusen C, Steer J, Voges I, Logoteta J, Dütschke P, Kramer H, Attmann T. Right ventricular outflow tract reconstruction with the labcor® stentless valved pulmonary conduit. *Eur J Cardiothorac Surg.* 2020; 57(2): 380-387.
142. Ioannis Tzanavaros ML. In: Performance of the labcor stentless valved pulmonary conduit in patients with congenital heart disease. . Annual scientific meeting; April 12-14, 2018; Stuttgart, Germany: The heart valve society; 2018.
143. Aupècle, B., Serraf, A., Belli, E., Mohammadi, S., Lacour-Gayet, F., Fornes, P., Planché, C. Intermediate follow-up of a composite stentless porcine valved conduit of bovine pericardium in the pulmonary circulation(article). *Annals of Thoracic Surgery.* 2002; 74(1): 127-132.
144. Chanda J, Kuribayashi R, Abe T. New-generation valved conduit: An experimental study. *J Thorac Cardiovasc Surg.* 1997; 114(2): 218-223.
145. Herijgers P, Ozaki S, Verbeken E, Van Lommel A, Meuris B, Lesaffre E, Daenen W, Flameng W. Valved jugular vein segments for right ventricular outflow tract reconstruction in young sheep. *J Thorac Cardiovasc Surg.* 2002; 124(4): 798-805.
146. Dave HH, Kadner A, Berger F, Seifert B, Dodge-Khatami A, Béttex D, Prêtre R. Early results of the bovine jugular vein graft used for reconstruction of the right ventricular outflow tract. *Ann Thorac Surg.* 2005; 79(2): 618-624.
147. Göber V, Berdat P, Pavlovic M, Pfammatter J, Carrel TP. Adverse mid-term outcome following RVOT reconstruction using the contegra valved bovine jugular vein. *Ann Thorac Surg.* 2005; 79(2): 625-631.
148. Beckerman Z, De León LE, Zea-Vera R, Mery CM, Fraser CD. High incidence of late infective endocarditis in bovine jugular vein valved conduits. *The Journal of thoracic and cardiovascular surgery.* 2018 Aug; 156(2): 728-734.e2.
149. Marianeschi SM, Iacona GM, Seddio F, Abella RF, Condoluci C, Cipriani A, Iorio FS, Gabbay S, Marcelletti CF. Shelhigh no-react porcine pulmonic valve conduit: A new alternative to the homograft. *Ann Thorac Surg.* 2001; 71(2): 619-623.
150. Pearl JM, Cooper DS, Bove KE, Manning PB. Early failure of the shelhigh pulmonary valve conduit in infants. *The Annals of Thoracic Surgery.* 2002 -08; 74(2): 542.

151. Design and manufacture of heart valve bioprosthesis and vascular graft [homepage on the Internet]. . 2021. Available from: <https://en.neocor.ru>.
152. Nichay NR, Zhuravleva IY, Kulyabin YY, Timchenko TP, Voitov AV, Kuznetsova EV, Soynov IA, Zubritskiy AV, Bogachev-Prokophiev A, Karaskov AM. In search of the best xenogeneic material for a paediatric conduit: An analysis of clinical data†. *Interact CardioVasc Thorac Surg*. 2018; 27(1): 34-41.
153. Ruffer A, Purbojo A, Cicha I, Glöckler M, Potapov S, Dittrich S, Cesnjevar RA. Early failure of xenogenous de-cellularised pulmonary valve conduits — a word of caution. *Eur J Cardiothorac Surg*. 2010 Jul; 38(1): 78-85.
154. Lü W, Zhang M, Wu Z, Hu T. Decellularized and photooxidatively crosslinked bovine jugular veins as potential tissue engineering scaffolds☆. *Interact CardioVasc Thorac Surg*. 2009; 8(3): 301-305.
155. Lü W, Zhang M, Wu Z, Hu T, Xu Z, Liu W, Hu Y. The performance of photooxidatively crosslinked acellular bovine jugular vein conduits in the reconstruction of connections between pulmonary arteries and right ventricles. *Biomaterials*. 2010; 31(10): 2934-2943.
156. van Rijswijk JW, Talacua H, Mulder K, van Hout, Gerardus P. J., Bouten CVC, Gründeman PF, Kluin J. Failure of decellularized porcine small intestinal submucosa as a heart valved conduit. *J Thorac Cardiovasc Surg*. 2020; 160(4): e201-e215.
157. Dominga Iacobazzi, Filippo Rapetto, Ambra Albertario, Megan M. Swim, Srinivas Narayan, Katie Skeffington, Tasneem Salih, Vincenza Valeria Alvino, Paolo Madeddu, Mohamed T. Ghorbel, and Massimo Caputo. Wharton's jelly-mesenchymal stem cell-engineered conduit for pediatric translation in heart defect. *Tissue Engineering Part A*. 2021 Feb; 27(3-4): 201-213.
158. Boethig D, Thies WR, Hecker H, Breymann T. Mid term course after pediatric right ventricular outflow tract reconstruction: A comparison of homografts, porcine xenografts and contegras. *Eur J Cardiothorac Surg*. 2005 Jan; 27(1): 58-66.
159. Nichay NR, Zhuravleva IY, Kulyabin YY, Timchenko TP, Voitov AV, Kuznetsova EV, Soynov IA, Zubritskiy AV, Bogachev-Prokophiev AV, Karaskov AM. In search of the best xenogeneic material for a paediatric conduit: An analysis of clinical data. *Interactive cardiovascular and thoracic surgery*. 2018 Jul 01,; 27(1): 34-41.
160. Congenital heart valve program [homepage on the Internet]. . 2021. Available from: https://www.childrenshospital.org/centers-and-services/programs/a_-e/congenital-heart-valve-program/advance-valve-imaging/pulmonary-valve.

161. Butany J, Ahluwalia MS, Munroe C, Fayet C, Ahn C, Blit P, Kepron C, Cusimano RJ, Leask RL. Mechanical heart valve prostheses:: Identification and evaluation (erratum). *Cardiovascular Pathology*. 2003; 12(6): 322-344.
162. Ionescu A, Payne N, Fraser AG, Giddings J, Grunkemeier GL, Butchart EG. Incidence of embolism and paravalvar leak after st jude silzone valve implantation: Experience from the cardiff embolic risk factor study. *Heart (British Cardiac Society)*. 2003 Sep; 89(9): 1055-1061.
163. Bortolotti U, Milano A, D'Alfonso A, Piccin C, Mecozzi G, Magagna P, Fabbri A, Mazzucco A. Evaluation of valve-related complications in patients with sorin bicarbon prosthesis: A seven-year experience. *The Journal of heart valve disease*. 2001 Nov; 10(6): 795-801.
164. Laczkovics A, Heidt M, Oelert H, Laufer G, Greve H, Pomar JL, Mohr FW, Haverich A, Birnbaum D, Regensburger D, Palatianos G, Wolner E. Early clinical experience with the on-X prosthetic heart valve. *The Journal of heart valve disease*. 2001 Jan; 10(1): 94-99.
165. Walther T, Falk V, Tigges R, Krüger M, Langebartels G, Diegeler A, Autschbach R, Mohr FW. Comparison of on-X and SJM HP bileaflet aortic valves. *The Journal of heart valve disease*. 2000 May; 9(3): 403-407.
166. Baudet E, Roques X, McBride J, Panès F, Grimaud JP. A 8-year follow-up of the edwards-duromedics bileaflet prosthesis. *Journal of cardiovascular surgery*. 1995 Oct; 36(5): 437-442.
167. Hemmer WB, Doss M, Hannekum A, Kapfer X. Leaflet escape in a TEKNA and an original duromedics bileaflet valve. *The Annals of thoracic surgery*. 2000 Mar; 69(3): 942-944.
168. Van Nooten G, Caes F, François K, Missault L, Van Belleghem Y. Clinical experience with the first 100 ATS heart valve implants. *Vascular*. 1996 Jun; 4(3): 288-292.
169. Milano A, Bortolotti U, Mazzucco A, Mossuto E, Testolin L, Thiene G, Gallucci V. Heart valve replacement with the sorin tilting-disc prosthesis. A 10- year experience. *The Journal of thoracic and cardiovascular surgery*. 1992 Jul 1; 103(2): 267-275.
170. Cho YH, MD, Jeong, Dong Seop, MD, PhD, Park, Pyo Won, MD, PhD, Park, Kay-Hyun, MD, PhD, Sung, Kiick, MD, PhD, Kim, Wook Sung, MD, PhD, Lee, Young Tak, MD, PhD. Serial changes of hemodynamic performance with medtronic hall valve in aortic position. *The Annals of thoracic surgery*. 2011; 91(2): 424-431.

171. Li HH, Jeffrey RR, Davidson KG, Seifert D, Körfer R, Grunkemeier GL. The ultracor tilting disc heart valve prosthesis: A seven-year study. *The Journal of heart valve disease*. 1998 Nov; 7(6): 647-654.
172. Seipelt RG, Vazquez-Jimenez JF, Seipelt IM, Franke A, Chalabi K, Schoendube FA, Messmer BJ. The st. jude "Silzone" valve: Midterm results in treatment of active endocarditis. *Ann Thorac Surg*. 2001; 72(3): 758-762.
173. Sakata K, Ishikawa S, Ohtaki A, Otani Y, Suzuki M, Kawashima O, Morishita Y. Malfunctioning starr-edwards mitral valve 21 years after installation. *Journal of cardiovascular surgery*. 1997 Feb; 38(1): 81-82.
174. Podesser BK, Khuenl-Brady G, Eigenbauer E, Roedler S, Schmiedberger A, Wolner E, Moritz A. Long-term results of heart valve replacement with the edwards duromedics bileaflet prosthesis: A prospective ten-year clinical follow-up. *J Thorac Cardiovasc Surg*. 1998; 115(5): 1121-1129.
175. Yoganathan AP, Corcoran WH, Harrison EC, Carl JR. The bjork-shiley aortic prosthesis: Flow characteristics, thrombus formation and tissue overgrowth. *Circulation*. 1978 Jul 01.; 58(1): 70-76.
176. Morse D, Steiner RM. Cardiac valve identification atlas and guide. In: Morse D, Steiner RM, Fernandez J, editors. *Guide to Prosthetic Cardiac Valves*. New York, NY: Springer New York; 1985. p. 257-346.
177. Nelson Leonardo Kerdahi Leite de Campos, Rubens Ramos de Andrade, Marcos Augusto de Moraes Silva. Anticoagulação oral em portadores de próteses valvares cardíacas mecânicas: Experiência de dez anos oral anticoagulation in carriers of mechanical heart valve prostheses: Experience of ten years. *Revista brasileira de cirurgia cardiovascular*. 2010 Dec 01.; 25(4): 457-465.
178. Cannegieter S,C., Rosendaal F,R., Briët E. Thromboembolic and bleeding complications in patients with mechanical heart valve prostheses. *Circulation*. 1994; 89(2): 635-641.
179. Deviri E, Sareli P, Wisenbaugh T, Cronje SL. Obstruction of mechanical heart valve prostheses: Clinical aspects and surgical management. *J Am Coll Cardiol*. 1991; 17(3): 646-650.
180. Bloomfield P. Choice of heart valve prosthesis. *Heart (British Cardiac Society)*. 2002 Jun; 87(6): 583-589.
181. Graf T, Fischer H, Reul H, Rau G. Cavitation potential of mechanical heart valve prostheses. *Int J Artif Organs*. 1991; 14(3): 169-174.

182. Donated heart valves [homepage on the Internet]. . 2021. Available from: <https://www.aatb.org/donated-heart-valves>.
183. Ketheesan N, Ingham E, Kearney JN, Rasaretnam R. Donor valves as substitutes for heart valve replacement. *Ceylon Med J*. 1997 Jun; 42(2): 85-90.
184. Koolbergen DR, Hazekamp MG, de Heer E, Bruggemans EF, Huysmans HA, Dion RAE, Bruijn JA. The pathology of fresh and cryopreserved homograft heart valves: An analysis of forty explanted homograft valves. *J Thorac Cardiovasc Surg*. 2002; 124(4): 689-697.
185. Harris C, Croce B, Cao C. Tissue and mechanical heart valves. *Annals of cardiothoracic surgery*. 2015 Jul; 4(4): 399.
186. Schlein J, Simon P, Wollenek G, Base E, Laufer G, Zimpfer D. Aortic valve replacement in pediatric patients: 30 years single center experience. *Journal of Cardiothoracic Surgery*. 2021; 16(1): 259.
187. Cebotari S, Mertsching H, Kallenbach K, Kostin S, Repin O, Batrinac A, Kleczka C, Ciubotaru A, Haverich A. Construction of autologous human heart valves based on an acellular allograft matrix. *Circulation*. 2002; 106(12): I-68.
188. Ozaki S, Kawase I, Yamashita H, Uchida S, Takatoh M, Hagiwara S, Kiyohara N. Aortic valve reconstruction using autologous pericardium for aortic stenosis. *Circulation Journal*. 2015; 79(7): 1504-1510.
189. Baird CW, Marathe SP, del Nido PJ. Aortic valve neo-cuspidation using the ozaki technique for acquired and congenital disease: Where does this procedure currently stand? *Indian Journal of Thoracic and Cardiovascular Surgery*. 2020; 36(1): 113-122.
190. Okada K, Inoue Y, Haida H, Suzuki S. Aortic valve reconstruction using autologous pericardium (ozaki procedure) for active infective endocarditis: A case report. *General Thoracic and Cardiovascular Surgery*. 2018; 66(9): 546-548.
191. Ozaki S, Kawase I, Yamashita H, Uchida S, Nozawa Y, Takatoh M, Hagiwara S. A total of 404 cases of aortic valve reconstruction with glutaraldehyde-treated autologous pericardium. *J Thorac Cardiovasc Surg*. 2014; 147(1): 301-306.
192. Marathe SP, Chávez M, Sleeper LA, Marx G, del Nido PJ, Baird CW. Modified ozaki procedure including annular enlargement for small aortic annuli in young patients. *Ann Thorac Surg*. 2020; 110(4): 1364-1371.

193. Ozaki S. Aortic valve reconstruction to treat aortic stenosis using autologous pericardium: Ozaki procedure. In: Kuniyama T, Takanashi S, editors. *Aortic Valve Preservation: Concepts and Approaches*. Singapore: Springer Singapore; 2019. p. 177-184.
194. Vyavahare N, Tam H. Bioprosthetic heart valves: From a biomaterials perspective. In: Sacks MS, Liao J, editors. *Advances in Heart Valve Biomechanics: Valvular Physiology, Mechanobiology, and Bioengineering*. Cham: Springer International Publishing; 2018. p. 337-382.
195. Umashankar PR, Mohanan PV, Kumari TV. Glutaraldehyde treatment elicits toxic response compared to decellularization in bovine pericardium. *Toxicology international*. 2012 Jan; 19(1): 51-58.
196. Schoen FJ. Cardiac valves and valvular pathology: Update on function, disease, repair, and replacement. *Cardiovascular pathology*. 2005 Jul; 14(4): 189-194.
197. Butany J, Fayet C, Ahluwalia MS, Blit P, Ahn C, Munroe C, Israel N, Cusimano RJ, Leask RL. Biological replacement heart valves: Identification and evaluation. *Cardiovascular pathology*. 2003; 12(3): 119-139.
198. Crick SJ, Sheppard MN, Ho SY, Gebstein L, Anderson RH. Anatomy of the pig heart: Comparisons with normal human cardiac structure. *American journal of anatomy*. 1998 Jul; 193(1): 105-119.
199. Flynn M, Iaccovoni A, Pathi V, Butler J, Macarthur KJ, Berg GA. The aortic elan stentless aortic valve: Excellent hemodynamics and ease of implantation. *Seminars in thoracic and cardiovascular surgery*. 2001 Oct; 13(4 Suppl 1): 48-54.
200. Fann JJ, Chronos N, Rowe SJ, Michiels R, Lyons BE, Leon MB, Kaplan AV. Evolving strategies for the treatment of valvular heart disease: Preclinical and clinical pathways for percutaneous aortic valve replacement. *Catheterization and Cardiovascular Interventions*. 2008 Feb 15; 45(4): 434-440.
201. Chiam, Paul T.L., MBBS, MRCP, Ruiz, Carlos E., MD, PhD, FACC, FESC. Percutaneous transcatheter aortic valve implantation: Evolution of the technology. *The American heart journal*. 2009; 157(2): 229-242.
202. Kidane AG, Burriesci G, Cornejo P, Dooley A, Sarkar S, Bonhoeffer P, Edirisinghe M, Seifalian AM. Current developments and future prospects for heart valve replacement therapy. *Journal of Biomedical Materials Research Part B: Applied Biomaterials*. 2009 Jan; 88B(1): 290-303.
203. Zilla P, Brink J, Human P, Bezuidenhout D. Prosthetic heart valves: Catering for the few. *Biomaterials*. 2007; 29(4): 385-406.

204. Suleiman T, Kavinsky CJ, Skerritt C, Kenny D, Ilbawi MN, Caputo M. Recent development in pulmonary valve replacement after tetralogy of fallot repair: The emergence of hybrid approaches. *Frontiers in surgery*. 2015; 2: 22.
205. Bapat V, FRCS CTh, Attia R, MRCS, Redwood S, FRCP, Hancock J, FRCP, Wilson K, MS, Young C, FRCS CTh, Thomas M, FRCP. Use of transcatheter heart valves for a valve-in-valve implantation in patients with degenerated aortic bioprosthesis: Technical considerations and results. *The Journal of thoracic and cardiovascular surgery*. 2012; 144(6): 1372-1380.
206. Kunadian, Babu, MBBS, MRCP, Vijayalakshmi, Kunadian, MBBS, MRCP, Thornley, Andrew R., MBBS, MRCP, de Belder, Mark A., MA, MD, FRCP, Hunter S, FRCS, Kendall, Simon, MD, FRCS, Graham, Richard, MD, MRCP, Stewart, Michael, MD, FRCP, Thambyrajah, Jeetendra, MD, MRCP, Dunning, Joel, MRCS, PhD. Meta-analysis of valve hemodynamics and left ventricular mass regression for stentless versus stented aortic valves. *The Annals of thoracic surgery*. 2007; 84(1): 73-78.
207. Katz NM, MD. The emerging specialty of cardiothoracic surgical critical care: The leadership role of cardiothoracic surgeons on the multidisciplinary team. *The Journal of thoracic and cardiovascular surgery*. 2007; 134(5): 1109-1111.
208. Cohen, Gideon, MD, PhD, Zagorski B, MSc, Christakis GT, MD, Joyner CD, MD, Vincent J, Sever J, Harbi S, MD, Feder-Elituv R, Moussa F, MD, Goldman BS, MD, Fremes SE, MD. Are stentless valves hemodynamically superior to stented valves? long-term follow-up of a randomized trial comparing Carpentier–Edwards pericardial valve with the toronto stentless porcine valve. *The Journal of thoracic and cardiovascular surgery*. 2010; 139(4): 848-859.
209. Khoo JP, Davies JE, Ang KL, Galiñanes M, Chin DT. Differences in performance of five types of aortic valve prostheses: Haemodynamic assessment by dobutamine stress echocardiography. *Heart (British Cardiac Society)*. 2013 Jan; 99(1): 41-47.
210. Perez de Arenaza D, Lees B, Flather M, Nugara F, Husebye T, Jasinski M, Cisowski M, Khan M, Henein M, Gaer J, Guvendik L, Bochenek A, Wos S, Lie M, Van Nooten G, Pennell D, Pepper J, on behalf of ASSERT (Aortic Stentless versus Stented valve assessed by Echocardiography Randomized Trial) Investigators. Randomized comparison of stentless versus stented valves for aortic stenosis: Effects on left ventricular mass. *Circulation*. 2005 Oct 25; 112(17): 2696-2702.
211. Ali A, Halstead JC, Cafferty F, Sharples L, Rose F, Coulden R, Lee E, Dunning J, Argano V, Tui S. In: Are stentless valves superior to modern stented valves?: A prospective randomized trial. Hagerstown, MD: Lippincott Williams & Wilkins; 2006. p. I535-540.

212. Mahjoub, Haïfa, MD, PhD, Dahou, Abdellaziz, MD, MSc, Dumesnil JG, MD, Pibarot, Philippe, DVM, PhD. Echocardiographic recognition and quantitation of prosthetic valve dysfunction. In: Practice of Clinical Echocardiography. Fifth Edition ed. ; 2017. p. 455-480.
213. Antman E, Sabatine M. Cardiovascular therapeutics: A companion to Braunwald's heart disease. 4th ed. Elsevier Health Sciences; 2013.
214. O'Brien MF, Goldstein S, Walsh S, Black KS, Elkins R, Clarke D. The SynerGraft valve: A new acellular (nongluteraldehyde-fixed) tissue heart valve for autologous recellularization first experimental studies before clinical implantation. *Seminars in thoracic and cardiovascular surgery*. 1999 Oct; 11(4 Suppl 1): 194-200.
215. Goldstein S, Clarke DR, Walsh SP, Black KS, O'Brien MF. Transpecies heart valve transplant: Advanced studies of a bioengineered xeno-autograft. *The Annals of thoracic surgery*. 2000; 70(6): 1962-1969.
216. Simon P, Kasimir MT, Seebacher G, Weigel G, Ullrich R, Salzer-Muhar U, Rieder E, Wolner E. Early failure of the tissue engineered porcine heart valve SYNERGRAFT® in pediatric patients. *Eur J Cardiothorac Surg*. 2003 Jun; 23(6): 1002-1006.
217. Research and Markets adds report: Global implantable medical devices market. *Health & Beauty Close-Up*. 2018 Jan 16,.
218. Mosaic tissue valve [homepage on the Internet]. . 2021. Available from: <https://professional.sjm.com/products/sh/tissue-valves/aortic-mitral/trifecta>.
219. Trifecta valve [homepage on the Internet]. . 2021. Available from: <https://professional.sjm.com/products/sh/tissue-valves/aortic-mitral/trifecta>.
220. ThermoFix description [homepage on the Internet]. . 2021. Available from: <http://www.edwards.com/eu/products/heartvalves/pages/thermafixdescription.aspx>.
221. Badylak SF, Gilbert TW. Immune response to biologic scaffold materials. *Seminars in immunology*. 2007; 20(2): 109-116.
222. Gilbert TW, Ph.D, Freund JM, B.S, Badylak, Stephen F., D.V.M., Ph.D., M.D. Quantification of DNA in biologic scaffold materials. *The Journal of surgical research*. 2009; 152(1): 135-139.
223. Gilbert TW, Sellaro TL, Badylak SF. Decellularization of tissues and organs. *Biomaterials*. 2006; 27(19): 3675-3683.

224. Faulk DM, Johnson SA, Badylak SF. 7 - decellularized biological scaffolds for cardiac repair and regeneration. In: Cardiac regeneration and repair. Elsevier Ltd; 2014. p. 180-200.
225. Zhang X, Chen X, Hong H, Hu R, Liu J, Liu C. Decellularized extracellular matrix scaffolds: Recent trends and emerging strategies in tissue engineering. *Bioactive materials*. 2021 Sep.
226. Aeberhard P, Grognez A, Peneveyre C, McCallin S, Hirt-Burri N, Antons J, Pioletti D, Raffoul W, Applegate LA. Efficient decellularization of equine tendon with preserved biomechanical properties and cytocompatibility for human tendon surgery indications. *Artificial organs*. 2020 Apr; 44(4): E161-E171.
227. Li X, Ni X, Qian S, Wang Q, Jiang R, Xu W, Zhang Y, Yu G, Chen Q, Shang Y, Zhao C, Yu H, Zhang T, Liu G, Deng H, Gao J, Ran X, Yang Q, Xu B, Huang X, Wu X, Bao Y, Chen Y, Chen Z, Liu Q, Lu G, Liu C, Wang R, Zhang G, Gu F, Xu H, Li Y, Yang T. Chinese guidelines for the diagnosis and treatment of hand, foot and mouth disease (2018 edition). *World J Pediatr*. 2018 Oct 3; 14(5): 437-447.
228. Ferdowsi Khosroshahi A, Soleimani Rad J, Kheirjou R, Roshangar B, Rashtbar M, Salehi R, Ranjkesh MR, Roshangar L. Adipose tissue-derived stem cells upon decellularized ovine small intestine submucosa for tissue regeneration: An optimization and comparison method. *Journal of cellular physiology*. 2020 Feb; 235(2): 1556-1567.
229. Rabbani M, Zakian N, Alimoradi N. Contribution of physical methods in decellularization of animal tissues. *Journal of medical signals and sensors*. 2021 Jan 1; 11(1): 1-11.
230. Yusof F, Sha'ban M, Azhim A. Development of decellularized meniscus using closed sonication treatment system: Potential scaffolds for orthopedics tissue engineering applications. *International journal of nanomedicine*. 2019; 14: 5491-5502.
231. Neumann A, Sarikouch S, Breymann T, Cebotari S, Boethig D, Horke A, Beerbaum P, Westhoff-Bleck M, Harald B, Ono M, Tudorache I, Haverich A, Beutel G. Early systemic cellular immune response in children and young adults receiving decellularized fresh allografts for pulmonary valve replacement. *Tissue engineering. Part A*. 2014 Mar; 20(ja): 1003-1011.
232. Taylor DA, Sampaio LC, Cabello R, Elgalad A, Parikh R, Wood RP, Myer KA, Yeh AT, Lee P. Decellularization of whole human heart inside a pressurized pouch in an inverted orientation. *Journal of Visualized Experiments*. 2018(141).

233. Willemse J, Verstegen MMA, Vermeulen A, Schurink IJ, Roest HP, van der Laan, Luc J.W, de Jonge J. Fast, robust and effective decellularization of whole human livers using mild detergents and pressure controlled perfusion. *Materials Science & Engineering C*. 2020 Mar; 108: 110200.
234. Saghizadeh M, Winkler MA, Kramerov AA, Hemmati DM, Ghiam CA, Dimitrijevič SD, Sareen D, Ornelas L, Ghiasi H, Brunken WJ, Maguen E, Rabinowitz YS, Svendsen CN, Jirsova K, Ljubimov AV. A simple alkaline method for decellularizing human amniotic membrane for cell culture. *PLoS one*. 2013; 8(11): e79632.
235. Golberg A, Bruinsma BG, Jaramillo M, Yarmush ML, Uygun BE. Rat liver regeneration following ablation with irreversible electroporation. *PeerJ (San Francisco, CA)*. 2016; 4: e1571.
236. Zager Y, Kain D, Landa N, Leor J, Maor E. Optimization of irreversible electroporation protocols for in-vivo myocardial decellularization. *PLoS one*. 2016; 11(11): e0165475.
237. Watanabe M, Yano K, Okawa K, Yamashita T, Tajima K, Sawada K, Yagi H, Kitagawa Y, Tanishita K, Sudo R. Construction of sinusoid-scale microvessels in perfusion culture of a decellularized liver. *Acta biomaterialia*. 2019 Sep 1; 95: 307-318.
238. Taylor DA, Ott HC, Matthiesen TS, Goh S, Black LD, Kren SM, Netoff TI. Perfusion-decellularized matrix: Using nature's platform to engineer a bioartificial heart. *Nature medicine*. 2008 Feb; 14(2): 213-221.
239. Guimaraes AB, Correia AT, Alves BP, Da Silva RS, Martins JK, Pêgo-Fernandes PM, Xavier NS, Dolhnikoff M, Cardoso PFG. Evaluation of a physical-chemical protocol for porcine tracheal decellularization. *Transplantation proceedings*. 2019 Jun; 51(5): 1611-1613.
240. Struecker B, Butter A, Hillebrandt K, Polenz D, Reutzel-Selke A, Tang P, Lippert S, Leder A, Rohn S, Geisel D, Denecke T, Aliyev K, Jöhrens K, Raschok N, Neuhaus P, Pratschke J, Sauer IM. Improved rat liver decellularization by arterial perfusion under oscillating pressure conditions. *Journal of tissue engineering and regenerative medicine*. 2017 Feb; 11(2): 531-541.
241. Aeberhard P, Grognez A, Peneveyre C, McCallin S, Hirt-Burri N, Antons J, Pioletti D, Raffoul W, Applegate LA. Efficient decellularization of equine tendon with preserved biomechanical properties and cytocompatibility for human tendon surgery indications. *Artificial organs*. 2020 Apr; 44(4): E161-E171.

242. Wilson SL, Sidney LE, Dunphy SE, Rose JB, Hopkinson A. Keeping an eye on decellularized corneas: A review of methods, characterization and applications. *Journal of functional biomaterials*. 2013 Jul 10;; 4(3): 114-161.
243. Decellularization of human stromal refractive lenticules for corneal tissue engineering [homepage on the Internet]. Nature Publishing Group. 2016. Available from: <http://scholarbank.nus.edu.sg/handle/10635/182470>.
244. Bader A, Steinhoff G, Strobl K, Schilling T, Brandes G, Mertsching H, Tsikas D, Froelich J, Haverich A. Engineering of human vascular aortic tissue based on a xenogeneic starter matrix. *Transplantation*. 2000; 70(1): 7-14.
245. Kasimir MT, Rieder E, Seebacher G, Silberhumer G, Wolner E, Weigel G, Simon P. Comparison of different decellularization procedures of porcine heart valves. *International journal of artificial organs*. 2003 May; 26(5): 421-427.
246. Kim B, Ventura R, Lee B. Functionalization of porous BCP scaffold by generating cell-derived extracellular matrix from rat bone marrow stem cells culture for bone tissue engineering. *Journal of tissue engineering and regenerative medicine*. 2018 Feb; 12(2): e1256-e1267.
247. Kajbafzadeh A, Khorramirouz R, Nabavizadeh B, Ladi Seyedian S, Akbarzadeh A, Heidari R, Masoumi A, Azizi B, Seyed Hossein Beigi R. Whole organ sheep kidney tissue engineering and in vivo transplantation: Effects of perfusion-based decellularization on vascular integrity. *Materials Science & Engineering C*. 2019 May; 98: 392-400.
248. Studies from Ferdowsi University have provided new information about bone scaffolds (development of a demineralized and decellularized human epiphyseal bone scaffold for tissue engineering: A histological study). *Biotech Business Week*. 2018 Dec 24, (117).
249. Verstegen MMA, Willemsse J, van den Hoek S, Kremers G, Luijckx TM, van Huizen NA, Willemsse FEJA, Metselaar HJ, IJzermans JNM, van der Laan, Luc J.W, de Jonge J. Decellularization of whole human liver grafts using controlled perfusion for transplantable organ bioscaffolds. *Stem cells and development*. 2017 Sep 15;; 26(18): 134-1315.
250. McCrary MW, Vaughn NE, Hlavac N, Song YH, Wachs RA, Schmidt CE. Sodium deoxycholate-based chemical decellularization method for peripheral nerve. *Tissue engineering. Part C, Methods*. 2019 Nov 14,(ja).
251. Rosmark O, Åhrman E, Müller C, Elowsson Rendin L, Eriksson L, Malmström A, Hallgren O, Larsson-Callerfelt A, Westergren-Thorsson G, Malmström J. Quantifying extracellular matrix turnover in human lung scaffold cultures. *Scientific reports*. 2018 Apr 3;; 8(1): 5409-13.

252. Simsa R, Padma AM, Heher P, Hellström M, Teuschl A, Jenndahl L, Bergh N, Fogelstrand P. Systematic in vitro comparison of decellularization protocols for blood vessels. *PloS one*. 2018; 13(12): e0209269.
253. Korossis SA, Booth C, Wilcox HE, Watterson KG, Kearney JN, Fisher J, Ingham E. Tissue engineering of cardiac valve prostheses II: Biomechanical characterization of decellularized porcine aortic heart valves. *The Journal of heart valve disease*. 2002 Jul; 11(4): 463-471.
254. Chen mao, zhu shaoxuan, liu xuebin, zheng lizhen, lin liwei, xu shuwen, wang yuping, yang wei, li yunfeng, ye fang, zhang xiaona, guangzhou pharmaceutical industrial research institute and guangzhou baiyunshan pharmaceutical co ltd guangzhou baiyunshan pharmaceutical factory submit patent application for N-heterocyclic substituent-containing antibiotic, preparation and use thereof. *Global IP News. Pharmaceutical Patent News*. 2014 May 15,.
255. Gupta SK, Mishra NC, Dhasmana A. Decellularization methods for scaffold fabrication. In: *Decellularized Scaffolds and Organogenesis*. New York, NY: Springer New York; 2017. p. 1-10.
256. Poornejad N, Schaumann LB, Buckmiller EM, Momtahan N, Gassman JR, Ma HH, Roeder BL, Reynolds PR, Cook AD. The impact of decellularization agents on renal tissue extracellular matrix. *Journal of biomaterials applications*. 2016 Oct; 31(4): 521-533.
257. Cornelison RC, Wellman SM, Park JH, Porvasnik SL, Song YH, Wachs RA, Schmidt CE. Development of an apoptosis-assisted decellularization method for maximal preservation of nerve tissue structure. *Acta biomaterialia*. 2018 Sep 1; 77: 116-126.
258. Casali DM, Handleton RM, Shazly T, Matthews MA. A novel supercritical CO₂-based decellularization method for maintaining scaffold hydration and mechanical properties. *The Journal of supercritical fluids*. 2018 Jan; 131: 72-81.
259. Wang Z, Sun F, Lu Y, Zhang B, Zhang G, Shi H. Rapid preparation method for preparing tracheal decellularized scaffolds: Vacuum assistance and optimization of DNase I. *ACS omega*. 2021 Apr 27; 6(16): 10637-10644.
260. Butler CR, Hynds RE, Crowley C, Gowers KHC, Partington L, Hamilton NJ, Cavalhos C, Platé M, Samuel ER, Burns AJ, Urbani L, Birchall MA, Lowdell MW, De Coppi P, Janes SM. Vacuum-assisted decellularization: An accelerated protocol to generate tissue-engineered human tracheal scaffolds. *Biomaterials*. 2017; 124: 95-105.
261. Cornelison RC, Wellman SM, Park JH, Porvasnik SL, Song YH, Wachs RA, Schmidt CE. Development of an apoptosis-assisted decellularization method for maximal preservation of nerve tissue structure. *Acta biomaterialia*. 2018 Sep 1; 77: 116-126.

262. Song YH, Maynes MA, Hlavac N, Visosevic D, Daramola KO, Porvasnik SL, Schmidt CE. Development of novel apoptosis-assisted lung tissue decellularization methods. *Biomaterials science*. 2021 May 4;; 9(9): 3485-3498.
263. Łopianiak I, Butruk-Raszeja BA. Evaluation of sterilization/disinfection methods of fibrous polyurethane scaffolds designed for tissue engineering applications. *International journal of molecular sciences*. 2020 Oct 30;; 21(21): 8092.
264. Qiu S, Rao Z, He F, Wang T, Xu Y, Du Z, Yao Z, Lin T, Yan L, Quan D, Zhu Q, Liu X. Decellularized nerve matrix hydrogel and glial-derived neurotrophic factor modifications assisted nerve repair with decellularized nerve matrix scaffolds. *Journal of tissue engineering and regenerative medicine*. 2020 Jul; 14(7): 931-943.
265. Mendes GC, Brandão TRS, Silva CLM. Modeling the inactivation of bacillus subtilis spores by ethylene oxide processing. *J Ind Microbiol Biotechnol*. 2011 Feb 5;; 38(9): 1535-1543.
266. Qing Q, Zhang Y, Yang J, Ning L, Zhang Y, Jiang Y, Zhang Y, Luo J, Qin T. Effects of hydrogen peroxide on biological characteristics and osteoinductivity of decellularized and demineralized bone matrices. *Journal of biomedical materials research. Part A*. 2019 Jul; 107(7): 1476-1490.
267. Wang W, Itoh S, Takakuda K. Comparative study of the efficacy of decellularization treatment of allogenic and xenogeneic nerves as nerve conduits. *Journal of biomedical materials research. Part A*. 2016 Feb; 104(2): 445-454.
268. Bombelli S, Meregalli C, Scalia C, Bovo G, Torsello B, De Marco S, Cadamuro M, Viganò P, Strada G, Cattoretti G, Bianchi C, Perego RA. Nephrosphere-derived cells are induced to multilineage differentiation when cultured on human decellularized kidney scaffolds. *The American journal of pathology*. 2018 Jan; 188(1): 184-195.
269. Clapp PA, Davies MJ, French MS, Gilbert BC. The bactericidal action of peroxides; an E.P.R. spin-trapping study. *Free radical research*. 1994; 21(3): 147-167.
270. Zvarova B, Uhl FE, Uriarte JJ, Borg ZD, Coffey AL, Bonenfant NR, Weiss DJ, Wagner DE. Residual detergent detection method for nondestructive cytocompatibility evaluation of decellularized whole lung scaffolds. *Tissue engineering. Part C, Methods*. 2016 May 1;; 22(5): 418-428.
271. Jayakrishnan A, Jameela SR. Glutaraldehyde as a fixative in bioprostheses and drug delivery matrices. *Biomaterials*. 1996; 17(5): 471-484.

272. Kim SS, Lim SH, Cho SW, Gwak SJ, Hong YS, Chang BC, Park MH, Song KW, Choi CY, Kim BS. Tissue engineering of heart valves by recellularization of glutaraldehyde-fixed porcine valves using bone marrow-derived cells. *Experimental & molecular medicine*. 2006 Jun 30; 38(3): 273-283.
273. Lee C, Kim SH, Choi S, Kim YJ. High-concentration glutaraldehyde fixation of bovine pericardium in organic solvent and post-fixation glycine treatment: In vitro material assessment and in vivo anticalcification effect. *Eur J Cardiothorac Surg*. 2011 Mar; 39(3): 381-387.
274. Pathak CP, Adams AK, Simpson T, Phillips Jr RE, Moore MA. Treatment of bioprosthetic heart valve tissue with long chain alcohol solution to lower calcification potential. *Journal of Biomedical Materials Research Part A*. 2004 Apr 1; 6(4): 140-144.
275. Vyavahare N, Hirsch D, Lerner E, Baskin JZ, Schoen FJ, Bianco R, Kruth HS, Zand R, Levy RJ. Prevention of bioprosthetic heart valve calcification by ethanol preincubation: Efficacy and mechanisms. *Circulation*. 1997 Jan 21; 95(2): 479-488.
276. Damink LHHO, Dijkstra PJ, van Luyn MJA, van Wachem PB, Nieuwenhuis P, Feijen J. In vitro degradation of dermal sheep collagen cross-linked using a water-soluble carbodiimide. *Biomaterials*. 1996; 17(7): 679-684.
277. Jorge-Herrero E, Fernández P, Turnay J, Olmo N, Calero P, García R, Freile I, Castillo-Olivares JL. Influence of different chemical cross-linking treatments on the properties of bovine pericardium and collagen. *Biomaterials*. 1999; 20(6): 539-545.
278. Sung H, Hsu C, Lee Y. Physical properties of a porcine internal thoracic artery fixed with an epoxy compound. *Biomaterials*. 1996; 17(24): 2357-2365.
279. Sung H, Chang Y, Chiu C, Chen C, Liang H. Crosslinking characteristics and mechanical properties of a bovine pericardium fixed with a naturally occurring crosslinking agent. *Journal of Biomedical Materials Research*. 1999 Nov; 6(4): 116-126.
280. Sung H, Liang I, Chen C, Huang R, Liang H. Stability of a biological tissue fixed with a naturally occurring crosslinking agent (genipin). *Journal of Biomedical Materials Research*. 2001 Jun 15; 55(4): 538-546.
281. Chang Y, Tsai C, Liang H, Sung H. In vivo evaluation of cellular and acellular bovine pericardia fixed with a naturally occurring crosslinking agent (genipin). *Biomaterials*. 2002; 23(12): 2447-2457.
282. Koob TJ, Willis TA, Hernandez DJ. Biocompatibility of NDGA-polymerized collagen fibers. I. evaluation of cytotoxicity with tendon fibroblasts in vitro. *Journal of Biomedical Materials Research*. 2001 Jul; 56(4): 31-39.

283. Han B, Jaurequi J, Tang BW, Nimni ME. Proanthocyanidin: A natural crosslinking reagent for stabilizing collagen matrices. *Journal of Biomedical Materials Research Part A*. 2003 Apr 1; 65A(4): 118-124.
284. Zhai W, Chang J, Lin K, Wang J, Zhao Q, Sun X. Crosslinking of decellularized porcine heart valve matrix by procyanidins. *Biomaterials*. 2006; 27(19): 3684-3690.
285. Zhai W, Chang J, Lü X, Wang Z. Procyanidins-crosslinked heart valve matrix: Anticalcification effect. *Journal of Biomedical Materials Research Part B: Applied Biomaterials*. 2009 Aug; 90B(2): 913-921.
286. Pennel T, Fercana G, Bezuidenhout D, Simionescu A, Chuang T, Zilla P, Simionescu D. The performance of cross-linked acellular arterial scaffolds as vascular grafts; pre-clinical testing in direct and isolation loop circulatory models. *Biomaterials*. 2014; 35(24): 6311-6322.
287. Luck G, Liao H, Murray NJ, Grimmer HR, Warminski EE, Williamson MP, Lilley TH, Haslam E. Polyphenols, astringency and proline-rich proteins. *Phytochemistry (Oxford)*. 1994; 37(2): 357-371.
288. Charlton AJ, Baxter NJ, Lilley TH, Haslam E, McDonald CJ, Williamson MP. Tannin interactions with a full-length human salivary proline-rich protein display a stronger affinity than with single proline-rich repeats. *FEBS letters*. 1996; 382(3): 289-292.
289. Isenburg JC, Simionescu DT, Starcher BC, Vyavahare NR. Elastin stabilization for treatment of abdominal aortic aneurysms. *Circulation*. 2007 Apr 3; 115(13): 1729-1737.
290. Vyavahare NR. Nanoparticle-based targeted delivery of pentagalloyl glucose reverses elastase-induced abdominal aortic aneurysm and restores aorta to the healthy state in mice. *PLoS ONE*. 2020 Jan 1; 15(3).
291. Wang X, Parasaram V, Dhital S, Nosoudi N, Hasanain S, Lane BA, Lessner SM, Eberth JF, Vyavahare NR. Systemic delivery of targeted nanotherapeutic reverses angiotensin II-induced abdominal aortic aneurysms in mice. *Scientific reports*. 2021 Apr 21; 11(1): 8584.
292. Torres-León C, Ventura-Sobrevilla J, Serna-Cock L, Ascacio-Valdés JA, Contreras-Esquivel J, Aguilar CN. Pentagalloylglucose (PGG): A valuable phenolic compound with functional properties. *Journal of functional foods*. 2017 Oct; 37: 176-189.
293. Zhai W, Lü X, Chang J, Zhou Y, Zhang H. Quercetin-crosslinked porcine heart valve matrix: Mechanical properties, stability, anticalcification and cytocompatibility. *Acta biomaterialia*. 2010; 6(2): 389-395.

294. Xiao J, Kai G, Yang F, Liu C, Xu X, Yamamoto K. Molecular structure-affinity relationship of natural polyphenols for bovine γ -globulin. *Molecular nutrition & food research*. 2011 May; 55(S1): S86-S92.
295. Pereira SC, Parente JM, Belo VA, Mendes AS, Gonzaga NA, do Vale GT, Ceron CS, Tanus-Santos JE, Tirapelli CR, Castro MM. Quercetin decreases the activity of matrix metalloproteinase-2 and ameliorates vascular remodeling in renovascular hypertension. *Atherosclerosis*. 2018 Mar; 270: 146-153.
296. Beck F, Ilie N. Antioxidants and collagen-crosslinking: Benefit on bond strength and clinical applicability. *Materials*. 2020 Dec 1; 13(23): 5483.
297. Miguez PA, Tuin SA, Robinson AG, Belcher J, Jongwattapanisan P, Perley K, de Paiva Gonçalves V, Hanifi A, Pleshko N, Barton ER. Hesperidin promotes osteogenesis and modulates collagen matrix organization and mineralization in vitro and in vivo. *International journal of molecular sciences*. 2021 Mar 22; 22(6): 3223.
298. Adamiak K, Lewandowska K, Sionkowska A. The influence of salicin on rheological and film-forming properties of collagen. *Molecules (Basel, Switzerland)*. 2021 Mar 16; 26(6): 1661.
299. Gao F, Zhang S. Salicin inhibits AGE-induced degradation of type II collagen and aggrecan in human SW1353 chondrocytes: Therapeutic potential in osteoarthritis. *Artificial cells, nanomedicine, and biotechnology*. 2019 Dec 4; 47(1): 1043-1049.
300. Song Y, Tian X, Wang X, Feng H. Vascular protection of salicin on IL-1 β -induced endothelial inflammatory response and damages in retinal endothelial cells. *Artificial cells, nanomedicine, and biotechnology*. 2019 Dec 4; 47(1): 1995-2002.
301. Rossetti D, Kielmanowicz MG, Vigodman S, Hu YP, Chen N, Nkengne A, Oddos T, Fischer D, Seiberg M, Lin CB. A novel anti-ageing mechanism for retinol: Induction of dermal elastin synthesis and elastin fibre formation. *International journal of cosmetic science*. 2011 Feb; 33(1): 62-69.
302. Chang Y, Kao Y, Hu D, Tsai L, Wu W. All-trans retinoic acid remodels extracellular matrix and suppresses laminin-enhanced contractility of cultured human retinal pigment epithelial cells. *Experimental eye research*. 2009; 88(5): 900-909.
303. Kim H, Park J, Shin J, Yang H, Lee H, Park I. TGF- β 1-induced HSP47 regulates extracellular matrix accumulation via Smad2/3 signaling pathways in nasal fibroblasts. *Scientific reports*. 2019 Oct 29; 9(1): 15563.

304. Axel DI, Frigge A, Dittmann J, Runge H, Spyridopoulos I, Riessen R, Viebahn R, Karsch KR. All-trans retinoic acid regulates proliferation, migration, differentiation, and extracellular matrix turnover of human arterial smooth muscle cells. *Cardiovascular research*. 2001 Mar; 49(4): 851-862.
305. Diabetes statistics [homepage on the Internet]. . 2021 April 13,. Available from: <https://www.who.int/news-room/fact-sheets/detail/diabetes>.
306. Krupyanko VI. Experimental biochemistry, by R.L. switzer and L.F. garrity, (third edition). W.H. freeman and company, new york, 1999, ix+451 pp., ISBN 0-7167-3300-5. *Process Biochemistry*. 2000; 36(4): 379.
307. Diabetes facts and figures [homepage on the Internet]. . Available from: <https://idf.org/aboutdiabetes/what-is-diabetes/facts-figures.html>.
308. Type 2 diabetes [homepage on the Internet]. . Available from: <https://www.niddk.nih.gov/health-information/diabetes/overview/what-is-diabetes/type-2-diabetes>.
309. Type 2 diabetes [homepage on the Internet]. . 2021 August 10,. Available from: <https://www.cdc.gov/diabetes/basics/type2.html>.
310. Type 2 diabetes [homepage on the Internet]. . 2021. Available from: <https://www.mayoclinic.org/diseases-conditions/type-2-diabetes/symptoms-causes/syc-20351193>.
311. Diabetes before pregnancy and congenital heart defects [homepage on the Internet]. . 2021 October 1,. Available from: <https://www.cdc.gov/ncbddd/heartdefects/features/keyfindings-diabetes-preg.html>.
312. Terranova A. The effects of diabetes mellitus on wound healing. *Plastic surgical nursing*. 1991; 11(1): 20-25.
313. Wysocki AB, Grinnell F. Fibronectin profiles in normal and chronic wound fluid. *Laboratory investigation*. 1990; 63(6): 825-831.
314. Frich LMH. Nursing interventions for patients with chronic conditions. *Journal of advanced nursing*. 2003 Oct; 44(2): 137-153.
315. Baltzis D, Eleftheriadou I, Veves A. Pathogenesis and treatment of impaired wound healing in diabetes mellitus: New insights. *Adv Ther*. 2014 Jul 29; 31(8): 817-836.
316. Tian-Shing Lee, Saltsman KA, Ohashi H, King GL. Activation of protein kinase C by elevation of glucose concentration: Proposal for a mechanism in the development of

diabetic vascular complications. *Proceedings of the National Academy of Sciences - PNAS*. 1989 Jul 1,; 86(13): 5141-5145.

317. Pradhan L, Nabzdyk C, Andersen ND, LoGerfo FW, Veves A. Inflammation and neuropeptides: The connection in diabetic wound healing. *Expert reviews in molecular medicine*. 2009 Jan 13,; 11: e2.

318. Blakytyn R, Jude E. The molecular biology of chronic wounds and delayed healing in diabetes. *Diabetic medicine*. 2006 Jun; 23(6): 594-608.

319. Yan SD, Schmidt AM, Anderson GM, Zhang J, Brett J, Zou YS, Pinsky D, Stern D. Enhanced cellular oxidant stress by the interaction of advanced glycation end products with their receptors/binding proteins. *The Journal of biological chemistry*. 1994 Apr 1,; 269(13): 9889-9897.

320. Kirstein M, Brett J, Radoff S, Ogawa S, Stern D, Vlassara H. Advanced protein glycosylation induces transendothelial human monocyte chemotaxis and secretion of platelet-derived growth factor: Role in vascular disease of diabetes and aging. *Proceedings of the National Academy of Sciences - PNAS*. 1990 Nov 1,; 87(22): 9010-9014.

321. Pradhan Nabzdyk L, PhD, Kuchibhotla S, BS, Guthrie P, BS, Chun M, BA, Auster ME, BA, Nabzdyk C, MD, Deso S, MD, Andersen N, MD, Gnardellis C, PhD, LoGerfo FW, MD, Veves, Aristidis, MD, DSc. Expression of neuropeptides and cytokines in a rabbit model of diabetic neuroischemic wound healing. *Journal of vascular surgery*. 2013; 58(3): 766-775.e12.

322. Ochoa O, Torres FM, Shireman PK. Chemokines and diabetic wound healing. *Vascular*. 2007 Dec 1,; 15(6): 350-355.

323. Desta T, Li J, Chino T, Graves DT. Altered fibroblast proliferation and apoptosis in diabetic gingival wounds. *Journal of dental research*. 2010 Jun; 89(6): 609-614.

324. Keratinocyte migration, proliferation, and differentiation in chronic ulcers from patients with diabetes and normal wounds. .

325. Expression of tissue inhibitor of metalloprotease 3 is reduced in ischemic but not neuropathic ulcers from patients with type 2 diabetes mellitus. .

326. Expression of matrix-metalloproteinases and their inhibitors in the wounds of diabetic and non-diabetic patients. .

327. Lobmann R, Schultz G, Lehnert H. Proteases and the diabetic foot syndrome: Mechanisms and therapeutic implications. *Diabetes care*. 2005 Feb; 28(2): 461-471.

328. Dinh T, Tecilazich F, Veves A, Kafanas A, Doupis J, Gnardellis C, Leal E, Tellechea A, Pradhan L, Lyons TE, Giurini JM. Mechanisms involved in the development and healing of diabetic foot ulceration. *Diabetes (New York, N.Y.)*. 2012; 61(11): 2937-2947.
329. Gin H, Brottier E, Aubertin J. Influence of glycaemic normalisation by an artificial pancreas on phagocytic and bactericidal functions of granulocytes in insulin dependent diabetic patients. *Journal of clinical pathology*. 1984 Sep; 37(9): 1029-1031.
330. Repine JE, Clawson CC, Goetz FC. Bactericidal function of neutrophils from patients with acute bacterial infections and from diabetics. *The Journal of infectious diseases*. 1980 Dec; 142(6): 869-875.
331. Cheng H, Tsui Y, Cheung KMC, Chan D, Chan BP. Decellularization of chondrocyte-encapsulated collagen microspheres: A three-dimensional model to study the effects of acellular matrix on stem cell fate. *Tissue engineering. Part C, Methods*. 2009 Dec; 15(4): 697-706.
332. Hughes O, Rakosi A, Macquhae F, Herskovitz I, Fox J, Kirsner R. A review of cellular and acellular matrix products: Indications, techniques, and outcomes. *Plastic and reconstructive surgery (1963)*. 2016 Sep; 138(3S Current Concepts in Wound Healing: Update 2016): 138S-147S.
333. Song JJ, Ott HC. Organ engineering based on decellularized matrix scaffolds. *Trends in molecular medicine*. 2011; 17(8): 424-432.
334. Chen R, Ho H, Tsai Y, Sheu M. Process development of an acellular dermal matrix (ADM) for biomedical applications. *Biomaterials*. 2004; 25(13): 2679-2686.
335. Pastar I, Stojadinovic O, Tomic-Canic M. Role of keratinocytes in healing of chronic wounds. *Surgical technology international*. 2008; 17: 105-112.
336. Zaulyanov L, Kirsner RS. A review of a bi-layered living cell treatment (apligraf (®)) in the treatment of venous leg ulcers and diabetic foot ulcers. *Clinical interventions in aging*. 2007; 2(1): 93-98.
337. Dickinson LE, Gerecht S. Engineered biopolymeric scaffolds for chronic wound healing. *Frontiers in physiology*. 2016; 7: 341.
338. Yonehiro L, Burleson G, Sauer V. Use of a new acellular dermal matrix for treatment of nonhealing wounds in the lower extremities of patients with diabetes. *Wounds (King of Prussia, Pa.)*. 2013 Dec; 25(12): 340-344.

339. Kirsner RS, Bohn G, Driver VR, Mills Sr JL, Nanney LB, Williams ML, Wu SC. Human acellular dermal wound matrix: Evidence and experience. *International wound journal*. 2015 Dec; 12(6): 646-654.
340. Litwiniuk M, Krejner A, Speyrer MS, Gauto AR, Grzela T. Hyaluronic acid in inflammation and tissue regeneration. *Wounds (King of Prussia, Pa.)*. 2016 Mar; 28(3): 78-88.
341. Cai H, Li G. Efficacy of alginate-and chitosan-based scaffolds on the healing of diabetic skin wounds in animal experimental models and cell studies: A systematic review. *Wound repair and regeneration*. 2020 Nov; 28(6): 751-771.
342. Kelechi, Teresa J., PhD, RN, Mueller M, PhD, Hankin CS, PhD, Bronstone A, PhD, Samies J, MD, Bonham, Phyllis A., PhD, RN. A randomized, investigator-blinded, controlled pilot study to evaluate the safety and efficacy of a poly-N-acetyl glucosamine–derived membrane material in patients with venous leg ulcers. *Journal of the American Academy of Dermatology*. 2011; 66(6): e209-e215.
343. Liu J, Zheng H, Poh PSP, Machens H, Schilling AF. Hydrogels for engineering of perfusable vascular networks. *International journal of molecular sciences*. 2015 Jul 14; 16(7): 15997-16016.
344. Thangavel P, Ramachandran B, Chakraborty S, Kannan R, Lonchin S, Muthuvijayan V. Accelerated healing of diabetic wounds treated with L-glutamic acid loaded hydrogels through enhanced collagen deposition and angiogenesis: An in vivo study. *Scientific reports*. 2017 Sep 6; 7(1): 10701-15.
345. McCarty SM, Percival SL. Proteases and delayed wound healing. *Advances in wound care (New Rochelle, N.Y.)*. 2013 Oct 1; 2(8): 438-447.
346. Laiva AL, O'Brien FJ, Keogh MB. SDF-1 α gene-activated collagen scaffold restores pro-angiogenic wound healing features in human diabetic adipose-derived stem cells. *Biomedicines*. 2021 Feb 6; 9(2): 160.
347. Liu J, Zheng H, Dai X, Sun S, Machens HG, Schilling AF. Biomaterials for promoting wound healing in diabetes. *Journal of tissue science & engineering*. 2017; 8(1).
348. Tokatlian T, Cam C, Segura T. Porous hyaluronic acid hydrogels for localized nonviral DNA delivery in a diabetic wound healing model. *Advanced healthcare materials*. 2015 May; 4(7): 1084-1091.
349. Losi P, Briganti E, Errico C, Lisella A, Sanguinetti E, Chiellini F, Soldani G. Fibrin-based scaffold incorporating VEGF- and bFGF-loaded nanoparticles stimulates wound healing in diabetic mice. *Acta biomaterialia*. 2013 Aug; 9(8): 7814-7821.

350. King AJ. The use of animal models in diabetes research. *British journal of pharmacology*. 2012 Jun; 166(3): 877-894.
351. Kahn SE. Insulin resistance and beta cell dysfunction. Oxford: Blackwell; 2002.
352. Kleinert M, Clemmensen C, Hofmann SM, Moore MC, Renner S, Woods SC, Huypens P, Beckers J, de Angelis MH, Schürmann A, Bakhti M, Klingenspor M, Heiman M, Cherrington AD, Ristow M, Lickert H, Wolf E, Havel PJ, Müller TD, Tschöp MH. Animal models of obesity and diabetes mellitus. *Nature reviews. Endocrinology*. 2018 Mar; 14(3): 140-162.
353. King AJ. The use of animal models in diabetes research. *British journal of pharmacology*. 2012 Jun; 166(3): 877-894.
354. Animal models of type 2 diabetes: Clinical presentation and pathophysiological relevance to the human condition.
355. Kottaisamy CPD, Raj DS, Prasanth Kumar V, Sankaran U. Experimental animal models for diabetes and its related complications—a review. *Laboratory animal research*. 2021 Aug 24; 37(1): 23.
356. Gheibi S, Kashfi K, Ghasemi A. A practical guide for induction of type-2 diabetes in rat: Incorporating a high-fat diet and streptozotocin. *Biomedicine & pharmacotherapy*. 2017 Nov; 95: 605-613.
357. Magalhães DAD, Kume WT, Correia FS, Queiroz TS, Allebrandt Neto EW, Santos MPD, Kawashita NH, França SAD. High-fat diet and streptozotocin in the induction of type 2 diabetes mellitus: A new proposal. *Anais da Academia Brasileira de Ciências*. 2019 Mar 21; 91(1): e20180314.
358. Jacobs ML. MD, MD, FRCS jaroslav F. stark marc R. de leval victor T. tsang surgery for congenital heart defects 3rd edition 2006 john wiley & sons west sussex, england 718 pp, illustrated, \$315.00 ISBN: 0470093161. *Ann Thorac Surg*. 2008; 85(1): 364.
359. Manji RA, Zhu LF, Nijjar NK, Rayner DC, Korbitt GS, Churchill TA, Rajotte RV, Koshal A, Ross DB. Glutaraldehyde-fixed bioprosthetic heart valve conduits calcify and fail from xenograft rejection. *Circulation*. 2006 Jul 25; 114(4): 318-327.
360. van Brakel, Thomas J., MD, PhD, Schoof, Paul H., MD, PhD, de Roo F, MPA, Nikkels, Peter G.J., MD, PhD, Evens FCM, MD, Haas F, MD. High incidence of dacron conduit stenosis for extracardiac fontan procedure. *The Journal of thoracic and cardiovascular surgery*. 2014; 147(5): 1568-1572.

361. Ozaki S, Kawase I, Yamashita H, Uchida S, Nozawa Y, Matsuyama T, Takatoh M, Hagiwara S. Aortic valve reconstruction using self-developed aortic valve plasty system in aortic valve disease. *Interact CardioVasc Thorac Surg*. 2011 Apr; 12(4): 550-553.
362. Marathe SP, Chávez M, Sleeper LA, Marx G, del Nido PJ, Baird CW. Modified ozaki procedure including annular enlargement for small aortic annuli in young patients. *The Annals of thoracic surgery*. 2020 Oct; 110(4): 1364-1371.
363. Schoen FJ, Levy RJ. Calcification of tissue heart valve substitutes: Progress toward understanding and prevention. *The Annals of thoracic surgery*. 2005; 79(3): 1072-1080.
364. Isenburg JC, Simionescu DT, Starcher BC, Vyavahare NR. Elastin stabilization for treatment of abdominal aortic aneurysms. *Circulation*. 2007 Apr 03; 115(13): 1729-1737.
365. Lu Q, Ganesan K, Simionescu DT, Vyavahare NR. Novel porous aortic elastin and collagen scaffolds for tissue engineering. *Biomaterials*. 2004; 25(22): 5227-5237.
366. Srokowski EM, Woodhouse KA. 2.20 decellularized scaffolds. In: Ducheyne P, editor. *Comprehensive Biomaterials II*. Oxford: Elsevier; 2017. p. 452-470.
367. Wong ML, Griffiths LG. Immunogenicity in xenogeneic scaffold generation: Antigen removal vs. decellularization. *Acta biomaterialia*. 2014; 10(5): 1806-1816.
368. Isenburg JC, Karamchandani NV, Simionescu DT, Vyavahare NR. Structural requirements for stabilization of vascular elastin by polyphenolic tannins. *Biomaterials*. 2006; 27(19): 3645-3651.
369. Xu K, Kuntz LA, Foehr P, Kuempel K, Wagner A, Tuebel J, Deimling CV, Burgkart RH. Efficient decellularization for tissue engineering of the tendon-bone interface with preservation of biomechanics. *PLOS ONE*. 2017; 12(2): e0171577.
370. Gilpin A, Yang Y. Decellularization strategies for regenerative medicine: From processing techniques to applications. *BioMed Research International*. 2017; 2017: 9831534.
371. Butler, Charles E., MD, FACS, Burns NK, MD, Campbell KT, MD, Mathur AB, PhD, Jaffari MV, BS, Rios CN, BS. Comparison of cross-linked and non-cross-linked porcine acellular dermal matrices for ventral hernia repair. *Journal of the American College of Surgeons*. 2010; 211(3): 368-376.
372. Alberti KA, Xu Q. Biocompatibility and degradation of tendon-derived scaffolds. *Regenerative biomaterials*. 2016; 3(1): 1-11.

373. Isenburg JC, Simionescu DT, Vyavahare NR. Tannic acid treatment enhances biostability and reduces calcification of glutaraldehyde fixed aortic wall. *Biomaterials*. 2005; 26(11): 1237-1245.
374. Chuang T, Stabler C, Simionescu A, Simionescu DT. Polyphenol-stabilized tubular elastin scaffolds for tissue engineered vascular grafts. *Tissue Engineering Part A*. 2009; 15(10): 2837-2851.
375. Luck G, Liao H, Murray NJ, Grimmer HR, Warminski EE, Williamson MP, Lilley TH, Haslam E. Polyphenols, astringency and proline-rich proteins. *Phytochemistry*. 1994; 37(2): 357-371.
376. Charlton AJ, Baxter NJ, Lilley TH, Haslam E, McDonald CJ, Williamson MP. Tannin interactions with a full-length human salivary proline-rich protein display a stronger affinity than with single proline-rich repeats. *FEBS letters*. 1996; 382(3): 289-292.
377. Sinha A, Nosoudi N, Vyavahare N. Elasto-regenerative properties of polyphenols. *Biochemical and biophysical research communications*. 2014 Feb 07; 444(2): 205-211.
378. Wang R, Ozsvar J, Yeo GC, Weiss AS. Hierarchical assembly of elastin materials. *Current Opinion in Chemical Engineering*. 2019; 24: 54-60.
379. Sivaraman B, Bashur CA, Ramamurthi A. Advances in biomimetic regeneration of elastic matrix structures. *Drug delivery and translational research*. 2012; 2(5): 323-350.
380. Li X, Wang X, Liu H, Peng Y, Yan Y, Ni T. Mechanism evaluation of the interactions between eight flavonoids and γ -globulin based on multi-spectroscopy. *Journal of molecular structure*. 2021 Feb 05; 1225: 129291.
381. Axel DI, Frigge A, Dittmann J, Runge H, Spyridopoulos I, Riessen R, Viebahn R, Karsch KR. All-trans retinoic acid regulates proliferation, migration, differentiation, and extracellular matrix turnover of human arterial smooth muscle cells. *Cardiovascular research*. 2001 Mar; 49(4): 851-862.
382. Crowe AR, Yue W. Semi-quantitative determination of protein expression using immunohistochemistry staining and analysis: An integrated protocol. *Bio-protocol*. 2019; 9(24): e3465.
383. Peter Bankhead. Analyzing fluorescence microscopy images with ImageJ. 2014 May.
384. Srokowski EM. Benefits and challenges of decellularization 370 2.221.2. decellularization methodology 371 2.221.2.1. physical methods 371 2.221.2.2. chemical methods 373 2.221.2.2.1. solvent extraction 373 2.221.2.2.2. alkaline and acid treatments 373 2.

385. Wong ML, Griffiths LG. Immunogenicity in xenogeneic scaffold generation: Antigen removal vs. decellularization. *Acta biomaterialia*. 2014; 10(5): 1806-1816.
386. Srokowski EM, Woodhouse KA. 2.20 decellularized scaffolds. In: Ducheyne P, editor. *Comprehensive Biomaterials II*. Oxford: Elsevier; 2017. p. 452-470.
387. Sengyoku H, Tsuchiya T, Obata T, Doi R, Hashimoto Y, Ishii M, Sakai H, Matsuo N, Taniguchi D, Suematsu T, Lawn M, Matsumoto K, Miyazaki T, Nagayasu T. Sodium hydroxide based non-detergent decellularizing solution for rat lung. *Organogenesis*. 2018; 14(2): 94-106.
388. Vyavahare N, Tam H. Bioprosthetic heart valves: From a biomaterials perspective. In: Sacks MS, Liao J, editors. *Advances in Heart Valve Biomechanics: Valvular Physiology, Mechanobiology, and Bioengineering*. Cham: Springer International Publishing; 2018. p. 337-382.
389. Wang R, de Kort BJ, Smits, Anthal I. P. M., Weiss AS. Elastin in vascular grafts. In: Walpoth B, Bergmeister H, Bowlin G, Kong D, Rotmans J, Zilla P, editors. *Tissue-Engineered Vascular Grafts*. Cham: Springer International Publishing; 2019. p. 1-32.
390. Madani MM, Golts E. Cardiovascular anatomy. In: *Reference Module in Biomedical Sciences*. Elsevier; 2014.
391. The components in fascia [homepage on the Internet]. Atlasbalans AB. 2020. Available from: <https://fasciaguide.com/fascia-anatomy-physiology/the-components-in-fascia/>.
392. Parasaram V. Targeted delivery of drug loaded albumin nanoparticles to emphysematous lungs to preserve elastin and mitigate matrix metalloproteinase activity [dissertation]. Clemson University Libraries.
393. Nosoudi N. Targeted nano-therapeutics for the reversal of calcification and ECM degradation in abdominal aortic aneurysms [dissertation]. Clemson University Libraries.
394. Chowdhury A, Nosoudi N, Karamched S, Parasaram V, Vyavahare N. Polyphenol treatments increase elastin and collagen deposition by human dermal fibroblasts; implications to improve skin health. *J Dermatol Sci*. 2021; 102(2): 94-100.
395. Miguez PA, Tuin SA, Robinson AG, Belcher J, Jongwattanapisan P, Perley K, de Paiva Gonçalves V, Hanifi A, Pleshko N, Barton ER. Hesperidin promotes osteogenesis and modulates collagen matrix organization and mineralization in vitro and in vivo. *International Journal of Molecular Sciences*. 2021; 22(6).

396. van Strijp, Augustinus J. P, Takatsuka T, Sono R, Iijima Y. Inhibition of dentine collagen degradation by hesperidin: An in situ study. *European journal of oral sciences*. 2015 Dec; 123(6): 447-452.
397. Hiraishi N, Sono R, Sofiqul I, Yiu C, Nakamura H, Otsuki M, Takatsuka T, Tagami J. In vitro evaluation of plant-derived agents to preserve dentin collagen. *Dental materials*. 2013; 29(10): 1048-1054.
398. Islam MS, Hiraishi N, Nassar M, Sono R, Otsuki M, Takatsuka T, Yiu C, Tagami J. In vitro effect of hesperidin on root dentin collagen and de/re-mineralization. *Dental materials journal*. 2012; 31(3): 362-367.
399. Sanaei K, Plotner S, Oommen Jacob A, Ramirez-Vick J, Vyavahare N, Nosoudi N. Effect of all-trans retinoic acid and pentagalloyl glucose on smooth muscle cell elastogenesis. *Biomed Mater Eng*. 2021; 32: 145-157.
400. Watson REB, Craven NM, Griffiths CEM, Kang S, Jones CJP, Kielty CM. A short-term screening protocol, using fibrillin-1 as a reporter molecule, for photoaging repair agents. *J Invest Dermatol*. 2001; 116(5): 672-678.
401. Schrenk S, Cenzi C, Bertalot T, Conconi M, Teresa, Di Liddo R. Structural and functional failure of fibrillin-1 in human diseases (review). *Int J Mol Med*. 2018; 41(3): 1213-1223.
402. Greco KV, Francis L, Huang H, Ploeg R, Boccaccini AR, Ansari T. Is quercetin an alternative natural crosslinking agent to genipin for long-term dermal scaffolds implantation? *Journal of tissue engineering and regenerative medicine*. 2018 Mar; 12(3): e1716-e1724.
403. Ciaravella JM, McGoon DC, Danielson GK, Wallace RB, Mair DD, Ilstrup DM. Experience with the extracardiac conduit. *J Thorac Cardiovasc Surg*. 1979; 78(6): 920-930.
404. Greutmann M. Tetralogy of fallot, pulmonary valve replacement, and right ventricular volumes: Are we chasing the right target? *Eur Heart J*. 2016; 37(10): 836-839.
405. Ong K, Boone R, Gao M, Carere R, Webb J, Kiess M, Grewal J. Right ventricle to pulmonary artery conduit reoperations in patients with tetralogy of fallot or pulmonary atresia associated with ventricular septal defect. *Am J Cardiol*. 2013; 111(11): 1638-1643.
406. van Steenberghe M, Schubert T, Gerelli S, Bouzin C, Guiot Y, Xhema D, Bollen X, Abdelhamid K, Gianello P. Porcine pulmonary valve decellularization with NaOH-based vs detergent process: Preliminary in vitro and in vivo assessments. *Journal of Cardiothoracic Surgery*. 2018; 13(1): 34.

407. Ruel M, Chan V, Mesana TG, Berard P, Kulik A, Ressler L, Khanh Lam B, Rubens FD, Goldstein W, Hendry PJ, Masters RG. In: Very long-term survival implications of heart valve replacement with tissue versus mechanical prostheses in adults
408. Kim DJ, Kim YJ, Kim W, Kim S. Xenograft failure of pulmonary valved conduit cross-linked with glutaraldehyde or not cross-linked in a pig to goat implantation model. *The Korean journal of thoracic and cardiovascular surgery*. 2012; 45(5): 287-294.
409. Gist, Katja M., DO, MA, Mitchell MB, MD, Jagers J, MD, Campbell DN, MD, Yu JA, MD, Landeck, Bruce F., MD, MS. Assessment of the relationship between congenital conduit size and early valvar insufficiency. *The Annals of thoracic surgery*. 2012; 93(3): 856-861.
410. Oliver JM, Garcia-Hamilton D, Gonzalez AE, Ruiz-Cantador J, Sanchez-Recalde A, Polo ML, Aroca A. Risk factors for prosthetic pulmonary valve failure in patients with congenital heart disease. *Am J Cardiol*. 2015; 116(8): 1252-1256.
411. Karamlou T, Ungerleider RM, Alsoufi B, Burch G, Silberbach M, Reller M, Shen I. Oversizing pulmonary homograft conduits does not significantly decrease allograft failure in children☆. *Eur J Cardiothorac Surg*. 2005; 27(4): 548-553.
412. Mery CM, Guzmán-Pruneda FA, De León LE, Zhang W, Terwelp MD, Bocchini CE, Adachi I, Heinle JS, McKenzie ED, Fraser CD, Jr. Risk factors for development of endocarditis and reintervention in patients undergoing right ventricle to pulmonary artery valved conduit placement. *J Thorac Cardiovasc Surg*. 2016 Feb; 151(2): 432-2.
413. Avolio E, Caputo M, Madeddu P. Stem cell therapy and tissue engineering for correction of congenital heart disease. *Frontiers in Cell and Developmental Biology*. 2015; 3: 39.
414. Gilbert TW, Sellaro TL, Badylak SF. Decellularization of tissues and organs. *Biomaterials*. 2006 Jul; 27(19): 3675-3683.
415. Schenke-Layland K, Vasilevski O, Opitz F, König K, Riemann I, Halbhuber KJ, Wahlers T, Stock UA. Impact of decellularization of xenogeneic tissue on extracellular matrix integrity for tissue engineering of heart valves. *J Struct Biol*. 2003 Sep; 143(3): 201-208.
416. Ootaki Y, Williams DA. 60 - pulmonary valve replacement: Indications and options. In: Ungerleider RM, Meliones JN, Nelson McMillan K, Cooper DS, Jacobs JP, editors. *Critical Heart Disease in Infants and Children (Third Edition)*. Philadelphia: Elsevier; 2019. p. 720-725.e2.

417. Flameng W, Meuris B, Yperman J, De Visscher G, Herijgers P, Verbeken E. Factors influencing calcification of cardiac bioprostheses in adolescent sheep. *J Thorac Cardiovasc Surg*. 2006; 132(1): 89-98.
418. Rosenblatt M, Peluso JV. Determination of tannins by photocolorimeter. *Journal of AOAC INTERNATIONAL*. 1941 Feb 1;; 24(1): 170-181.
419. Singleton VL, Orthofer R, Lamuela-Raventós RM. Analysis of total phenols and other oxidation substrates and antioxidants by means of folin-ciocalteu reagent. In: *Methods in Enzymology*. Elsevier Science & Technology; 1999. p. 152-178.
420. Tam H, Zhang W, Feaver KR, Parchment N, Sacks MS, Vyavahare N. A novel crosslinking method for improved tear resistance and biocompatibility of tissue based biomaterials. *Biomaterials*. 2015 Oct; 66: 83-91. PMID: PMC4522354.
421. Annor AH, Tang ME, Pui CL, Ebersole GC, Frisella MM, Matthews BD, Deeken CR. Effect of enzymatic degradation on the mechanical properties of biological scaffold materials. *Surg Endosc*. 2012; 26(10): 2767-2778.
422. Tam H. Novel chemical crosslinking to stabilize extracellular matrix for bioprosthetic heart valve materials to resist calcification and structural degradation [dissertation]. Clemson University Libraries; 2016.
423. Robinson-Bennett B, Han A. 30 - role of immunohistochemistry in elucidating lung cancer metastatic to the ovary from primary ovarian carcinoma. *Handbook of Immunohistochemistry and in Situ Hybridization of Human Carcinomas*. 2006; 4: 537-545.
424. Shinde AV, Humeres C, Frangogiannis NG. The role of α -smooth muscle actin in fibroblast-mediated matrix contraction and remodeling. *Biochim Biophys Acta Mol Basis Dis*. 2017 Jan; 1863(1): 298-309. PMID: PMC5163362.
425. Ito S, Nagata K. Roles of the endoplasmic reticulum-resident, collagen-specific molecular chaperone Hsp47 in vertebrate cells and human disease. *The Journal of biological chemistry*. 2019; 294(6): 2133-2141.
426. Manavitehrani I, Ebrahimi P, Yang I, Daly S, Schindeler A, Saxena A, Little DG, Fletcher DF, Dehghani F, Winlaw DS. Current challenges and emergent technologies for manufacturing artificial right ventricle to pulmonary artery (RV-PA) cardiac conduits. *Cardiovasc Eng Tech*. 2019 -02-14; 10(2): 205.
427. Rastan AJ, Walther T, Daehnert I, Hamsch J, Mohr FW, Janousek J, Kostelka M. Bovine jugular vein conduit for right ventricular outflow tract reconstruction: Evaluation of risk factors for mid-term outcome. *The Annals of thoracic surgery*. 2006; 82(4): 1308-1315.

428. Ichikawa Y, Noishiki Y, Kosuge T, Yamamoto K, Kondo J, Matsumoto A. Use of a bovine jugular vein graft with natural valve for right ventricular outflow tract reconstruction: A one-year animal study. *J Thorac Cardiovasc Surg.* 1997; 114(2): 224-233.
429. Fiore AC, Ruzmetov M, Huynh D, Hanley S, Rodefeld MD, Turrentine MW, Brown JW. Comparison of bovine jugular vein with pulmonary homograft conduits in children less than 2 years of age☆. *Eur J Cardiothorac Surg.* 2010; 38(3): 318-325.
430. Hiemann NE, MD, Mani M, MD, Huebler M, MD, Meyer, Rudolf, MD, PhD, Hetzer, Roland, MD, PhD, Thieme R, MD, Bethge, Christian, MD, PhD. Complete destruction of a tissue-engineered porcine xenograft in pulmonary valve position after the ross procedure. *The Journal of thoracic and cardiovascular surgery.* 2010; 139(4): e67-e68.
431. Hoerstrup SP, Kadner A, Breymann C, Maurus CF, Guenter CI, Sodian R, Visjager JF, Zund G, Turina MI. Living, autologous pulmonary artery conduits tissue engineered from human umbilical cord cells. *Ann Thorac Surg.* 2002 Jul; 74(1): 46-52; discussion 52.
432. van Rijswijk JW, Talacua H, Mulder K, van Hout, Gerardus P. J., Bouten CVC, Gründeman PF, Kluin J. Failure of decellularized porcine small intestinal submucosa as a heart valved conduit. *J Thorac Cardiovasc Surg.* 2020; 160(4): e201-e215.
433. Simon P, Kasimir MT, Seebacher G, Weigel G, Ullrich R, Salzer-Muhar U, Rieder E, Wolner E. Early failure of the tissue engineered porcine heart valve SYNERGRAFT® in pediatric patients. *Eur J Cardiothorac Surg.* 2003; 23(6): 1002-1006.
434. Wright GA, Faught JM, Olin JM. Assessing anticalcification treatments in bioprosthetic tissue by using the new zealand rabbit intramuscular model. *Comp Med.* 2009; 59(3): 266-271.
435. Barnhart J. National failure and international disregard. In: *The Consequences of Humiliation.* Cornell University Press; 2020. p. 15.
436. Mako WJ, Shah A, Vesely I. Mineralization of glutaraldehyde-fixed porcine aortic valve cusps in the subcutaneous rat model: Analysis of variations in implant site and cuspal quadrants. *J Biomed Mater Res.* 1999; 45(3): 209-213.
437. Levy RJ, Schoen FJ, Levy JT, Nelson AC, Howard SL, Oshry LJ. Biologic determinants of dystrophic calcification and osteocalcin deposition in glutaraldehyde-preserved porcine aortic valve leaflets implanted subcutaneously in rats. *The American journal of pathology.* 1983; 113(2): 143-155.

438. Dearani JA, Danielson GK. Congenital heart surgery nomenclature and database project: Ebstein's anomaly and tricuspid valve disease. *The Annals of thoracic surgery*. 2000; 69(3): 106-117.
439. Waller BF, Howard J, Fess S. Pathology of aortic valve stenosis and pure aortic regurgitation: A clinical morphologic assessment—Part II. *Clinical cardiology (Mahwah, N.J.)*. 1994 Mar; 17(3): 150-156.
440. Waller B, Howard J, Fess S. Pathology of aortic valve stenosis and pure aortic regurgitation a clinical morphologic assessment—part I. *Clinical cardiology (Mahwah, N.J.)*. 1994 Feb; 17(2): 85-92.
441. Waller BF, Howard J, Fess S. Pathology of pulmonic valve stenosis and pure regurgitation. *Clin Cardiol*. 1995; 18(1): 45-50.
442. Suleiman T, Kavinsky CJ, Skerritt C, Kenny D, Ilbawi MN, Caputo M. Recent development in pulmonary valve replacement after tetralogy of fallot repair: The emergence of hybrid approaches. *Frontiers in surgery*. 2015; 2: 22.
443. Myers PO, Mokashi SA, Horgan E, Borisuk M, Mayer JE, del Nido PJ, Baird CW. Outcomes after mechanical aortic valve replacement in children and young adults with congenital heart disease. *The Journal of thoracic and cardiovascular surgery*. 2019 Jan; 157(1): 329-340.
444. Umashankar PR, Mohanan PV, Kumari TV. Glutaraldehyde treatment elicits toxic response compared to decellularization in bovine pericardium. *Toxicology international*. 2012 Jan; 19(1): 51-58.
445. Fuller SM, Borisuk MJ, Sleeper LA, Bacha E, Burchill L, Guleserian K, Ilbawi M, Razzouk A, Shinkawa T, Lu M, Baird CW. Mortality and reoperation risk after bioprosthetic aortic valve replacement in young adults with congenital heart disease. *Seminars in thoracic and cardiovascular surgery*. 2021 Jun.
446. Nomoto R, BA, Sleeper LA, ScD, Borisuk, Michele J., MSN, CPNP, Bergerson, Lisa, MD, MPH, Pigula FA, MD, Emani S, MD, Fynn-Thompson F, MD, Mayer JE, MD, del Nido, Pedro J., MD, Baird CW, MD. Outcome and performance of bioprosthetic pulmonary valve replacement in patients with congenital heart disease. *The Journal of thoracic and cardiovascular surgery*. 2016; 152(5): 1333-1342.e3.
447. Ruel M, Chan V, Mesana TG, Bedard P, Kulik A, Ressler L, Khanh LAM B, Rubens FD, Goldstein W, Hendry PJ, Masters RG. In: Very long-term survival implications of heart valve replacement with tissue versus mechanical prostheses in adults

448. Huang HS, Lu J. Biaxial mechanical properties of bovine jugular venous valve leaflet tissues. *Biomech Model Mechanobiol.* 2017 Jun 19,; 16(6): 1911-1923.
449. Davis FM, De Vita R. A nonlinear constitutive model for stress relaxation in ligaments and tendons. *Ann Biomed Eng.* 2012 May 31,; 40(12): 2541-2550.
450. Hinds MT, Courtman DW, Goodell T, Kwong M, Brant-Zawadzki H, Burke A, Fox BA, Gregory KW. Biocompatibility of a xenogenic elastin-based biomaterial in a murine implantation model: The role of aluminum chloride pretreatment. *Journal of Biomedical Materials Research Part A.* 2004 Apr 1,; 6(4): 55-64.
451. Macleod TM, Williams G, Sanders R, Green CJ. Histological evaluation of permacol™ as a subcutaneous implant over a 20-week period in the rat model. *British journal of plastic surgery.* 2005; 58(4): 518-532.
452. Tam H. Novel chemical crosslinking to stabilize extracellular matrix for bioprosthetic heart valve materials to resist calcification and structural degradation [dissertation]. Clemson University Libraries.
453. Shakya S, Asosingh K, Mack JA, Maytin EV. Optimized protocol for the preparation of single cells from cutaneous wounds for flow cytometric cell sorting and analysis of macrophages. *MethodsX.* 2020; 7: 101027.
454. Wilson L, Fathke C, Isik F. Tissue dispersion and flow cytometry for the cellular analysis of wound healing. *BioTechniques.* 2002 Mar 1,; 32(3): 548-551.
455. VeDepo MC, Detamore MS, Hopkins RA, Converse GL. Recellularization of decellularized heart valves: Progress toward the tissue-engineered heart valve. *Journal of Tissue Engineering.* 2017 Aug 24,; 8: 2041731417726327.
456. Hopkins R. From cadaver harvested homograft valves to tissue-engineered valve conduits. *Progress in pediatric cardiology.* 2006; 21(2): 137-152.
457. Vesely I. Heart valve tissue engineering. *Circ Res.* 2005; 97(8): 743-755.
458. Schoen FJ, Hoerstrup SP. Chapter II.6.10 - heart valve tissue engineering. In: Ratner BD, Hoffman AS, Schoen FJ, Lemons JE, editors. *Biomaterials Science (Third Edition)*. Academic Press; 2013. p. 1246-1261.
459. Argento G, Simonet M, Oomens CWJ, Baaijens FPT. Multi-scale mechanical characterization of scaffolds for heart valve tissue engineering. *Journal of biomechanics.* 2012; 45(16): 2893-2898.

460. Iop L, Renier V, Naso F, Piccoli M, Bonetti A, Gandaglia A, Pozzobon M, Paolin A, Ortolani F, Marchini M, Spina M, De Coppi P, Sartore S, Gerosa G. The influence of heart valve leaflet matrix characteristics on the interaction between human mesenchymal stem cells and decellularized scaffolds. *Biomaterials*. 2009; 30(25): 4104-4116.
461. Li F, Li W, Johnson SA, Ingram DA, Yoder MC, Badylak SF. Low-molecular-weight peptides derived from extracellular matrix as chemoattractants for primary endothelial cells. *Endothelium (New York, N.Y.)*. 2004; 11(3-4): 199-206.
462. Argento G, Simonet M, Oomens CWJ, Baaijens FPT. Multi-scale mechanical characterization of scaffolds for heart valve tissue engineering. *Journal of biomechanics*. 2012; 45(16): 2893-2898.
463. VeDepo MC, Buse EE, Quinn RW, Williams TD, Detamore MS, Hopkins RA, Converse GL. Species-specific effects of aortic valve decellularization. *Acta biomaterialia*. 2017 Mar 1; 50: 249-258.
464. Liao J, Joyce EM, Sacks MS. Effects of decellularization on the mechanical and structural properties of the porcine aortic valve leaflet. *Biomaterials*. 2007; 29(8): 1065-1074.
465. Korossis SA, Booth C, Wilcox HE, Watterson KG, Kearney JN, Fisher J, Ingham E. Tissue engineering of cardiac valve prostheses II: Biomechanical characterization of decellularized porcine aortic heart valves. *The Journal of heart valve disease*. 2002 Jul; 11(4): 463-471.
466. Converse GL, Armstrong M, Quinn RW, Buse EE, Cromwell ML, Moriarty SJ, Lofland GK, Hilbert SL, Hopkins RA. Effects of cryopreservation, decellularization and novel extracellular matrix conditioning on the quasi-static and time-dependent properties of the pulmonary valve leaflet. *Acta biomaterialia*. 2012 Jul; 8(7): 2722-2729.
467. Modolo R, Miyazaki Y, Onuma Y, Soliman OI, Serruys PW. Biorestorative valve for transcatheter aortic valve implantation: Tomorrow's world from preclinical to clinical. In: *Transcatheter Aortic Valve Implantation*. Cham: Springer International Publishingp. 539-547.
468. Chronic hemodynamic performance of a biorestorative transcatheter heart valve in an ovine model. *EuroIntervention : journal of EuroPCR in collaboration with the Working Group on Interventional Cardiology of the European Society of Cardiology*. 2021 Jul 20,.
469. Syedain Z, Bradee A, Kren S, Taylor DA, Tranquillo RT. Decellularized tissue-engineered heart valve leaflets with recellularization potential. *Tissue engineering. Part A*. 2013 Mar; 19(ja): 759-769.

470. Syedain ZH, Meier LA, Reimer JM, Tranquillo RT. Tubular heart valves from decellularized engineered tissue. *Ann Biomed Eng.* 2013 Jul 30; 41(12): 2645-2654.
471. Syedain Z, Reimer J, Schmidt J, Lahti M, Berry J, Bianco R, Tranquillo RT. 6-month aortic valve implantation of an off-the-shelf tissue-engineered valve in sheep. *Biomaterials.* 2015; 73: 175-184.
472. Quinn RW, PhD, Hilbert, Stephen L., MD, PhD, Bert AA, MD, Drake BW, MD, Bustamante JA, RN, Fenton JE, RN, Moriarty SJ, BS, Neighbors SL, RNFA, Lofland GK, MD, Hopkins RA, MD. Performance and morphology of decellularized pulmonary valves implanted in juvenile sheep. *The Annals of thoracic surgery.* 2011; 92(1): 131-137.
473. Quinn RW, Hilbert SL, Converse GL, Bert AA, Buse E, Drake WB, Armstrong M, Moriarty SJ, Lofland GK, Hopkins RA. Enhanced autologous re-endothelialization of decellularized and extracellular matrix conditioned allografts implanted into the right ventricular outflow tracts of juvenile sheep. *Cardiovasc Eng Tech.* 2012 Feb 2; 3(2): 217-227.
474. Dohmen PM, Lembcke A, Hotz H, Kivelitz D, Konertz WF. Ross operation with a tissue-engineered heart valve. *The Annals of thoracic surgery.* 2002; 74(5): 1438-1442.
475. Dohmen PM. Clinical results of implanted tissue engineered heart valves. *HSR proceedings in intensive care & cardiovascular anesthesia.* 2012; 4(4): 225-231.
476. Dohmen, Pascal M., MD, PhD, Lembcke A, MD, Holinski S, MD, Pruss, Axel, MD, PhD, Konertz, Wolfgang, MD, PhD. Ten years of clinical results with a tissue-engineered pulmonary valve. *The Annals of thoracic surgery.* 2011; 92(4): 1308-1314.
477. Dohmen, Pascal M., MD, PhD, Lembcke A, MD, Holinski S, MD, Kivelitz D, PhD, Braun JP, MD, Pruss A, PhD, Konertz, Wolfgang, MD, PhD. Mid-term clinical results using a tissue-engineered pulmonary valve to reconstruct the right ventricular outflow tract during the ross procedure. *The Annals of thoracic surgery.* 2007; 84(3): 729-736.
478. Dohmen PM, Hauptmann S, Terytze A, Konertz WF. In-vivo repopularization of a tissue-engineered heart valve in a human subject. *The Journal of heart valve disease.* 2007 Jul; 16(4): 447-449.
479. Bejleri D, Davis ME. Decellularized extracellular matrix materials for cardiac repair and regeneration. *Advanced healthcare materials.* 2019 Mar 7; 8(5): e1801217-n/a.
480. Mase J, Vincent J, Hsu JR, Wolf SE, Wenke JC, Baer DG, Owens J, Badylak SF, Walters TJ. Clinical application of an acellular biologic scaffold for surgical repair of a large, traumatic quadriceps femoris muscle defect. *Orthopedics (Thorofare, N.J.).* 2010 Jul 13; 33(7): 511.

481. Greising SM, Rivera JC, Goldman SM, Watts A, Aguilar CA, Corona BT. Unwavering pathobiology of volumetric muscle loss injury. *Scientific reports*. 2017 Oct 13,; 7(1): 13179-14.
482. De Coppi P, Bellini S, Conconi MT, Sabatti M, Simonato E, Gamba PG, Nussdorfer GG, Parnigotto PP. Myoblast–acellular skeletal muscle matrix constructs guarantee a long-term repair of experimental full-thickness abdominal wall defects. *Tissue engineering*. 2006 Jul; 12(7): 1929-1936.
483. Koláčná L, Bakesová J, Varga F, Kostáková E, Plánka L, Necas A, Lukás D, Amler E, Pelouch V. Biochemical and biophysical aspects of collagen nanostructure in the extracellular matrix. *Physiological research*. 2007; 56 Suppl 1: S51-S60.
484. Xu F, Zhang C, Graves DT. Abnormal cell responses and role of TNF- α in impaired diabetic wound healing. *BioMed research international*. 2013 Jan 20,; 2013: 754802-9.
485. Jiamboonsri P, Pithayanukul P, Bavovada R, Leanpolchareanchai J, Yin T, Gao S, Hu M. Factors influencing oral bioavailability of thai mango seed kernel extract and its key phenolic principles. *Molecules (Basel, Switzerland)*. 2015 Nov 30,; 20(12): 21254-21273.
486. Lin M, Chang F, Hua M, Wu Y, Liu S. Inhibitory effects of 1,2,3,4,6-penta-O-galloyl- β -d-glucopyranose on biofilm formation by staphylococcus aureus. *Antimicrobial Agents and Chemotherapy*. 2011 Mar 1,; 55(3): 1021-1027.
487. Skovso S. Modeling type 2 diabetes in rats using high fat diet and streptozotocin. *Journal of diabetes investigation*. 2014 Jul; 5(4): 349-358.
488. Srinivasan K, Viswanad B, Asrat L, Kaul CL, Ramarao P. Combination of high-fat diet-fed and low-dose streptozotocin-treated rat: A model for type 2 diabetes and pharmacological screening. *Pharmacological research*. 2005; 52(4): 313-320.
489. Zhang M, Lv X, Li J, Xu Z, Chen L. The characterization of high-fat diet and multiple low-dose streptozotocin induced type 2 diabetes rat model. *Experimental diabetes research*. 2008 Nov 30,; 2008: 704045-9.
490. Suckow MA, Duke Boynton FD, Johnson C. Use of a rat model to study ventral abdominal hernia repair. *Journal of Visualized Experiments*. 2017(128).
491. Vogels RRM, Kaufmann R, van den Hil, L. C. L, van Steensel S, Schreinemacher MHF, Lange JF, Bouvy ND. Critical overview of all available animal models for abdominal wall hernia research. *Hernia*. 2017 Oct; 21(5): 667-675.

492. Crowe AR, Yue W. Semi-quantitative determination of protein expression using immunohistochemistry staining and analysis: An integrated protocol. *Bio-protocol*. 2019 Dec 20;; 9(24).